Department of Forest Products Technology

The Effect of Web Structure on Wet Web Runnability

Markku Ora

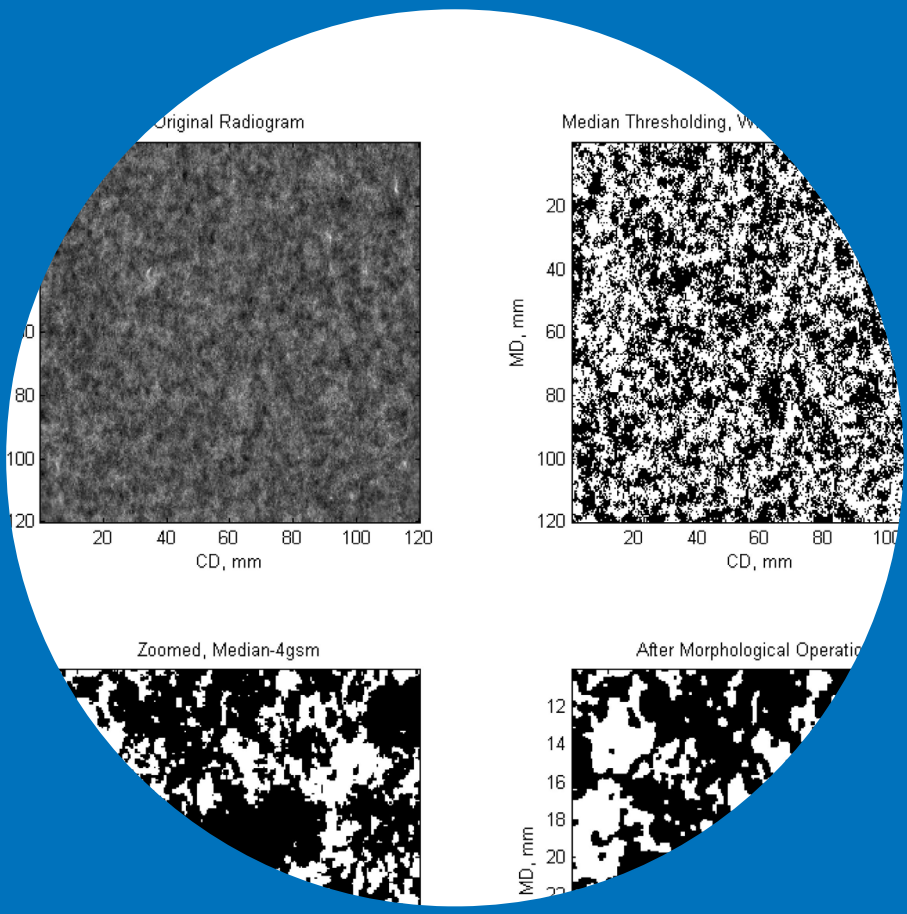

Aalto University

DOCTORAL DISSERTATIONS

Aalto University publication series
DOCTORAL DISSERTATIONS 38/2012

The Effect of Web Structure on Wet Web Runnability

Markku Ora

Doctoral dissertation for the degree of Doctor of Science in Technology to be presented with due permission of the School of Chemical Technology for public examination and debate in Auditorium (Forest Products Building 2) at the Aalto University School of Chemical Technology (Espoo, Finland) on the 20th of April 2012 at 12 noon.

Aalto University
School of Chemical Technology
Department of Forest Products Technology

Supervisor
Professor Thaddeus Maloney, Aalto University

Instructors
Professor Emeritus Hannu Paulapuro, Aalto University
Dr. Isko Kajanto, UPM-Kymmene Corporation

Preliminary examiners
Assistant Professor Artem Kulachenko, Royal Institute of Technology (KTH), Sweden
Dr. Ari Kiviranta, M-Real Corporation, Finland

Opponents
Assistant Professor Artem Kulachenko, Royal Institute of Technology (KTH), Sweden
Dr. Kari Räisänen, Metso Corporation, Finland

Aalto University publication series
DOCTORAL DISSERTATIONS 38/2012

ISBN 978-952-60-4568-9 (printed)
ISBN 978-952-60-4569-6 (pdf)
ISSN-L 1799-4934
ISSN 1799-4934 (printed)
ISSN 1799-4942 (pdf)

Unigrafia Oy
Helsinki 2012

Finland

The dissertation can be read at http://lib.tkk.fi/Diss/

441 697
Printed matter

Aalto University

Abstract

Aalto University, P.O. Box 11000, FI-00076 Aalto www.aalto.fi

Author
Markku Ora

Name of the doctoral dissertation
The Effect of Web Structure on Wet Web Runnability

Publisher School of Chemical Technology

Unit Department of Forest Products Technology

Series Aalto University publication series DOCTORAL DISSERTATIONS 38/2012

Field of research Paper and Printing Research

Manuscript submitted 30 May 2011 **Manuscript revised** 28 February 2012

Date of the defence 20 April 2012 **Language** English

☒ **Monograph** ☐ **Article dissertation (summary + original articles)**

Abstract

The effect of paper structure on wet web strength properties was studied by running the re-wetted mill-made paper reels on a pilot runnability device at the dry solids contents (DSC) typical to the press section and the first part of the drying section. In order to run those reels with low DSC, a new re-wetting procedure was developed. In addition, one trial was conducted with measuring the wet web strength in situ on the press section of a pilot Fourdrinier. The benefit of these approaches is the ability to measure the strength properties in more realistic conditions compared with standard laboratory methods.

According to the results, if formation is good—as it presumably is on modern paper machines—further formation improvement does not improve average wet strength properties. Only when formation is poor—as it can be on a Fourdrinier-type machine—does improved formation result in improved average wet tensile strength and tensile stiffness. Instead, the fibre orientation had a strong effect on these strength properties. Interestingly, the orientation profile in the z-direction did not affect the wet strength properties if the average orientation remained constant. This suggests that it does not matter whether the machine runs the jet-wire-ratio in the rush or drag side.

Formation has an influence on the tensile strength variation of wet and dry papers. In addition, the effect depends on the scale of formation and dry solids content. In wet papers, large scale formation has the strongest effect on the strength variation. Conversely, in dry papers the strength variation is controlled by small scale formation. In addition, it is suggested that the poorer the formation the lower the DSC at which the variability due to the effect of formation appears. Contrary to formation, fibre orientation does not affect the strength variation.

The strength distribution of dry paper can be described by an extreme value model, such as the 2-parameter Weibull. Instead, the strength distribution of wet webs appears Gaussian, meaning that the wet papers do not show either weak-link behaviour or weak-link scaling. In addition, even large defects do not impair wet web runnability on the press section or in the first part of the drying section, at least if the defects are not located just at the edge of the web.

Keywords Formation, orientation, paper machine, runnability, strength distribution, strength properties, structure, wet web

ISBN (printed) 978-952-60-4568-9 **ISBN (pdf)** 978-952-60-4569-6

ISSN-L 1799-4934 **ISSN (printed)** 1799-4934 **ISSN (pdf)** 1799-4942

Location of publisher Espoo **Location of printing** Helsinki **Year** 2012

Pages 198 **The dissertation can be read at** http://lib.tkk.fi/Diss/

Tekijä
Markku Ora

Väitöskirjan nimi
Rainan rakenteen vaikutus märän rainan ajettavuuteen

Julkaisija Kemian tekniikan korkeakoulu

Yksikkö Puunjalostustekniikan laitos

Sarja Aalto University publication series DOCTORAL DISSERTATIONS 38/2012

Tutkimusala Paperi- ja painatustekniikka

Käsikirjoituksen pvm 30.05.2011 **Korjatun käsikirjoituksen pvm** 28.02.2012

Väitöspäivä 20.04.2012 **Kieli** Englanti

☒ **Monografia** ☐ **Yhdistelmäväitöskirja (yhteenveto-osa + erillisartikkelit)**

Tiivistelmä

Työssä tutkittiin paperin rakenteen vaikutusta märän rainan lujuuksiin ajamalla uudelleen kostutettuja tehdasvalmisteisia paperirullia ajettavuuspilotissa. Tutkimusta varten kehitettiin uusi kostutusmenetelmä, jolla päästiin paperikoneen puristin- ja alkukuivatusosan kuiva-ainepitoisuuksiin. Lisäksi yksi koesarja ajettiin tasoviiratyyppisellä pilotpaperikoneella, jossa märän rainan lujuus mitattiin suoraan puristinosalla. Laboratoriomittaisiin menetelmiin verrattuna käytetyt menetelmät tarjoavat realistisemman ympäristön lujuusmittauksille.

Tulosten mukaan formaation ollessa hyvä, kuten se tyypillisesti on moderneilla paperikoneilla, formaation edelleen parantaminen ei paranna märän rainan lujuusominaisuuksia. Vain jos formaatio on huono, kuten se voi olla tasoviiratyyppisillä koneilla, formaation parantaminen lisää märän paperin vetolujuutta ja vetojäykkyyttä. Kuituorientaatiolla on sitä vastoin voimakas vaikutus edellä mainittuihin ominaisuuksiin. Mielenkiintoinen havainto oli se, että orientaatioprofiililla z-suunnassa ei ole vaikutusta märän rainan lujuusominaisuuksiin, jos keskimääräinen kuituorientaatio pysyy vakiona. Tästä voidaan päätellä, että märän rainan lujuuden kannalta ei ole väliä ajetaanko paperikonetta ali- vai yliperällä.

Formaatio vaikuttaa märkien ja kuivien papereiden vetolujuusvaihteluun. Vaikutus riippuu formaation mittakaavasta ja paperin kuiva-ainepitoisuudesta. Märissä papereissa suurimittakaavaisella formaatiolla on voimakkain vaikutus ja kuivissa papereissa pienimittakaavaisella. Lisäksi näyttää siltä, että mitä huonompi formaatio on sitä alemmassa kuiva-ainepitoisuudessa lujuusvaihtelu formaation vaikutuksesta alkaa. Sitä vastoin kuituorientaatiolla ei ole vaikutusta vetolujuusvaihteluun.

Kuivan paperin lujuutta voidaan kuvata ääriarvojakaumalla, kuten esimerkiksi kaksiparametrisella Weibull-jakaumalla. Sitä vastoin märän paperin vetolujuus on normaalijakautunut, joten märällä paperilla ei ole "weak-link" -ominaisuutta (katkeaminen heikoimmasta kohdasta) eikä "weak-link scaling" -ominaisuutta (pienen näytekappaleen lujuus on suurempi kuin suuremman näytteen). Lisäksi suuretkaan viat eivät haittaa märän rainan ajettavuutta puristin- ja alkukuivatusosalla, ainakaan jos viat eivät ole aivan radan reunassa.

Avainsanat Ajettavuus, formaatio, lujuusjakauma, lujuusominaisuudet, märkä raina, orientaatio, paperikone, rakenne

ISBN (painettu) 978-952-60-4568-9 **ISBN (pdf)** 978-952-60-4569-6

ISSN-L 1799-4934 **ISSN (painettu)** 1799-4934 **ISSN (pdf)** 1799-4942

Julkaisupaikka Espoo **Painopaikka** Helsinki **Vuosi** 2012

Sivumäärä 198 **Luettavissa verkossa osoitteessa** http://lib.tkk.fi/Diss/

PREFACE

The idea for this thesis was born when I worked at a paper mill where the paper machines suffered from a big number of press and drying section breaks. It is well known among the papermakers that there are several issues affecting the break rate, for example, technical solutions, housekeeping, strength properties of the web etc. Structural technical solutions are not easily changed. In addition, possibilities to change furnish properties were limited at the mill in question. As a consequence, two questions arose. Firstly, what are the forces stressing the wet web and secondly, is it possible to reduce the break rate by improving the wet web tolerance to the stressing forces by altering the web structure. This thesis tries to answer those questions by means of a literature study and own experiments.

I would like to express my gratitude to my instructors Professor Emeritus Hannu Paulapuro and Dr. Isko Kajanto and supervisor Professor Thaddeus Maloney for their valuable advice during the course of this work. Especially, I would like to thank professor Paulapuro for his clever way keeping my studies alive when I was burying myself in daily work.

In addition, I wish to thank preliminary examiners Professor Artem Kulachenko and Dr. Ari Kiviranta for their constructive comments. Professor Kulachenko's contribution is especially acknowledged.

I also want to thank Jaakko Asikainen, Dr. Rolf Wathén and Dr. Atsushi Tanaka for their indispensable input in the pilot runs. In addition, I wish to thank Tiina Pöhler and Asko Sneck for the ESEM measurements and Dr. Jukka Ketoja and Professor Kaarlo Niskanen for good discussions related to paper physics and Dr. Pekka Salminen for discussions concerning water absorption into paper.

Furthermore, I want to express my sincere thanks to Dr. Olli Saarela for his unselfish input in developing the computation algorithms needed in the work and fruitful discussions during the course of this work.

I wish to thank Anna-Leena Erkkilä and Tiina Hälikkä for the β-radiography and layered orientation measurements as well as Terhi Saari for the β-radiography measurements.

The list of the persons to whom I am grateful is so long that it is impossible to mention everybody by name. So thank you former and present colleagues, laboratory technicians in UPM Research Centre and mill people for your contribution. However, I would like to mention and give special thanks to my present and former colleagues Dr. Jouko Lehto, Klaus Jernström, Maarit Saloranta, Dougie Briggs and Mikko Pirinen for their contribution and very good co-operation. In addition, I would like to thank Mirva Hakuli and Jenni Ukkonen from our Information Service for their excellent work finding and supplying me with the articles and information needed during the course of this work. I also want to thank Sirje Liukko for her indispensable help in the finishing phase of this dissertation.

I would like to express my gratitude to Dr. Eeva Jernström and Pekka Hurskainen from UPM R&D who rendered this work possible. I hope this work pays off!

My sincere thanks go to Markku Taavitsainen, my friend of many years, for his endless support and curiosity regarding the progress of the work.

Finally, my warmest thanks belong to my brother Pekka and his family Heljä, Nea and Theo for their encouragement, support and pleasant time together.

Lappeenranta, March 16, 2012

Markku Ora

LIST OF ABBREVIATIONS

AIC	Akaike's information criterion
AICc	A second-order variant of AIC, used for small samples
AFM	Atomic force microscopy
AHMA	Runnability pilot device
CD	Cross machine direction
COV	Coefficient of variation
CSF	Canadian Standard Freeness
DIP	Deinked pulp
DDJ	Dynamic drainage jar
DSC	Dry solids content
ESEM	Environmental scanning electron microscopy
FEM	Finite element method
FR	Forming roll
FSP	Fibre saturation point
GW	Groundwood
KCL	Oy Keskuslaboratorio-Centrallaboratotium AB
LWC	Light weight coated paper
MFS	Multifoil shoe
MD	Machine direction
NIR	Near-infrared
PGW	Pressurised groundwood
PM	Paper machine
RBA	Relative bonded area (dry samples)
RCA	Relative contact area (wet samples)
RCF	Recycled fibre
RH	Relative humidity
RMS	A method used to characterise surface roughness
RSS	Residual sum of squares
SBK	Semi-bleached kraft
SC	Supercalendered paper
SD	Standard deviation
Stdev	Standard deviation
TSI	Tensile stiffness index
TMP	Thermo mechanical pulp
VTT	Technical Research Centre of Finland
WRV	Water retention value
ZD	Z-direction

LIST OF SYMBOLS

Latin

a	Pixel size or parameter
b	Parameter
c	Coverage (the number of fibres in the z-direction scanning line) or parameter
C	Fibre coarseness
C_{af}	Average air friction coefficient between the web and surrounding air
d	Parameter
D	Diffusion coefficient
e_i	(minor axis of ellipse i) / (major axis of ellipse i)
$1 - e_i$	Anisotropy for layer i
$1 - e$	Layered anisotropy = anisotropy for the whole paper
f	Unknown reality that produces the strength data
F	Fraction of the amount of water taken up in time t relative to the amount taken up at infinite time
g	Gravitational constant
g_i	Candidate model to approximate the unknown reality f
$G(\sigma)$	Cumulative distribution function for Gumbel distribution
$G_{mod}(\sigma)$	Cumulative distribution function for modified Gumbel distribution
h	Pore height
K	The number of estimable parameters in a candidate model
l	Penetration depth
L	Length of the web in an open draw or length of test draw section in AHMA or fibre length
$L(\theta \mid x, g)$	Likelihood function of the model parameters θ, given the data x and the model g
T	Outer wire tension or tensile strength
m	Basis weight
m_i	Mass of a paper layer when measuring layered anisotropy
m_o, m_t, m_∞	Amount of water taken up at times 0, t and at fibre saturation respectively
m_{cp}	Added mass (affected by surrounding air) per surface area for the centripetal force component
n	Sample size
p	Pressure
p_e	External pressure
Δp	Pressure difference between the upper and lower surface of the web
P	Fibre perimeter of the average fibre cross-section
r	Capillary or pore radius
r_c	Radius of curvature of the water meniscus
R	Radius of the web in an open draw or local radius of the curvature of the wire
t	Time or penetration time in water absorption or time elapsed from the introduction of water in diffusion

t_{ramp}	Ramp time
Tg	Glass transition temperature
z	Initial thickness of paper
v	Velocity
v_J	Velocity of headbox jet
v_{FS}	Velocity of free suspension in the wire gap
v_1	Web speed in the brake nip
v_2	Web speed in the pulling nip
V	Volume of the entire paper sheet
V_f	Volume occupied by fibres
W	Work of adhesion
$W(\sigma)$	Cumulative distribution function for Weibull distribution

Greek

α	Parameter
β	Weibull shape parameter or Weibull modulus
Δ_i	AIC or AICc differences, relative to the smallest AIC or AICc values in the set of candidate models
ε	Strain
ε_{app}	Speed difference between the nips and called apparent strain
ε_{max}	Maximum applied strain
ε_{min}	Initial strain
ε_{real}	Real strain
γ	Surface tension of water
ϕ	Porosity
γ	Surface tension
η	Viscosity of liquid
φ	Take-off angle
μ	Location parameter or the minimum stress below which the paper cannot fail or the coefficient of friction
ρ	Density or paper density
ρ_a	Air density
ρ_f	Fibre density (includes the porosity of the cell wall and uncollapsed lumen space of the fibres)
σ	Stress or web tension
θ	Generic model parameter or contact angle between the liquid and the capillary wall
$\hat{\theta}$	Estimator of the generic model parameter

TABLE OF CONTENTS

1 INTRODUCTION

1.1 Background

Papermaking is very challenging nowadays due to cost pressure and efficiency requirements. In order to respond to these challenges, a papermaker tries to maximise production and minimise the amount of quality-related broke, and to do both in a cost-effective manner. There are three ways in which the papermaker can maximise production: reduce the number and duration of breaks, reduce the number of unplanned shutdowns (due to machine failures) and increase the machine speed. The concept of paper machine runnability involves these three options.

Web runnability is a part of the paper machine runnability concept and comprises both the number of breaks and the speed of the paper machine. To enable good runnability the strength properties of the paper web need to be adequate and of the right type in order to tolerate all the stress influencing it when running through the paper machine.

The critical areas from a web runnability point of view are the first open draw between the press section and drying section—where the wet web is transferred from one supporting surface to another without any support—and the first part of the drying section, even though this would be the single-tier type. The reason for this is the low dry solids content of the web: typically 40–50% after the press section, leading to low strength values; for example, at that location the tensile stiffness of the web is only 10–15% of that of dry paper (Kurki et al. 2010). The bonding mechanisms and rheological behaviour in wet and dry paper are different. As such, it is good to differentiate the runnability of the wet web from that of the dry web.

1.2 Research problem

Much research has been carried out concerning wet web rheology, wet web behaviour in an open draw, the effect of furnish and chemistry-related issues on wet web strength properties, bonding mechanism and the rupture mechanism. However, very little attention has been paid to the effect of web structure on wet web strength properties. Certainly there are publications where the topic has been approached with modelling (Miettinen et al. 2007a, 2007b, Kulachenko et al. 2008, 2009 and Lindström et al. 2009), but due to computational restrictions the size of the simulated specimens have been too small to allow study of the effects of formation scale grammage variation. In addition, Yang and Thorpe (1977, 1979) executed some exercises using finite element simulations and experimental analysis. In addition to these publications, there are results available concerning the effect of fibre orientation on the tensile strength of the wet web (Kouko et al. 2007). However, the current knowledge related to the effect of web structure on wet web strength properties is limited. For example, what is the effect of formation on wet web strength properties?

In addition, it is questionable whether the strength of wet paper follows any extreme value distribution at all—as dry paper does—and whether the wet web strength shows any weak-link scaling, meaning that the strength of a large specimen is smaller than that of a smaller specimen. These issues are closely related to the failure mechanism of the paper specimen or paper web.

Because there is a structural hierarchy in paper, i.e. the structure exists at a variety of scales (cf. Table 1), the structural level of interest needs to be defined first. After this the structure at all scales below the scale of interest can be ignored and represented by a set of properties. Note that the scales overlap in the table. In addition, fibre morphology and paper microstructure are presented separately, although they could have been grouped together because of the same basic size range. However, the original division by Kortschot (1997) is retained.

In this thesis, the structural level of interest extends from the microstructure to mesostructure because the relative bonded area (RBA), fibre orientation, different type of z-direction distributions and formation, which are expected to affect wet strength properties, belong to these categories

Table 1. *The hierarchical structure of paper, adapted from Kortschot (1997). The table continues on the next page. MD denotes machine direction and CD cross machine direction.*

Scale	Structural component	Structural parameters	Properties dependent on structure at this scale
0.1 – 10 nm	**Molecular structure and packing** • cellulose • hemicellulose • lignin • other components	• chemical composition — (type and number of bonds, functional groups etc.) • degree of crystallinity • crystal structure • aspect ratio of elementary fibrils (crystallites) • fibrillar defects • etc.	• hydrogen bonding potential • tensile modulus and strength of fibrils • Tg of lignin • influence of moisture on Tg, stiffness • viscosity • etc.
10 nm – 1 μm	**Internal structure of the fibre** • softwood tracheids • hard wood fibres • hardwood vessels • ray cells • compression wood • tension wood	• volume fraction and position of various cell components (e.g. P, S1, S2, S3 and W layers) • wall thickness • lumen diameter • pit location and density • fibril angle in each wall layer • cracks • internal fibrillation, porosity • external fibrillation	• stiffness and strength of the fibre • anisotropy • distribution of weak spots along fibre • bond strength • moment of inertia of cell walls • light scattering • fibre saturation point • swelling potential

Table 1. Continued

1 µm – 10 mm	**Fibre morphology** • different for different types of fibres	• length, width, thickness • moment of inertia • coarseness • curl, kinks • microcompressions • specific surface area • fines content and type ("quality")	• fibre strength, distribution of strength • fibre modulus, stress-strain curve • shear and torsional properties • fibre flexibility • collapsibility • hygrothermal properties (transverse and axial)
1 µm – 10 mm	**Paper micro-structure**	• relative bonded area (RBA) • fibre orientation distribution • density • fines distribution (location) • porosity, pore size distribution • z-direction distributions – two-sidedness • surface texture	• local sheet properties – strength modulus, stress-strain curve • fracture toughness • peel strength/delamination resistance • viscoelastic properties • absorbency • printability • linting • opacity
1 mm – 10 cm	**Paper meso-structure**	• distribution of mass • distribution of regions with net differences in microstructure such as average local fibre orientation, local density or local RBA	• optical formation • printability • tensile strength of the sheet
5 mm – 30 m	**Paper macro-structure**	• MD and CD variations in sheet and roll structure • roll structure (thickness profiles etc.) • roll defects • multilayered structure	• converting performance • end use performance

1.3 Objectives and hypothesis

The main objective of this work is to clarify how the web structure on the microscale and mesoscale affects wet web strength properties, which in turn provides means to affect wet web runnability. Special attention is paid to the effects of formation and fibre orientation distribution because the papermaker can control these properties to some extent by altering the settings of the headbox and wire section. The hypothesis to be clarified is that by altering these parameters it is possible to affect the strength properties of the wet web.

The second objective is to develop a relevant methodology to study re-wetted paper reels on a pilot scale, which enables the measurement of dynamic MD strength

properties at the dry solids content (DSC) typical to the first open draw, located between the press section and drying section, and the first part of the drying section.

The third objective is to clarify whether, as in the case of dry paper, the strength distribution of the wet web can be described by an extreme value strength distribution; does the wet web demonstrate a weak-link behaviour, i.e. breaking from the weakest point in the web, and does the wet web show any weak-link scaling, i.e. the tensile strength of a large specimen is lower than that of a small specimen?

1.4 Research methods

Literature is widely used in determining the relevant strength properties from a wet web runnability point of view, in the method development for running re-wetted webs on the pilot scale and in building a connection between the bonding mechanism, fracture mechanism and the strength distribution in a wet web.

The strength measurements were mainly conducted with the AHMA runnability pilot device (Niskanen et al. 2003) by using re-wetted mil-made paper webs. Compared with standard laboratory methods, web breaks occur in AHMA under dynamic and more realistic conditions and specimen dimensions enable both microscale and mesoscale structural research. In addition, it provides good possibilities for studying break statistics. In addition to the AHMA trials, one pilot trial was run on a pilot Fourdrinier by measuring breaking tension in situ by the wet web winder installed right after the third press (Tanaka et al. 2009).

1.5 Scope of the research

This research focuses on the effects of web structure on the strength, strength distribution and runnability of the wet web. This means that furnish or machinery-related issues are reviewed only to the extent that supports achieving the set research objectives.

Papers used for the AHMA trials were newsprint and LWC base papers from different paper mills, typically made on a gap former. In order to provide a wide formation range, two trial papers were made on a gap former equipped with loadable blades. In addition, one trial was run on a pilot Fourdrinier in order to test paper whose formation was clearly worse than that of the mill papers.

1.6 Outline of the thesis

The following provides the outline of the thesis. This thesis consists of eight chapters with the following content:

Chapter 1 is the introduction.

Chapter 2 discusses and makes conclusions on the important wet strength properties affecting the web runnability in an open draw and in the first part of the drying section. It then discusses the importance of a statistical approach. After that, it reviews the effect of furnish properties, bonding mechanism, paper structure and machinery on wet strength properties.

Chapter 3 discusses the methodology used in the thesis. At first, the congruence between the web in the first open draw on the paper machine and the re-wetted web is discussed. This is based on clarifications of fibre-water interactions, fibre hornification, possible structural hornification in the re-wetted paper structure and the comparison of the AHMA runnability pilot with in situ measurements on a pilot paper machine. In addition, the on-line re-wetting systems developed to restore the dry paper webs close to the state in the first open draw after the press section is discussed. It is shown that running re-wetted webs on AHMA is a relevant method for studying the effect of paper structure on the strength properties of wet paper webs. Chapter 3 then describes the computation method developed, which allowed fairly accurate strength results on AHMA in spite of unexpected intense cyclic variation and a noise component in the measured signals in the main trials.

Chapter 4 concentrates on the effect of formation and fibre orientation on the strength properties. Different types of methods to characterise the formation and fibre orientation are used. It is shown that, on modern paper machines where formation is good or fairly good, any further formation improvement does not have any influence on average wet strength properties. Instead, when formation is poor—as it can be on Fourdriniers—the improvement of formation increases both average tensile strength and average tensile stiffness of the wet web. In addition, it is concluded that fibre orientation has a strong effect on average wet strength properties, greater than on the dry strength properties. It is also concluded that the orientation profile in the z-direction does not have any influence on average strength properties in wet webs, indicating that it does not matter whether the machine runs the jet-wire-ratio in the drag or rush side.

Chapter 5 discusses strength distributions and the effect of paper structure on them. It is shown that formation has an influence on the tensile strength variation of wet and dry papers. It is suggested that the effect depends on the scale of formation and dry solids content. In wet papers, large scale formation has the greatest effect on the strength variation. Conversely, in dry papers the strength variation is controlled by small scale formation. In addition, it is suggested that the poorer the formation the lower the DSC at which the effect of formation appears. Contrary to formation, fibre orientation does not affect the strength variation. It is also shown that paper strength at dry solids contents typical to the press section and the first part of the drying section follows the Gaussian distribution rather than any extreme value distribution. This also means that the rupture process of wet paper does not originate from a single weak spot. Neither does wet paper show weak-link scaling typical to dry papers.

Chapter 6 discusses the effect of defects on the strength of wet papers. It is demonstrated that even large defects, simulated by CD centre notches in the AHMA webs, do not affect runnability on the press section or in the first part of the drying section.

Chapter 7 discusses the main findings of this study.

Chapter 8 draws the main conclusions.

1.7 Scientific contribution

- A research method enabling the study of wet web strength properties at low DSC (i.e. typical to the press section and the first part of drying section) with running re-wetted paper reels in a pilot scale runnability device.
- The effect of formation on the wet web tensile strength, tensile stiffness and tensile strength variation at low DSC.
- Deeper knowledge concerning the effects of fibre orientation on the wet web tensile strength, tensile stiffness and tensile strength variation.
- The strength of wet paper is normally distributed, which means that wet paper does not show the weakest link behaviour or weak-link scaling.
- Even large defects in the wet web do not disturb its runnability on the press section or in the first part of the drying section, at least if they are not located in the very edge of the web.

The author was responsible for the experimental design, the method development and the analysis of the results with the following exception: the computation algorithms needed in the main trial were developed by Dr. Olli Saarela from KCL (Oy Keskuslaboratorio-Centrallaboratotium AB), currently VTT (Technical Research Centre of Finland), with the author's contribution being brainstorming together with the developer, testing the algorithms and providing him with feedback.

2 LITERATURE REVIEW

2.1 Requirements for wet strength properties derived from the forces affecting the web in an open draw and single-felted dryer group

The behaviour of wet paper is viscoelastic-plastic (Hauptmann and Cutshall 1977, Ketoja et al. 2007) and the wet web experiences both creep and relaxation while running through the paper machine. Due to viscoelasticity, the stress-strain interaction is time dependent. This was confirmed, for example, by Kouko et al. (2006a) who altered the strain rate between 1%/s and 1000%/s. The dry solids content of the papers varied between 45% and 57%. At fast strain rates the elastic modulus and measured stress (tensile strength) were higher than at slow strain rates. Interestingly, strain at break was not sensitive to the strain rate. It can be simply said that there is less time available for inelastic plastic deformation and paper is "stiffer" when the strain rate is high. Viscoelastic deformations are reversible, unlike plastic or viscoplastic ones which are irreversible. Considering the stress-strain curve, the linear section ends at a yield point, and plastic elongation only becomes significant above this point. However, the yield point has no unique definition because the deviation from a linear stress-strain curve begins to grow gradually when elongation increases (Alava and Niskanen 2008). In wet papers the plastic strain is considerably larger than in dry papers.

In the following, the word draw has been used both for the speed difference between an upstream and downstream roll and for the open gap between the same two rolls. However, the context always clarifies which one of the meanings is valid. In the first open draw between the press and the drying section (paper guiding roll), where the web is stretched most, the dwell time is typically 5–20 ms (Jantunen 1985, Kurki 2005). In open draws between the top and bottom drying cylinders in a double-felted dryer configuration, the dwell time is about 100 ms (Jantunen 1985). The work of Hauptman and Cutshall (1977), Kurki (2005) Ketoja et al. (2007) and Edvardsson and Uesaka (2010) suggests that in an open draw the tension level is essentially constant throughout the draw length and the major part of creep strain occurs quickly at the beginning of the open draw. In addition, studies done by Österberg (1962) and Mardon et al. (1975) suggest that most of the web extension occurs during or immediately after peeling from the press roll. Irrespective of the draw length, there exists significant creep, which influences the paper properties.

The web dry solids content after the press section is 33–55% depending on the paper grade and press section design (Kuhasalo et al. 2000) and ranges from 40% to 45% (Paulapuro 2007) after the third nip in common three-nip press configurations, see Figure 1. The strength and elastic modulus of a wet web are low compared with the corresponding values of dry paper. Typically, the tensile strength of wet paper after the press section is only one tenth of the dry paper strength (Kurki 2005). This is a challenge for wet web transfer in open draws, especially in the first open draw between the centre roll and dryer section where most of strain occurs. In practice, the release from the centre roll and the path through the first part of the drying section run very often at the limit of wet paper tolerance. Thus, it is quite plausible in these

circumstances that web defects, a variation in the web properties or external disturbances can cause a web break. In an open draw, web tension is needed to release the web from a supporting surface and transfer it unsupported onto another supporting surface. The required tension is induced by stretching the web by using speed difference between the downstream and upstream supporting surfaces of an open draw. This stretching in conjunction with the load-elongation properties of the wet web generates the required web tension.

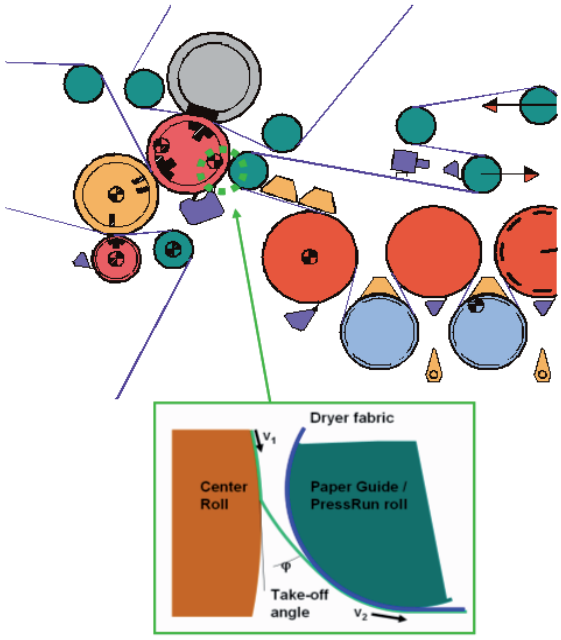

Figure 1. *Three-nip press configuration with an open draw located between the centre roll and paper guide roll. Modified from the references of Kurki (2001, 2004).*

Several researchers have studied the wet web behaviour in an open draw with the main interest being experimental work on the peeling of wet webs and its associated theory (Österberg 1962, Shallhorn and Karnis 1975, Mardon 1976, 1979, Oliver 1982, Pye et al. 1985, McDonald et al. 1988, Pikulik et al. 1993, Ahrens et al. 2004.) and modelling the wet web performance (Wahren 1981, 1989, Parker 1985, Pakarinen et al. 1993, Kurki et al. 1995, 1997, Ahrens et al. 2004, Kurki 2005, Edvarsson and Uesaka 2009a, 2009b, 2010). Edvardson and Uesaka developed and applied a novel particle-based system dynamics model. Compared with the earlier publications, it allows the investigation of complex interactions between web property fluctuations and system parameters without any constraints of a particular geometrical web shape or boundary conditions assumed a priori. The model provides information on the phenomenon of how the open draw becomes unstable and the factors defining a safe operating window.

During the transfer in an open draw, several different types of external forces influence the web and the web tension needs to be high enough to carry all these forces. The affecting forces include pressure, centrifugal, adhesion, friction (caused by the surrounding air) and gravitational forces. The most intense pressure forces occur in pockets between the rotating centre roll or drying cylinder and the moving web leaving or entering the nip causing under and over-pressure respectively. This is due to boundary air flows, which follow the moving surfaces bringing air to the closing pocket and dragging it out from the opening pocket. Under and over-pressure cause movement in the web, which can be a steady-state type of deflection or an unstable time-dependent web flutter. Over and under-pressure development with web velocity is somewhere between quadratic and linear accentuating pressure effects on high-speed machines. Other important forces acting on high-speed machines are centrifugal forces due to their quadratic dependence on web speed. The effect of friction forces between the web and air as well as gravitational force is small in short open draws. (Pakarinen et al. 1993, 1995, Kurki et al. 1995, 1997, Kurki 2005.) Several variables affect the strength of adhesion between the wet web and the centre roll surface, for example surface topology and material, surface energy, furnish, build-up of impurities on the roll surface such as resin, surface and sheet temperature, web moisture and application pressure (Ahrens et al. 2004). Neither speed nor a web take-off angle in the normal range of 10–35° influences the adhesion.

In addition to external forces, there exists an important internal force in the web — drying tension (Htun and de Ruvo 1978). This affects the required draw in the open gaps. However, because the drying tension is caused by drying shrinkage originating from the emergence of hydrogen bonds, the drying tension cannot have any significant influence on the wet web in the press section or in the first part of the drying section.

The forces affecting the web tension in the open draw between the centre roll and the transfer roll are shown schematically in Figure 2 as a function of speed. As the figure demonstrates, centrifugal and pressure forces clearly strengthen as the running speed increases.

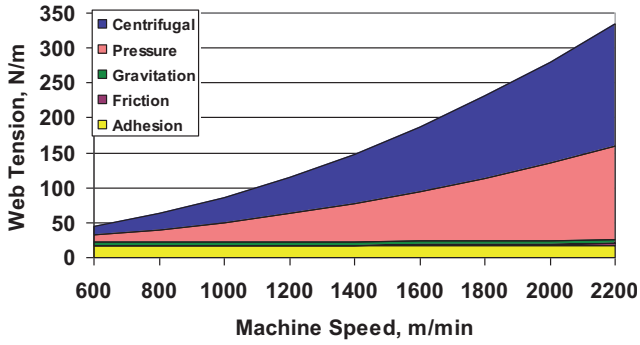

***Figure 2**. A schematic depiction of the forces affecting the web tension in the open draw between the centre roll and the paper guide roll as a function of web velocity. Constant web radius and take-off angle (Kurki 2001).*

The interaction between the web tension and influencing parameters in an open draw can also be presented by the following steady-state model by assuming the shape of the web to be an arc (Kurki 2005).

.

$$\sigma = \Delta pR + (m + m_{cp})v^2 + \frac{W}{(1-\cos\varphi)} + mgR + C_{af}\rho_a L v^2 \qquad (1)$$

where σ is the web tension
Δp is the pressure difference between the upper and lower surface of the web
R is the radius of the web in the open draw
m is the basis weight of the web
m_{cp} is the added mass (affected by surrounding air) per surface area for the centripetal force component
v is the web velocity
W is the work of adhesion
φ is the take-off angle
g is the gravitational constant
C_{af} is the average air friction coefficient between the web and air
ρ_a is the air density
L is the web length in the open draw.

The effect of the last two terms, gravitational and friction term, is small in short open draws and the terms can be omitted (Kurki 2005).

Equation (1) provides the first prerequisite for wet web runnability in an open draw. The web tension, achieved by straining the wet web, needs to balance the sum effect of the external forces. To meet this requirement, the tensile strength of wet paper needs to equal the web tension, or preferably, to exceed it.

The first prerequisite can simply be stated as follows:

(I) Wet web tensile strength > wet web tension = sum effect of external forces.

In an ideal situation, the paper machine runs for long periods with no breaks and web tension changes are at a minimum. In practice, however, such stability is unusual and the process is more or less subjected to various time-dependent disturbances that can have a significant effect on runnability. Especially in the first open draw, where the wet web is weak, the external forces in the presence of peeling force form a very sensitive, complex and time-dependent runnability system. One essential feature of this system is its self-adjustment capability. For modest transient disturbances and modest step-wise changes in external conditions (speed, draw, aerodynamic effects and adhesion between the web and centre roll etc.) or web properties (DSC, elastic modulus and basis weight etc.), simultaneous adjustments occur to the take-off angle and web curvature to restore the original tension and strain level. (Kurki et al. 1997, Kurki 2005, Edvardsson and Uesaka 2009a, 2009b, 2010.) According to practical experience from paper machines, the take-off angle is the primary adjusting variable when web speed increases (Kurki 2005).

Depending on the combination of parameters (e.g. web speed, draw and wet web properties), the open draw may lose its self-adjustment capability due to sudden external disturbances or a sudden fluctuation in web properties (Edvardsson and Uesaka 2009a, 2009b, 2010). Figure 3 provides an example to clarify the phenomenon.

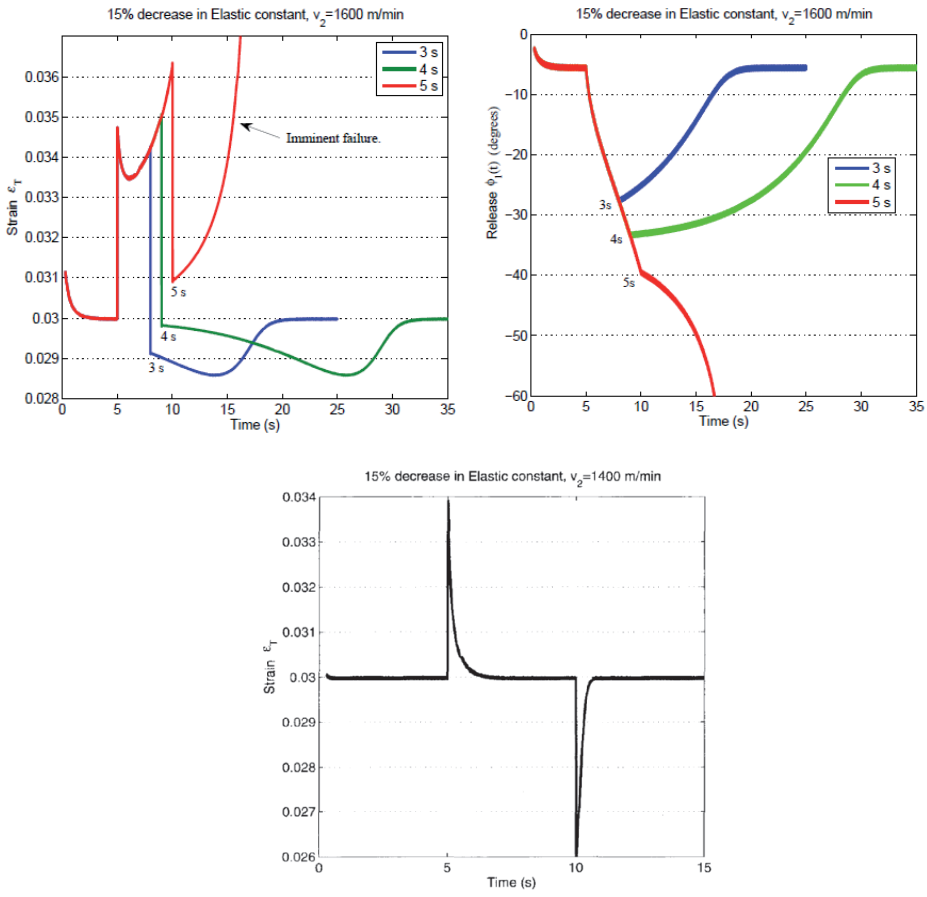

Figure 3. *Top left: Total strain ε_T as a function of time. The elastic modulus is decreased by 15% at t = 5 s. Duration of the disturbances is 3 s, 4 s or 5 s. Speed 1600 m/min and draw 3%. Top right: The corresponding evolution of the release point. In both figures, the 2 s long transient behaviour in the beginning of the curve is caused by the starting phase of the simulation and it does not describe the real web behaviour. Bottom: The elastic modulus is decreased by 15% at t = 5 s and the duration of the disturbances is 5 s. Speed is only 1400 m/min and draw is 3%. (Edvarsson and Uesaka 2009b, 2010).*

The web is running at 1600 m/min with the draw being 3%. At t = 5 s, the elastic modulus suddenly decreases by 15%, for example due to a reduction in DSC, and the strain surges up to almost 3.5% (top left picture). The system attempts to adjust itself

to a new condition seen as a reduction in strain to about 3.35%. However, the disturbance together with the quite high machine speed makes the system unstable. If the duration of the disturbance is short enough (less than 5 s in this case), the system is capable of recovering. However, when the stiffness of the web is restored after 5 s, the web length in the open draw has already increased so much due to the changed release point and web curvature that the system cannot cope with the increased centrifugal and gravity forces. The unstable behaviour therefore becomes irreversible and the strain continuously grows without any sign of recovery and web failure is imminent. The top right figure displays the corresponding evolution of the release point. The bottom figure shows that, with a less challenging parameter combination (i.e. web speed 1400 m/min), the same 5 s disturbance does not jeopardise stability. In addition, another simulation at 1400 m/min and 3% draw showed that if the 15% reduction in elastic modulus occurred slowly, for example over 2 s instead of 0.1 s, the strain peak reduced from 3.24% to 3.05% and was thus less dangerous (Edvarsson and Uesaka 2009a).

Generally, according to the results of Edvarsson and Uesaka (2009a), it seems that sudden disturbances and their continuation are dangerous but slow variations are much less harmful. In addition, according to Wahren (1989), the open draw cannot adjust to accommodate high frequency disturbances as it does for slow disturbances. To avoid or minimise flutter and keep within the bounds of tolerable web strain, any potentially flutter-inducing disturbance must be slow, i.e. gradual changes extending for several or tens of times the length of the open draw. The recommended rate of change is of the same order of magnitude as aforementioned example, where elastic modulus decreased 15% in 2 s causing only a minor strain increase.

At a given set of web property parameters and draw, even if there are no disturbances at all, there exists a critical machine speed at which the unstable behaviour starts. The parametric sensitivity study carried out by Edvarsson and Uesaka (2009a) showed that out of five investigated parameters—wet web elastic modulus, thickness, mass density (i.e. fibre-water mixture), adhesion strength to the centre roll and draw—the highest impact factors were draw, elastic modulus and mass density (in the order of importance). In contrast to mass density, an increase in the draw and elastic modulus had a positive effect on the critical speed. In addition, the dry solids content had a strong influence on the elastic modulus. The research (2009a) calculated that the increase of DSC from 40% to 45% increased the critical speed by 25% when the draw was kept constant.

Normal values for the take-off angle are 10–35° (Kurki 2005). With higher values the behaviour of the release is very unstable. Even a small variation in adhesion between the web and centre roll surface, in furnish properties, in basis weight, in moisture and in speed due to inaccuracies of the drive system can initiate web flutter (i.e. release point moving back and forth on the centre roll). Instabilities in web transfer between the press and dryer section can in turn lead to web breaks. Higher web tension levels increase web stability and reduce the risk of sheet flutter. (Österberg 1962, Wahren 1981, Wahren 1989.) However, excessively high web tension levels will permanently deform the web causing a reduction in paper quality, such as increased porosity, oil absorption, reduced Scott Bond and stretch at break (Baum et al. 1984, Pikulik 1997, Juppi and Kaihovirta 2002, Ilvespää et al. 2003), and web breaks either as early as the

press section or due to lack of sufficient residual strain later in the drying section and in converting and printing processes (Mardon 1976, Barnet and Harvey 1979, 1980, Wahren 1989, McDonald et al. 1990, Ahrens et al. 2004, Juppi 2006). This is quite understandable because the effect of web straining in paper machine draws is cumulative (Barnet and Harvey 1980, McDonald et al. 1988) and high draws exhaust the strain capability of the web.

The parametric sensitivity study of Edvarsson and Uesaka (2009a) provides information on the parameters controlling the web release point. The parameters studied were wet web elastic modulus, thickness, mass density, adhesion strength to the centre roll, draw and machine speed. The outcome of the study was that the machine speed (the most important), elastic modulus and draw had the largest effect on the web release point. When the draw and web speed were kept constant, the results showed that during normal operation it is the variation in elastic modulus that dominates the release point.

Based on the discussion above, it is obvious that the draw, enabling the required tension to the web, and elastic modulus have key roles in stabilising the web run in an open draw and in speeding up the machine to higher running velocities. A natural outcome from the draw requirement is a high enough tensile strength, presented already as a prerequisite (I). In addition, in order to induce the required tension without ruining the paper quality by excessively harsh straining, the elastic modulus must be sufficiently high. If it can be expected that the web experiences strong and very sudden disturbances in an open draw, the outcome may be high transient strains occurring in the web (Kurki et al. 1997, Edvarsson and Uesaka 2009a). Under such circumstances, the wet web needs to have a large enough stretch at break.

As a conclusion, the second runnability prerequisite from a wet web strength point of view can be stated as follows:

(II) The wet web elastic modulus needs to be as high as possible.
In addition, the stretch at break needs to be large enough if sudden strong disturbances are likely.

At the end of the open draw, located between the press and the first dryer group (paper guide roll) in Figure 1, the wet web is attached onto the dryer fabric in a strained state. The speed level remains the same inside the whole first drying group. Therefore the strain level does not increase, but the web tension decreases due to relaxation. This means that the primary tension behaviour is tension relaxation after the open draw. Loss of wet web tension is typically 50–60% and most of the loss occurs within 0.5 s (Kurki et al. 2004, 2010). The web tension is therefore remarkably reduced already in the first opening pocket, point A in Figure 4. This is important because, in the first part of the dryer section, good stabilisation of the wet web depends highly on web tension. This is induced by a speed difference in the open or closed draw preceding every dryer group.

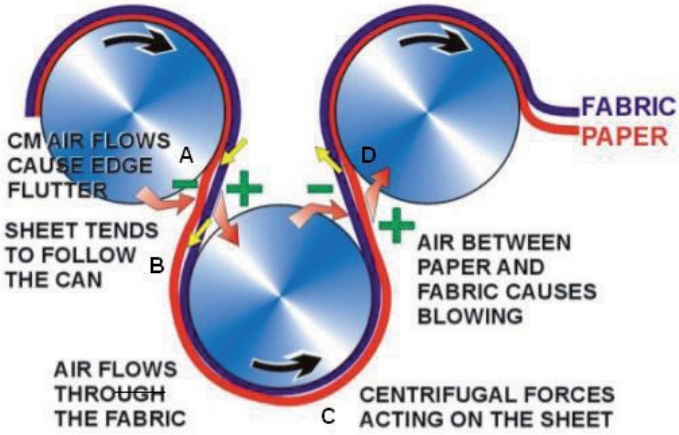

***Figure 4**. Problems caused by air flows in single-felted dryers. Modified from the reference of Kurki et al. (2005).*

Inside the double-felted dryer groups, the external forces affecting the web in the free draws between the top and bottom cylinders are the same as those in the open draw between the press and the dryer section. With rising machine speeds, impaired web runnability is a significant problem in the wet region of this type of dryer section. The problem appears in the form of web flutter and wrinkles, especially at the edges in the free draws (Kuhasalo et al. 2000).

In single-felted dryer groups, the situation is different due to the support provided by the drying fabric. However, the critical area is the opening pocket. If the web tension is too low, the web forms an open draw by following the dryer due to under-pressure and adhesion between the web and cylinder surface, point A in Figure 4. The stronger the deflection, the larger the stress. The second critical point is the closing nip, where overpressure—caused by air transported by the fabric and roll surfaces—tends to detach the paper web from the fabric, point B. The air penetration between the web and fabric at points A and B can cause runnability problems at points C and D where the extra air forced out produces a cross-directional flow (Pakarinen et al. 1995). The web running without fabric support is subject to disturbances due to centrifugal and flutter-related forces. The first dryer groups are the most critical due to rapid web tension relaxation in the wet web. The slackening of the wet web causes wrinkling, bagging, fluttering and weaving of the web, which may lead to web breaks (Kurki et al. 2010).

The more extensive the strain in the web transfer, the higher the relaxation rate (Jantunen 1985, Miettinen et al. 2009). In addition, the higher the strain rate, the stronger the tension relaxation (Retulainen and Salminen 2009, Kekko et al. 2009). The results of Kekko et al. (2009) suggest that the residual tension after straining at a high rate cannot be predicted from slow-strain-rate results. This is because straining at low rate did not affect the residual tension at all. The results of Retulainen, Salminen and Kekko suggest that a short open draw may be worse than a long open

one in terms of tension relaxation because the same stretching is performed at a higher rate in the shorter draw.

According to the results of Kouko et al. (2007), when DSC was altered between 41% and 47% by wet pressing, the wetter the web the quicker the relaxation. However, Jantunen's (1985) experiments with newsprint show that the relaxation speed decreases only slightly when the dry solids content is increased from 35% to 75%. Above the 75% limit, the relaxation speed declines markedly with increasing solids content.

It has been noticed that there is a correlation between residual tension (tension after relaxation) and paper machine dryer section runnability (Kouko et al. 2006b). Figure 5 provides strong evidence of this by demonstrating that the higher the residual tension, the lower the vacuum required in the runnability stabilising equipment.

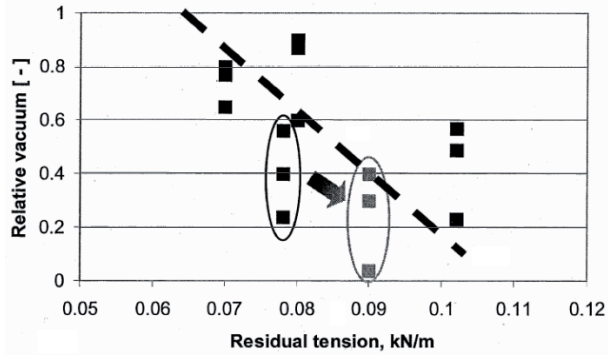

Figure 5. *Correlation between the measured residual tension of pulps and the vacuum required in a runnability stabilising component at the first dryer group on a pilot PM to stabilise the wet web. Machine speed, draws, basis weight, press solids content and fibre orientation were kept constant. The arrow and lighter dots mark the effect of the reduction of kraft on TMP base (Kouko et al. 2006b).*

Based on the discussion above, the third wet web strength-related prerequisite can be stated as follows.

(III) Wet web residual tension needs to be as high as possible.

A special device is needed for residual tension measurements because the relaxation rate of tensile strength is very high in wet paper, tens of percent within less than 0.5s (Kurki et al. 2004, 2010). The latest research has utilised the fast tensile rig IMPACT (Kurki et al. 2004) as a special device where wet and dry specimens are stretched to the targeted strain with a very high elongation velocity. The initial tension (i.e. the maximum tension either at 1 or 2% strain) and the development of tension are monitored. The residual tension for wet papers is the tension measured 0.475 s after straining is stopped. For dry papers the respective time is 9.5 s.

Because of the need of a special device it would be tempting to use the tensile strength as an indicator for the residual tension. Indeed, residual tension can be determined, at least to some accuracy, through tensile strength. Kouko et al. (2007) noticed a fairly good linear relationship between the residual tension and tensile strength in dry paper, cf. Figure 6. According to the authors, the linear relationship was stronger in dry than wet papers.

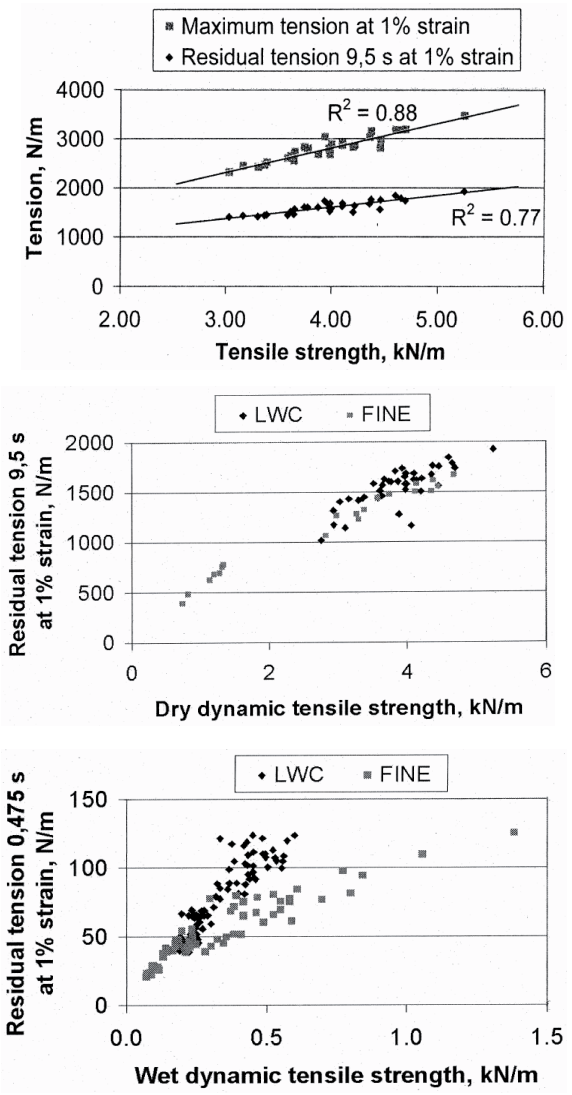

***Figure 6**. Top: Maximum and residual tension in dry hand sheets as a function of dry paper tensile strength (Kouko et al. 2007). Middle: Residual tension of dry LWC and Fine blends as a function of dry tensile strength (Kurki et al. 2004). Bottom: Residual tension of wet LWC and Fine blends as a function of wet tensile strength (Kurki et al. 2004). All the measurements were taken by the Impact device.*

Also the results of Kurki et al. (2004) with LWC and Fine blends suggest that residual tension correlates with tensile strength, although there was a fair amount of variation, see Figure 6. In the case of dry paper, the correlation seemed to be independent of pulp type. Instead, in the case of wet paper, Fine pulps had a lower slope compared with LWC blends when the residual tension was examined as a function of tensile strength.

Under some circumstances, the use of tensile strength as an indication of residual tension may be misleading, cf. the effect of kraft addition into mechanical pulps in Figure 8 (Page 37) or consider the opposite effect of a high straining rate on residual tension and tensile strength, c.f. Pages 21 and 28.

Without going into any detail, it can be speculated that variation in the relationship between the tensile strength and residual tension under different circumstances originates from different types of physical phenomena. Tensile strength testing involves a considerable amount of fibre movement until rupture, but there cannot be a significant amount of mutual fibre movement in residual tension testing.

In any case, the results of Kurki et al. (2004) and Kouko et al. (2007) suggest that the tensile strength can be used as a rough indication of the residual tension when this is done with caution. This underlines the importance of tensile strength as an important runnability parameter.

In conclusion, there are two options for improving wet web runnability: the improvement of wet web strength properties and the mitigation of the effects of external forces affecting the wet web. The key strength properties for wet web runnability in an open draw are tensile strength and elastic modulus. In addition, if sudden and strong disturbances are likely to occur in the open draw, the higher the stretch at break, the better the runnability. As regards to runnability in the first part of the drying section, the higher the residual tension, the better the runnability. The tensile strength can be used to some degree as an indication of the residual tension. The mitigation of the effects of external forces is discussed in Chapter 2.3.4.

Not only are the averages of the web strength properties and external forces important but also their variation. Load-strength interaction is a very important aspect in runnability, and the ways in which the load and strength are distributed affect the probability of breaks. For example, assume that there are two paper webs with the same average strength properties but one has a long weak tail in its tensile strength distribution. It is easy to come to the conclusion that this web is more vulnerable to web breaks. Because the scope in this thesis is paper properties, the variation of the load and load distributions are not covered.

2.2 Failure statistics

2.2.1 The importance of statistical approach

Although taken from printing house runnability studies, the following examples illustrate the importance of controlling strength distributions. Uesaka et al. (2001) showed in their parametric study that, of the paper-related properties, the uniformity of machine direction (MD) tensile strength had the strongest effect on press room break frequency followed by MD elastic strain (tensile strength divided by elastic modulus) and average MD tensile strength. The distribution of tensile strength was described by the two-parameter Weibull distribution. The Weibull shape parameter β (called also Weibull modulus or uniformity parameter) describes the uniformity of the strength distribution. The smaller the value of β, the heavier the weak tail of low strength values and thus the wider the distribution.

Deng et al. (2005) collected break and strength data from both printing houses and paper mills to examine whether there is any relation between routinely measured strength properties, such as MD tensile strength, MD stretch, MD TEA, CD tear and burst and press room breaks. The total number of rolls examined for each press room was between 10,000 and 50,000, and seven press rooms were investigated. The paper grades involved were newsprint, directory and SC. It turned out that tensile strength was most consistent in predicting printing house runnability. Conversely, CD tear strength was not a reliable parameter for web breaks in press rooms. Not only the tensile strength but also its variation, described as the tensile strength uniformity parameter β, proved to be a significant factor in press room runnability.

Figure 7 shows a break rate vs. the strength uniformity parameter β. The uniformity parameter was determined from MD tensile strength measurements performed over a three-year period at a Canadian newsprint mill, between 1998 and 2000. Tensile strength was measured at three locations in the cross machine direction for each jumbo reel. Printing data is from one press room. During the three years, the average tensile strength remained constant but the break rate decreased considerably (from about 12% to less than 5%) when the tensile strength uniformity improved from about 13 to 17.5.

Web breaks on a paper machine are a fairly rare phenomenon. It can be estimated that two to eight breaks occur per day on a typical news machine. If we assume that the speed is 1500 m/min, an average distance between breaks varies from 270 km to 1080 km. If the web width is 8 m, the respective areas are 2.16 km^2 and 8.64 km^2. However, breaks are not evenly distributed as a function of web length and they can be very infrequent events. The statistical approach is therefore very logical. It must be emphasised, that in spite of it being a rare phenomenon, web breaks can cause significant production losses. For example, by assuming the average break duration to be 12 min eight breaks per day results in a production loss of approximately 7%.
.

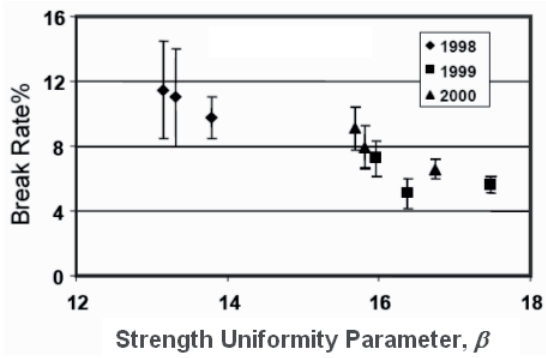

***Figure** 7. Press room break rate vs. tensile strength uniformity. Newsprint. (Deng et al. 2005.)*

2.2.2 Strength distribution in dry paper

In the following, the focus is on the interrelation of the breaking mechanism and strength distribution. Web strength varies across the sheet and along its length as a complicated function of basis weight, furnish, formation, fibre orientation, moisture and other factors. In addition, the local mechanical properties like elastic modulus, strain to failure etc. may vary from point to point and cause the stress and strain fields to be highly non-uniform. The consequence of all this is that failure phenomena obey extreme value statistics, i.e. the fracture of a paper web is controlled by a local minimum value rather than by the average of strength. (Niskanen 1993, Korteoja et al. 1998a.)

Traditionally, Weibull and (modified) Gumbel distributions, based on a "weakest-link" approach, have been widely used to describe the strength of brittle materials (Zapperi and Nukala 2006). According to the micro structural approach of Duxbury et al. (1994), if the size distribution of initial flaws or micro cracks of the specimen is algebraic (described by a power law), the macroscopic strength obeys the Weibull distribution. The physical origin of an algebraic flaw population may be that the flaw population in many materials evolves via nucleation and growth process (Curtin and Scher 1992, Duxbury et al. 1994) or plastic yielding or diffuse damage may alter the shape of the flaw size distribution and thus lead to e.g. Weibull-type strength distribution (Korteoja 1998b). If the flaw size distribution is exponential, the Gumbel (4) or modified Gumbel distribution (3) arises (Duxbury et al. 1994).

Hristopulos and Uesaka (2003) provide a good synthesis for the fracture process of heterogeneous materials like paper: as the tensile stress increases, some of the structural elements, such as bonds and fibres, start failing locally. This causes stress redistribution among intact structural elements. Initially such failed areas are almost randomly distributed throughout the entire system. As the stress continues to increase, the neighbouring failed areas interact and coalesce with each other, creating clusters of damaged areas. These "damage" or critical clusters behave almost as independent

elements. A group containing several critical clusters forms a mesoscopic "link", and the whole material can be viewed as a chain of such links. The final failure is determined in this case by the weakest of the links. According to experimental evidence, the length scale of the links is about 20 mm, and the dimensions of critical clusters are expected to be approximately on the millimetre scale (Hristopulos and Uesaka (2003, 2004).

Based on the discussion above, it is natural to expect that the tensile strength of paper approximately follows the Weibull distribution. Indeed, several studies (Gregersen 1998, Uesaka et al. 2001, Hristopulos and Uesaka 2003, 2004, Wathén and Niskanen 2006) have confirmed this. According to the Weibull statistics, the cumulative failure probability $W(\sigma)$ of a material subjected to a stress σ is given by a three-parameter Equation (2) (Bury 1975, p. 414).

$$W(\sigma) = 1 - \exp\left[-\left(\frac{\sigma - \mu}{\alpha} \right)^{\beta} \right] \tag{2}$$

where $\sigma \geq \mu$

β is the shape parameter, $\beta > 0$

μ is the location parameter, $\mu \geq 0$

α is the scale parameter, $\alpha > 0$

The shape parameter β allows the Weibull distribution to assume a wide variety of shapes. The location parameter μ shifts the values of α, median and mode of the distribution, but it does not change the shape of the distribution function. On the other hand, μ denotes a threshold stress below which no failure will occur. If the location parameter μ is set to zero, the two-parameter Weibull model arises.

Wathén et al. (2006) compared the two and three-parameter Weibull distributions and modified Gumbel (3) distribution. They employed the KCL AHMA pilot-scale strength testing machine for running paper webs (Niskanen et al. 2003). All together, 60 25-cm-wide LWC and fine paper rolls (30 trial points) were tested with the number of breaks varying from 52 to 148 per roll. The paper was made on a hybrid pilot paper machine with different fibre mixes, refining degrees and basis weights.

When the three distributions were fit to the 60 experimental distributions, the best fit was generally given by the two-parameter Weibull distribution, which failed only once in the χ^2 test. The other two distributions had more no-fit cases. At smaller shape parameter values, below 20, only the two-parameter Weibull distribution gave good fits. The shape parameter varied from 9 to 36, with the higher values indicating better tensile strength uniformity.

The usage of the location parameter μ is well justified because it is impossible to make a paper web with zero strength because such a web would have broken even before leaving a paper machine (Korteoja 1997). However, the results of Gregersen (1998) and Wathén and Niskanen (2006) show that the tensile strength of dry paper

can be described in practice by the two-parameter Weibull distribution where μ is set to zero. This is also supported by the study of Lu et al. (2002) obtained from both numerical simulations and real data. Their results with glass and ceramics showed that as long as sample data is limited in number and the threshold stress μ is not too high, a clear distinction cannot be made between the two and three-parameter Weibull distributions. As such, the flexible two-parameter Weibull distribution is preferred over the three-parameter version. However, the influence of μ becomes more important as β increases.

The cumulative failure probability $G_{\mathrm{mod}}(\sigma)$ for the modified Gumbel distribution is given by Korteoja et al. (1998b):

$$G_{\mathrm{mod}}(\sigma) = 1 - \exp\left\{ - \exp\left[- a\left(\frac{b}{\sigma - \mu} - 1 \right) \right] \right\} \tag{3}$$

where $\sigma > \mu$, $\mu \geq 0$ and $a, b > 0$.

Korteoja et al. (1998b) compared the three-parameter Weibull, Gumbel and modified Gumbel distributions. They measured tensile strength of four paper samples exhibiting a variety of brittle-to-ductile properties (MD and CD samples of copy paper and newsprint). 1005 tensile specimens were measured in each case. The Gumbel distribution failed to fit the data. Statistical comparisons (Kolmogorov-Smirnov and χ^2 tests) of the Weibull and modified Gumbel distributions were inconclusive. However, according to visual observations the modified Gumbel distribution fit better than the Weibull one regardless of ductility of the material. This suggests that tensile strength of paper is governed by exponentially distributed micro cracks. Thus the stress redistribution due to plastic yielding, micro-crack coalescence or crack propagation should have only a minor effect on fracture in quasi-static loading conditions (Korteoja 1997 and Korteoja et al. 1998b).

The Gumbel distribution, also called Type I extreme distribution, is widely used to describe the strength of materials. The cumulative distribution function for the left tailed distribution is (Bury 1975, p. 377):

$$G(\sigma) = 1 - \exp\left[- \exp\left(\frac{\sigma - \mu}{\alpha} \right) \right] \tag{4}$$

where $\mu \geq 0$ and $\alpha > 0$.

In the Gumbel distribution, in contrast to the two and three-parameter Weibull and modified Gumbel distributions, there is a finite probability of failure—even at zero stress—as can be noticed from Equation (4), $G_{min}(\sigma \to 0) > 0$. As such, the Gumbel distribution overestimates the failure probability at low stress levels, which are far from the median stress level. However, near its median the cumulative failure

distribution usually approaches either the Weibull or Gumbel form (Duxbury et al. 1994).

To conclude, although the two-parameter Weibull distribution has proved to be a suitable model to describe the strength distribution of paper, it is not unambiguously clear that it always provides the best fit to the strength data at hand.

2.2.3 Weak-link scaling

An interesting aspect related to the tensile strength distribution is the size effect (Duxbury et al. 1994, Curtin 1998, Hristopulos and Uesaka 2003, 2004, Kulachenko et al. 2009). The average tensile strength of larger paper samples is usually lower than that of smaller ones. For example, a long test specimen shows smaller tensile strength than a short one. This behaviour is known, in a more general term, as "strength scaling" or "weak-link scaling". The size effect in tensile strength and the statistical distribution of tensile strength are intimately related. For example, a material that can be described by the two-parameter Weibull distribution should exhibit an algebraic size effect, and a material described by the Gumbel or modified Gumbel distribution should exhibit a logarithmic size effect. Conversely, a material with the Gaussian distribution should exhibit no size effect at all. (Duxbury et al. 1994.)

2.3 Phenomena affecting the strength and runnability of a wet web

2.3.1 The effect of furnish properties

The effect of kraft and mechanical pulp type

Although the addition of kraft to mechanical pulp furnishes increases dry strength properties, this is not the case with wet strength properties of strong mechanical pulps (Jantunen 1985, Kouko et al. 2006b). As an example, Figure 8 shows that at constant DSC the addition of kraft improves neither wet tensile strength nor elastic modulus of strong PGW2 and TMP when the beating degree of chemical pulp is kept at a practical level. Only weak PGW1 benefits from kraft addition. Kraft dosage has a clear negative effect on the residual tension of strong TMP and PGW2 and basically no influence on weak PGW1.

Comparison of the wet tensile strength and residual tension of 100% PGW1, PGW2 and TMP shows the relative differences between the pulps to be very close, irrespective of whether the comparison is made using tensile strength or residual tension. However, the response to the addition and beating of kraft is not alike, see Figure 8. This means that the wet tensile strength can be used only as a rough indicator for the wet residual tension.

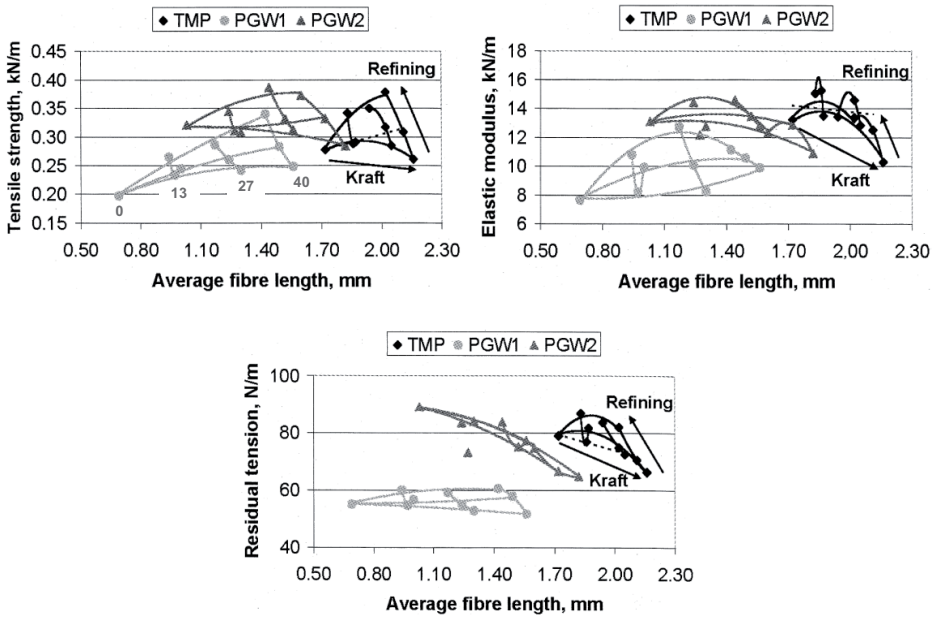

Figure 8. *The effect of kraft addition on mechanical pulps. DSC 40%. Kraft dosage 0, 13, 27 and 40% and CSF levels 680, 605 and 315 ml. PGW2 is an SC pulp type with CSF, fines content, length weighted fibre length and tensile index of 34 ml, 33.8%, 1.00 mm and 49.4 Nm/g respectively. The respective figures for LWC-type PGW1 are 58 ml, 37.5%, 0.67 mm and 37.6 Nm/g, and the figures for LWC-type TMP are 75 ml, 25.6%, 1.67 mm and 48 Nm/g. Average fibre length denotes the fibre length of the mix. (Kouko et al. 2006b).*

Jantunen (1985) also noticed clear differences between different types of mechanical pulps. He studied the effect of furnish on tensile stiffness. The comparison of mechanical pulps, TMP, PGW and GW, was carried out at the same CSF level: 90 ml. 12.5% of semi-bleached kraft (SBK), SR 20, was added to each mechanical pulp. The differences between the mixes were widest at a DSC of 35% to 55%. For example, at a DSC of 45% the TMP/SBK mix had approximately 38% and 74% higher tensile stiffness than the PGW/SBK and GW/SBK mixes respectively. These proportional differences between the mixes diminished significantly as DSC increased. As a comparison, at low DSC the tensile stiffness of the plain SBK was markedly below the value of the mixes, while at DSC exceeding 60% it settled above the respective values of the mixes.

Jantunen's (1985) results with GW and SBK are fairly comparable to the PGW1 results. SBK was added to GW at a proportion of 0, 12.5 and 20%. Below a DSC of 60%, the lower SBK content did not improve tensile stiffness at all. Only when the proportion was increased to 20% was an improvement also seen at lower dry solids contents. The increase of the proportion of semi-bleached pine kraft, SR 22, from 5% to 20% in a newsprint furnish had hardly any effect on stress relaxation speed (DSC 40–80%). Interestingly, the stress relaxation was quicker without any kraft in the furnish (the lower the DSC the greater the difference). Where the furnish consisted of

GW (80%) and SBK (20%), beating from SR 13 to SR 22 or SR 41 increased the speed of stress relaxation when DSC was below 65% (the lower the DSC the larger the difference).

Ionides et al. (1977) studied the effect of variations in the kraft pulp content and refining degree on wet tensile strength. The furnish was a mix of unrefined SBK and GW. The DSC rose approximately from 35 to 38% at equivalent wet pressing conditions when the proportion of unrefined SBK was increased from 25% to 35%. In addition, the wet tensile strength improved by 25%. The improvement was also clear at constant DSC. It turned out that only slight refining is beneficial to wet tensile strength. When the SBK component was beaten from CSF 700 ml (unrefined) to CSF 610 ml, the DSC decreased approximately from 43% to 41% but the wet tensile index increased by 7% at equal wet pressing conditions. Further refining did not improve wet tensile strength but only reduced DSC.

Regarding to the start-up of a TMP plant at one newsprint mill, Ionides et al. (1977) compared newsprint furnishes consisting either of kraft (24%) and GW (76%) or solely 100% TMP. There was virtually no difference in DSC or maximum wet tensile strength between the two cases at equal wet pressing. However, elastic modulus was better in the 100% TMP furnish. This finding was confirmed as draws reduced in the press section, up to 30%, when TMP was the only component of the furnish. In addition, the wrinkling tendency diminished.

To summarise, the discussion above strongly suggests that the wet strength properties of kraft are worse than those of strong mechanical pulps. Thus, the wet web strength properties of TMP and strong PGW cannot be improved by adding kraft to the furnish. Only when the kraft proportioning increases the DSC of the wet web, the higher kraft proportion is useful.

The effect of fines

Corson and Lobben (1980) extracted fines from bleached pine kraft and mixed them with the unbeaten or beaten fibre fraction. The primary and secondary fines significantly improved the wet tensile index of the beaten and unbeaten fibre fraction, irrespective of whether the comparison was made at constant wet pressing pressure or constant DSC, see Figure 9. However, the secondary fines were more effective than the primary fines when mixed with the unbeaten fibre fraction, especially when they were present in high proportions (15%).

When the fines extracted from spruce TMP, CSF 175 ml, were mixed with different types of TMP fibre fractions, the increase in wet tensile index was generally very small when the comparison was made at fixed wet pressing conditions. The amount of fines in the blends extended up to approximately 38%. When the comparison was made at a constant DSC, the increased quantities of fines made a significant positive contribution to the development of the wet tensile index of all fibre fractions. (Corson and Lobben 1980.)

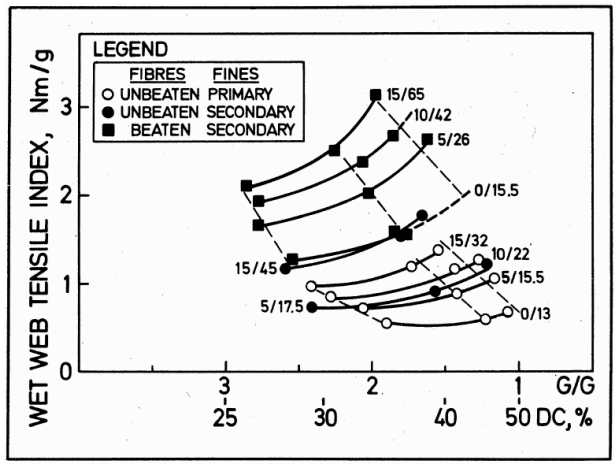

Figure 9. *Wet tensile index of the blends of the fines and fibre fraction. Bleached pine kraft. The numbers refer to the fines percentage/SR number of the blend. The dashed lines link points of equal pressing conditions. (Corson and Lobben 1980.)*

Retulainen and Salminen (2009) studied the effect of fines on the long fibre fraction of bleached softwood kraft, beaten to SR° 25, and TMP, CSF 45 ml. The long fibre fractions used in the tests were Bauer McNett +25 and fines fractions Bauer McNett -200. Kraft fines for the tests were separated from the pulp beaten to SR° 75. Table 2 shows that the TMP fines were fairly ineffective in improving strength properties of the long fraction of TMP. Conversely, the kraft fines significantly improved the wet tensile strength of the TMP and kraft fibres. In addition, the original difference between the long fibre fractions remained approximately the same. Interestingly, the long fibre fraction of TMP experienced much stronger improvement in residual tension than the kraft fibres. The effect is even clearer at a constant DSC of 50%.

Table 2. *The effect of fines (Bauer McNett -200) addition on the long fibre fraction (Bauer McNett +25) of bleached soft wood kraft (SR° 25) and TMP (CSF 45 ml). Data is extracted from the figures of the reference of Retulainen and Salminen (2009).*

Fines addition	Constant wet pressing, 350 kPa				DSC 50%	
	Wet tensile index, Nm/g		Wet residual tension, N/m		Wet residual tension, N/m	
	TMP fibres	Kraft fibres	TMP fibres	Kraft fibres	TMP fibres	Kraft fibres
No fines added	1.5	4.9	31	46	10	32
10% TMP fines	2.3	-	52	-	-	-
20% TMP fines	2.9	-	68	-	43	-
10% kraft fines	8.4	13.4	110	81	-	-
20% kraft fines	12.9	16.5	134	87	114	66

Tanaka et al. (2009) studied the effect of TMP fines on wet web strength properties. They fractionated two pulps in a pilot scale, one TMP and one kraft pulp, both having high long fibre content. The pulps are marked "TMP (fines removed)" and "Kraft (fines removed)" in Figure 10. The third tested pulp, marked as "Kraft (fines removed) + TMP fines" was made by adding fines from the TMP fractionation to the fractioned kraft with the aim being the same fines content as in the original TMP. The fourth tested pulp was the original TMP. Papers were made on a pilot Fourdrinier and wet strength properties were measured by means of the wet web winder, installed on the press section of the pilot paper machine, see Figure 62 (Page 130). The linear loads on the press section were kept constant.

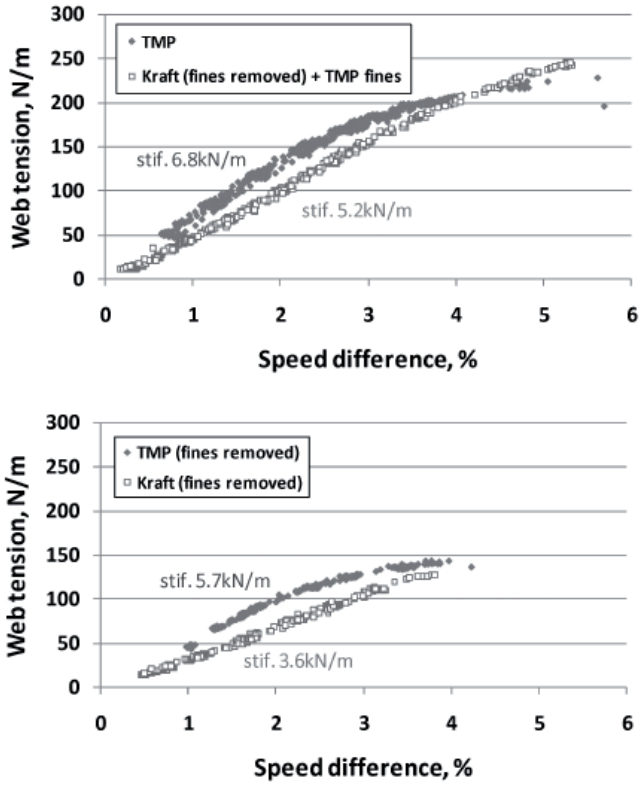

Figure 10. *Relationship between wet draw and web tension (i.e. tensile strength) on a pilot paper machine (wet web winder). The top figure refers to furnish with TMP fines, the bottom figure to furnishes from which fines have been removed. (Tanaka et al. 2009.)*

Again the effect of fines was remarkable, and as in Table 2, the wet tensile strength of TMP and kraft fibres improved similarly due to the addition of fines. Interestingly, the stiffness of the fibres seems to have an influence on the wet tensile stiffness although not on the tensile strength, as Figure 10 shows. This assumption gets support from the modelling work of Miettinen et al. (2007b) and Miettinen and Ketoja (2008). According to their results, the fibre network tensile strength is unaffected by the fibre

stiffness although the network stiffness increases with increasing fibre stiffness. Furthermore, Kulachenko's modelling work (2008) showed that the fibre elastic modulus does not affect the tensile strength of a wet fibre network when the elastic modulus is varied within a reasonable range.

To conclude, the fines have a significant influence on the tensile strength, residual tension and stiffness of a wet web. The better the bonding ability of the fines, the stronger the effect. It is very likely that, compared with (good-quality) mechanical pulps, the inferior performance of chemical pulps and fine papers—especially regarding residual tension (e.g. see Figure 8)—originates from a significantly lower fines content.

2.3.2 Bonding mechanism in wet webs

Campbell (1933) suggested that wet paper was held together by capillary forces arising from an attractive capillary pressure in liquid bridges between fibres. Page (1993) extended this idea and presented that the wet web tensile strength can be considered in terms of the frictional shear strength of the fibre-fibre crossings that are pulled into contact by the surface tension forces in the water menisci. He derived the following expression for the tensile strength of wet paper:

$$T = \frac{\mu\gamma PLRBA}{12Cr_c} \tag{5}$$

where μ is the coefficient of friction
γ is the surface tension of water
P is the fibre perimeter of the average fibre cross-section
L is the fibre length
RBA is the relative bonded area in the sheet but means in this context of the proportion of the fibre surface that is contained within a water meniscus holding adjacent fibres together
C is the fibre coarseness
r_c is the radius of curvature of the water meniscus.

Shallhorn (2002) modified Page's theory by taking into account the effect of wet pressing on fibre thickness and relative bonded area. His results suggest that surface tension forces are responsible for wet web tensile properties over a wide range of moisture contents corresponding to dry solids contents ~ 20–60%. The model he used is limited to the fibre fraction of softwood kraft. As such, no fines were involved. In any case, there was good conformity with the predicted and measured tensile strength values for unbeaten black spruce kraft as a function of moisture content.

In contrast to Shallhorn's findings, theoretical and experimental work carried out by Alince et al. (2006), de Oliveira et al. (2008), van de Ven (2008) and Tejado and van de Ven (2009a, 2009b, 2009c) suggest that, in dry solids contents typical to the open draw from the press to the drying section and in the beginning of the drying section, capillary forces cannot be a major contributor to the wet strength. Figure 11 illustrates

this matter. Van de Ven (2008) showed that when two wet paper sheets are pressed gently together and dried to various solids contents, the friction force between the sheets could be fairly well described by capillary forces acting between fibres, caused by liquid bridges in fibre crossings. This force can be measured by measuring the force required to slide the sheets over each other. The friction reaches the maximum value when all the water is located only in isolated liquid bridges at fibre crossings and in the fibre wall. When water is further removed, capillary forces and the friction between the sheets reduce and finally become zero when the volume of water in liquid bridges comes zero, roughly at the FSP, see Figure 11.

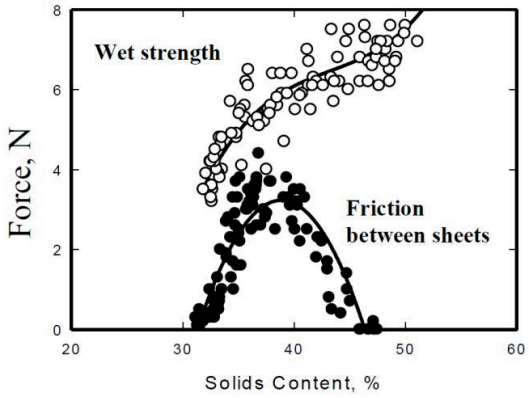

Figure 11. *Tensile strength of wet sheets and friction between wet sheets as a function of DSC (Alince et al. 2006 and de Oliveira et al. 2008).*

However, tensile strength measured from wet sheets increased irrespective of the reduction of capillary forces. In addition, theoretical calculations showed that the predicted maximum wet tensile strength based on capillary forces (all the water located only in isolated liquid bridges at fibre crossings and in the fibre wall) underestimates the wet tensile strength by at least one order of magnitude (van de Ven 2008). There must therefore be other forces present to provide wet tensile strength. It is proposed that entangled elastic fibres generate stress into the fibre crossings in a sheet, causing an entanglement friction that keeps the fibres in the sheet together and provides the wet tensile strength, see Figure 12, (de Oliveira et al. 2008, van de Ven 2008, Tejado and van de Ven 2009a, 2009b, 2009c). Naturally, no entanglements occur between the surfaces of two wet sheets.

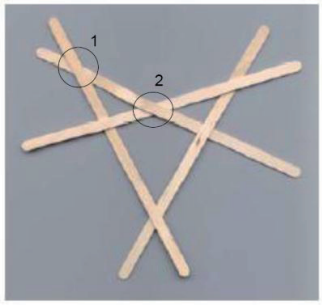

***Figure 12**. An idealised illustration of fibre entanglement: Coherent structure of 4 wooden sticks, kept together by entanglement, in the absence of any attractive force. Elastic force acting on a fibre crossing near the end of a fibre (1) and sandwiched between two crossings (2) (Tejado and van de Ven 2009a).*

Even if a sheet was made from infinitely dilute fibre suspensions in which the fibres are depositing on a forming sheet one by one, entanglements would be expected. Even in this case, entanglements may form by individual fibres settling at an angle upon a mat of fibres and penetrating the web to a certain depth. When such fibres get covered by other fibres, entanglements are likely to occur. The entanglements formed during sheet consolidation are likely to be distributed fairly uniformly throughout the sheet and should therefore strengthen it. (Tejado and van de Ven 2009a.) This type of entanglement needs to be distinguished from fibre entanglement in fibre flocs, which do not strengthen wet paper and are usually already present before the sheet is formed. Increased consistency, fibre flexibility and flexible microfibrils increase the entanglement. In addition, the positive effect of entanglement friction caused by microfibrils becomes more pronounced upon dewatering. (de Oliveira et al. 2008.)

Alince, de Oliveira, Tejado and van de Ven do not provide any detailed explanation for the entanglement friction. However, the mechanism can be conjectured based on the studies of Andersson et al. (2000), Kulachenko (2008), Kulachenko et al. (2008) and Huang et al. (2009). It has been noticed, especially in Atomic Force Microscopy (AFM) measurements, that friction force between fibres is the sum of the coefficient of friction multiplied by normal force and an initial adhesive force that is independent of normal force (Andersson and Rasmuson 1997, Huang et al. 2009). The initial adhesive force is called henceforth the initial tangent adhesive force to emphasise its role in total friction. The initial tangent adhesive force arises due to the contribution of various attractive forces, such as capillary, electrostatic, van der Waals and chemical bonding under different circumstances (Maboudian and Howe 1997).

AFM measurements with TMP fibres showed that increasing fibre surface nanoscale roughness (RMS roughness from 17 nm to 71 nm), caused by refining, had a different kind of effect on the coefficient of friction and initial tangent adhesion force (RH 35-45%, T 20–23°C). The coefficient of friction increased but the initial adhesion force clearly decreased, the reason being a higher separation distance between the surface means. DSC had a strong influence on the coefficient of friction, which grew from 0.07 to 0.58 when DSC increased from 6% to 90%. (Huang et al. 2009.) According to

AFM measurements, the increase of relative humidity (from 20% to 80%) reduced the coefficient of friction but increased the initial tangent adhesive force of TMP fibres and fibre saturation with water further increased the force (Kulachenko 2008).

Andersson et al. (2000) used a contact point method for friction measurements. Their coefficient of friction results for wet (submerged in water) and dry kraft fibres, an average 0.68 and 0.57 respectively, are higher and opposite to the results of Huang et al. (2009). In the results of Andersson et al. (2000), the initial tangent adhesive force was clearly higher for wet fibres. Refining increased the coefficient of friction and reduced the initial adhesive force of dry fibres. Thus the result is congruent with the results of Huang et al. (2009). Conversely, refining did not have any effect on the respective properties of wet fibres.

Kulachenko (2008) and Kulachenko et al. (2008) utilised a fibre network model in clarifying the effects of friction components on wet web strength. The model features a detailed description of fibre-to-fibre interaction, which is based on results of AFM measurements conducted on TMP fibres. The results suggest that the number of contacts and the initial tangent adhesion force have a high impact on wet web tensile strength, even stronger than that of the coefficient of friction. One of the sources of the tangent adhesion is shear resistance of the water meniscus. Fibre elastic modulus had a low impact on tensile strength. The result is congruent with the simulation result of Miettinen et al. (2007b) and Miettinen and Ketoja (2008). This result can be compared to a theoretical speculation of Tejado and van de Ven (2009a), which indicates highly flexible fibres to reduce wet strength. However, more flexible fibres are likely to result in more entanglements and thus more fibre crossings, and consequently to improved wet strength. According to Tejado and van de Ven (2009a), wet web strength increases steeply with the amount of fibre crossings per fibre.

Nanko's and Ohsawa's (1989) experiments with beaten and unbeaten bleached Japanese beech kraft suggest that secondary fines fill the spaces between the fibres and, in addition, they form together with randomly orientated external macro and micro fibrils a more or less continuous bonding layer in the bonding areas between fibres. The macro fibrils lie mostly parallel to the fibre surface and they are not deeply entangled through the bonding zone (Nanko and Ohsawa 1989). Instead, it is likely that microfibrils are freer for entanglement and thus capable of increasing the entanglement friction supporting the results of de Oliveira et al. (2008) related to the effect of microfibrils.

Depending on the morphology, mechanical pulp fines perform different kinds of structural functions in a fibre network (de Silveira et al. 1995, Görres et al. 1996). For example, fines that are small fragments of the primary wall or ribbon-like fragments of the secondary cell wall split off radially and may then deposit on the outside of fibres acting as the "filling" in a "sandwich" and forming bonds between two fibres. It is generally assumed that the width of microfibrils is 4–10 nm. This is close to 20–30 nm, the width of TMP fibrils after the second reject refining stage (evaluated from the FE-SEM image in Kangas 2007, p. 56). Based on the results of de Oliveira et al. (2008) and Huang et al. (2009), these fines, when "sandwiched" between fibres, should increase the entanglement friction.

Fines that are portions of fibres split axially from the fibre wall appear to be filling interstices and bridging gaps in the fibre network. Consequently, in wet pressing this shortens the required deflection distance between fibres to constitute additional fibre contacts. Without the bridging fines, the deflection distance would be too great for fibre contacts to be generated. (de Silveira et al. 1995, Görres et al. 1996). This would lead to a weaker wet web as discussed above.

By taking FSP values 1.47 and 0.99 (Table 3 in Appendix 1) for unbeaten chemical pulp and TMP respectively, we obtain the respective DSC values of 40% and 50%. Based on the entanglement friction theory, this suggests that capillary forces could only have a minimal influence, if any, on wet web strength in the open draw after the press section and in the first part of the drying section. Thus the friction force, the coefficient of friction multiplied by the normal force originating from the elasticity of the fibre network, would be the major factor for wet tensile strength. In addition, the initial tangent adhesion, originating from van der Waals force, contributes to the wet tensile strength.

However, it is likely that wet pressing removes water unevenly from the fibre network. This may leave at least some water menisci in the fibre/fibre and fibre/fines contacts contributing to the initial tangent adhesion. Especially in the case of mechanical pulps, there must be plenty of water menisci in the fibre contacts. This can be deducted from the aforementioned DSC value 50%. In addition, if the coefficient of friction for wet fibres is really as low as that measured by Huang et al. (2009), an inevitable question arises as to whether the normal force originating from the elastic fibre network is strong enough to provide the required friction force. If not, the initial tangent adhesion originating from the shear resistance of water menisci could have a stronger role than expected based on the work of Alince et al. (2006), de Oliveira et al. (2008), van de Ven (2008) and Tejado and van de Ven (2009a, 2009b, 2009c).

To conclude, the bonding mechanism in dry solids contents typical to the open draw after the press section and in the first part of the drying section is not fully understood. However, the entanglement friction has an important role in wet strength with the friction force and initial tangent adhesion force acting on the fibre contacts. It is likely that nanoscale surface roughness on the fibre contact areas increases the coefficient of friction but simultaneously reduces the initial tangent adhesion, irrespective of the working mechanism: van der Waals force or shear resistance caused by water menisci on fibre contact points.

2.3.3 The effect of web structure

Paper is a disordered and essentially layered structure that consists of fibres of varying lengths (up to a few millimetres), fibre fragments, fines and various inorganic fillers. In addition, paper structure is anisotropic due to the preferential alignment of fibres along a principal direction. However, there are local variations around the alignment axis caused by the paper-forming process involving fibre flocculation and turbulence. For the same reason, the basis weight varies locally. In addition, circumstances on the wire section have an effect on the z-direction distribution.

Consequently, spatial variation exists in paper structural parameters. (Deng and Dodson 1994, Niskanen and Pakarinen 2008.) Of these, formation and local fibre orientation are probably the most important structural characteristics what can be expected to have an influence on the strength and strength uniformity of a wet web. This is based on the following deduction: generally, it can be assumed that the greater the extent of fibre-fibre interaction in a wet web, the longer the failure is postponed so that both the stress and strain at which failure occur are higher. However, the fibre-fibre interaction is not evenly distributed in the fibre network as discussed above. Instead, the structural disorder of the fibre network affects the number of contacts per fibre, the area of regions of contact and the spatial distribution of inter-fibre contacts. If the contacts are not evenly distributed throughout the whole network, the distribution of stresses and strains and therefore strength varies locally within a sheet during loading.

This deduction gets support from the analytical studies of Seth et al. (1984), Page (1993), Seth (1995) and Tejado and van de Ven (2009a) and computer simulations of Miettinen et al. (2007a, 2007b), Kulachenko et al. (2008) and Lindström et al. (2009) with wet fibre networks. Their results show that wet strength depends strongly on the extent of fibre-fibre interaction or number of inter-fibre contacts. Thus, if formation and local fibre orientation have an effect on the distribution of inter-fibre contacts, they should also affect the strength uniformity of the wet fibre network. However, when considering the influence of formation, it is worth keeping in mind that it is not unambiguously related to paper strength. The effect of formation on paper strength depends on the type of changes in paper making conditions used to generate the changes in formation (Norman 1989, Norman and Söderberg 2001).

In addition, local fibre orientation and local grammage variation are partly interrelated. This was investigated by Hasuike et al. (1987), who produced softwood kraft paper sheets with a basis weight of 60 g/m² using different forming units on STFI's pilot paper machine. The forming units studied were blade former (pulsating dewatering pressure), roll former (constant dewatering pressure) and Fourdrinier. Both local orientation and grammage variation were measured from 1x1 mm² fields by soft x-ray micro radiography. The local anisotropy ratio of MD to CD varied widely in the sheet. In spite of that, a tendency for the degree of the local anisotropy ratio of MD to CD to be higher in the lower grammage regions was found. The tendency was more pronounced in highly orientated sheets. The arrangement of fibres in high grammage regions was more random than that in low grammage regions.

Comparison of the local major/minor axis ratio (a measure of local alignment of fibres irrespective of their average orientation angle) with the local MD/CD ratio showed that, in the sheets formed with a low headbox consistency of 4 g/l (better formation), the difference between the ratios was small. This indicates alignment of local orientation with the MD. This was valid for both the roll and blade former. However, in the sheets formed with a higher headbox consistency of 10 g/l (poorer formation), larger deviations of the local orientation from the MD were observed. In the roll former, however, the tendency was that the low grammage spots were clearly more aligned with the MD than the higher grammage spots. In the blade former paper of poorer formation, the major/minor ratio was much greater than the MD/CD ratio, indicating more spread in the orientation angle even in low grammage spots, see

Figure 13. The sheets made by the Fourdrinier former had characteristics of an anisotropic structure similar to that of the roll former sheets. (Hasuike et al. 1987.)

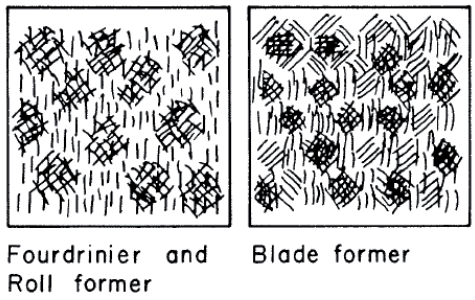

Figure 13. *Illustration of the principal anisotropic structure for the sheets made by roll former, Fourdrinier and blade former (Hasuike et al. 1987).*

Although the results above show local grammage and local fibre orientation (anisotropy and misalignment angel) to be related to some degree, Bernard and Charlebois (1991) did not find any correlation between local grammage and local anisotropy or local fibre alignment when measuring photocopier paper. This was also the case with Praast and Göttsching (1997), who did not find any significant correlation between formation and anisotropy of fibres or flocs and between formation and fibre or floc alignment. Correlation between the anisotropy of flocs and the equivalent property of fibres was poor. However, the correlation between floc and fibre alignment was better. The floc orientation measurements were based on the power spectrum determined from light transmission images of 100x100 mm² taken at 100 mm intervals across the web. Bernard and Charlebois (1991) utilised a far-infrared laser technique with the spatial resolution varying from 1 mm to 5 mm.

There seems to be a discrepancy between the results of Hasuike et al. and those of Bernard et al. and Praast et al. However, Hasuike et al. searched for a possible correlation between formation and local orientation separately for flocs and voids, whereas the others searched for the correlation for the whole sheet. The results can be summarised to state that, although the local fibre orientation and formation are interrelated to some degree, they can be measured and treated as separate entities. However, in practice it seems that inside one paper machine type it is not easy to control local fibre orientation and formation separately if the alteration is made only with headbox consistency, jet-wire-ratio and wire section control parameters.

Because formation and local fibre orientation were considered to be important parameters affecting wet web strength, a literature survey was carried out with the aim of clarifying how the wet web structure deforms when loaded and the effect of the aforementioned parameters on wet strength properties. However, the literature related to the topic is very scarce.

How does the wet web deform under loading and what is the role of formation and fibre orientation?

Seth et al. (1984) studied the effect of formation with laboratory sheets made of unbleached never-dried softwood kraft, yield 45%. The forming consistency was kept constant but the drainage time was varied from 4.4 s to 30.5 s by changing the orifice of the drain on the sheet machine. No formation figures were provided. At constant DSC, the alteration of formation did not affect the wet tensile strength and the reduction in wet strain was only marginal. The DSC range studied was 15–53%.

Kulachenko et al. (2009) studied the strength behaviour of wet fibre networks by fibre level network simulations. The fibre networks for the strength simulations were prepared by simulating the web produced on a twin-wire former (Lindström and Uesaka 2008) from furnish consisting of 50% fines-free TMP and 50% kraft pulp. The mean dry basis weight was 41 g/m². The size of the simulation box was 6.5x5 mm² and the length and the width of the test specimens cut from the simulation box varied from 2.5 mm to 6.5 mm and from 1 mm to 5 mm respectively. The same normal and tangent adhesion was assigned for all the fibre pairs, meaning that the variation in the system was solely introduced by geometry (disordered structures).

Deformation of the wet network was found to be driven by continuous stick-slip behaviour at the fibre level. The same phenomenon is also visible in the results of Miettinen et al. (2007b). Figure 14 illustrates the evolution of damages and the corresponding stress-strain curve of network A. The fibre-fibre contacts are visualised by small dots in the coloured contact status plots B to D. Because some of the fibres may have many contacts along the fibre length (especially long kraft fibres) and all the contacts are shown, it looks like there was a sparse fibre network in plots B to D.

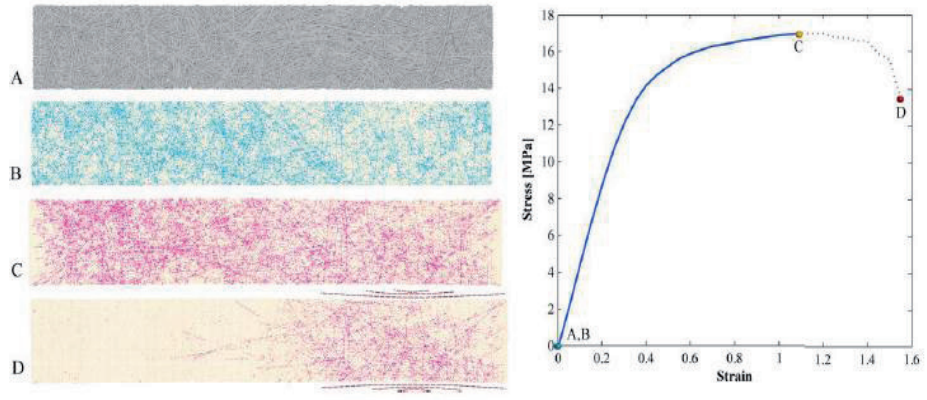

***Figure 14**. Evolution of damage (specimen size 5 mm x 1 mm) in wet paper (Kulachenko et al. 2009).*

Originally, all the fibre contacts are in the sticking state as shown by the blue dots in plot B. The plot shows that the contact concentration is not even; there are areas with lower and higher contact concentration density. At point C in the stress-strain curve,

most of the contacts are in the slipping state as shown by the red in plot C. The entire network is engaged in the deformation and the load is shared between most of the contacts. At the failure point D, however, the number of slipping contacts decreases, since the damage is localised near the weakest area of the sheet, which is usually the one with lowest concentration of contacts, and necking develops. Based on the results of Kulachenko et al. (2009), the length of the localisation area seems to be 2–2.5mm.

Also, Miettinen et al. (2007a, 2007b) employed fibre level network simulations when they studied the tensile strength behaviour of thin (16 g/m²), isotropic, wet and fines-free fibre networks. The simulated area was 2 L_{MD} x 2 L_{CD} where L denotes fibre length. The results suggest that the fibre network deforms evenly and the number of fibre contacts changes by only a very small amount when stretched to the maximum tensile strength value. These results are consistent with the findings of Kulachenko et al. (2009).

In addition, the results of Miettinen et al. (2007a) suggest that the stronger the fibre orientation anisotropy, the smaller the number of inter-fibre contacts. However, the effect is insignificant for networks of practical interest.

In contrast to the above described results, the study of Lappalainen and Kouko (2011) suggests the deformation to be unevenly distributed in the wet specimen, at least close to the rupture point. The researchers used a digital image correlation method to determine local strains in 180 mm long and 20 mm wide paper strips during a tensile test. The grammage of never dried LWC base paper from a pilot paper machine was 38 g/m² and the dry solids content ranged from 50 to 70%. The studied area was located in the middle of the strips. Figure 15 shows an example of the local strains close to the rupture point and the original location of the markers used to determine the local strains.

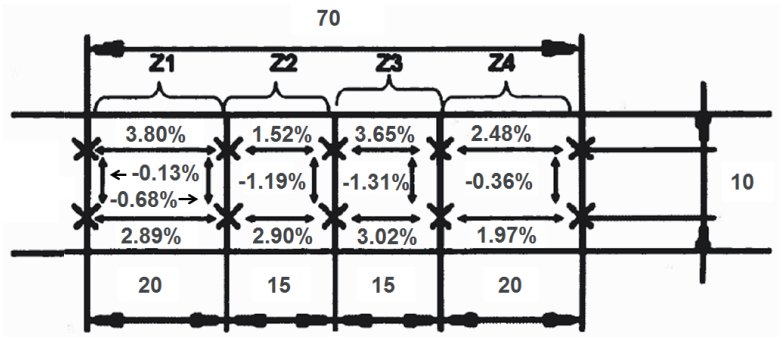

Figure 15. *An example of the results. The original positions of the markers (distances as millimetres) and the measured local strains and shrinkages. Strain at break was 2.4%. Never dried LWC base paper, basis weight 38 g/m², measurement in MD. Straining speed 10 mm/s. The fracture started from zone Z2. Redrawn from Lappalainen and Kouko (2011).*

In the MD specimens, the ratio between the maximum local strain and the strain at break was on average 1.35. Typically, the fracture started from the zone with the largest or second largest difference between the strain values.

The simulation results of Kulachenko and Uesaka (2012) suggests the strain field to develop as a form of shear bands. They used a finite element model for 3D random orientated fibre network to study the deformation and failure behaviour of wet fibre networks. Figure 16 demonstrates the accumulated strain field at different phases along the stress-strain curve. In the linear region, point A, there is no clear sign of strain localization. Instead, the strain field shows a presence of distinct shear bands (a non-uniform "criss-cross" pattern). At the point of the maximum stress, point B, the development of localisation is already apparent as seen in the presence of some nucleation. However, the propagation zone is not yet formed. It is only at the point C (point D in Figure 14), when there exists a clear localization of failure across the network and most of the slippage between fibres occurs in this region. The width of localization approximately equals the length of the fibre.

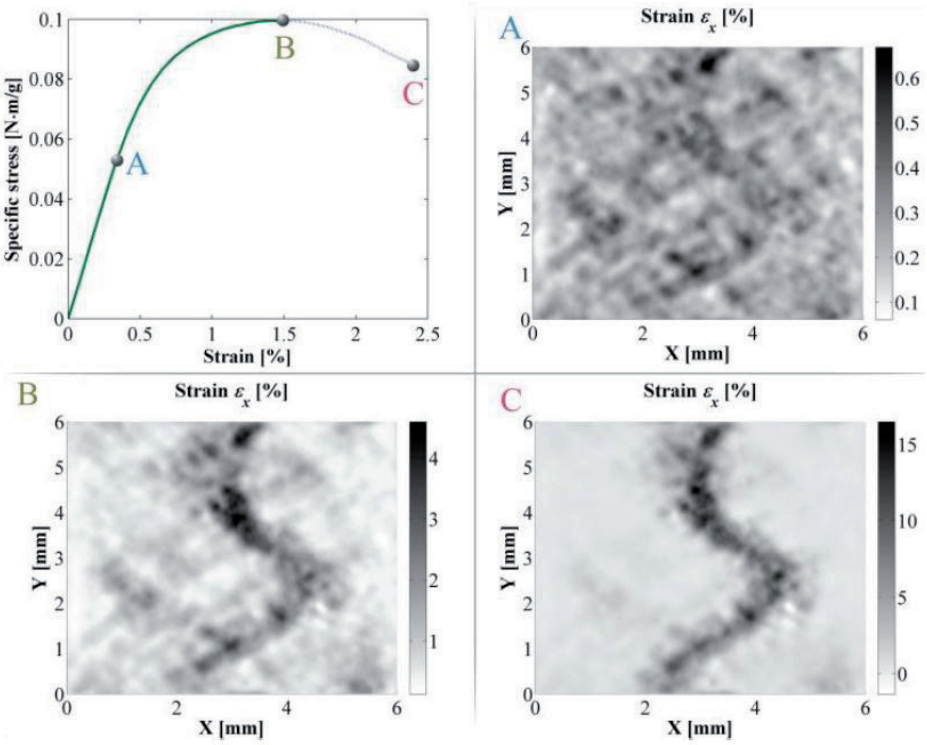

***Figure 16**. Evolution of damage in a wet fibre network. Fibre length 0.8 mm, no fines. The size of the network 6 mm x 6 mm. (Kulachenko and Uesaka 2012.)*

Generally, localised deformation patterns are experimentally observed in many ductile materials (such as metal, alloy, granular material and plastic) as a precursor to rupture. When deformed sufficiently into the plastic range, deformation occurs highly localised in the form of a shear band. (Rice 1976, Corso 2009.) In addition, dry paper may also exhibit shear band behaviour. At least Ranger and Hopkins (1962) found plastic deformations to concentrate along lines that traverse across the paper specimen at a 30°–40° angle to the external stress. Korteoja et al. (1996) reported that

in CD newsprint and CD virgin pine kraft linerboard specimens, small "lines" and then patterns of lines began to become apparent with the onset of nonlinearity in the measured stress-strain curves, became profuse as strain increased toward failure, and eventually formed distinct diagonal patterns. Interestingly, in both reports the lines were too indistinct to measure or were missing when MD samples were used. Instead, a MD specimen of sack kraft, when weakened by wetting, tended to fracture along a diagonal line by shear (Ranger and Hopkins 1962).

Yang and Thorpe (1977) studied the strain behaviour of wet (solids content 12–15%) isotropic specimens consisting of bleached softwood kraft. They employed both finite element simulations and experimental analysis. The total area, analysed and simulated, was 20 x 16 mm² (length x width) and consisted of 1 mm^2 squares. Local basis weight variation was measured from β-radiographs, which were established from freeze-dried samples. Straining from 0% to 8% at increments of 2% resulted in a linear reduction in the average basis weight. According to the results, wet specimens seemed to elongate fairly evenly as a whole until at some straining level elongation seemed to be concentrated in areas of initial low basis weight. However, these areas were not only individual formation scale voids but large entities. These initial low grammage areas became single selective zones of straining accompanied by a rapid decrease in basis weight.

Thorpe and Young (1979) continued their finite element analysis with wet groundwood newsprint (DSC 24%). Local basis weight variation was not substantially increased by straining to 5%. In contrast to the sizeable increases in basis weight variation found in straining the kraft softwood specimens, only small variations in basis weight were observed. The writers suggest that the differences between chemical and groundwood pulps in length and flexibility probably account for the different results. Short, stiff GW fibres or fibre pieces would be expected to strain more uniformly than the longer, perhaps mechanically entangled, chemical fibres.

Thorpe and Young (1979) also studied the effect of formation on wet straining. The simulated samples were again groundwood newsprint (DSC 24%). According to their results, even a substantial improvement in formation, from a level of 3.9–4.7 g/m² to 2.6 g/m², did not appear to yield much gain in the ability of the wet web to withstand straining. Breaking strain of the specimen would have increased from approx. 5% to approx. 6% only.

Effect of formation on the fracture phenomenon of dry paper

To gain more perspective on the effect of formation on the fracture mechanism of wet paper, a literature survey was carried out with the aim of clarifying the same issue in dry paper.

Wong et al. (1996) studied the effect of formation scale basis weight variation on local strain fields. Formation was measured using β-radiography. The strain fields in uncalendered handsheet specimens subjected to uniaxial tension were measured experimentally using video image correlation and were also simulated using a finite element method (FEM) with the plate elements in the model being 1 mm² in area.

Handsheets with a nominal grammage of 60 g/m² were made of beaten unbleached kraft. The width of the specimen was 2 cm and the gauge length was 5 cm. Local displacements were measured every mm in MD and CD. The results showed that local grammage and local strain were inversely proportional, although the degree of correlation was not strong. Thus there have been other additional factors contributing to the local strain. For example, the local fibre orientation distribution is most likely an influential factor. In addition, it is known that local strain is affected not only by the condition at the point itself, but also by surrounding regions. A low-grammage region with high-grammage regions next to it in the direction perpendicular to the load could be shielded from the load. Conversely, high-grammage regions sandwiching a low grammage region in the direction of the load may magnify the local deformation of the thinner region (Thorpe 1981, Kimura and Shimizu 1985, Wong et al. 1996).

In any case, the fracture always initiated from a region of high local strain and the initiation zone followed the low-grammage/high-strain contour quite well. After the fracture initiation, the fracture line tended to run perpendicular to the direction of applied strain, regardless of local grammage variation.

Moffat et al. (1976) performed tensile tests with 15 mm wide uncalendered newsprint specimens and found failure lines largely passing through areas of below average grammage.

The studies of Korteoja et al. (1996, 1997, 1998c) provide more support to the interdependence of formation and the rupture process. They studied the effect of formation-like non-uniformity on the strength properties and the rupture process of paper. They employed both computer simulations based on the elastic-plastic continuum mechanical model (1997) and saturation of paper specimens with silicone (1996, 1998c). The silicone treatment makes the emerging fracture lines and patterns visible due to increasing local reflectance caused by micro-failures. The evolution of local damage and strains were measured simultaneously and changes in the latter were determined by the digital image correlation system (1998c). The size of the measurement area in the middle section of the specimens was 20 mm x 40 mm. The grammage distribution of unstrained specimens was measured from β-radiographs.

The findings can be summarised as follows. Paper formation affects the way external elongation is distributed through paper specimens into local strains. The local strain variations in turn control the accumulation of local damage and the ultimate failure of the specimen. The low grammage points clearly accumulate more strain and damage than the high grammage points. "Poor" formation emphasises this tendency; strains and damage localise in the low grammage areas more than they would if formation was "good". The final rupture path seems to go through the areas that have the highest damage levels prior to rupture. This all means that the variation of tensile strength is attributed to the variation in local breaking strains, not the variation of local strengths, and the higher the variation in local strains the lower the tensile strength. (Korteoja et al. 1996, 1997, 1998c.)

Hristopulos and Uesaka (2003) showed that formation on the length scale smaller than a few mm, comparable to the size of critical or "damage" clusters (cf., Chapter

2.2.2), has an effect on the tensile strength distribution. Conversely, the grammage variation on length scales higher than a few millimetres was shown to have a minor effect only.

Conclusions

The results above and discussion in Chapter 2.2.2 strongly support the following rupture concept for dry papers under external straining. The damage accumulates in low grammage points throughout the whole specimen or paper web but the final rupture process always starts from a single weak spot and then propagates through the areas that have the highest damage levels prior to rupture. Formation is therefore an important structural parameter affecting the strength properties, tensile strength and breaking strain of dry paper webs. For example, the simulations (Korteoja et al. 1996) suggest that, in all paper grades, plastic deformations take place in less than a quarter of the paper area when paper is loaded. Increased formation-type disorder reduces this fraction. Naturally this means increased local strain variation and reduced tensile strength of the paper.

The research reviewed suggests that the rupture mechanism for wet papers differs from that of dry papers. In wet papers, most of the fibre contacts slip during straining, although not at the same rate due to the development of shear bands. Deformation localises more to those bands and finally, after the maximum stress, a failure path forms across the specimen or paper web and most of the slippage of fibres concentrates in this region.

In dry papers, the crucial formation length scale related to paper strength seems to be smaller than a few millimetres (i.e. micro scale in Table 1). Clearly this is not the case for wet papers. However, because the size of modelled and measured wet specimens was small, it cannot be concluded whether basis weight variation on a larger length scale would have an influence on wet strength properties. For example, assume that paper with very poor formation is produced on a Fourdrinier. It is likely that there are a substantial number of large thin spots in that paper with the diameter of the spots being possibly 1 cm or more. Inevitably, the question arises as to whether this kind of paper could show any weak-link behaviour.

2.3.4 Effect of machinery — means to improve runnability

A powerful means to improve wet web strength is to increase its solids content (Pye et al. 1985, McDonald et al. 1988 and Lange 1996), see Figure 17. This can be achieved either by improving wet web dewatering properties or by intensifying wet pressing. This review concentrates on the improvement in runnability that can be achieved using machinery. In recent years, a four-roll, three-nip press section with a separate fourth press has been a very popular concept for fast printing and writing paper making machines. The fourth press was introduced to improve paper two-sidedness and after-press solids content. However, in dry solids content gains are small, 1–2 percentage units (Ilvespää 1998). Also, an extra open draw compared with the three-nip press section increases a risk of runnability problems.

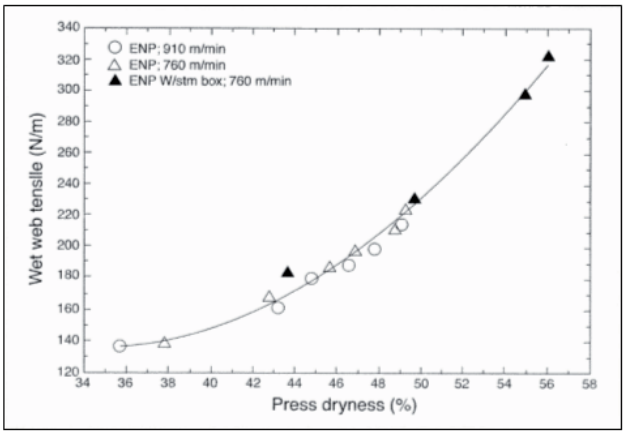

Figure 17*. Wet web tensile strength vs. solids content in pressing (newsprint 49 g/m²) (Lange 1996).*

Dwell time is more significant for solids content than peak pressure. As such, a higher dewatering capacity is achieved mainly with longer nip dwell times. As a comparison, nip dwell times in conventional roll nips are typically 1–2 ms and in shoe presses between 6 ms and 10 ms. (Ilvespää 1996.) This explains the higher post-press dryness. For example, when comparing the standard four-roll, three-nip press section with the same type of press section with a shoe press in the third nip, a 4–10 percentage unit increase in solids content (depending on the paper grade) together with increased running speed has been reported (Ilvespää 1998).

The most effective way to improve wet web runnability is to replace open draws with what is known as a closed transfer. In that arrangement, a supported wet web is at first transferred to come into contact with a new supporting surface, for example a drying fabric. At the contact point, the wet web is released from the previous surface and attached to the new one by vacuum. Although some web stretching is also still required in the closed web transfer (Lauterbach 1990, Adams 1991), this type of arrangement reduces web tension dramatically, enabling a high running speed. Modern press configurations with closed web transfer from the press section to the drying section have moved the breaking occurrence to the first drying cylinder. The reason is that wet paper tends to follow the drying cylinder rather than the dryer fabric supporting the web, see Figure 4 (Page 28). This tendency is increased if no draw is applied between the press and the dryer section to create web tension (Mayer 2002, Ilvespää et al. 2003). Machine suppliers have improved runnability in this critical area as well in the first groups of the drying section by providing runnability components to ease web release from the cylinder surface and to keep the web better attached to the supporting drying fabric (Mayer 2002, Ilvespää et al. 2003, Juppi 2006, and Kurki et al. 2010).

The development of paper machine technology has at the same time increased paper machine runnability and speed. For example, it can be seen from the reference (Kurki et al. 2004) that the operating speed of the best news, SC, LWC and fine paper

machines increased by approximately 45% between 1988 and 2001. It seems that whatever the machine configuration of the new or rebuilt machines is, the general tendency seems to favour speeding up the machine to the limit that can be withstood by the wet paper. Furthermore, when it is considered that there are only a few paper machines up to now running without an open draw from the press to the drying section (Paulapuro 2008), and also the high costs of machine rebuilds, the importance of improving wet web strength is evident.

3 METHODOLOGY

Because the research of wet web strength properties is mainly based on re-wetted paper webs in this thesis, the possibility of whether fibre hornification or possible hornification in a paper structure could violate the comparison and study of the wet web strength properties based on re-wetted paper webs will be discussed. The correspondence between the wet strength properties measured from the re-wetted webs in the runnability device utilised in this thesis and the wet strength properties measured directly on a paper machine will also be discussed. The trial papers will also be introduced. Finally, the development of the re-wetting procedure as well as the analysis procedure for the measured data from the runnability device will be discussed.

3.1 What is the congruence between the web taken from the press section and the re-wetted web?

Although the aim of re-wetting is to restore the dry web to the state after the press section, it is clear that this target cannot be met in full. The reason for this is that, on re-wetting, the dried pulp—especially low-yield pulp—absorbs less water than before drying due to reduced fibre swelling. This loss of swelling, a manifestation of hornification, is caused by irreversible changes to the cell wall structure. (Scallan 1977, de Ruvo and Htun 1981, Kitayama et al. 1983, Laivins and Scallan 1993, Weise 1998, Maloney 2000, Wang et al. 2003, Park et al. 2006.) In addition, it is possible that the original entanglement state of microfibrils affecting the wet web strength, as discussed in Chapter 2.3.2, cannot fully be restored. Although only the structural alterations were considered above, there are also chemical changes affecting hornification, of which Weise (1998) provides a good summary.

At first, the extent to which the rew-wetted web differs from the web taken directly from the press section will be evaluated. The evaluation is based on hornification, its emergence, its consequences and the degree to which wet fibre properties can be restored in re-wetting without any mechanical treatment. In addition, the possibility of the sheet structure also experiencing some kind of irreversible changes when dried and re-wetted will be studied. When considering the paper grades used in our trials, there are in principle two sub-processes on a paper machine that may cause a significant reduction in fibre swelling during re-wetting: drying and wet pressing. This is kept in mind during the evaluation.

3.1.1 Cell pore structure and its interaction with water

The fibre cell wall consists of the thin primary cell wall layer, P, and the much thicker secondary wall layer, which is almost entirely made up of three different layers, S1, S2 and S3. The layers have different fibril orientations and chemical compositions. The fibrils in each layer are built up of cellulose microfibrils, which in turn are composed of bundles of cellulose chains (Hakkila and Verkasalo 2009). According to

Shmulski et al. (2007), approximately two-thirds of the cellulose is in crystalline form and the rest is in amorphous form. The hemicelluloses occur primarily in the amorphous areas in the spaces between microfibrils, like a mantle, to bond the microfibrils together. In spite of extensive studies, the exact ultrastructure and locations of different wood polymers are still uncertain. In any case, it is believed that the wood fibre cell wall consists of a lamellar structure. (Stone and Scallan 1968a, Scallan 1974, Kerr and Goring 1975, Lindström 1986, Scallan and Tigerström 1992, Vuorinen and Alén 1998, Alén 2000, Fahlén and Salmén 2003).

According to the wood fibre model of Kerr and Goring (1975), the microfibrils form a coaxial interrupted lamella structure bonded together on their radial surfaces, see Figure 18. These lamellae are covered with roughly 1/3 of all the hemicelluloses associated with the microfibrils and the remaining 2/3 are evenly distributed in the hemicellulose-lignin gel or matrix. Dissolution of the lignin-hemicellulose matrix in pulping allows the interrupted lamellae to merge, leading to thicker and more continuous lamellae than those in wood fibres (Stone et al. 1968b, Kerr and Goring 1975). Stone and Scallan (1967, 1968a) called the gaps between the lamellae "macropores" and referred to a smaller class of intralamellar pores as "micropores".

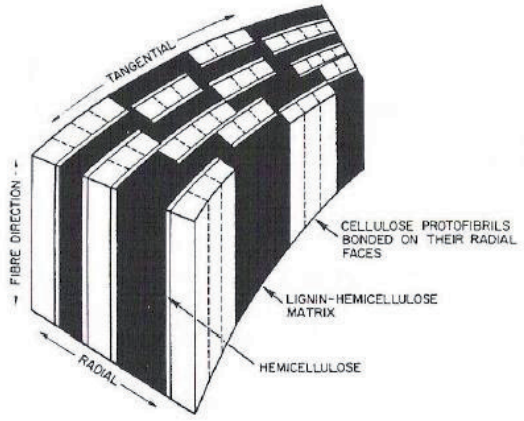

Figure 18. *Pictorial representation of the proposed interrupted lamella model for the ultrastructural arrangement of lignin, cellulose and hemicelluloses in the wood cell wall (Kerr and Goring 1975).*

When speaking about pores and porosity of the fibre cell wall, it must be remembered that the cell wall is a hydrogel, i.e. the pores only exist when the fibre is saturated with water (Maloney 2000). Dissolution of lignin and hemicelluloses shifts the pore size distribution from mainly small pores in TMP towards larger pores with a lower portion of smaller pores for unbleached kraft, see Table 3. This trend is even more pronounced for bleached kraft. The pore size was measured by the inverse size-exclusion chromatography technique (ISEC). In this method, the pore size is determined with the use of the hydrodynamic dimensions of various probe molecules. The detected pore sizes are therefore dependent on the ability of the probe molecules to penetrate a pore. As such, the actual shape of pores (bottle necks, slits between lamellae, spheres or cylinders) affects the results. The pore size is therefore called the

apparent pore size. The size of the slits between the lamellae is underestimated in particular. This is evident based on the results of Li et al. (1992), who used the pulsed gradient spin-echo (PGSE) method. Their results indicate that the pores of never-dried bleached softwood kraft are elongated along the fibre axis with lengths ranging from a few micrometres up to 20 μm. However, the measurements of Berthold et al. (1997) provide a good basis for the comparison of pore size distribution of mechanical and chemical pulps.

The results of Stone and Scallan (1968a), based on the solute exclusion technique, showed that the micro-reticular or intra-lamellar pores (< 2.5 nm) re-opened in re-wetting but macro-reticular or inter-lamellar pores (> 2.5 nm) did not fully recover.

Table 3. *The apparent pore size distribution and water retention value, WRV, for never-dried TMP and two never-dried unbeaten kraft pulps. Pore size intervals given in terms of the radii of the pores. The contribution to the total pore volume coming from each interval is given as a percentage. (Berthold et al. 1997.)*

Pulp	Total pore volume ml/g	WRV ml/g	< 2.2 nm ml/g	2.2–7.0 nm ml/g	> 7.0 nm ml/g
TMP	0.8 ± 0.1	-	0.57 ± 0.01 71%	0.13 ± 0.04 15%	0.12 ± 0.03 14%
Unbleached kraft	1.1 ± 0.4	1.6	0.50 ± 0.03 45%	0.48 ± 0.02 44%	0.11 ± 0.01 11%
Bleached kraft	1.0 ± 0.6	1.4	0.31 ± 0.02 31%	0.52 ± 0.02 53%	0.16 ± 0.01 16%

3.1.2 Hornification

The results of Forsström et al. (2005) using different never-dried chemical pulps suggest that drying significantly lowers the average pore size in re-slushed pulp without drastically changing the overall fibre wall volume. The writers suggest that a decrease in pore size is due to the formation of local contacts between the lamellae due to longitudinal and tangential irreversible pore closure during drying. The work of Stone et al. (1965, 1968a, 1968c), Laivins and Scallan (1993), Weise and Paulapuro (1995), Maloney and Paulapuro(1999) and Wang et al. (2003) indicate that the lamellae are to some extent irreversibly linked or collapsed together during drying. That is because the evaporation of water from these slit-shaped pores leads to capillary forces on the pore walls, which pull the lamellae together. The contact of lamellae is more complete in the outer part of the cell wall than in the inner part. This presumably leads to a larger number of—and possibly more water-resistant—bonds between adjacent microfibrils. The pores in the inner part are therefore more capable of re-opening and refilling during re-wetting (Weise and Paulapuro 1995). The bonds formed are possibly both hydrogen and Van der Waals bonds (Maloney and Paulapuro 1999). The irreversible coagulation of fines and bonding of external fibrils contribute to hornification (Weise et al. 1996).

Scallan and Tigerström (1992) showed that, above a yield of 65%, the elastic modulus of never-dried kraft pulps (without fines < 200 mesh) hardly changed when air dried and re-wetted. However, at low yields, the elastic modulus was increased beyond that of the never-dried pulps. For the unbleached (yield 45%) and bleached low-yield kraft (43%), elastic modulus was doubled. Measurements of single bleached kraft fibres also showed that their flexibility lessened when air dried and re-wetted (Dulemba et al. 1999). Together with the irreversible partial collapse of lamellae discussed above, these results suggest that re-wetted low-yield pulp fibres are stiffer than never-dried ones. As discussed in Chapter 2.3.1, the stiffness of wet fibres seems to affect the wet web tensile stiffness but not the tensile strength. Brancato and Banerjee (2010) noticed that recycling (without chemicals) reduced the nanoscale roughness of the surface of kraft fibres but that TMP fibres were relatively unaffected. The measurements were done for dry samples in 50% relative humidity. The lower the nanoscale roughness was, the higher the initial adhesion.

The strongest reduction in swelling occurs after the first drying-re-wetting cycle and the reduction is more pronounced for beaten pulps than for unbeaten pulps (Tables 1 and 2 in Appendix 1). In the following cycles, the change is much smaller (Weise and Paulapuro 1999, Park et al. 2006). Contrary to macro pores, bonding within a micro-reticular system (i.e. amorphous polymer network in the cell wall) appears to be largely reversible, meaning that micropores re-open during re-wetting (Maloney and Paulapuro 1999). Laivins and Scallan (1996) showed that the fines of both never-dried and once-dried pulp are more swollen than the respective fibres by a factor of about two. This factor is maintained through the range of yields from mechanical pulps to more swollen chemical pulps, see Table 3 in Appendix 1.

The pore structure of fibre cell walls of mechanical pulps differs from that of chemical pulps because mechanical pulping creates micropores, large cracks and dislocations but no macropores. It is believed that the opening of micropores is due to the formation of small cracks in the cell wall and this is related to internal fibrillation. (Maloney and Paulapuro 1999.) Because mechanical pulping does not remove the lignin-hemicellulose matrix, mechanical pulp fibres and fines should show only minimal hornification, if any. Thus it is understandable that published results generally show small or inconsequential hornification values for mechanical pulps, especially compared with beaten kraft (Stone and Scallan 1965, Scallan and Tigerström 1992, Laivins and Scallan 1996, Weise 1997, Park et al. 2006). See also Tables 1–4 in Appendix 1. Hornification of deinked pulp (DIP) is also fairly small because the pulp consists of mechanical and chemical pulp fibres and fines that have been processed several times, see Table 1 in Appendix 1.

According to the results of Luukko and Maloney (1999), mechanical pulp fines show only a small reduction in swelling, irrespective of the fibrillar/flake ratio, see Figure 19. As a comparison, the writers reported the fibre saturation point (FSP) change for bleached kraft pine pulp from 1.38 to 0.97 g/g due to drying. The degree of swelling of mechanical pulp fines correlates with the proportion of fibrillar material and swelling of fibrillar fines is on a level comparable with unbeaten kraft fibres, see Tables 3 and 4 in Appendix 1.

A high drying temperature, for example 105–120°C instead of 25°C, reduces the degree of swelling of chemical pulps further. However, this effect is relatively much smaller than that of drying as such. (Lundberg and de Ruvo 1978, Weise 1997, Maloney and Paulapuro 2000). A high drying temperature makes swelling restrictions to some degree permanent because even prolonged beating may not be able to restore the swelling to the original value. For example, the formation of relatively strong bonds between microfibrils may be one reason, or micropores may partially collapse irreversibly. The results achieved with kraft suggest that the amount of hornification increases with drying temperature after about 70°C (Maloney and Paulapuro 2000).

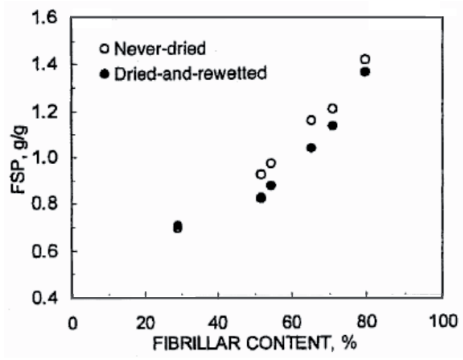

***Figure 19**. Fibre saturation point of the never-dried and dried-and-re-wetted TMP fines as a function of fibrillar content (the mass-weighted percentage of fibrillar particles in the sample). (Luukko and Maloney 1999.)*

Surprisingly, the results of Weise (1997) show a fairly high total swelling reduction for TMP and DIP when dried at 105°C, though smaller than that for chemical pulps (Table 1 in Appendix 1). He centrifuged an intact remoistened sheet instead of a pad formed from dispersed fibres, which is the standard procedure. It may be possible that high temperature somehow coagulates fines in the fibre-fines network of the sheet and therefore reduces pore volume between fines particles.

The web temperature on a paper machine during the constant rate period, when the web is saturated with water, is typically 60–75°C (Kiiskinen et al. 2000). After that, the uniform water film appears, the surface of the web is partly dry and the web temperature increases. Based on a simulation, the web can reach temperatures over 100°C (Heikkilä et al. 2000). As discussed above, this increases hornification of chemical pulps to some degree at least.

Wet pressing increases hornification of wet sheets made of chemical pulps with the effect being larger for beaten than unbeaten pulp (Carlsson and Lindström 1984, Maloney et al 1997). The likely reasons for this are the flexible walls of the beaten fibres collapsing more easily and the higher amount of fines. The fines can be considered to form a porous network between the fibres. When this network is compacted during wet pressing, the fines may irreversibly coagulate in part. (Maloney et al. 1997.) In contrast to chemical pulps, mechanical pulps are virtually unaffected by wet pressing (Carlsson and Lindström 1984). However, the results of

Maloney et al. (1997) suggest that drying at 105°C causes an irreversible increase of hornification of the wet pressed TMP sheet. It is possible that the fines, compacted in wet pressing, coagulate irreversibly to some degree during drying at a high temperature. The effect of drying at 105°C on TMP hornification is congruent with the results of Weise (1997).

3.1.3 Is the sheet structure affected by hornification?

A test series was conducted in order to gain a more comprehensive impression of hornification, see Figure 20. The aim was to clarify whether wet pressing followed by drying have any effects on the sheet structure of a re-wetted sheet. The WRV and FSP values were also measured to compare possible structural effects to the changes in fibres.

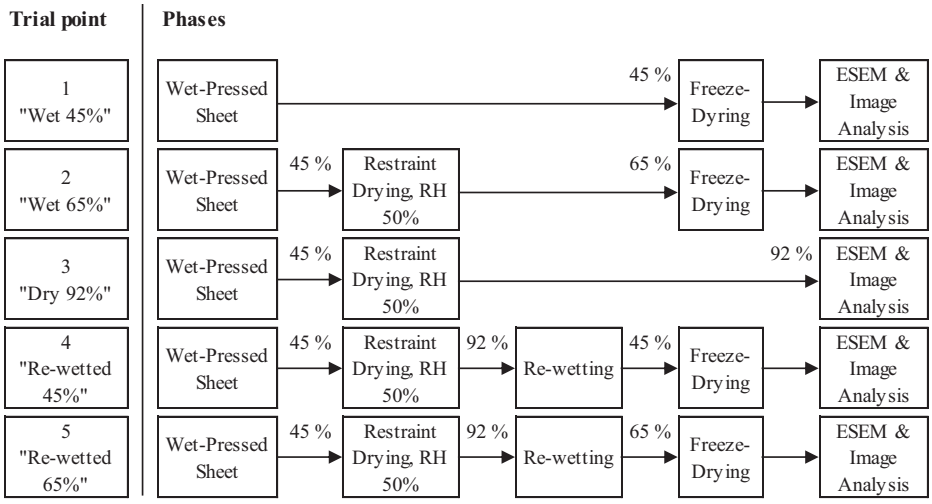

Figure 20. *Trial program for testing possible hornification effects on the sheet structure.*

The laboratory sheets were formed and wet pressed in an identical manner at all trial points with the Formette Dynamique Sheet Former and its wet pressing unit. The wire speed was 899 m/min. Wet pressing was done in two stages (1 bar + 2 bar) and dry solids content after pressing was approximately 46%. The basis weight (ISO 536:1995, MD/CD tensile ratio (ISO 1924-2:1994), bulking density (ISO 5270:1998) and Ambertec formation were 51.3 g/m², 2.16, 358 kg/m^3 and 3.47 g/m² respectively. The furnish was a mixture of bleached Scandinavian softwood kraft (30%) and TMP (70%). The kraft pulp was beaten to CSF 590 ml (ISO 5267-2:2001) with a Voith Sulzer refiner and the TMP was disintegrated in the same device for 10 min with 55°C tap water, consistency 4%. The sheets in trial points 2–5 were restraint dried in air (50% RH and 23°C) using ISO-brightness rings. Re-wetting in trial points 4 and 5 was carried out with deionised water using the KCL Nozzle Applicator. The selected application method provided an even water layer on the sheet, which was visually confirmed by adding 0.1% Amarant dye into the water. After re-wetting, the sample

was placed on a plate and sealed together with the plate in a plastic bag for one hour before die-cutting to allow moisture to even out through the sample. Die-cutting was done similarly to all the wet and re-wetted samples (trial points 1, 2, 4 and 5). Two pieces (5 cm x 6 cm) of each trial point were die-cut through the plastic bag against the plate.

After die-cutting, all the wet and re-wetted samples were deep-frozen in liquid nitrogen and then dried frozen in a vacuum, which led to the sublimation of water. A deep-freezing method was experimentally tested by measuring in-plane (x-y) dimensions of the sample at the wet stage before and after the freeze-drying procedure. The in-plane (x-y) dimensional stability of the samples was good with almost identical dimensions in both samples (difference of 2% between the wet and freeze-dried samples). Although the dimensional stability in the z-direction was not explicitly tested, it was assumed that this procedure kept the original wet structure of the samples thoroughly or very close to unchanged.

Four small sheet slices (20 mm x 10 mm) per test point were embedded in epoxy resin. Two of those slices were for CD measurements and two for MD measurements, see Figure 21. The embedded sample blocks were ground and polished using lapping oil as a lubricant. The cross-sections were imaged in an environmental scanning electron microscope (ElectroScan ESEM 2020) in high vacuum back-scattered electron mode. 30 images both in CD and MD were taken (i.e. 15 images per sample block). The magnification was 250x. The structural parameters were determined from binary images, size 512 x 512 pixels. The pixel size in the images was 0.7 μm. Noise was removed with median filtering, after which the images were treated by a differential contrast enhancement (DCE) operation. In order to determine the porosity parameters and effective thickness, the top and bottom surface of the fibre layer in every image was defined manually. The porosity parameters were measured both with lumen filled and lumen open. Lumen filling was done manually. The total porosity was measured as the ratio of total void area divided by the total network area. Effective thickness, pore height and pore width were measured by combining the binary ESEM image and an image of a grid mask of either vertical or horizontal straight lines at 4-pixel intervals. A Boolean AND operation was used to combine the images. The result is a sum image where the length of the lines shows the dimensions of the measured parameters (effective thickness, pore height or pore width).

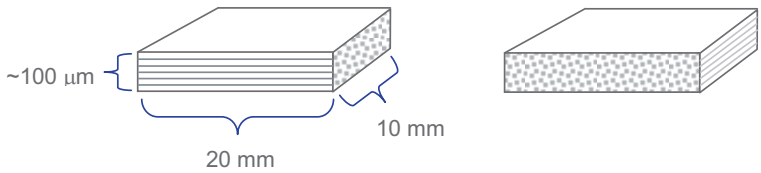

Figure 21. *Illustration of the sample blocks for image analysis (ESEM). The left picture depicts the block for MD measurements and the right picture depicts the block for CD measurements. The ESEM images were always taken from the longer side. The lines in the blocks denote fibre orientation.*

Relative bonded area (RBA), the bonded fraction of the total fibre surface area, was estimated by using the model (6) developed by Niskanen and Rajatora (2002). The model allows the estimation of RBA based on the measurement of the mean pore height and fibre coverage from the sheet cross-section images. Due to the lack of hydrogen bonds in wet paper, RBA is called henceforth relative contact area (RCA). When dealing with RBA/RCA values, it is important to keep in mind that any measurement of those values relies on a threshold separation below which two fibre surfaces are considered bonded together.

In order to determine RCA, the number of fibre layers was measured from the dry sample, trial point 3. This was done by magnifying 30 images of dry sample 3 to 10 cm x 10 cm, drawing 10 vertical lines for each image (1 cm apart) and counting manually how many times the fibres intersected each line.

$$RCA = \frac{a}{\langle h \rangle}\left[1 - \frac{1}{c}\left(1 - e^{-c}\right)\right] \tag{6}$$

where a is the pixel size, µm
h is the mean pore height without lumen, µm
c is the coverage, i.e. the number of fibres in a z-direction scanning line.

The model presumes that sheet structure is random in the z-direction and hence pore heights are exponentially distributed. If this is not true, then the calculated RBA is not correct (Niskanen and Rajatora. 2002). The presumption of the exponential distribution is violated, at least to some degree, if the interaction forces between fibres are effective enough to close small inter-fibre pores. This kind of situation occurs, for example, in drying. Because we are comparing wet and not very dense samples with each other, strong interaction forces do not exist between fibres. Thus an exponential distribution can be expected. Figure 22 shows that the z-direction (ZD) porosity distribution is curved with the surface layers being denser than the middle layer. However, the exponential distribution can be expected to be valid for both layers. As a comparison, the pore height distribution in the handsheets in the study of Niskanen and Rajatora (2002) was approximately exponential.

Table 4 shows the effect of drying and re-wetting on the structure parameters and relative contact area (RCA). Only the results measured without lumen (i.e. lumen filled) are shown. On average, there was only 1.7% difference in the mean pore height and 0.1% difference in mean pore width between the measurements taken with lumen filled and lumen open, when the calculation included both the CD and MD measurements. The difference in total porosity was more distinct. When the measurements were taken with lumen filled, the values were on average 8.5% smaller compared with the values done with lumen open.

The RCA value for the dry sample, roughly 0.09, is surprisingly small compared with the RCA values of Niskanen and Rajatora (2002). They measured for dry handsheets an RCA of 0.16 irrespective of the furnish concept, either 100% PGW or a mix of 60% PGW and 40% kraft. In addition, their total porosity and mean pore height values were on average 43.5% and 4 µm respectively. These values are clearly

smaller than the respective values in Table 4. The resolution used does not explain the difference. The most probable reason is that the wet pressing procedure employed was not able to provide a dense enough fibre network for some reason. This is evident when the total porosity and mean pore height values of newsprint E are examined, see Appendix 3. These values, 40.9% and 3.3 µm, are comparable to the results of Niskanen and Rajatora. Due to a lack of coverage values, the RCA was not calculated but based on the numbers above it can be estimated to be in the region of 0.19. To compare, RCA values for dry samples of mechanical pulps were typically slightly below 0.2 in Lehto's measurements (2004).

Although the dry and wet samples are not as dense as expected, the behaviour between the trial points seems logical and there is no reason not to consider the results reliable.

Table 4 *Influence of drying and re-wetting on effective thickness, porosity parameters and relative contact area (RCA). The values are measured with lumen filled.*

Sample	tp 1 Wet 45%	tp 4 Re-wetted 45%	tp 2 Wet 65%	tp 5 Re-wetted 65%	tp 3 Dry
	CD values				
Total porosity, %	62.1	60.3	58.4	58.3	52.2
Effective thickness, µm	131.7	122.8	116.8	111.7	90.5
Mean pore height, µm	8.9	8.7	8.6	8.6	6.8
Mean pore width, µm	14.2	14.6	14.1	14.4	11.5
RCA	0.065	0.066	0.067	0.067	0.085
	MD values				
Total porosity, %	57.5	56.7	52.5	55.9	54.3
Effective thickness, µm	115.8	110.4	104.0	98.9	90.0
Mean pore height, µm	7.7	7.6	7.2	7.5	6.6
Mean pore width, µm	14.4	14.3	14.4	13.9	12.4
RCA	0.075	0.076	0.080	0.077	0.087

There is a systematic level difference between the CD and MD measurements. In addition, the porosity distribution of dry sample 3 differs more from that of the wet and re-wetted samples when measured in the CD than the MD. These differences most likely originate from fibre orientation. The pore height and pore width did not change during drying and re-wetting, see Table 4. Porosity distribution did not change either, as seen in Figure 22. The important issue is the invariability of RCA, contact area between wet fibres, because RCA has a direct effect on the strength of a wet web. Only the total porosity and effective thickness of re-wetted samples 4 and 5 showed a minor reduction compared with wet samples 1 and 2. The results therefore suggest that drying followed by re-wetting does not change the sheet structure, i.e. no sheet structural hornification exists.

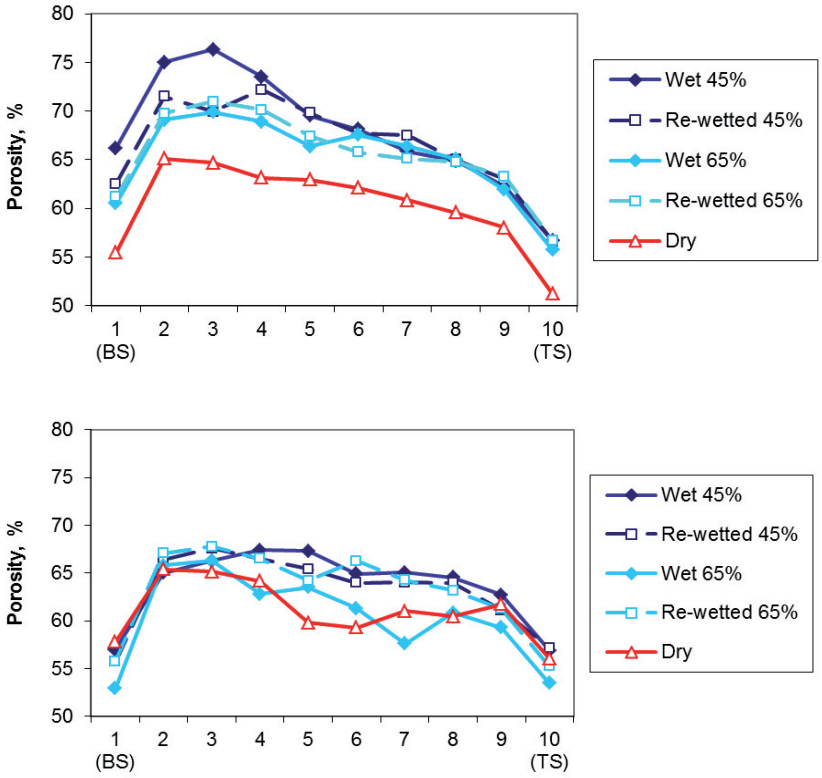

***Figure 22**. CD (top) and MD porosity distributions (bottom). The values are measured with lumen filled. BS and TS denote the bottom and top side of the sample respectively.*

Fibre hornification was determined by measuring WRV (SCAN-C 62:00, modified) and FSP (by solute exclusion method according to the internal method of Helsinki University of Technology) from trial point 1 (sheet wet pressed to 45%), trial point 2 (sheet wet pressed to 45% and dried restraint to 65%) and trial point 3 (sheet wet pressed to 45% and dried restraint). The sheets in trial points 1–3 were disintegrated in deionised water before the measurements. The WRV was measured from the furnish also, see Figure 23.

Wet pressing to DSC 45% did not increase hornification. This is understandable due to the large proportion of TMP. The result is therefore congruent with the results of Carlsson and Lindström (1984). Drying from DSC 45% to DSC 65% belongs to the phase where macropore water is removed from the fibre cell wall, causing irreversible hornification. Weise et al. (1998) calls this phase “wet hornification”. It is possible that some kind of irreversible fines coagulation may also occur in this phase. In any case, the reduction in WRV and FSP for mechanical pulps is small, as discussed in the previous chapter. The measured changes in WRV and FSP were -11.7% and -8.2% respectively. The corresponding WRV change for TMP calculated from the WRV 1 and WRV 3 values, presented in Table 1 in Appendix 1, is -10.7%. Thus the

figures are very similar. The last drying phase starts approximately at DSC 70% (Weise et 1997, 1998, Weise and Paulapuro 1998), where practically all free water has disappeared. The removal of bound water from the micropores and accessible hydration sites is largely reversible (Maloney and Paulapuro 1999). This means that the last drying phase does not increase hornification, with the exception being drying at high temperature as discussed above. Thus the measured negligible reductions of -4.2% and -1.1% in WRV and FSP respectively are understandable.

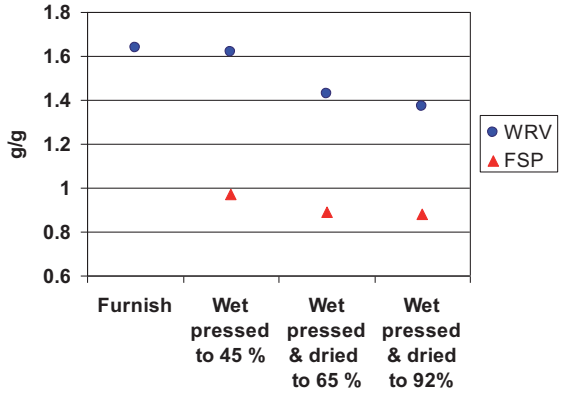

Figure 23. *WRV and FSP results (g water / g oven dry pulp).*

One method to investigate whether the sheet microstructure experiences to any extent the same type of hornification as fibres is to calculate percent changes between trial points 1 and 4 and between trial points 2 and 5, see Table 5. Computation for the values measured is performed with lumen filled. The change in WRV is consistent with the respective DIP values, 11.6–15.3%, computed from Table 1 in Appendix 1. In addition, the absolute results are well in line with the values shown in Tables 1–3 in Appendix 1.

Table 5. *Percentage change in FSP and WRV as well as in sheet structural parameters (lumen filled) due to drying and re-wetting. Structural results are averages from CD and MD measurements*

	Wet and re-wetted DSC 45%	Wet and re-wetted DSC 65%
Change in total porosity, %	-2.1	3.2
Change in effective thickness, %	-5.7	-4.6
Change in pore height, %	-1.2	2.2
Change in pore width, %	0.8	-0.7
Change in RCA, %	1.2	-2.1
Change in WRV, %	15.4	-
Change in FSP, %	9.3	-

As Table 5 shows, drying and re-wetting had, practically speaking, no effect on the structural parameters; only the effective thickness decreased by approximately 5%. The independence of RCA is especially important. As discussed above, drying at high temperature increases fibre level hornification. Thus, analogically, high temperature could also have an influence on the structural parameters. However, because the structural changes were inconsequential, the possible additional increase due to increased temperature would also be inconsequential.

3.1.4 Can the re-wetted web simulate the wet web on a paper machine?

This question will be considered based on the review of bonding mechanisms in the wet web, Chapter 2.3.2, the review of fibre and fines hornification, Chapter 3.1.2, and the tests related to possible structural hornification, Chapter 3.1.3.

It is shown that while the wet web runs from the press section to the reel-up, fibres and fines experience hornification to a different degree due to differences in morphology and chemical composition. Typically, kraft fibres and fines—especially of beaten pulp—show a clear irreversible reduction in swelling when re-wetted. In addition, an irreversible coagulation of fines leading to a reduced pore volume between them and bonding of external fibrils contribute to hornification.

Due to the structure and chemical composition, mechanical pulp fibres and fines should show only insignificant hornification. The results of Luukko and Maloney (1999), which show only a minor loss in swelling for mechanical pulp fines in re-wetting, are notable. The importance of this result is related to the fact that mechanical pulp fines, especially fibrillar ones, have a large effect on wet strength. However, the results of Maloney et al. (1997) suggest that a high drying temperature together with wet pressing seems to coagulate fines irreversibly to some degree. According to the results of Weise (1997), even high temperature alone may be enough.

Because DIP consists of recycled chemical and mechanical pulps with some fibres and fines being recycled many times, it is natural to expect DIP to resemble mechanical pulps in terms of hornification.

Wet pressing without any additional drying causes hornification to beaten unbleached kraft, but the effect on unbeaten kraft is clearly smaller (Maloney et al. 1997). When considering the effect of wet pressing, it must be remembered that both the wet web on a paper machine and the dried and re-wetted web on the AHMA runnability pilot (cf. Figure 24), used in this thesis, have experienced the same kind of wet pressing treatment on a paper machine. The difference is that, in the dried web, the wet pressing has contributed to drying-induced hornification. In addition, the re-wetted web experiences additional wet pressing in the brake nip in AHMA (item 12 in Figure 24). This additional pressing is useful because it condenses the structure of the re-wetted web, which most likely has been loosened by swelling of the fibres.

Due to the reduced fibre swelling and smaller pore volume between fines, there is less water in the cell wall and more water between fibres and fines at constant DSC.

According to the general relationship between strength and moisture, the outcome should be slightly reduced tensile strength and elastic modulus compared with wet paper made of never-dried pulp. In addition, the partially irreversible coagulation of fines may reduce, to some degree, their capability to act as bridge makers between fibres in a re-wetted web compared with a never-dried web. This may lead to slightly reduced wet strength properties.

Hornification increases the elastic modulus of kraft fibres but not that of TMP fibres. This means improved stiffness for kraft-based wet webs at constant DSC. However, the improved elastic modulus does not affect the tensile strength of the wet web.

Hornification is likely to reduce the nanoscale roughness of kraft fibres but not TMP fibres. This means a higher initial tangent adhesive force between kraft fibres but a reduced coefficient of friction.

Drying and re-wetting seem to have no effect on RCA. This suggests that the irreversible changes are restricted to fibre material only.

Based on the reasoning above, the following conclusions can be made:

- The results from this work and from references reviewed suggest that drying and re-wetting do not cause any that kind of irreversible changes to the paper microstructure that could violate the comparison and study of wet web strength properties based on re-wetted papers.
- Even if the target is to investigate the effect of different type of furnishes on wet strength, e.g. a furnish containing a considerable share of chemical pulp compared with a furnish having only a minor portion of chemical pulp, drying and re-wetting most likely mitigate the absolute differences between the furnishes but do not change their mutual order and do not lead to erroneous conclusions.

3.2 Trial papers

The trial program comprised of four separate trial series, see Table 6. Series I–III were run on the AHMA runnability device (Niskanen et al. 2003) and series IV on a pilot Fourdrinier. The middle position reels for the AHMA trials were collected from the paper mill winders. Reels initially 50 cm wide were slit to 25 cm wide at KCL. In series IV, the wet web strength properties were measured in situ by the wet web winder installed right after the third press (Tanaka et al. 2009). Paper properties are discussed in the following chapters when necessary.

***Table 6**. Newsprint and LWC base papers used in AHMA trials and run on a pilot Fourdrinier. The dominant pulp component in each furnish is mentioned first. RBG denotes roll-blade gap former and LB denotes loadable blades.*

Trial series	Papers	Grade	Basis weight	Furnish	Former	Utilisation
I	A	News	45	TMP/RCF	Hybrid	Re-wetting procedure Effect of defects
I	B	News	45	RCF/TMP	RBG	Re-wetting procedure Effect of defects
II	C	News	45	RCF/TMP	RBG	Re-wetting procedure
II	D	News	45	RCF	RBG	Re-wetting procedure
III	E1–E6	News	45	RCF	RBG	Effect of web structure Effect of defects
III	A1	LWC	40	TMP/kraft	RBG	Re-wetting procedure Effect of web structure Effect of defects
III	A2–A3	LWC	40	TMP/kraft	RBG & LB	Re-wetting procedure Effect of web structure Effect of defects
III	B1–B2	LWC	48	PGW/kraft	RBG	Effect of web structure Effect of defects
IV	Pilot1–Pilot4	News	58	TMP	Fourdrinier	Effect of poor formation

3.3 Runnability pilot

Five trial series out of six were carried out on the KCL AHMA pilot-scale strength testing machine for running paper webs (Niskanen et al. 2003). The selection of KCL AHMA for the testing device was based on the following reasons:

- Wet web tensile strength, elastic modulus and residual tension were considered to be important parameters affecting wet web runnability, see Chapter 2.1. In addition, the strain at break was also considered to be an important parameter for paper machines that typically have sudden strong perturbations. The first two properties can easily be studied with AHMA. The strain at break can also be determined but it is not a straightforward measurement for re-wetted paper rolls as will be discussed later.
- It is possible to measure a large number of breaks at each trial point, enabling detailed information on web break statistics. This is an advantage because not only are the averages of web strength properties important but also their variation.
- Compared with standard laboratory methods, web breaks occur under more realistic conditions as the web suddenly enters an open draw, where it experiences a rapid increase in tension and the majority of creeping occurs quickly at the beginning of the open draw. For this reason, the tensile strength and tensile stiffness measured in AHMA are often called dynamic tensile strength and dynamic tensile stiffness. However, for simplicity the terms tensile strength or breaking tension and tensile stiffness are used in this thesis.

- Specimen dimensions are large enough to enable the study of mesoscale structural effects as well as the effects of microstructure.

The device consists of the unwinder, notching device, three moistening units, storage path to control the web length from moistening to testing, special test draw section and shredding unit, see Figure 24. Pre-tensions (items 5, 8 and 11 in Figure 24) are controlled to the set values by speed differences from the unwinder to the brake nip. Web breaks occur in the one-meter long test section starting from the brake nip and ending at the pulling nip. When paper strength is measured using "web break mode" (Niskanen et al. 2003), as in this thesis, the pulling nip repeatedly accelerates so that paper strain increases until the web breaks. The accelerating rate is controllable. The brake nip runs all the time at a constant speed. The web tension in the test draw is measured by two tension sensors integrated into the brake nip. One sensor is located on the tending side and the other on the driving side. The tension values and the respective strain values are recorded at 10 ms intervals. The device recovers automatically from a web break and the next acceleration ramp starts immediately after recovery. The automatic web break recovery uses rubber bands that carry the broken web into the pulling nip. In our tests, it was typically possible to measure 4 to 6 breaks per minute.

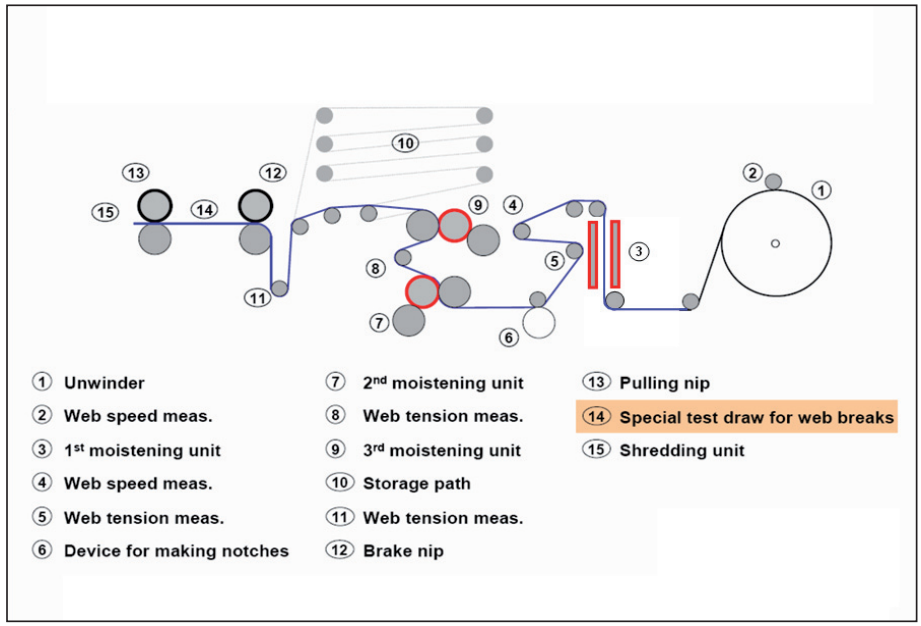

***Figure 24**. The main components of the KCL AHMA runnability pilot.*

Another possibility when running AHMA is to use "rheology mode" (Niskanen et al. 2003). The speed difference in the test draw is kept constant between successive speed increments. This is a robust method used to produce strain-tension curves. However, the method is time consuming and the amount of breaks remains low.

Because break distributions are one of the interests in this work, “rheology mode" was not used.

The same nip loads were used in all the AHMA trials: 11.5 kN/m in the moistening units and 28 kN/m in the pulling and brake nips. With the respective nip lengths being 20 mm and 7 mm the average nip pressures were 5.5 bar and 40 bar respectively. The latter is of the same order of magnitude as the average nip pressures on a paper machine press section.

The strain (ε) experienced by the paper web in the test draw depends on whether the speed difference between the nips is constant or accelerating. When strength measurements are carried out using "web rheology mode", strain can be calculated easily from the speeds of the brake and pulling nips v_1 and v_2 respectively:

$$\varepsilon = \frac{v_2 - v_1}{v_1} \tag{7}$$

However, this is not the case with the accelerating speed difference. In order to get realistic strain values—which in turn enables realistic tensile stiffness values—the following equation, derived from the law of mass conservation, was used (Wathén 2003):

(8)

$$\varepsilon_{real}(\varepsilon_{app}) = \varepsilon_{\min} + \frac{(\varepsilon_{\max} - \varepsilon_{\min})L}{t_{ramp} v_1 (1+\varepsilon_{\min})^2}\left[\exp\left(-\frac{v_1 t_{ramp}(\varepsilon_{app} - \varepsilon_{\min})(1+\varepsilon_{\min})}{L(\varepsilon_{\max} - \varepsilon_{\min})}\right) - 1\right] + \frac{\varepsilon_{app} - \varepsilon_{\min}}{1+\varepsilon_{\min}}$$

Where $\varepsilon_{\text{real}}$ is the real strain

$\varepsilon_{\min}$ is the initial strain (i.e. the initial speed difference)

$\varepsilon_{\max}$ is the maximum applied strain (i.e. the maximum speed difference)

v_1 is the web speed in the brake nip

t_{ramp} is the ramp time

L is the length of test draw section

ε_{app} is the speed difference of the nips, called apparent strain and computed by Equation (9)

$$\varepsilon_{app}(t) = \varepsilon_{\min} + \left(\frac{\varepsilon_{\max} - \varepsilon_{\min}}{t_{ramp}}\right) * t \tag{9}$$

Where t is the time until break.

The accelerating rate is controlled by the ramp time t_{ramp}, which is the time needed to reach the maximum speed difference ε_{max} from the minimum speed difference ε_{min}. In trial series I and II, News A, B, C and D, ε_{min}, ε_{max} and t_{ramp} were set to 0.1%, 1.5% or 4.3% and 10 s or 30 s respectively, allowing a straining speed of 0.14%/s. In trial series III, News E and LWC base papers A and B, settings for moistened papers were

slightly different. ε_{min} was varied between 0.3% and 0.6%. ε_{max} and t_{ramp} were 5% and 10 s respectively. These settings allowed a straining speed of 0.44–0.47 %/s.

The logic of the system is built so that the tension in the test draw measured by both of the sensors always needs to be higher than 25% of the first measured pretension (item 5 in Figure 24) to allow the speed of the pulling nip to be increased. The minimum web tension is controlled by ε_{min}.

3.4 Correspondence between wet strength properties measured on the runnability pilot and in situ on the press section

When using KCL AHMA to study the wet strength of re-wetted paper rolls, the following question is unavoidable: how well do the strength properties measured on the pilot device simulate the real wet strength properties of the very same paper run on a paper machine?

By utilising a new wet web winder installed right after the 3rd press on a pilot PM (speed 80m/min), Tanaka et al. (2009) were able to measure wet strength properties both in situ and on AHMA 1–2 hours later. The wet reels were wound on the wet web winder (Figure 62, Page 130) and transported to AHMA for measurements. According to the results, a good correlation exists between the wet tensile strength measured on a pilot PM and on AHMA, see Figure 25. However, breaking strain values measured on AHMA were much smaller and tensile stiffness higher than those measured directly from the press section. The straining history was different for the web on the pilot PM and on AHMA because before the test draw the web had already experienced about 2.5% straining on the wet web winder plus straining due to the pre-tension on AHMA.

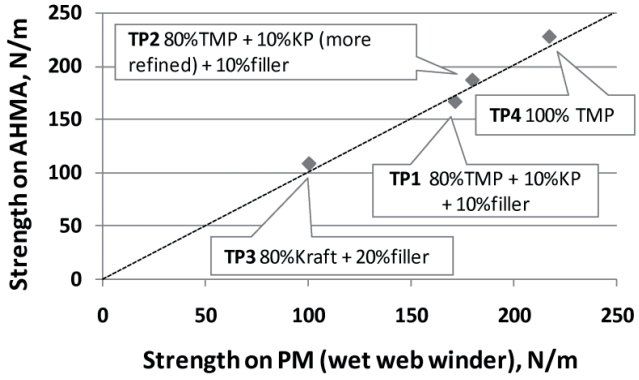

***Figure 25**. Comparison of wet tensile strength measured on AHMA and immediately after the press section on a pilot paper machine. The quality of TMP, refining degree of kraft pulp (KP) and filler content were varied between the trial points. (Tanaka et al. 2009.)*

Barnet and Harvey (1980) explored the properties of a wet web on a pilot PM running at 55 m/min. The furnish was a mixture of TCMP and GW. The web was sampled in three open draws for testing. Their results support the independence of the total strain from the straining history, see Table 7. This suggestion is supported by the results of Tanaka et al. (2009). They reported the total breaking strain to remain constant when wet paper reels taken from a pilot PM were run on AHMA using two clearly different pretensions, 42 N/m and 208 N/m.

Table 7*. Total break strain with different straining combinations. The results are recalculated from the results of Barnet and Harvey (1980).*

Couch draw %	1st press draw %	2nd press draw %	Draw to break at	Draw to break %
7.1			couch	7.1
2.6	4.2		1st press	6.8
2.6	2.1	2.5	2nd press	7.2

Mäkinen (2003) produced wet LWC base paper reels on a 700 m/min running hybrid pilot PM equipped with a shoe press and one ordinary nip press. The DSC of the final paper was approximately 49%. The wet draw over the pilot PM was varied approximately between 5.3% and 8.6% with the changes being made between the first press and the dryer. The wet reels were transported to AHMA for strength measurements. The increase in the wet draw on the pilot PM was only partially compensated by the reduced breaking strain on AHMA, with the outcome being a clear difference in the total breaking strain, see Table 8. However, in spite of a significant increase in the paper machine draw, the wet tensile strength remained practically unchanged (difference 3.9%). Tensile stiffness naturally increased due to the reduced breaking strain and fairly constant tensile strength on AHMA.

Table 8*. The effect of wet straining on a pilot PM on the total strain and tensile strength of the wet web. The breaking strain on AHMA includes the strain (0.7–0.8%) due to the pre-tension. Results are recalculated from the results of Mäkinen (2003).*

Draw over pilot PM %	Breaking strain on AHMA, %	Total breaking strain %	Tensile strength kN/m	Tensile stiffness kN/m
5.3	3.3	8.6	184	8.1
8.6	2.0	10.7	191	10.1

The results above suggest that the tensile strength of the wet web is independent from the wet straining history. In addition, the same also seems to be valid for the total breaking strain when the variation in the wet straining history is not large. If pre-straining is fairly constant between trial points, the stretch-at-break and tensile stiffness values measured on the test draw of AHMA are comparable with each other, although on a different level with the in situ measurements on a paper machine. These are important results.

Based on the results of this chapter and the discussion in Chapter 3.1.4, it is safe to conclude that running re-wetted webs on AHMA is a relevant method for studying the effect of paper structure on strength properties of wet paper webs.

3.5 Development of the moistening procedure

At first, water sorption mechanisms over short times are reviewed to the extent needed to evaluate the adequacy of the delay time from rewetting to the test draw. Because the trial papers were produced without any hydrophobic sizing, the review is limited only to unsized papers.

3.5.1 Short-term water absorption

It is generally accepted that the pore dimensions of conventional papers allow capillary penetration, but the water transport into the fibres is primarily diffusion controlled (Salminen 1988).

Generally, the water transport rate into paper is affected by external pressure, the chemical properties of the fibre surfaces (e.g. solid-liquid contact angle), surface tension, the temperature and the viscosity of the water (Bristow 1986, Salminen 1988, Neimo 1999). The complex pore structure also plays an important role in this transport phenomenon (Kent and Lyne 1989, Roberts et al. 2003a). In addition, the swelling of fibres by water affects the water transport (Bristow 1986).

Water transport mechanisms into unsized paper (i.e. no hydrophobic sizing) can be viewed as a sum of several co-existing sub-processes. However, the pores and roughness pits need to be filled before capillary penetration can begin (Hoyland 1977a, 1977b, Bristow 1986, Salminen 1988, Neimo 1999 and references therein, Fabritius 2007):

- filling of pores and roughness pits at the paper surface
- capillary penetration through pores and cavities
- diffusion along fibre surfaces (through fibre-fibre contact = intrafibre penetration)
- diffusion into and inside fibres = interfibre penetration
- diffusion transport of vapour formed above the liquid surface in pores

Of the sub processes, capillary penetration is probably the most important transport mechanism quantitatively and the external water pressure is a decisive factor for the rate of water transport (Eklund and Salminen 1987, Salminen 1988). Diffusion into and inside fibres controls fibre and paper expansion (Hoyland 1977a, Bristow 1986). The dynamic capillary pressure, the main driving potential for capillary penetration under no external pressure, is influenced by sorption of water molecules from the vapour phase onto the fibre wall, as well as by surface chemical changes in the fibres caused by the water molecules diffusing in the fibre network ahead of the liquid front (Salminen 1988).

The Lucas-Washburn theory has often been used to model water penetration into paper where the rate of penetration is a function of the balance between surface tension forces and viscous drag. When the external pressure is included, the model can be presented in the following form (Salminen 1988):

$$l = \sqrt{\frac{2r\gamma\cos\theta + p_e r^2}{4\eta}}\sqrt{t} \tag{10}$$

where l is the penetration depth
r is the capillary radius
γ is the surface tension
θ is the contact angle between the liquid and the capillary wall
p_e is the external pressure
η is the viscosity of liquid
t is the penetration time.

Equation (10) predicts that the penetration depth of water is proportional to the square root of the penetration time. However, the model does not take into account the complex internal structure because the pore morphology is reduced to an equivalent cylindrical pore. Neither does the model take into account the simultaneous fibre absorption and swelling during penetration. In addition, the model assumes the contact angle between the liquid and the capillary wall to be constant. All this is a gross oversimplification and leads to a deviation from the square root relationship between time and penetration depth at zero or low external pressure. (Hoyland et al. 1973, Hoyland 1977a, Bristow 1986, Salminen 1988, Ramaswamy et al. 2002, Roberts et al. 2003a.)

On the other hand, Yakahashi et al. (1997) studied water imbition into cellulosic fibre matrices using the dynamic spiral nuclear magnetic resonance (NMR) imaging technique. The results indicated two different processes: water penetration into capillaries and slower water diffusion into fibres. In addition, the advancing liquid front is primarily determined by the water capillary flow and can be quantitatively described by Lucas-Washburn theory.

Based on cryo-scanning electron microscopy, Roberts et al. (2003a, 2003b) and Senden et al. (2007) provide another view for the common description of capillary penetration. According to them, the continuous displacement of the water meniscus along the bulk pores is highly unlikely due to the presence of discontinuities in the pore morphology halting the advancement in the pores. The only mechanism for water to advance beyond discontinuities in the pore structure is via a film flow. Thus, if the frontal meniscus cannot advance down a pore, water will flow as a film along the edges of the pores. In addition, the results of Roberts et al. (2003a, 2003b) indicate that water movement into kraft papers is due primarily to the advance of water in the form of capillary pressure-driven water films along the channels formed by fibre overlaps. These channels form a highly interconnected, dense network of flow paths that efficiently transport water. Pores saturate by thickening of the advancing films. The smaller pores saturate first, while the largest pores may remain

only partially wetted along the edges. The pore filling via a film swelling process is defined as snap-off of the wetting fluid in the small pores.

In TMP papers, fines seem to accumulate in the fibre overlap channels and in the pore spaces of the paper sheet. The increasing fines content impedes water penetration in the fibre overlap channels. As a result, the dominant flow mechanism seems to be via the largest channels, which form a connected pathway for water. Furthermore, water seems to flow along the pathways provided by the network of fines. (Senden et al. 2007.) The penetration mechanism suggested by Roberts et al. (2003a, 2003b) and Senden et al. (2007) further confirms that the Lucas-Washburn theory oversimplifies the penetration phenomenon.

Water penetration will be strongly sped up if water is applied to the sheet under external pressure (Salminen 1988, Roberts et al. 2003a) with the driving potential being the sum of the external pressure and the capillary pressure, see Equation (10). However, when the external pressure is released, capillary transport will again dominate the flow mechanisms, and any excess water and water within the pores will continue to penetrate via films (Roberts et al. 2003a). The results of Salminen (1988) with two 52 g/m² groundwood containing coating base papers show that water penetration already at 0.5 atm external pressure is a relatively linear function of the square root of penetration time. Instead, at zero external pressure water transport is often linearly dependent on the penetration time, rather than being proportional to the square root of time (Salminen 1988).

The diffusion into and within the fibre wall material differs from the capillary flow in inter-fibre pores. In addition to the breakage of the inter-fibre bonds and separation of the fibres, the diffusing water penetrates between the hydrogen-bonded microfibrils and the lamellae in the fibre wall. This causes swelling of the fibres and hence the paper. As a first approximation, it can be assumed that only water absorption into the fibres increases the paper volume directly by the volume of absorbed water. In contrast, pore penetration does not increase paper volume. (Hoyland 1977a, Bristow 1986, Lyne 1993, Takahashi 1997.) The results of Skowronski et al. (1988) suggest that swelling of the fibre wall is the primary process in chemical pulp fibres while, in mechanical pulp fibres, fibre shape recovery predominates over swelling. Both mechanisms lead to paper swelling. The main driving potentials for diffusion are probably the concentration gradient of water and osmotic pressure between the interior and exterior of the fibres (Salminen 1988, Scallan & Tigerström 1992).

Under ideal conditions, the general solution of the classical diffusion equation, Fick's second law, yields a square root of time relationship. However, this is approximately true for liquid water diffusion in paper too (Hoyland 1977a), although the diffusion constant is a function of the moisture content of the fibres (Hoyland 1977a, Ramarao et al. 2003). Hoyland (1977a) proposed that the following solution of Fick's second law should describe the penetration of liquid water into paper by diffusion:

$$F = \frac{m_t - m_o}{m_\infty - m_o} = \frac{2}{z}\left(\frac{Dt}{\pi}\right)^{0.5} \qquad (11)$$

where F is the fraction of the amount of water taken up in time t relative to the amount taken up at infinite time

m_o, m_t, m_∞ are the amounts of water taken up at times 0, t and at fibre saturation respectively

t is the time elapsed from the introduction of water

z is the initial thickness of paper

D is the diffusion coefficient

In addition, Salminen's (1988) experiment with an unlacquered 35g/m² cellophane film (made of regenerated cellulose and having probably a pore structure that prevents capillary transport but allows diffusion) and water up to DSC 50% showed a very good square root of time relationship for water diffusion. His results also showed that diffusion is independent of the external pressure.

This all means that, at least at short time intervals, the liquid water amount transported by the diffusion mechanism is proportional to the square root of time.

Although slower than the capillary penetration process, the diffusion process is very fast (Salminen 1988, Skowronski et al. 1988, Kartovaara 1989, Huang and LePoutre 1996, Heikkinen 1998, Ketoja et al. 2001, Lehtonen 2005, Paaso 2007). This is contrary to what has been generally assumed. In the Salminen's cellophane test, DSC 50% was achieved in 13–14 s. Kartovaara (1989) measured the swelling of individual GW, PGW, TMP and bleached kraft fibres with a surplus of applied water. Swelling was measured as a percentage value of the maximum width, which in turn was achieved by monitoring the swelling until the width did not increase anymore with time. Kartovaara's results show that mechanical pulp fibres achieved 50% and 75% of their maximum possible swelling on average in 0.12 s and 0.25 s respectively. The corresponding figures for bleached kraft fibres were 0.07 s and 0.15 s. Heikinen (1998) utilised Kartovaara's method by measuring the swelling of bleached chemical pulp fibres and swelling was monitored for 1 s. At first, fibre swelling was very fast but at the end of the time scale swelling approached asymptotically the value measured at 1 s. Heikkinen's results show that 25%, 50% and 75% of the swelling achieved at 1 s was achieved in 0.07 s, 0.13 s and 0.21 s respectively.

Although several sorption models, developed to overcome the shortcomings of the Lucas-Washburn approach (Hoyland et al. 1973, Yamazaki 1995, Ketoja et al. 2001, Ramaswamy et al. 2002), provide some possibilities to evaluate the adequacy of the delay time used in our trials, more modelling work is needed. However, that kind of modelling is out of the scope of this thesis and a more practical approach was therefore selected. Firstly, the rates of capillary penetration and diffusion were evaluated by measurements. Secondly, measurement results were reviewed from the literature comprising papers similar to our trial papers, see Table 11 (Pages 85–86).

3.5.2 Initial tests

The first task was to develop a moistening procedure for KCL AHMA to simulate the state of the wet web after the press section. The idea was to use the lower and upper moistening nips (items 7 and 9 in Figure 24 respectively) and a two-sided spray unit consisting of several nozzles (item 3). In each nozzle, water was pumped at high speed through a very small opening, causing the jet to disperse into small droplets when it collided with air. The nozzles were positioned to provide even moistening coverage.

Two different newsprints, News A and News B (trial series I), were used for the tests. News A was manufactured on a hybrid former and News B on a roll-blade gap former. The TMP/RCF ratio was 51/49 and 10/90 respectively. The basis weight for both papers was 45 g/m². Formation was measured by Ambertec and by β-radiographic method, see Chapter 4.1.1. Fines from the disintegrated paper were separated by a dynamic drainage jar (DDJ) equipped with a 200 mesh wire. Ash content (525°C) in turn was determined from the fines according to ISO 1762:2001. MD and CD tensile strength values for MD/CD tensile ratio were determined according to ISO 1924-2:1994. Table 9 shows the paper properties.

Table 9. *Initial tests (trial series I), paper properties. Fibre orientation is measured as tensile strength MD/CD ratio. Total DDJ fines include both fibre fines and ash (525°C). Formation is given as Ambertec numbers and grammage variation in wavelength bands 0.3–3 mm and 3–30 mm from β-radiography measurements.*

Trial paper	MD/CD tensile ratio	DDJ fines, %			Ambert	β-radiography	
		Total	Fibre fines	Ash 525°C	σ g/m²	$\sigma_{0.3\text{-}3mm}$ g/m²	$\sigma_{3\text{-}30mm}$ g/m²
News A	3.20	31.2	25.6	5.5	3.9	4.3	3.0
News B	3.61	34.9	20.0	14.9	3.3	4.2	2.8

The adequacy of the delay time was tested by altering the delay and by monitoring whether the wet strength properties changed. The delay from the upper moistening unit and from the spray to the test draw was varied from 0.75 s to 2.75 s and from 1.8 s to 4.9 s respectively by altering the web speed between 2 and 4 m/s and the length of the web lead by utilising the storage path (item 10 in Figure 24). Re-wetting down to a DSC level of 80% was done only with two nip moistening units (2nd and 3rd moistening units in Figure 24). Further reduction in DSC needed to be done with the two-sided spray only because the joint use of the three moistening devices caused picking between the moistened web surface and the soft backing roll in both nips. However, newsprint B was too weak to be re-wetted to DSC 70% with the spray only. All re-wetting was done with distilled water. The measurements were taken from two reels in each settings combination, referred to here as trial points. At the trial points connected with an arrow, Figure 26**,** the same two reels were run at both trial points (the first part of the reels at a speed of 4 m/s and the last part at 2 m/s). 171 breaks per trial point were measured on average.

According to Figure 26, the measured breaking tension values do not change—irrespective of DSC or web speed—when the delay is controlled by altering the length of the web lead. This can be seen by comparing trial points 3 and 5 with each other, trial points 2 and 6 with each other, trial points 7 and 8 with each other and trial points 9 and 10 with each other. In contrast, the delay control with the web speed affects strength properties in nip re-wetting. This can be seen by comparing trial points 1 and 3 with trial points 2 and 4. The detrimental effect of speed increase is also very prominent when comparing trial points 2 and 5 with each other. Re-wetting at a web speed of 4 m/s may be somehow too harsh, causing structural damage to the paper structure and leading to a considerable reduction in strength. At DSC 80%, the reduction in breaking tension was 400–500 N/m when the web speed was increased from 2 m/s to 4 m/s.

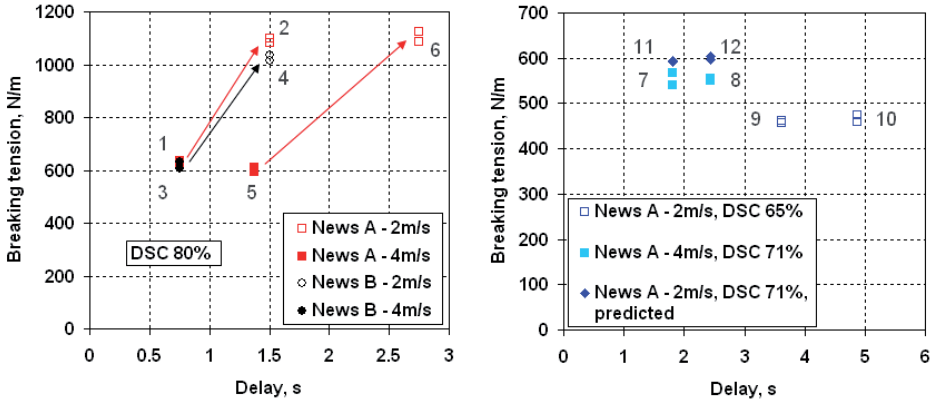

***Figure 26**. Breaking tension as a function of delay arranged by altering running speed and the length of web lead. The trial points connected with arrows were measured from the same paper reel. Two reels were run at every trial point. Re-wetting to DSC 80% with two nip moistening units and to 71% and 65% with two-sided spray moistening.*

In order to see whether the increase of web speed also causes strength reduction with spray moistening, breaking tension at a web speed of 2 m/s was modelled as a function of DSC. A second-order polynomial model was computed based on DSC and breaking tension values of dry paper and trial points 2, 6, 9 and 10. R^2 of the model was 0.99. With the aid of the model, the breaking tension values corresponding to trial points 7 and 8 were computed, marked by numbers 11 and 12 in Figure 26. As can be seen, only small differences are detectable between trial points 7–8, run at 4 m/s, and predicted points 11–12, web speed 2 m/s. Thus it can be concluded that spray moistening can be executed at both web speeds. In addition, it can be concluded that the delay of 1.5 s seems to be long enough in two-sided nip moistening when the target is DSC 80% and 3.7 s seems to be a long enough delay in two-sided spray moistening when the target DSC is 65%.

3.5.3 Second tests

In order to verify the findings of the first test, two other newsprints were tested. Both papers were manufactured on a roll-blade gap former to a basis weight of 45 g/m². The effect of the delay was studied by running one reel of both trial papers C and D Trial series II), see Table 10. This allowed 60 breaks per trial point on average. The settings for AHMA were similar to those in the first test run. However, only nip moistening was employed this time. The delay was varied between 0.75 s and 2.75 s by altering the length of the web lead between 3 m and 5.5 m and web speed between 2 m/s and 4 m/s.

***Table 10**. Papers for trial series II. Fibre orientation is measured as tensile strength MD/CD ratio and β-formation figures are given for wavelength bands 0.3–3 mm and 3–30 mm.*

Trial paper	Furnish		MD/CD tensile ratio	β-formation, g/m²	
				$\sigma_{0.3-3mm}$	σ_{3-30mm}
News C	TMP/RCF	40/60	NA	3.7	3.0
News D	RCF	100	3.80	3.8	3.0

The AHMA results confirmed the findings of the first test. Firstly, re-wetting at a speed of 4 m/s leads to low breaking tension values. Secondly, the delay can be controlled without affecting the breaking tension when it is done by altering the length of the web lead. Thirdly, 1.5 s seems to be a long enough delay for the two-sided nip application at DSC 80%.

3.5.4 Fastness of capillary penetration and diffusion

As a part of the estimation of the minimum required delay time from moistening to the test draw, the speed of the capillary penetration and diffusion was measured. The speed of capillary penetration through the paper was measured with KCL Clara (Lamminmäki et al. 2010). Distilled water was used. The measurement is based on the change in capacitance due to the movement of the average position of the liquid front after water is applied to one side of paper. Readings were recorded at 1 ms intervals over a period of 10 s. The measurements were taken with two small overpressures in the liquid chamber, 0.15 bar and 0.3 bar, to keep the samples straight during the measurement. When 95% of the maximum capacitance value was achieved, water was considered to have penetrated through the paper.

As Figure 27 illustrates, water penetrated through News A and B in 0.77 s and 0.83 s respectively when the overpressure was 0.15 bar. The corresponding values for 0.3 bar overpressure were 0.74 s and 0.73 s. These results are consistent with the result of Karppinen (2008) with an "infinite" amount of water available, see Table 11 (Pages 85–86). His measurement was done without any external pressure. The results show the capillary penetration to be very fast, even with no external pressure, when there is enough water available to fill the inter-fibre pores so that water does not need

to diffuse through the paper. A very rough estimate for the "infinite" water amount can be calculated with the aid of Equation (12) (Kajanto et al. 1998):

$$\phi = \frac{V - V_f}{V} * 100 = \left(1 - \frac{\rho}{\rho_f}\right) * 100 \qquad (12)$$

Where ϕ is the porosity

V is the volume of the entire sheet

V_f is the volume occupied by the fibres

ρ is the paper density

ρ_f is the fibre density (includes the porosity of the cell wall and uncollapsed lumen space of the fibres).

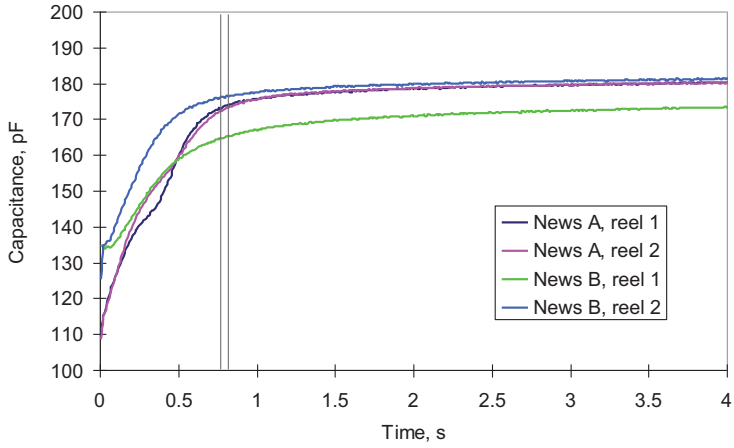

Figure 27*. Capillary penetration through the sheet. Basis weight 45 g/m². Over-pressure 0.15 bar. Distilled water. The verticals denote the point in time when 95% of the maximum capacitance was achieved, 0.77 s for News A and 0.83 s for News B.*

By selecting values 700 kg/m^3 for ρ and 1050 kg/m^3 for ρ_f, Equation (12) yields a porosity value of 33.3%. This value is close to the average value 30.3% measured for News E, see Appendix 3. These values correspond to a water volume 17.7 g/m² and 16.1 g/m² respectively, if all the added water was located solely in the inter-fibre pores (no fibre swelling). The corresponding DSC would be 66% and 68% respectively. Because the applied water amounts were 6.8 g/m² for 80% DSC and 18.7 g/m² for DSC 65% in AHMA, it is clear that water diffusion from fibre to fibre is of importance in water transport, especially at the lower application level.

In order to obtain an estimate for the speed of water diffusion into the fibres, the papers were tested with KCL Vesikko (Kananen 2003). The device measures the speed of in-plane dimensional changes. In the equipment, water is applied to a stationary paper web by a wetting roller attached to a moving sledge. Images of the bottom surface of the paper are taken through a glass table with a high-speed CCD

camera. The size of the imaging area is 40 mm x 40 mm. From the series of images obtained, the time-dependent expansion in CD and MD can be determined by image correlation analysis. The idea for the measurement was that, in order to induce dimensional changes to the fibres, which are further transferred to dimensional changes of the fibre network, water needs to be absorbed by the fibres. The point in time when no changes in the fibre network dimensions occur can be considered to reflect the situation when all the available water has diffused into the fibres.

The distilled water amount was 5.5 g/m² into newsprint C and 7.2 g/m² into newsprint D, measured by a lithium tracer mixed into the water. The corresponding DSC values were 82% and 79% respectively. The Vesikko settings were: web tension 150 N/m, nip speed 0.5 m/s and loading 4.8 kN/m, corresponding to an average nip pressure of 4.8 bar with an estimated 10 mm nip length. The estimated dwell time in the nip was 20 ms. High external pressure accelerates the capillary penetration remarkably. For example, the sorption model of Ketoja et al. (2001) predicted the 4 g/m² water film to penetrate into the inter-fibre pores of 45 g/m² newsprint within 20 ms in KCL Vesikko. This is 1/10 of the time taken when there is no external pressure, see Table 11 (Pages 85–86). See also the results of Salminen (1988), Table 11.

In contrast to capillary penetration, the water transport into the fibres is primarily diffusion controlled, which means that the external pressure does not have any influence on the water transport rate into the fibres (Salminen 1988). In addition, fibre swelling and fibre network expansion are controlled by water diffusion into and inside fibres, not by capillary penetration (Hoyland 1977a, Bristow 1986, Takahashi et al. 1997, Lyne 2002). Thus KCL Vesikko is a suitable device for monitoring water diffusion into and inside the fibres as a function of time. The frequency of the CCD camera was 160 frames/s. Figure 28 shows the results as an average of five measurements.

Because swelling is the inverse phenomenon to shrinkage, the shape of the curves in Figure 28 can be considered on these grounds. During water removal, both chemical and mechanical pulp fibres suddenly shrink at the end of drying with the removal of the last water fraction, non-freezing bound water, from the amorphous domains in the fibre wall. This isotropic shrinkage phenomenon, shrinkage phase two, occurs approximately beyond DSC 85%. During the preceding shrinkage phase, the removal of free water from the large pores in the cell wall causes the lamellae to approach each other. This leads to shrinkage perpendicular to the lamellae layers with change in the shape of the fibre cross-section and possible lumen collapse but without changes in fibre width, shrinkage phase one. (Nanko et al. 1991, Weise et al. 1996, Weise and Paulapuro 1998.) Thus the steep increase in the fibre network expansion curves in Figure 28 reflects the recovery from shrinkage phase two with the modest increase reflecting recovery from shrinkage phase one.

According to the results (Figure 28), water absorption into the fibres was completed in 1.5–2.5 s. These values are highly congruent with the result of Ketoja et al. (2001), according to which 90% of applied water was absorbed into the fibres within 1.5 s. However, 3 s was required to reach an absorption level close to 100%. See also the values concluded from the results of Paaso (2007) and Karppinen (2008), Table 11. A possible explanation for the difference between our results and close to 100%

absorption results is the measurement method. Ketoja et al. and Paaso and Karppinen measured the water penetration directly but we measured the water-induced expansion of a fibre network. The last diffusing water fraction may cause such an insignificant change in network expansion that it remains unnoticeable. The estimate for the adequate absorption time may therefore remain too low in the Vesikko measurements.

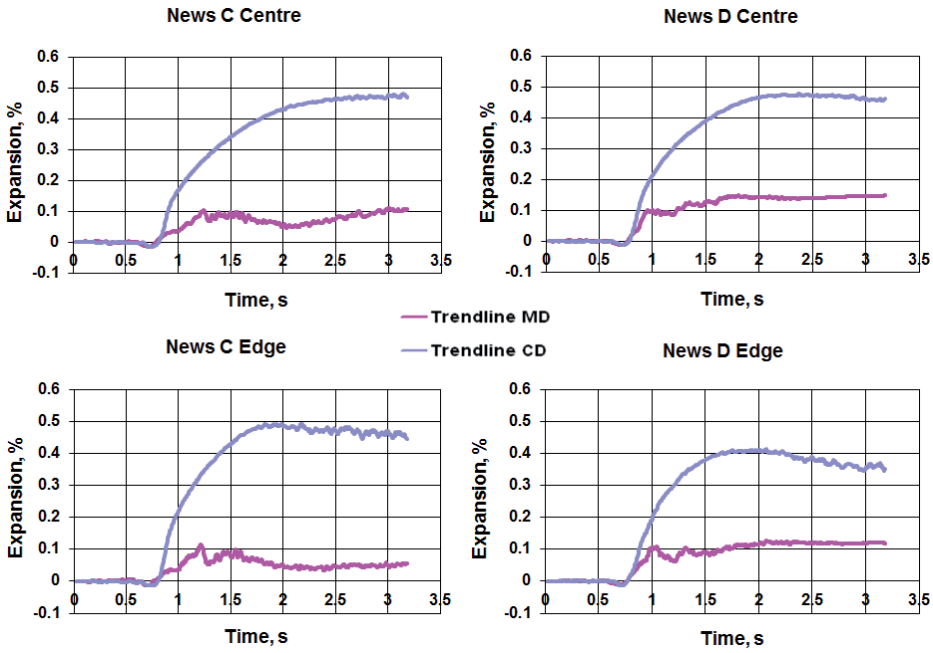

***Figure 28**. Expansion of paper in KCL Vesikko as a function of time. The moistening nip passes the strain calculation area between 0.72 s and 0.80 s. The samples are taken from the centre and edge position reels.*

Based on the results of Table 11, it can be estimated that with the target DSC being 80%, approximately 3 s is enough for water absorption into the fibres to be nearly completed in a one-sided nip application. Based on Equation (11), it can be estimated that the delay of 3 s would be only 0.75 s in a two-sided nip application (the penetration depth is reduced by 50%). This delay appears surprisingly short. However, if the results achieved in AHMA at a web speed of 4 m/s are accepted, the delay of 0.75 s appears to be long enough. This is evident when comparing trial points 1 and 5 with each other in Figure 26. In any case, the AHMA results at a web speed of 2 m/s showed 1.5 s to be long enough.

Table 11. *Water penetration into paper as a function of time. In the event of momentary water application, time in any result row denotes the time starting immediately after moistening (table continues on the next page).*

Reference	a) Paaso 2007 b) Lehtonen 2005	Karppinen 2008	Ketoja et al. 2001	Salminen 1988
Paper grade	Wood containing base paper for coating	Wood containing pilot paper	Newsprint	Two wood-containing base papers for coating
Basis weight, g/m²	a) - b) 41	50	45	52
Measuring method	NIR spectroscopy: transmission and reflection	Light transmission and reflection	Light transmission (KCL Vesikko) and modelling	Volumetric measurement for applied water
Type of information	Semi-quantitative	Semi-quantitative	Quantitative	Quantitative
Outcome	Water movement in ZD and water location as a function of time	Water movement in ZD and water location as a function of time	Water movement in ZD and water location as a function of time	Volume of absorbed water as a function of time
Application method	One-sided momentary spraying	a) One-sided momentary spraying (100 ms) or b) injection of large water droplet [1)]	One-sided roll application	One-sided nozzle application
Amount of transferred or available water	Water film on the paper surface. Film thicker in b) than in a)?	a) 12.6 g/m² corresponding to DSC 76% b) "Infinite"	4 g/m² corresponding to DSC 85%	"Infinite", DSC controlled by the contact time with the nozzle
Quality of water	-	Distilled / deionised	-	-
External pressure p_e	0	0	>0 during application, 0 after that	Adjustable

1) The droplet diameter was much larger than the thickness of the sample and the diameter of the observed area.
NIR denotes near-infrared spectroscopy.

***Table 11**. Continuation.*

Reference	a) Paaso 2007 b) Lehtonen 2005	Karppinen 2008	Ketoja et al. 2001	Salminen 1988
Results	Water film disappeared within 0.2 s for (a) and (b)		Water film disappeared within 0.02 s	DSC 76% achieved within 0.2–0.6s [4] (p_e = 0 atm)
Results	Transition from capillary dominant to diffusive dominant absorption at approx. 0.6 s (a) and 0.5 s (b)	Transition from capillary dominant to diffusive dominant absorption at approx. 0.6 s (a) and 0.5 s (b) [2]		DSC 56% achieved within 0.8–2.3s [4] (p_e = 0 atm)
Results	a) Water absorption into fibres nearly completed within 3 s [2]	a) Water absorption into fibres nearly completed within 5 s [2]	90% of applied water absorbed into fibres within 1.5 s [4] and nearly 100% within 3 s	DSC 56% achieved within 0.2–0.4s [4] (p_e = 0.15 atm)
Results	Even moisture profile in ZD at approx. 30 s (a)[3] and 3.5 s (b)	b) Major water transition occurred in ZD at approx. 1s	Roughly even moisture profile in ZD at approx. 10s	DSC 56% achieved within 0.05–0.06 s [4] (p_e = 0.6 atm)

2) Concluded by the writer, based on the comparison of the results in the references Paaso 2007, Lehtonen 2005, Karppinen 2008 Salminen 1988.
3) Extrapolated from the graph.
4) Estimated from the graph

Because the amount of applied water to reach DSC 65% in a two-sided spray application was fairly high, 18.7 g/m², and close to the theoretical "infinite" water amount of 16.1 g/m² (based on News E), it is reasonable to utilise the linear relationship to estimate the required delay time. Salminen (1988, 2010) noticed that, with zero external pressure and with "infinite" water resources, water transport into paper, rather than being proportional to the square root of time, is often linearly dependent on the penetration time until the paper starts to be fully saturated. For example, in his material for three modern LWC base papers the linear relation continued up to an applied water amount of 20–30 g/m² depending on the paper. Of course, this linear relationship does not tell us anything about water distribution between inter-fibre pores and fibres. However, diffusion into fibres is fast, as

discussed in Chapter 3.5.1. In addition, diffusion into fibres and capillary penetration are coexistent phenomena. Thus the usage of the linear relation is justified. If 1.5 s is considered a long enough delay for DSC 80% also in spray moistening, a delay of 4.2 s is enough for DSC 65% according to the linear relation. This result is highly congruent with the results of the first AHMA test, trial points 9 and 10 in Figure 26.

It is likely that an even moisture profile in the z-direction cannot be achieved within the delay times used in AHMA tests, see Table 11. However, based on all the discussion above, it is assumed in any case that most of the water reaches "the final destination", meaning that the final equalisation would have only a minor effect on the measured wet strength properties. Thus the following conclusions can be made:

- A web speed of 4 m/s is unsuitable for re-wetting in nip moistening.
- In two-sided nip moistening down to DSC 80%, the delay of 1.5 s is long enough.
- The delay of 3.7 s (based on the measured results, Figure 26) is long enough in two-sided spray moistening with the target DSC being 65%.

3.5.5 Development of a new re-wetting system

Although the effect of a probably uneven ZD moisture profile was not seen to have any influence on wet strength, a new re-wetting system was tested. The target was to develop a system enabling a fundamentally longer delay time than that possible with online moistening. The idea was to perform re-wetting with a spray on a separate winder and to seal the re-wetted reel after this in a plastic sack for 1–2 hrs to allow moisture equalisation. The only possible place for the spray was in front of the winding stack of the separate winder used to slit AHMA rolls. However, the DSC profile was strongly U-shaped due to air flows generated by the rotating reel ends. Plates situated close to the reel ends were tested as air flow dampers but the result was insufficient. Another problem was that wrinkles were created in the paper when the reel was kept in a plastic sack for 1–2 hrs. As a result of these problems, the decision was to do re-wetting in AHMA.

Because of the failure of the old spray device, new equipment consisting of a low pressure spray set with pump and flow control unit was installed by Metso Automation. In the system, the water is mixed with air at the nozzle exit, producing small water droplets. The water flow for each nozzle can be controlled independently from the other nozzles with rotameters. The nozzles were located in four rows to provide even coverage, see Figure 29. An embossed metal plate was installed to support the web in spraying.

The new re-wetting system was utilised in the last trial series with the target DSC levels being 56% and 68%. The spray was used together with the upper nip moistening unit to reach the lower target DSC. For the higher target DSC, the nip moistening was turned off but the nip was kept closed. In order to avoid picking, the lower moistening nip was kept open in all the runs with the new system. This arrangement therefore led to one-sided water application. As a result, the web speed was reduced to 1 m/s, allowing a delay of 12.2 s from the last spray nozzles to the test

draw and 8.5 s from the upper moistening nip to the test draw. Distilled water was used in all the runs and the re-wetting system worked well.

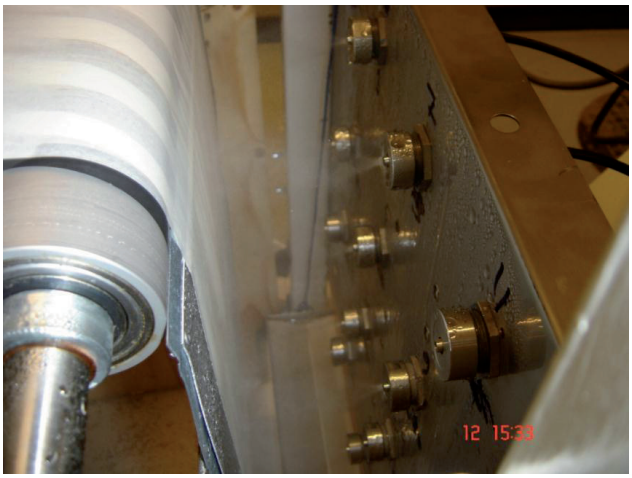

***Figure 29**. The spray unit (mounted between two white pillars). All the nozzles are in use except no. 11.*

Reaching DSC 56% and 68% in trial papers E1–E6 requires a water application of 28.9 g/m² and 15.9 g/m² respectively. The "infinite" water amount for News E is on average 16.1 g/m², as discussed above. By using the linear relation between the penetration time and water transport, it can be calculated that 3.7 s is a long enough delay at DSC 65% with a two-sided spray and 6.3 s is adequate for a one-sided spray at DSC 68%. Using Equation (11), the respective value is 10.7 s. As such, the 12.2 s delay from the spray to the test draw is long enough.

When DSC 56% is targeted, roughly half of the water is applied by the spray and half by the moistening nip. Filling of inter-fibre pores is a very fast phenomenon, firstly because nip application with an average pressure of 5.5 bar and dwell time of 20 ms causes an effective piston method of filling of the inter-fibre pores, secondly because there is a surplus of water to fill the expanding fibre network after the pressure pulse and thirdly because inter-fibre pores full of water provide an adequate water resource for fast water diffusion into the fibres. Thus it can be concluded that the combination of delay times, 12.2 s from the last spray nozzles to the test draw and 8.5 s from the upper moistening nip to the test draw, is adequate.

3.6 Development of analysis procedure for the measured data of the runnability pilot

3.6.1 Background

According to the author's knowledge, there are no published results related to running press dry reels in AHMA using the "web break mode". Instead, the "rheology mode" has been employed (Tanaka et al. 2009). This method is robust in that signal noise does not affect the measured tension values. The reason is that each tension value is an average of 300 readings of the tension signal recorded at 10 ms intervals when running AHMA at a constant speed difference. However, because one of the research aims was to investigate the statistical properties of press dry papers, the "web break rate mode" was employed instead of the "rheology mode" to ensure a sufficiently large number of breaks. The target was to run 100 breaks per trial point. Wathén and Niskanen (2006) suggest that at least 75 breaks need to be measured in order to obtain a reliable estimate for the Weibull modulus.

In the two first trials (News A, B, C and D), there was an intense noise in the tension signal, which was filtered with a 3 Hz low pass filter (Figure 30) and the maximum values were used as tensile strength values. Based on visual evaluation, this procedure seemed to enable fairly accurate results.

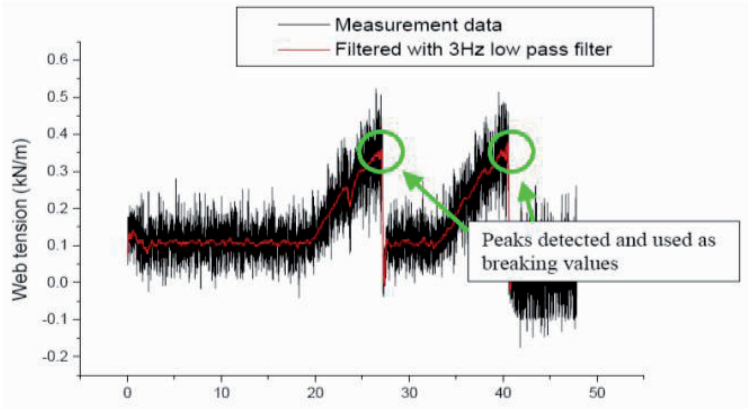

***Figure 30**. An example of the tension data from the first two trials.*

The situation was different in the third trial with News E and LWC base papers A and B. Analysis of the tension and strain signals after the trial revealed that a clear 0.61 s cyclic variation had appeared in the tension signals in addition to the noise present already in the previous measurements. The combination of those two disturbances was so intense compared with the average tension values of wet papers that it hampered the analysis of the results. The same disturbances were also noticeable with dry papers but their impact on the results computed from the tension signals remained

tolerable because of high average values. Noise and the cyclic variation could also be observed in the strain signals, though clearly to a lesser degree.

Another challenge at the lower dry solids content, 56%, was the small tension difference between the high initial tension, on average 185 N/m, and the breaking tension, on average 250 N/m. According to the system logic, the measured initial tension in the test draw always needed to be higher than 25% of the first measured pretension (item 5 in Figure 24) to allow the speed of the pulling nip to be increased. Although the first pretension was set very low at 80 N/m (item 5 in Figure 24), the initial tension in the test draw needed to be set high to keep the measured tension constantly above the control limit due to the combined effect of noise and cyclic variation in the measured tension signal. The initial tension is controlled by the minimum speed difference between the pulling and braking nips. The other pretensions were set to 80 N/m and 88 N/m respectively (items 8 and 11 in Figure 24).

Inevitable questions arose as to whether the wet paper experienced some additional cyclic straining in the test draw and what caused the variation. A study was therefore carried out to investigate the reasons for the disturbances noticed and possible consequences in wet paper. AHMA was run at different speeds with and without the dry trial paper News E4. The roll diameters in AHMA were measured with a slide gauge. Rotating frequencies were measured with a stroboscope (Bryel & Kjaer type 4912). Vibrations were measured with portable CSI apparatus and analysed using AMS Suite Machinery Health Manager Software. The vibration sensor was mounted using a magnet. Vibration was examined both as speed and displacement. In addition, paper from the same roll ran in AHMA was taken to The TAPIO® Paper Machine Analyzer (Hilden and Paerento 2000) to discover any possible paper-related reasons for the cyclic variation in the tension signal.

The only noteworthy cyclic variation found in the paper was thickness variation. All the basis weight variations were residual variations only. The paper variations were found neither in the tension nor in the vibration signals. The paper roll rotating frequency was not found in the tension either.

There were no fluctuations in the rotating speed of the rolls in the brake and pulling nips (measurement accuracy +/- 0.002 Hz). It turned out that the vibration of the brake and/or draw nip top rolls was transferred to the tension sensor, causing a major part of the disturbance in the tension signals. The band pulleys in the test draw, driving the wires that carry the broken web to the pulling nip in tail feeding, contributed to the signal disturbance. The important thing is that the maximum displacement of the tension sensor caused by the vibration was only 80 μm when driving 10 m/s without paper. The lower the speed was, the smaller the vibration. When running with the paper, the vibration reduced further. Because the vibration sensor is integrated into the brake nip, the displacement of the brake nip cannot be larger than that of the sensor. The observed 80 μm displacement corresponds to 0.008% length change in the 1 m long test draw. This means that the web had not experienced any consequential strain due to the vibration.

As an additional control, two data sets measured when running a paper at DSC 56% were visually examined break by break. It was investigated whether the web break frequency was concentrated at a specific point of the cycle. The cycle was divided into four sections: top, descending, bottom and ascending. The break frequency seemed to be distributed fairly evenly, with the highest share of 28% being in the descending section and the smallest share of 22% in the bottom section. This confirms the aforementioned conclusion about the vibration not having a considerable effect on web strain.

However, due to the intensity of the measurement disturbances in relation to the low strength of the moist paper web, it was clear that the procedure described in Figure 30 to produce strength and strain values when running AHMA by the "web break mode" was not suitable. Instead, a new procedure needed to be developed.

3.6.2 Development of the computation procedure

The following questions needed to be answered when developing the computation procedure:

- Where exactly does each web break occur?
- What is σ just before each break (i.e. breaking tension)?
- Where exactly does each ramp begin?

It is relatively easy to find answers to those questions with the naked eye, but developing a robust algorithm is not as simple. Various options for identifying breaks and breaking tension were tested. For example, the tension signal was filtered either by median or low-pass filter and the maximum value preceding a break (tension < 0 N/m) was determined. However, this option was rejected because filtering strong enough to attenuate the fluctuation distorted the original signal, resulting in breaking tension estimates that were too low, see Figure 31.

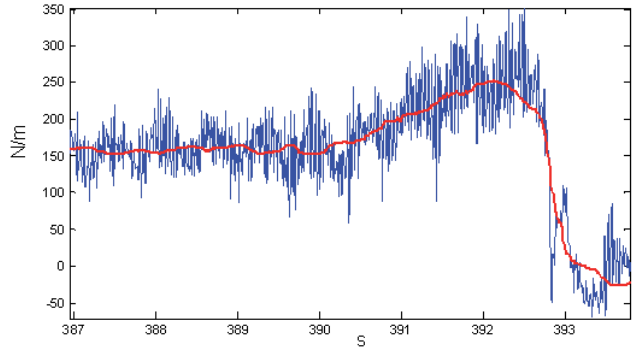

Figure 31*. Tension signal, original (blue) and filtered with 101 point median filter (red). DSC 56%.*

To give another example, line fitting was tested as means of filtering, see Figure 32. From the breaking point (tension < 0 N/m), it was moved 10 data points backwards

(100 ms) because sometimes the tension decreased gradually. From this point, a straight line was fitted for 1.2 seconds of data. The upper end of the line was taken as breaking tension. The length 1.2 s was selected because it corresponds to two cycle lengths of the strong 0.61 s noise component. The problem with this method was that breaking sometimes occurred in much less time than 100 ms, pushing the starting point of the line fitting to the left, see the left break in Figure 32. This led to underestimating of the maximum tension. At the same time, however, the tension reduction in some breaks was so gradual that 100 ms was not enough. This caused a negative slope for the fitting line, making the determination of the breaking tension very questionable, see Figure 33. As such, this method was also rejected.

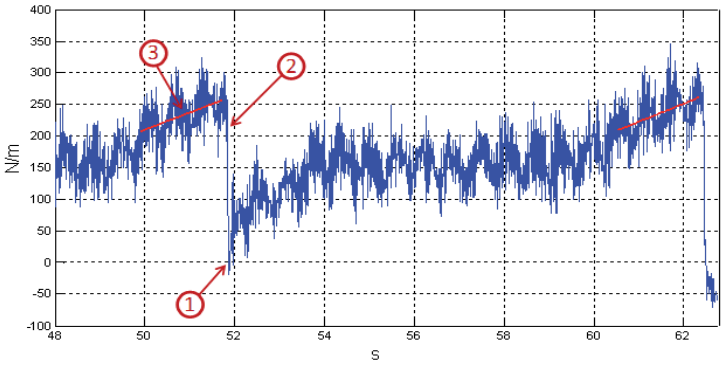

***Figure 32**. Line fitting: 1. Break point (tension < 0 N/m), 2. 10 data points backwards => starting point for line fitting, 3. Fitting a line for 1.2 seconds of data. DSC 56%.*

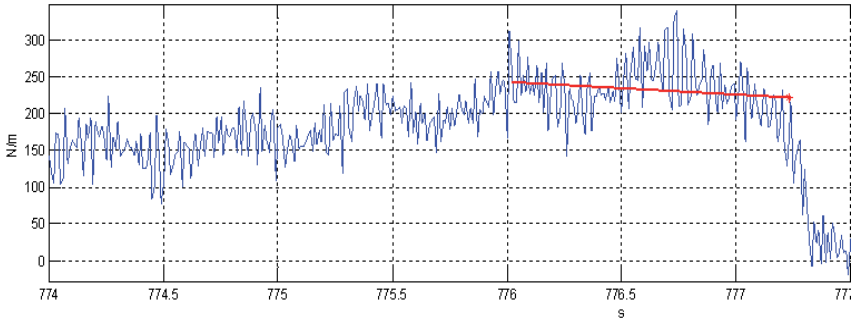

***Figure 33**. Line fitting when the tension reduction is very gradual. 10 data points backwards is not enough => fitting line very questionable. DSC 56%.*

3.6.3 Non-linear curve fitting

When analysing the data, it was noticed that the average rupture behaviour followed a certain pattern, although the behaviour of individual breaks varied. For example, some breaks at DSC 68% seemed to be just a straight line. The average rupture pattern can be easily seen when the measured tension values (raw data) of individual

breaks are superimposed from 0 s backwards, see Figure 34. The end point 0 s denotes the point in time 100 ms backwards from the point where tension had reached the level 0 N/m. At DSC 68%, all the papers followed, on average, the pattern plotted in red. At DSC 56%, the average behaviour was more variable. LWC base papers A2 and A3 followed the pattern plotted in blue, but LWC base papers A1, B1 and B2 displayed the pattern plotted in red. The pattern for newsprint was between the two shapes described in Figure 34. Interestingly, Robertson (1959) found the same three behaviours when determining stress-strain curves for wet laboratory samples at different dry solids contents.

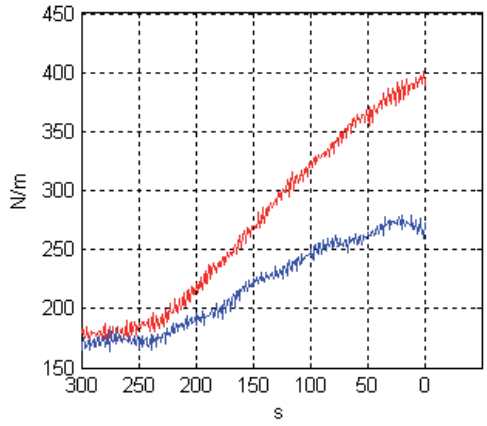

Figure 34. *An average tension development as a function of time until rupture at the point 0 s (i.e. 100 ms to the left from the point where tension has dropped to 0 N/m). LWC base paper A3 at DSC 56% (blue) and 68% (red).*

It was considered that differences in the rupture pattern could reflect not only the effect of DSC but also the effect of differences in the paper structure. Thus in order to model the breaking behaviour of all different types of breaks accurately enough, a non-polynomial model was considered necessary. However, before carrying out any fitting the beginning of the ramp needed to be defined for each break. This was done by utilising the speed difference ramp because there was only mild variation in the speed difference signal, see the top diagram in Figure 35. The reason for the variation is the same as in the tension signal.

The starting point for ramping was determined by iteration as follows: the upper end point was selected from the speed difference ramp at the point in time that corresponds to the point 300 ms backwards from the breaking point (tension < 0 N/m), point (1) in Figure 35. The lower end point (2) was taken 1.2 s earlier. A line was fitted between these two points (3) by utilising the least squares method. After the fitting, the line was interpolated or extrapolated until it intersected the minimum speed difference (e.g. 0.6% for newsprint) + 0.2% (4). The intersection point was recorded and the respective data point (5) was used as the lower end point in the next iteration. A line (6) was fitted between the new lower end point and constant upper end point. The intersection point with the minimum speed difference (7) was recorded

and used as the lower end point in the next iteration. Typically, the fitting did not improve after the second or third iteration round. The final lower end point was selected as the starting point for ramping.

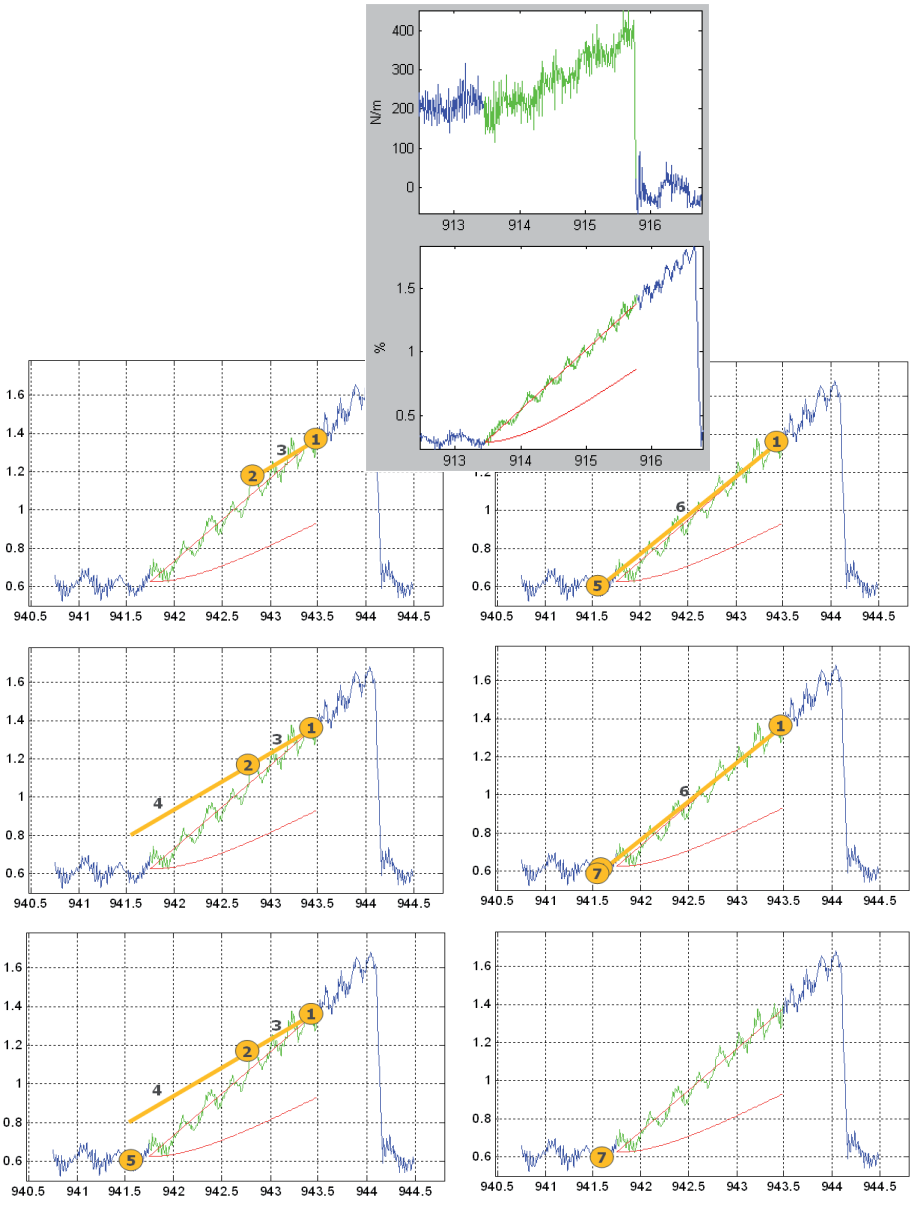

***Figure 35**. Top diagram: Tension development as a function of speed difference, and a speed difference ramp. Bottom diagrams: The iteration principle. x-axis as seconds. DSC 68%.*

The reason for selecting the higher intersection level, minimum speed difference + 0.2%, instead of the minimum speed difference only was that in some newsprint breaks at DSC 56% the ramp was so short that without selecting the higher intersection level the fitted line would not have been located in the ascending ramp. This would have led to difficulties in determining the ramp starting point. The tension as a function of speed difference and the speed difference ramp in the upper diagram are not related to the lower diagrams. The idea is to demonstrate the variation difference in the tension and speed difference signals. In addition, the diagram shows the linear rupture pattern seen occasionally in some breaks. The lines drawn in the bottom diagrams are not real fittings. Line 3 is clearly slanted in order to demonstrate the iteration idea.

A non-polynomial model was developed to represent the shapes of the observed stress-strain curves. In order to reduce the risk of over-fitting (i.e. using more parameters than needed for adequate presentation of the phenomena generating the data), the model was to include only a reasonably small number of parameters to be identified from the data. In the developed model (13), the parameters a and d represent the linear part of the stress-strain curve. Parameters b and c affect the slope of the curve; they determine at what level of strain and how rapidly the slope starts to decrease.

$$\sigma(\varepsilon) = a(1 - \exp(b\varepsilon + c))\varepsilon + d \tag{13}$$

$$\sigma(\varepsilon) = a\varepsilon + d \tag{14}$$

where σ is the tension
ε is the strain
a, b, c, d are the parameters to be identified from data.

The non-polynomial model (13) and the straight line (14) were fitted to each break with the fitting domain extending from the ramp starting point to the breaking point (i.e. 10 data points backwards from the point where tension < 0 N/m). Strain ε was computed as a real strain according to Equation (8). A non-zero value for the offset parameter d is needed only when there is already some tension in the web before ramping begins. This is the case on AHMA, where the initial tension affects the web in the test draw before ramping.

The reason for using model (13) instead of the 3rd degree polynomial, typically used to model the stress-strain curve, was the idea mentioned earlier of utilising the plateau and descending part of the curve as sort of a characteristic for the interaction of the web structure and rupture mechanism.

3.6.4 Akaike's information criterion

After the set of candidate models (g_i) , in our case models (13) and (14), have been identified, the parameter fitting and the selection of the best model can be performed based on Akaike's information criterion (AIC) (Akaike 1973).

$$AIC = -2\log(L(\hat{\theta})) + 2K \qquad (15)$$

where log denotes natural logarithm

$\log(L(\hat{\theta}))$ is the maximised value of the log-likelihood function $\log(L(\theta))$ and

$L(\theta)$ is the likelihood function of the estimable model parameters θ, given the data and the model g_i

K is the number of estimable parameters in a candidate model.

AIC is computed for each of the candidate models g_i and the model with the smallest value of AIC is selected as best. It is this model that is estimated to be "closest" to the unknown reality f that generated the data, or in other words, the least amount of information is lost when g_i is used to approximate f (Kullback-Leibler Information) (Burnham and Anderson 2002). Because the maximum likelihood function $\log(L(\theta))$ favours over-fitting and the maximised log-likelihood value is biased, a bias correction or penalty term (the second term on the right-hand side in Equation (15)) is needed. When K increases, the first term on the right-hand side decreases and at the same time the second term increases. This leads to a balance between under-fitting and over-fitting.

3.6.5 Method used

For simplicity, models (13) and (14) were fit to the measured data at every single break by the least squares method instead of computing maximum likelihood estimates. AIC values were computed with the formula (Burnham and Anderson 2002):

$$AIC = n \cdot \log(\hat{\sigma}^2) + 2K \qquad (16)$$

where n is the sample size

$\hat{\sigma}^2$ is RSS/n

RSS is the residual sum of squares

K is the number of estimable parameters in a candidate model +1 (1 for σ^2).

When using method (16), all the candidate models should assume normally distributed errors with a constant variance in order to provide the same AIC value with method (15) (Burnham et al. 2002). It cannot be expected that model (13) meets this criteria. This means that in those breaks where the AIC values of both candidate models are close to each other, methods (15) and (16) may rank the models differently. This would cause a small difference in estimated tensile strength. However, the number of this kind of occasion is most likely limited and secondly, the

effect on tensile strength is small. This means that the average strength and strength distribution of the whole break population would not change considerably. This justifies the usage of the mathematically simpler method (16), i.e. the likelihood function does not need to be formulated.

The fitting of the non-linear model (13) was based on iteration, which was continued until the model did not improve any more. The iteration started with fitting the line (14). This provided parameter values *a* and *d*, which were selected as starting values for fitting the curved part of the model (13).

The algorithms developed to compute the starting point for ramping and real strain, to carry out model fitting and, based on AIC values, to select the better model from the candidate models (13) and (14) were implemented in Matlab. A visual check revealed that although model (13) was able to describe fairly well the larger shape of the tail of the stress-strain curve (Figure 36), the fitting was, however, quite frequently prone to model the shape of the last cycle of the measurement disturbance instead (Figure 37). Accurate visual evaluation, comprising a large number of breaks, showed that this led to slightly erroneous breaking tensions. Due to this reason and because the stress-strain curve at DSC 68% typically did not show any bending downwards, the computation was changed. An iteration for finding the maximum breaking tension was done so that the curve tail was not allowed to bend downwards. In practice, this was executed by omitting the last few data points one by one until the criterion was met, see Figure 37. After the modification of the computation procedure, all the curve fittings done for newsprint and LWC base papers at DSC 68% were evaluated visually. The outcome was that model (13) now provided a good fit.

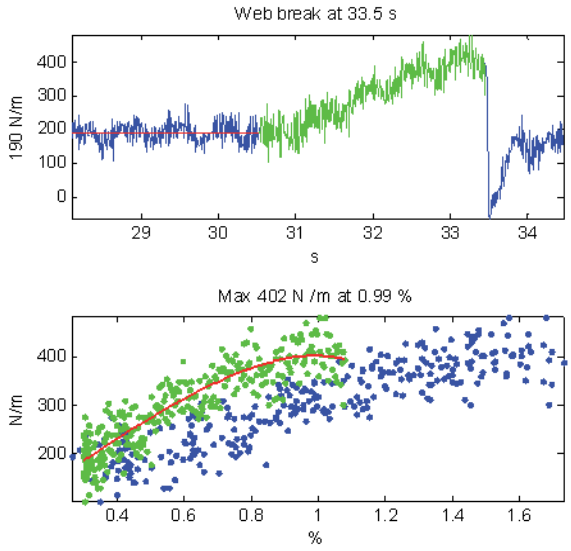

***Figure 36**. An example of curve fitting. Upper diagram: Raw data, initial tension 190 N/m. Lower diagram: Fitting models the shape of raw data fairly well. Fitted curve (red), speed difference between the pulling and brake nips in AHMA measured in 10 ms intervals (blue dots), and corresponding strain values (green dots).*

Because the pattern of the stress-strain curve was more variable for breaks at DSC 56%, the original calculation method was employed. However, the modelling was checked visually. In those breaks where the fitting clearly modelled the last cycle of the measurement disturbance, the fitting was amended by omitting the last few data points as shown in Figure 37. This provided a better fit.

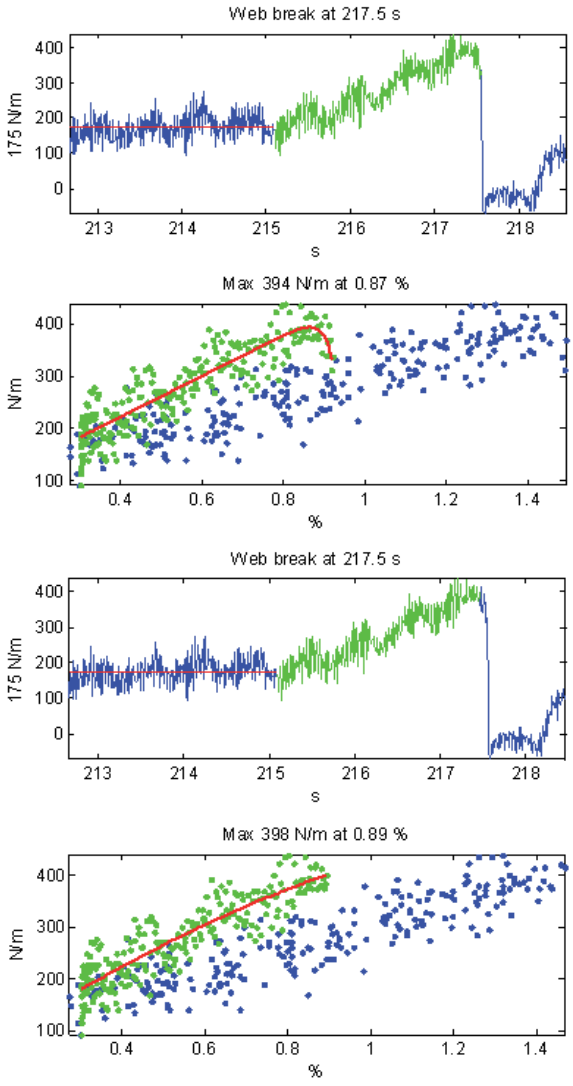

Figure 37*. An example of curve fitting. 1st diagram at top: Raw data, initial tension 175 N/m. 2nd diagram: Fitting models the shape of the last cycle of the measurement disturbances instead of showing the overall shape. 3rd diagram: The new iteration routine omits the last few data points to avoid the curve tail bending downwards. 4th diagram: Tension as a function of straining. Fitted curve (red), speed difference between the pulling and brake nips in AHMA measured in 10 ms intervals (blue dots), and corresponding strain values (green dots).*

The cyclic variation caused challenges in curve fitting and thus the original idea to utilise the plateau and descending part of the stress-strain curve as a sort of characteristic for the interaction of the web structure and rupture mechanism was abandoned.

The same algorithm, used for wet webs, was used for computing the maximum breaking tension of dry papers. The bottom of Figure 38 shows a good fit. However, in some occasions neither model (13) nor (14) provided a good fit as the bottom of Figure 39 shows. Due to this reason the procedure was changed for all dry papers by fitting only the data 2.4 s backwards from the breaking point (tension < 0 N/m). Based on the visual evaluation the fit was very good, see the top of Figures 38 and 39. On average, it was better than the achievement possible when fitting from the ramp starting point onwards. Instead, the tensile stiffness was determined as the initial slope of the curve/line fit for the entire data.

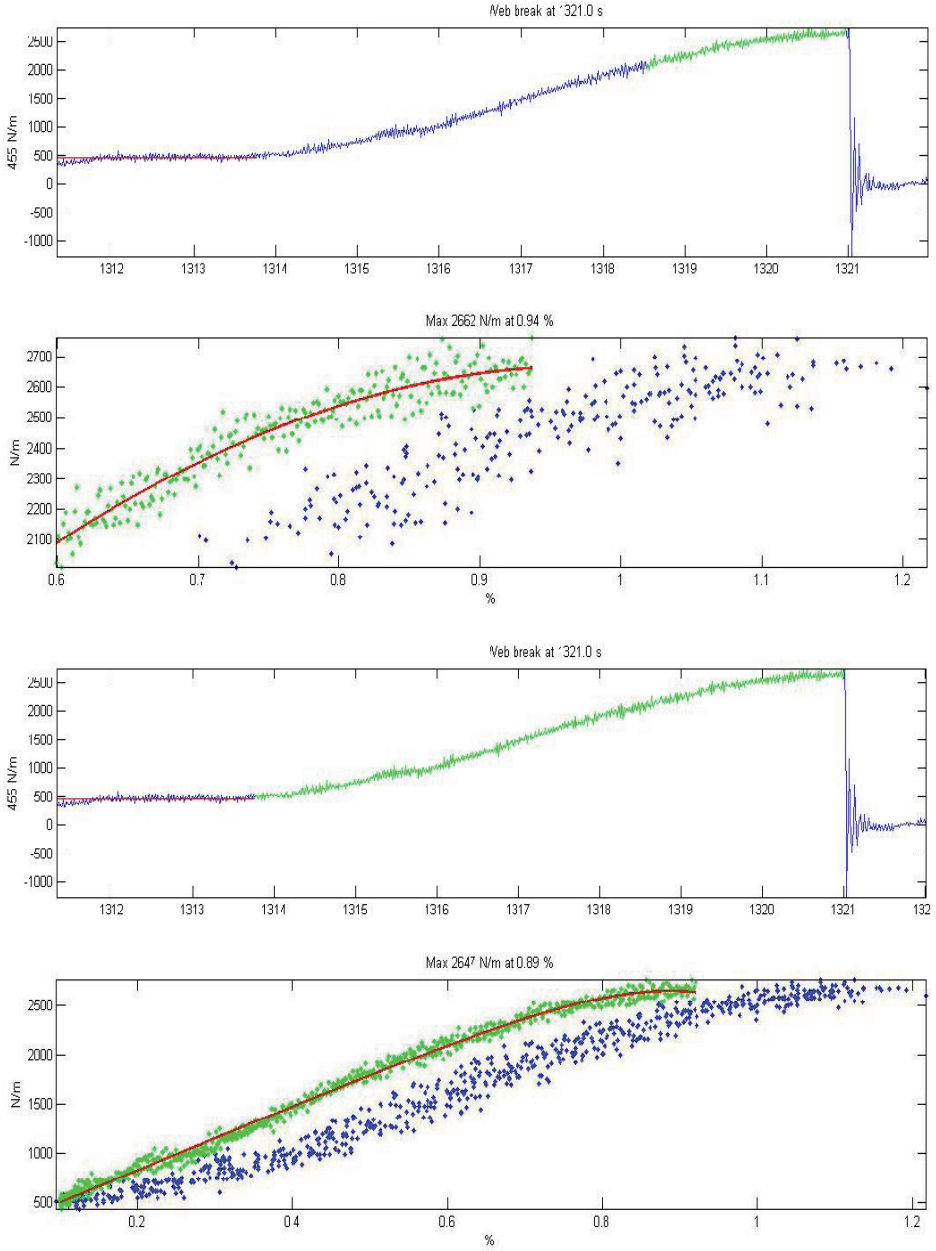

Figure 38. *An example of curve fitting. Speed difference between the pulling and brake nips in AHMA measured at 10 ms intervals (blue dots), and corresponding strain values (green dots). 1st diagram at top: Raw data, of which 2.4 s backwards from the break is marked in green. 2nd diagram: Model (red) for the last 2.4 s of data. 3rd diagram: The entire raw data (green) to be modelled. 4th diagram: Model (red) for the entire data, good fit. Both models give approximately the same breaking tension, 2662 N/m and 2647 N/m.*

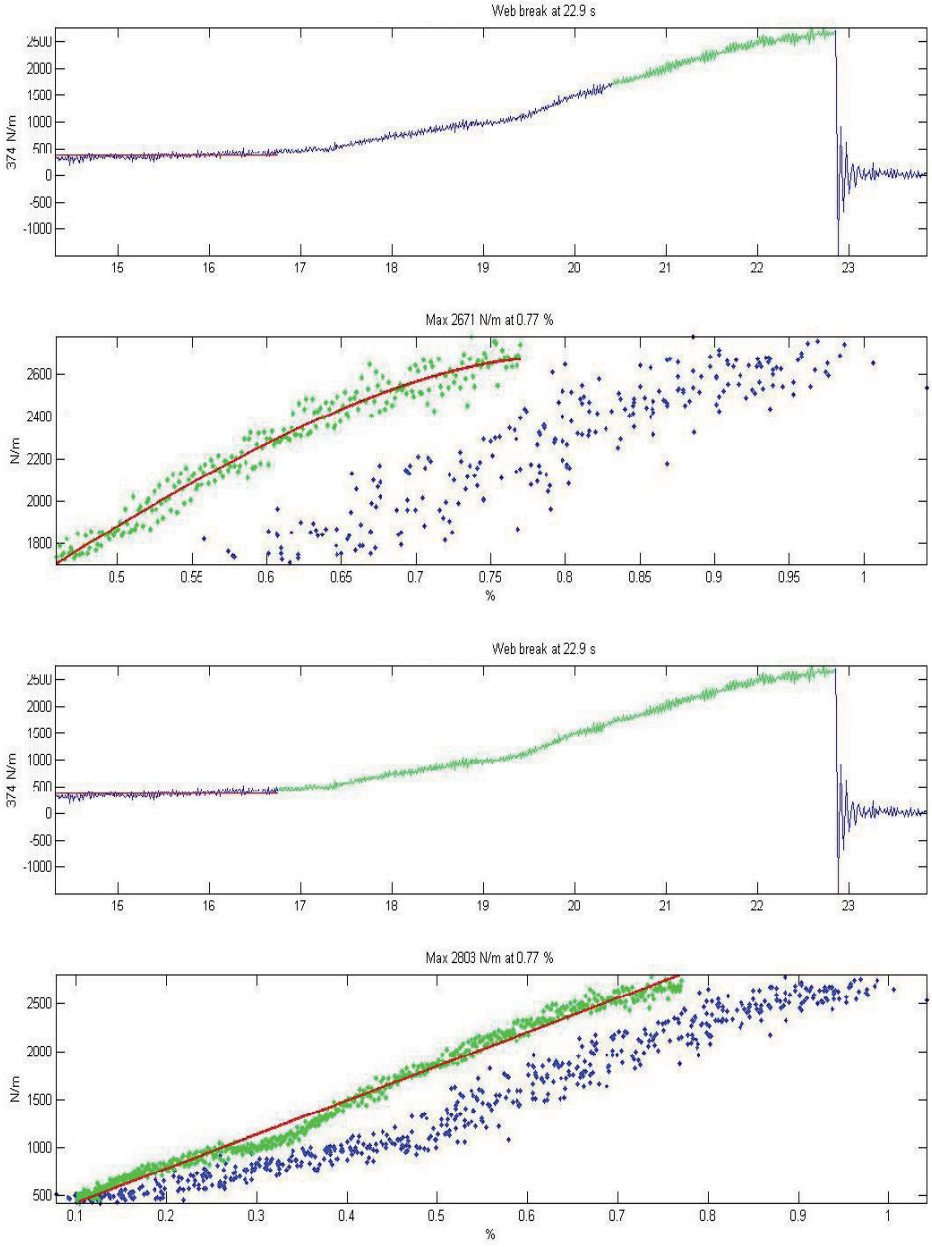

Figure 39. *An example of curve fitting. Speed difference between the pulling and brake nips in AHMA measured at 10 ms intervals (blue dots), and corresponding strain values (green dots). 1st diagram at top: Raw data, of which 2.4 s backwards from the break is marked in green. 2nd diagram: Model (red) for the last 2.4 s of data. 3rd diagram: The entire raw data (green) to be modelled. 4th diagram: Model (red) for the entire data, poor fit. The models give different breaking tensions, 2671 N/m and 2803 N/m.*

4 EFFECT OF PAPER STRUCTURE ON TENSILE STRENGTH AND TENSILE STIFFNESS

4.1 Structure measurements

In the following section, the paper structure is described by local grammage variation, different type of fibre orientation methods, filler distribution and different porosity parameters. The results are based on trial series III (News E1–E6, LWC base papers A1–A3 and B1–B2) and trial series IV (pilot papers 1–4).

4.1.1 Measurement of local grammage variation

The formation of the specimens was measured by a β-radiographic method. Each specimen, together with Mylar basis weight standards, was sandwiched between a reusable storage phosphor screen (SPS) and with uniform β-radiation (^{14}C) source (Avikainen and Erkkilä 2003). The image on the screen was then digitised into a matrix of grey level data using a Fuji BAS-1800 II SPS scanner. A high-pass filter was used to cut wavelengths longer than 70 mm. For News samples A–D (trial series I and II), the resolution was 100 µm/pixel and the size of the grammage map was 150 mm x 150 mm (results shown in Tables 9 and 10). The respective values for News samples E1–E6 and all the LWC base paper samples (trial series III) were 50 µm/pixel and 120 mm x 120 mm. Grammage variation is reported as standard deviation in the wavelength range of 0.25–32 mm and referred to as total formation. News samples E1–E6 were also measured with the Ambertec Formation Tester.

In addition, grammage variation up to a wavelength of 2048 mm was measured from trial papers E1–E6 and all the LWC base papers. The variation was determined by measuring from each trial paper four 100 m long lines that were located 1.6 cm apart. The device employed was The TAPIO® Paper Machine Analyzer (Hilden and Paerento 2000). The aperture size was 1 mm and the radiation source was Promethium 147.

However, to get a more comprehensive picture of the paper structure, void distribution was studied by utilising Matlab Image Processing Toolbox™. The reason for focussing on voids instead of flocs is their possible effect on structure yielding when the web is strained. Before median thresholding, the original resolution of the grey-scale images was reduced from 50 µm to 100 µm because the theoretical maximum resolution is twice the sheet thickness. After that, a visual study was undertaken to determine which threshold level for voids best classified the paper samples. Threshold levels median minus 2, 4 and 6 g/m² were studied. The median minus 4 g/m² was considered the best because it did well in segregating voids from each other without squeezing the overall void area too much. The value median – 4 g/m² means those pixels whose value is at least 4 g/m² smaller than the median value are considered to belong to voids. The following morphological operations were used in the image analysis:

- “Filling” to fill isolated interior pixels and “cleaning” to remove isolated pixels.
- “Majority” to set a pixel to 1 if five or more pixels in its 3x3 neighbourhood are 1 s; otherwise, it sets the pixel to 0.
- “Closing” with 2x2 structuring element to eliminate specific image details smaller than the structuring element — the global shape of the objects is not distorted. “Closing” connects objects that are close to each other, fills up small holes and smoothes out the object outline by filling narrow gulfs. “Closing” consists of a “dilatation” operation followed by an “erosion” operation. (Sonka et al. 1998.)
- “Connectivity 8” to count two voids as one void if one or more of their pixels are connected at the edge or corner.

Both 2x2 and 3x3 structuring elements were tested. The larger element seemed to distort the image by sometimes connecting voids that, according to visual evaluation, were separate units. This slightly increased the total floc area and reduced the number of flocs. As an example, for News E1 the overall void area was 13.8% after majority, filling and cleaning operations, and 13.9% after the closing operation with the 2x2 structuring element. Instead, the closing operation with the 3x3 structuring element increased the overall void area to 14.7%. The number of voids was 6180 for the smaller structuring element and 5240 for the larger one. Based on the tests, the smaller element was selected.

As Figures 40 and 41 demonstrate, the method brings forth the characteristics of the papers very well. News E5 in Figure 40 represents the best formation in the News series E1–E6. Figure 41 on the other hand is an example of poor formation, pilot paper 2.

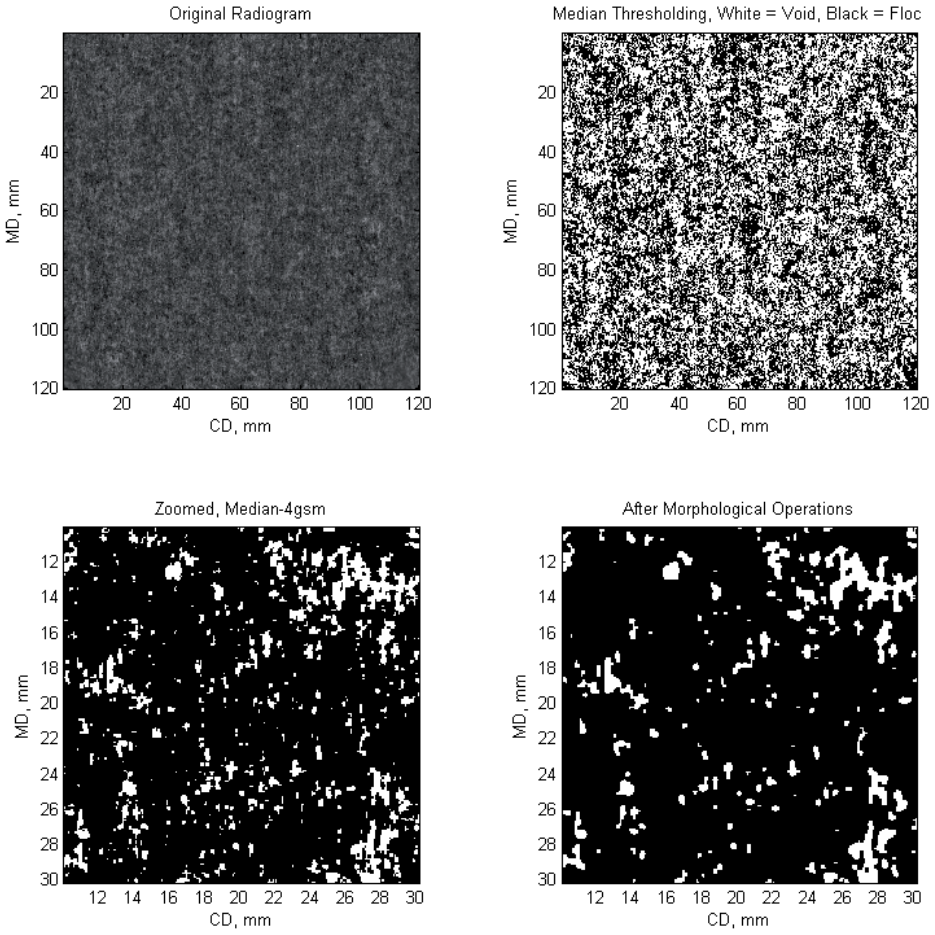

Figure 40. *An example of the image analysis. Top left: original radiogram. Top right: threshold median – 4 g/m². Bottom left: the same image zoomed. Bottom right: the image after the morphological operations. News E5.*

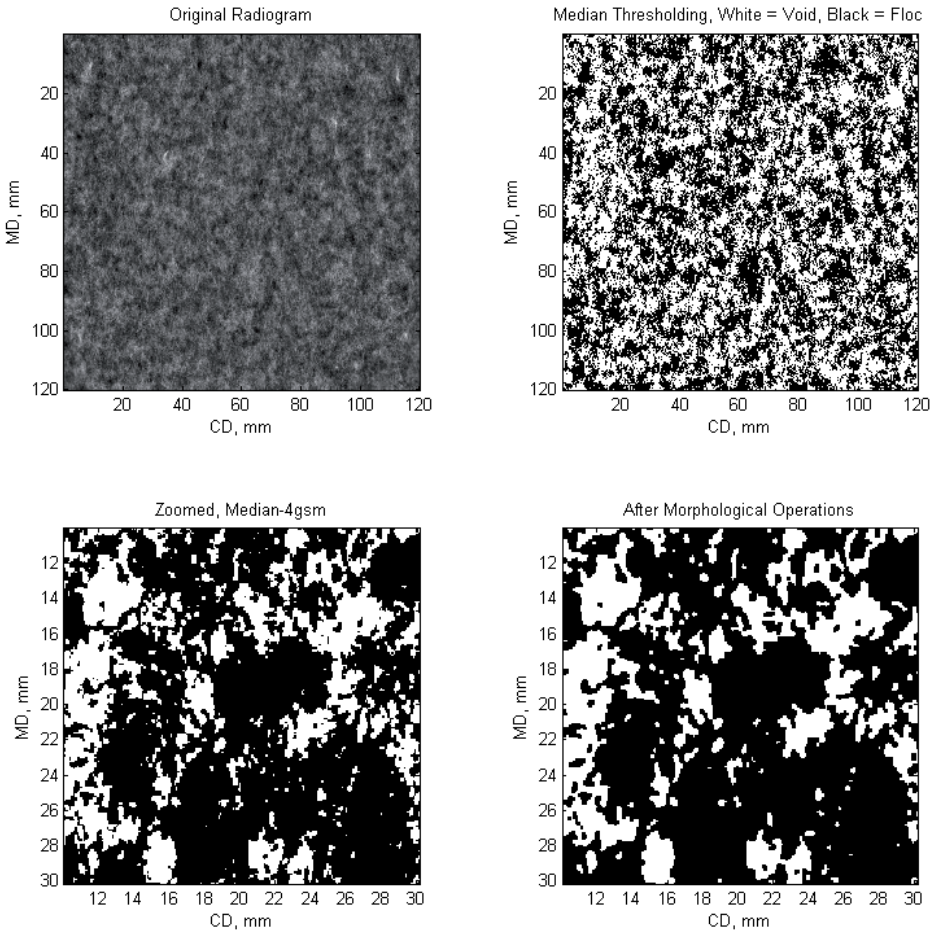

***Figure 41**. An example of the image analysis. Top left: original radiogram. Top right: threshold median – 4 g/m². Bottom left: the same image zoomed. Bottom right: the image after the morphological operations. Pilot paper 2.*

4.1.2 Layered fibre orientation measurements

In principle, the dewatering process can be of two different kinds, filtration or thickening. However, the filtration type of dewatering dominates conventional forming. This means that fibres are successively deposited flat on a wet web as the suspending water is removed, and free suspension with the same concentration as that in the jet from the headbox is still present above the wet web. This mechanism

produces a strongly layered web structure. The dewatering of fibre flocs in the free suspension takes place according to the thickening principle. (Norman 2008.)

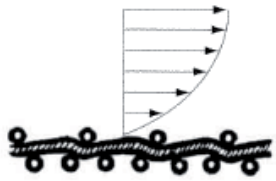

***Figure 42**. Oriented shear (Parker 1972).*

Oriented shear, Figure 42, caused by a velocity difference between the free suspension and the previously drained fibre mat or wire, influences fibre orientation anisotropy. When one end of a fibre is deposited on the wet web surface during dewatering, the shear field will tend to align the fibre in the direction of shear. (Niskanen 1989.) The oriented shear, however, does not stay constant. When the jet from the headbox enters the wire gap of a roll-former unit, it is met by a dewatering pressure p gradually rising to $p = T/R$, which means that the jet decelerates (Norman 2008). According to Bernoulli's equation, the following relationship (17) exists between the jet velocity v_J and the decelerated free suspension velocity v_{FS} between the wires when energy losses are neglected (Norman 2008):

$$\frac{1}{2}\rho\left(v_J^2 - v_{FS}^2\right) = \frac{T}{R} \tag{17}$$

where ρ is the density of free suspension
T is the outer wire tension
R is the local radius of curvature of the wire

Another fibre-orienting phenomenon is an accelerating flow in the headbox nozzle. The larger the nozzle contraction ratio (inlet divided by outlet cross sectional area) is and the closer the unit point (point between rush and drag) the paper machine runs, the clearer the effect of the accelerating flow (Nordström and Norman 1994, 1995, Ullmar 1998, Nordström 2003). Modelling work of Hämäläinen and Hämäläinen (2007) revealed that not all the fibre orientation developed in the slice channel survives to the end of the jet. This is because the orientation in the jet tends to randomise rapidly during the first centimetres and is then slower after that. The reason for the reduction of the orientation is the absence of acceleration and shear forces in the jet.

For roll-blade gap formers, the practical control parameters affecting the drainage and flow field of the suspension in the dewatering zone are jet-to-wire ratio, controlling oriented shear, slice opening, forming roll vacuum, multifoil shoe vacuum or vacuum and loading level of the loadable blade module (Erkkilä 1995, Odell 2000, Odell and Pakarinen 2003, Norman 2008). However, when considering jet-to-wire ratio as a

control parameter, it needs to be remembered that the deceleration of the free suspension in the wire gap reduces oriented shear when running on the rush side and the opposite being valid for running on the drag side. Because each individual section in the z-direction of the web forms in different locations along the forming zone, the layers may have experienced very different forming history. This presents the possibility of producing various paper structures. Fibre orientation throughout the whole thickness of the sheet is affected as a minimum.

To gain a more comprehensive impression of fibre orientation, layered fibre orientation measurements (Erkkilä 1995, Erkkilä et al. 1998, 1999) were implemented. The method is based on the tape-stripping technique and image analysis of the resulting layers. Good tape stripping requires uniform and appropriate tape adhesion. In addition, the tape should be non-stretching. The tape and the laminating machine employed were Brother LC-9L2R 23 cm x 20 cm cold laminating tape and a GBC 3500 Pro Series laminating machine. The paper specimens were conditioned and the whole stripping procedure was carried out under standard atmospheric conditions (RH 50%, T 23°C). The average grammage and max-min range for the layers were fairly similar in all the tested papers, with typical values being 5 g/m² and 3.3–6.2 g/m² respectively. The stripping procedure used is described in detail elsewhere (Lipponen et al. 2009).

Each specimen layer was placed against a dark background and scanned with the UltraScan 5000 flatbed scanner from the fibre side (in contrast to the tape side) with 30 μm/pixel resolution using reflective illumination. The fibres and fibre bundles are distinguished as lighter against the dark background. In the image analysis, intensity variations are sharpest at the fibre boundaries. This result is used in the form of gradients to establish the magnitude and direction of fibres in every image element throughout the whole image area. Three areas of 180 mm x 40 mm (CD x MD) were measured from every layer. By plotting the result for each layer using polar co-ordinates, an ellipse-type of fibre orientation distribution pattern is obtained, Figure 43.

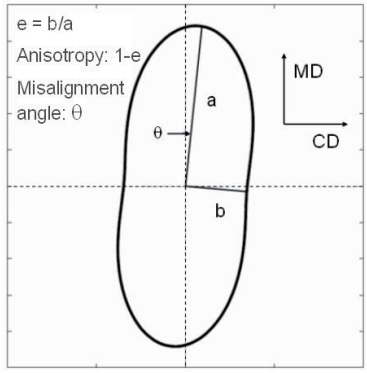

***Figure 43**. Orientation distribution pattern and parameter definition (Erkkilä 1995).*

Parameters such as anisotropy (deviation between the perfect circle and the measured distribution pattern) and misalignment angle (deviation between MD and the max. axis of the ellipse) can be determined from the shape of the distribution pattern. After this, ZD anisotropy and misalignment angle profiles can be established. (Erkkilä et al. 1998, Lipponen et al. 2009.)

Anisotropy (1 – e) for the whole paper consisting of i layers can be computed using Equation (18) and called henceforward layered anisotropy.

$$1 - e = \frac{\sum_i m_i (1 - e_i)}{\sum_i m_i} \tag{18}$$

where 1- e_i is the anisotropy for layer i

e_i is (minor axis of ellipse i) / (major axis of ellipse i)

m_i is the mass of layer i.

With both axes being equal, the anisotropy is 0. The maximum value for anisotropy is 1 (all the fibres oriented to the direction of the major axis).

In addition to the ZD orientation profile, orientation magnitude maps were determined for every trial paper (Erkkilä et al. 1999, Odell and Pakarinen 2001, Lipponen et al. 2009). The measured area in each layer was 180 mm (CD) x 120 mm (MD). The whole area in each layer was divided into small 2 mm x 2 mm squares and the ellipses were computed for each of those squares. The result is shown as a "stick" diagram where the length and angle of each line segment represents anisotropy and misalignment respectively, see Figure 44. The line segments depict orientation vectors whose MD components were used to compute orientation magnitude maps.

To create the MD orientation magnitude CD profile, Figure 44, the average of the MD components was computed for every 2 mm wide and 120mm long MD strip (90 strips and 60 measurements per strip) in each paper layer. These averages from all the layers constitute the orientation magnitude CD profile. The profile represents the MD effective shear that was prevailing at the time that the fibre layer was drained (Odell and Pakarinen 2001).

In order to clarify the evenness of the MD orientation magnitude over the x-y plane, another type of MD orientation magnitude map was computed, the x-y distribution of MD orientation magnitude, Figure 44. This time the average of the MD components was computed for the columns whose cross-section was 2 mm x 2 mm and height was the number of paper layers. The standard deviation of the averages was also determined, which was considered a measure of orientation evenness.

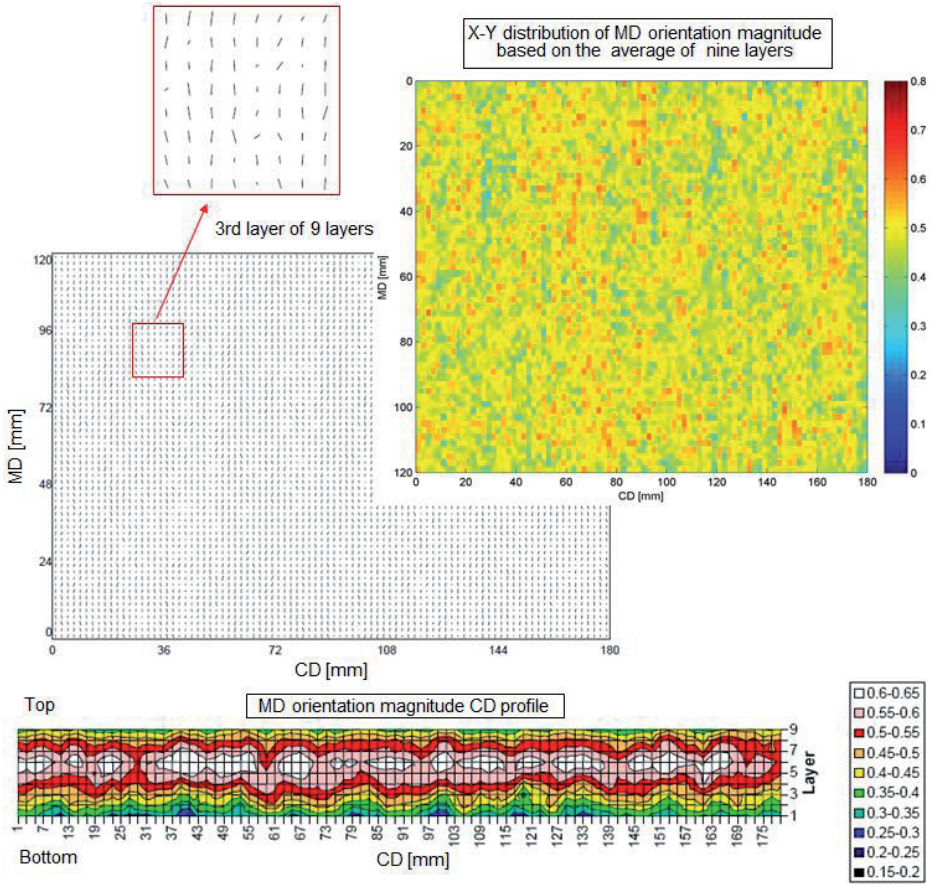

Figure 44. *Left: A "stick" diagram for a layer consisting of 2 mm x 2 mm squares. The length and direction of the line segments describes the degree of anisotropy and the misalignment angle in every square. Bottom: MD orientation magnitude CD profile. Right: X-Y distribution of MD orientation magnitude based on the mean of nine layers. News E4.*

4.1.3 Porosity and ash distribution measurements

The wet paper samples for porosity measurements were taken right before the AHMA brake nip, which was the last possible sampling point to get a proper sample. The wet samples were immediately placed on a satin caul and two pieces, 20 cm x 25 cm, were cut off. The samples on top of the satin caul were sealed in a plastic bag. The wet samples were die-cut to 50 mm x 60 mm through the plastic bag and were then deep-frozen in liquid nitrogen and dried as frozen in a vacuum. The porosity parameters were determined by means of image analysis (ESEM) as described in Chapter 3.1.3 with the exception being a stronger magnification and more accurate resolution. The magnification was 600x instead of 250x and the pixel size was 0.29

µm instead of 0.7 µm. In addition, only CD images were taken this time and the number of images per trial point was larger, altogether 50 CD images from four small sample blocks instead of 30 from two sample blocks.

Filler distribution in z-direction was determined using tape splitting. The ash-free tape with known grammage was applied to both the top and bottom sides of the samples measuring 50 x 180 mm². Typically, the samples were split in 11 layers. The basis weight of each layer was measured according to ISO 536:1995 standard method and ash content according to ISO 1762:2001 standard method at 525°C.

4.2 Results for News E1–E6

4.2.1 Running parameters

Trial papers News E1–E6 were manufactured on a roll-blade gap former consisting of a "constant dewatering" zone by the forming roll wrap area followed by a "pulsating dewatering" zone of a multifoil shoe, see the layout of the wire section in Appendix 7. The basis weight was 45 g/m² and ash content 9.2% (525°C). Paper structure was altered by changing forming roll vacuums (2/4–12/15 kPa), multifoil shoe vacuums (2/3–8/15 kPa), slice opening (6.8–7.5 mm) and jet-to-wire ratio (1.045–1.075). The unity point (change from rush to drag) was 1.015. The trial settings are discussed in detail in Chapter 4.2.5 (Pages 120–121). The other running parameters and furnish, 100% RCF, were standardised. However, the broke proportion needed to be increased from 19% to 45% when running the last trial papers E4–E6; the reason was unsuccessful tail feeding when trying to change from rush to drag according to the original trial plan. The outcome was the two broke towers becoming full of wet broke from the couch pit and a higher broke dosage for the last three trial papers. Because the furnish was 100% RCF, hornification of wet and dry broke does not substantially differ from that of the original RCF. In addition, the measured furnish characteristics remained fairly constant as Appendix 2 shows. Thus the furnish can be concluded to have been fairly constant throughout the whole trial. The total draw from the wire to the reel-up was 5.7%

4.2.2 Possible correlation between grammage variation and fibre orientation

In order to distinguish between the effect of local grammage variation and fibre orientation on the strength properties, the variables should not be correlated. To clarify whether this was the situation for the News series E1–E6, an investigation was conducted by means of visual evaluation and statistical methods. The grammage variation was described by total formation (β-radiography and Ambertec), variation in different wavelength bands (β-radiography and Tapio), and variation in the total area of voids (cf. Chapter 4.1.1) belonging to different size classes.

As Figure 45 and Appendix 4 show, there was no correlation between formation scale grammage variation and fibre orientation. The result was valid irrespective of the

orientation parameter used, layered anisotropy or tensile MD/CD ratio. There was no statistically significant correlation at a 95% confidence level, not even at 90%, between fibre orientation and grammage variation in different wavelength bands or void size classes, and there was no correlation based on visual evaluation either. The result is understandable because formation was not altered by the jet-to-wire ratio.

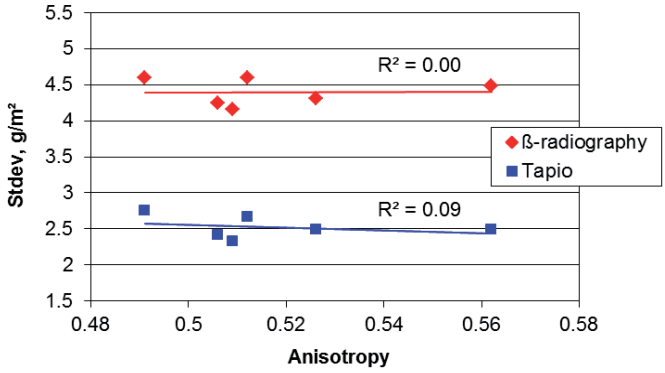

***Figure 45**. Correlation between formation and fibre orientation measured as layered anisotropy. Formation was measured by β-radiography and Tapio Paper Machine Analyser with a wavelength band of 0.25–32 mm and 2–32 mm respectively.*

In order to clarify whether local fibre orientation, measured in small 2 mm x 2 mm areas in paper layers, has some self-contained influence on strength properties irrespective of layered anisotropy, orientation evenness (described in Chapter 4.1.2) was computed for News E1–E6, LWC base papers A1–A3 and B1–B2, as well as pilot papers 1–3. The orientation evenness should not correlate with mean fibre orientation in order to differentiate the effect of local fibre orientation from that of mean fibre orientation. However, as Figure 46 shows, the correlation is very strong in newsprint and LWC base papers. The consequence of the result is that the method tested is unsuitable for the aimed purpose and will not be studied further.

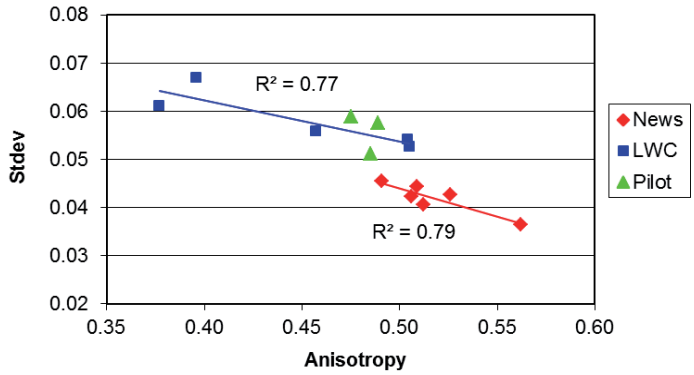

***Figure 46**. Correlation between layered anisotropy and standard deviation of effective shear, i.e. orientation evenness. The latter was computed from the mean anisotropy values of the columns whose cross-section was 2 mm x 2 mm and height was the number of paper layers. R² values are computed for News and LWC base papers.*

4.2.3 Effect of grammage variation on strength properties

According to the Ambertec results, the parameter combination enabled a considerable difference in formation, 0.5 g/m² between the best and worst trial paper. This is a significant change generated by machine parameters only. The β-radiography and Tapio measurements confirm the clear difference between the extremes. Table 12 shows a selection of different formation parameters, Figure 47 shows standard deviation in different wavelength bands and Figure 48 total area of voids (median – 4 g/m²) belonging to different size classes. The tensile MD/CD ratio was measured according to ISO 1924-3:2005 and the specimens for measurements were collected from the beginning and the end of each AHMA trial point.

***Table 12**. Some formation parameters and fibre orientation for News E1–E6. Formation parameters include standard deviation, standard deviation in different wavelength bands (mm scale) and floc size. Formation measurements were taken with Ambertec Formation Tester, β-radiography and Tapio Paper Machine Analyzer.*

	A-tec	β-radiography				Tapio		
	SD g/m²	$SD_{0.25-2}$ g/m²	SD_{2-8} g/m²	SD_{8-32} g/m²	Floc size mm	SD_{4-16} g/m²	SD_{16-64} g/m²	Tensile MD/CD
News E1	3.2	3.27	2.53	1.22	2.22	1.89	1.35	3.78
News E2	3.4	3.36	2.84	1.33	2.39	2.04	1.49	3.88
News E3	3.2	3.40	2.66	1.22	2.26	1.91	1.29	4.56
News E4	3.4	3.35	2.85	1.36	2.39	2.12	1.53	3.75
News E5	2.9	3.21	2.36	1.19	2.15	1.75	1.18	3.64
News E6	3.0	3.31	2.44	1.05	2.11	1.86	1.20	3.83

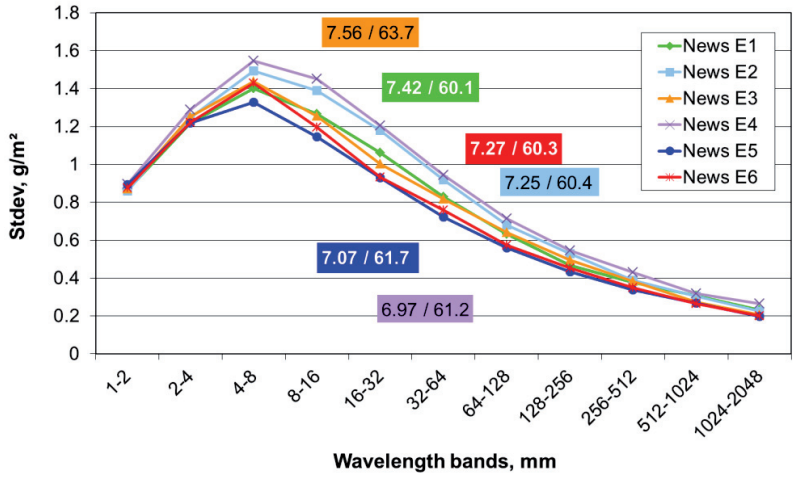

***Figure 47**. Standard deviation in octave bands from Tapio measurements. The averages of tensile indices at DSC 56% and 68% are shown in colour-coded boxes together with tensile indices of dry papers. The distance between the boxes in the vertical direction denotes the relative difference in the average wet tensile indices of the trial papers.*

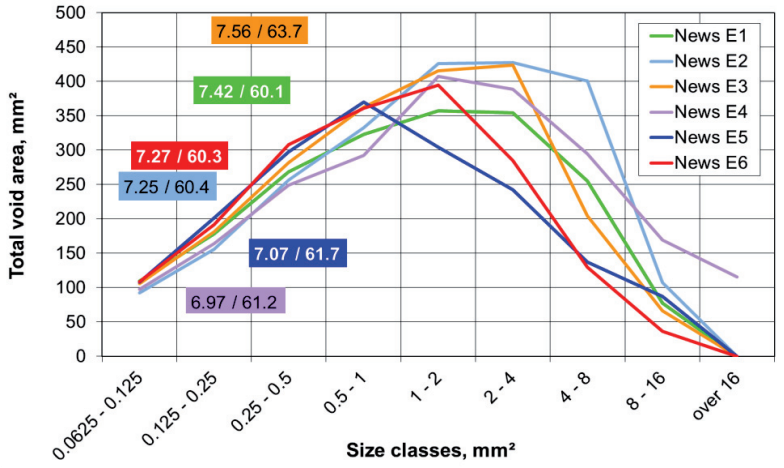

***Figure 48**. Total area of voids (median – 4 g/m² from β-radiogram measurements) belonging to different size classes. The averages of tensile indices at DSC 56% and 68% and tensile indices of dry papers are shown in colour-coded boxes. The distance between the boxes in the vertical direction denotes the relative difference in the average wet tensile indices of the trial papers. The size of the measured area was 12 cm x 12 cm.*

According to Table 12, there is only a small difference in grammage variation between the trial papers in the wavelength band 0.25–2 mm. This is understandable because of the fairly constant furnish. In the other wavelength bands, the differences are clearer.

Figure 48 shows that the trial papers differ in terms of total area of voids belonging to the different size classes. Differences are especially considerable in the 4–16 mm² size range. Although only one image analysis per trial point was performed, the method differentiated the good (E5 and E6), intermediate (E1 and E3) and poor (E2 and E4) formation papers.

Figures 47 and 48 suggest that grammage variation measured either in formation or mesoscale does not correlate with wet or dry strength properties (tensile indices shown in colour-coded boxes whose distance in the vertical direction denotes the relative difference between the trial papers). Visual evaluation and statistical investigation were carried out to confirm this. Strength properties were correlated with total formation (Ambertec, β-radiography) and grammage variation in different wavelength bands and void size classes, see Appendix 5. The visual evaluation and correlation investigation (p value < 0.05) confirmed that the measured data did not provide support to the hypothesis of the effect of formation or mesoscale grammage variation on the wet or dry tensile index and on the wet or dry tensile stiffness index (TSI), not even at a confidence level of 90%. See Figure 49 as an example. Although the results were unequivocal, it needs to be mentioned, however, that based on a visual evaluation there existed an indication at DSC 68% that total void area in the size class 8–16 mm² may affect tensile index (p value 0.11).

TSI was determined only at DSC 68% and for dry papers. The reason is that, typically, the difference between the initial tension and breaking tension was small at DSC 56% due to the high initial tension, see Chapter 3.6.1. Thus the measured tension-strain curves represent only a fraction of the real tension-strain curves, bringing the relevance of the usage of the slope as an indicator for TSI into question. The situation was quite different at DSC 68% due to higher breaking tension values.

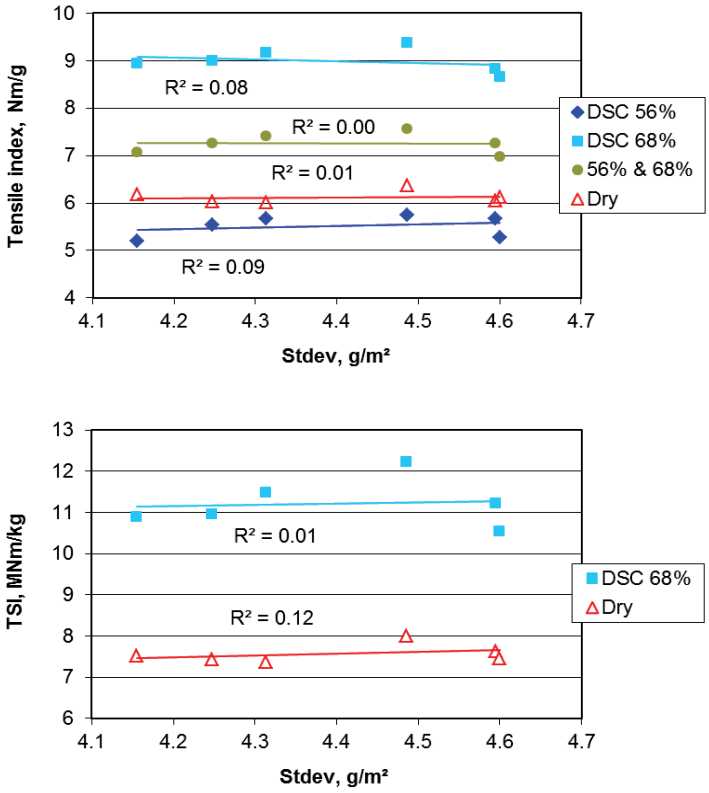

***Figure 49**. Tensile index (top) and tensile stiffness index (bottom) as a function of standard deviation (β-radiography, wavelength band 0.25–32 mm). 56% & 68% denotes the average of tensile indices measured at DSC 56% and 68%. Tensile index values for dry papers are divided by 10 and tensile stiffness index values for wet papers are multiplied by 10 to accommodate the curves in the same figures. News E1–E6.*

4.2.4. Effect of fibre orientation on strength properties

In contrast to grammage variation, Figure 50 suggests both wet and dry strength properties correlate with orientation magnitude. However, only in the case of TSI are the correlations statistically significant at a confidence level of 95%, see Table 13 (Page 119). In addition, all the correlations are strongly affected by one high tensile MD/CD value. More support for the interdependence is available when fibre orientation is measured by layered anisotropy, which is calculated as a weighted average from the anisotropy values of single paper layers, Equation (18). The correlations between wet strength properties (tensile index and TSI) and orientation magnitude are now clear, see Table 13 and Figure 51**.** However, the same does not apply to dry tensile index.

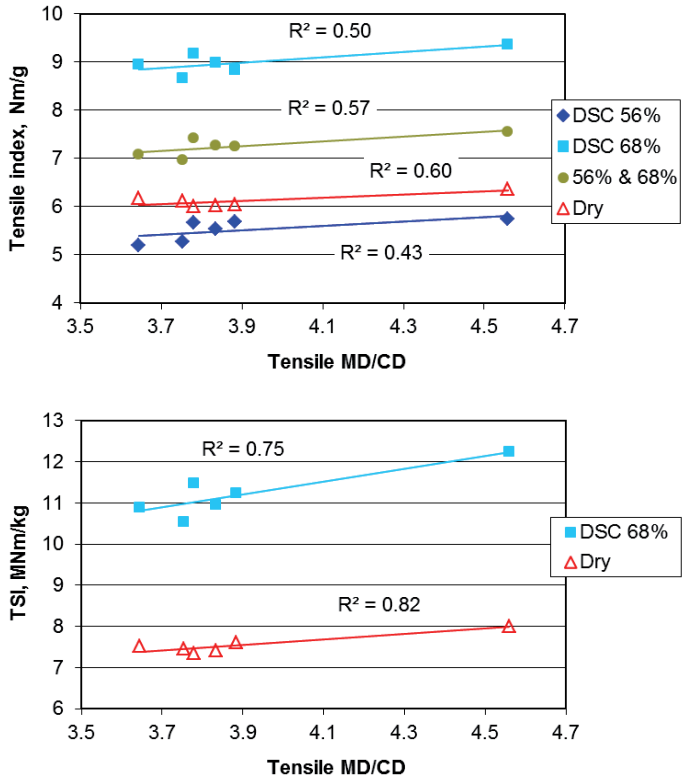

Figure 50. *Tensile index (top) and tensile stiffness index (bottom) as a function of tensile MD/CD at different DSC levels. 56% & 68% denotes the average of tensile indices measured at DSC 56% and 68%. Tensile index values for dry papers are divided by 10 and tensile stiffness index values for wet papers are multiplied by 10 to accommodate the curves in the same figures. News E1–E6.*

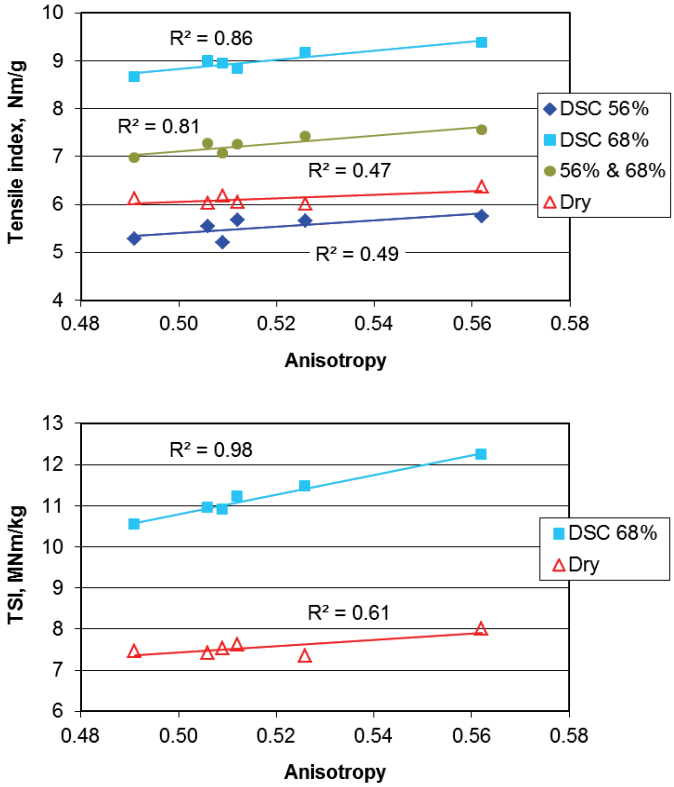

Figure 51. *Tensile index (top) and tensile stiffness index (bottom) as a function of layered anisotropy at different DSC levels. 56% & 68% denotes the average of tensile indices measured at DSC 56% and 68%. Tensile index values for dry papers are divided by 10 and tensile stiffness index values for wet papers are multiplied by 10 to accommodate the curves in the same figures. News E1–E6.*

***Table 13**. Correlation coefficients, t and p values for the correlations between strength properties at different dry solids contents and orientation magnitude measured as tensile MD/CD ratio and layered anisotropy. Highlighted correlations are statistically significant at p < 0.05. News E1–E6.*

Variables	DSC, %	R	t	p
Tensile index vs. Tensile MD/CD	56	0.656	1.74	0.157
Tensile index vs. Tensile MD/CD	68	0.709	2.01	0.115
Tensile index vs. Tensile MD/CD	56 & 68	0.753	2.29	0.084
Tensile index vs. Tensile MD/CD	dry	0.773	2.44	0.071
TSI vs. Tensile MD/CD	68	0.866	3.46	0.026
TSI vs. Tensile MD/CD	dry	0.908	4.33	0.012
Tensile index vs. Layered anisotropy	56	0.700	1.96	0.122
Tensile index vs. Layered anisotropy	68	0.929	5.01	0.007
Tensile index vs. Layered anisotropy	56 & 68	0.902	4.18	0.014
Tensile index vs. Layered anisotropy	dry	0.683	1.87	0.135
TSI vs. Layered anisotropy	68	0.988	12.60	0.000
TSI vs. Layered anisotropy	dry	0.780	2.50	0.067

Although the correlation between layered anisotropy and MD/CD tensile ratio is significant at a 95% confidence level with p value, t value and correlation coefficient being 0.022, 3.63 and 0.88 respectively, it is not perfect, cf. Figure 52. It is quite likely that layered anisotropy is more sensitive and more able to differentiate minor differences between the trial papers than tensile MD/CD ratio. This means that layered anisotropy should be more reliable at indicating the differences between fibre orientation and wet strength properties.

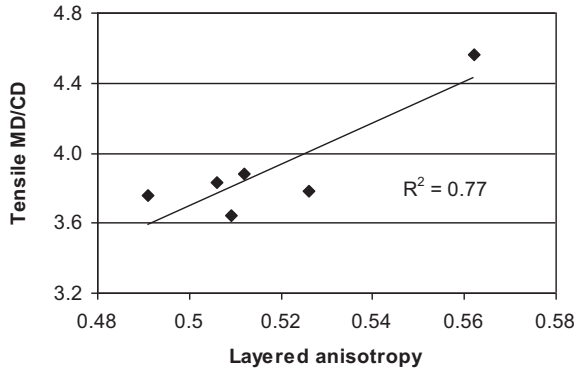

***Figure 52**. Correlation between layered anisotropy and tensile MD/CD ratio. News E1–E6.*

4.2.5 Detailed analysis of layered anisotropy and its effects on strength properties

Figure 53 shows the anisotropy profiles in the z-direction as well as the settings for the control parameters. The originally set target for the trial to produce substantially different structures was met, as was seen already in the case of formation.

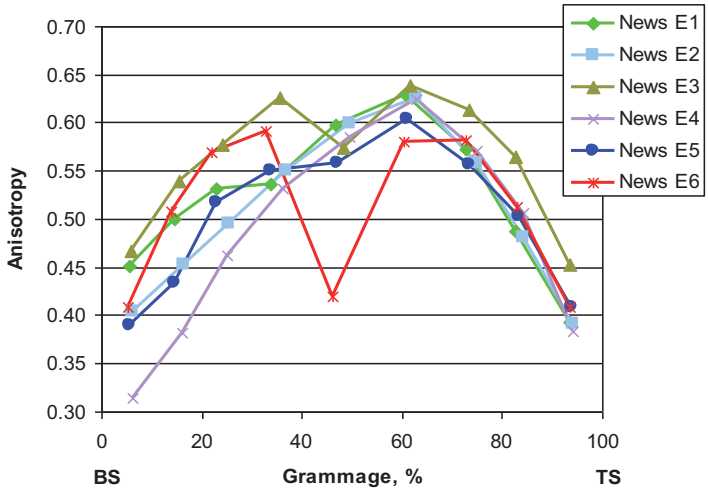

Tp.	Jet-to-wire ratio	Slice opening mm	FR vacuums 1 / 2 kPa	MFS vacuums 1 / 2 / 3 kPa	Profile type	Layered anisotropy	Tensile MD/CD ratio
E1	1.045	6.8	2 / 4	0 / 2 / 7	One max.	0.526	3.78
E2	1.045	6.8	12 / 15	0 / 8 / 15	One max.	0.512	3.88
E3	1.075	6.8	12 / 15	0 / 6 / 14	Seagull	0.562	4.56
E4	1.045	7.5	12 / 15	0 / 7 / 14	One max.	0.491	3.75
E5	1.045	7.5	2 / 4	0 / 2 / 3	One max.	0.509	3.64
E6	1.062	7.5	2 / 4	0 / 3 / 6	Seagull	0.506	3.83

***Figure 53**. Anisotropy in different paper layers starting from bottom side, control parameters and mean layered anisotropy. FR denotes forming roll and MFS multifoil shoe. Unity point 1.015. News E1–E6.*

The trial papers can be separated into two different categories according to the anisotropy profile in z-direction. Papers E3 and E6, manufactured with a high jet-to-wire ratio, show a symmetric seagull type of anisotropy profile around the sheet centre. This type of anisotropy profile is typical for roll-blade gap formers running in rush (Erkkilä et al. 1998, 1999, Odell 2000). The four other trial papers, run with the lower jet-to-wire ratio of 1.045, demonstrate a more or less asymmetric profile type with one maximum. However, this is not a unique phenomenon for running in rush. For example, in Erkkilä's study (1995) on a pilot and a production roll-blade gap former the anisotropy profile changed from the seagull type to a more or less asymmetric one maximum type when the jet wire ratio was reduced close to the unity

point. Thus by choosing the parameter values suitably it is possible to produce very different anisotropy profiles without changing from rush to drag.

The comparison between trial points E1 and E2 as well as between trial points E4 and E5 shows that the increase of forming roll and multifoil shoe vacuums together reduced fibre orientation in the bottom layers, leading to a reduced overall layered anisotropy value. In addition, formation was inferior with high vacuums, cf. Table 12 (Page 113) and the table in Figure 53. It may be that higher multifoil shoe vacuums evoke excessive pulsation, breaking the already formed fibre mat. Both low vacuum papers (E1 and E5) have a plateau in the anisotropy profile reminiscent of the seagull profile type.

Not only the vacuums but also the slice opening had an influence on the anisotropy profile. This is evident when a comparison is made between trial points E1 and E5 and between trial points E2 and E4. The wider slice opening together with high vacuums led to smaller anisotropy values in the bottom layers and smaller overall layered anisotropy. When the vacuums were low, the reduction in anisotropy was distributed more evenly between the layers, i.e. more layers contributed to the lowered overall layered anisotropy. The effect of the slice opening on formation was contradictory.

The findings can be summarised as follows. The usage of the smaller slice opening together with small vacuums at a jet-to-wire ratio of 1.045 led to a maximised overall layered anisotropy. The opposite settings led to a minimised layered anisotropy.

The high jet-to-wire ratios of 1.062–1.075 behaved quite differently compared with the low one of 1.045, causing the papers to feature a local orientation minimum in the middle layer. This is a natural consequence of the deceleration of the suspension core between the already infiltrated fibre mats. The wider slice opening together with low vacuums caused trial paper E6 to feature a deep reduction in the orientation anisotropy in the middle layer. Jet-to-wire ratio was therefore unable to increase the overall layered anisotropy value.

The universally applicable lower degree of anisotropy towards paper surfaces is probably caused by the following reasons at least (Norman 2008): Firstly, when the jet hits the wires, the evolving dewatering pressure decelerates the suspension between the wires. Secondly, due to the acceleration of low-velocity boundary layers in the emerging free jet, the jet surfaces will become more uneven further away from the lip opening (Söderberg and Alfresson 1998). In addition, any turbulence in the jet leaving the headbox nozzle will contribute to jet roughness. When the rough jet surface hits the forming fabric surface, local flows will be generated and will decrease fibre orientation anisotropy on the web surfaces. Thirdly, fibre orientation anisotropy at the jet surfaces is reduced due to boundary layer effects in the headbox nozzle (Asplund and Norman 2004, Carlsson 2007).

Because of the two different types of profile, the question arises as to whether there are any strength differences originating from the profile types. Tensile and tensile stiffness indices were studied as a function of overall layered anisotropy, see Figure

54. As the figure shows, it cannot be concluded that there are any notable differences between the profile types, at least where wet papers are concerned.

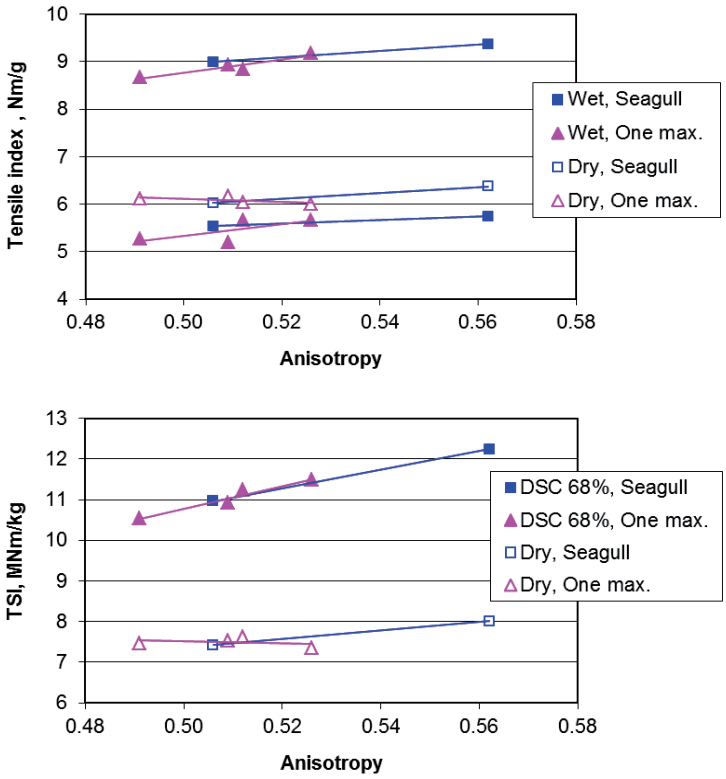

Figure 54. *Tensile and tensile stiffness indices of the seagull and one maximum anisotropy profile types as a function of layered anisotropy. In the upper diagram, the uppermost curve denotes tensile index at DSC 68% and the undermost curve at DSC 56%. Tensile index values for dry papers are divided by 10 and tensile stiffness index values for wet papers are multiplied by 10 to accommodate the curves in the same figures. News E1–E6.*

The misalignment angle profile in the z-direction was very even in all the trial papers with the average angle varying from layer to layer between -3° and +3°. Thus there are no practical differences between the papers and the misalignment profile will not be discussed.

4.2.6 Effect of porosity and ash distribution on strength properties

Porosity parameters were measured using an image analysis method as described in Chapter 3.1.3. The measurements were executed both with the fibre lumen filled and lumen open. Lumen filling was performed manually. Appendix 3 shows the results. The upside down U-profile originates from wet pressing (Szikla and Paulapuro 1989).

In spite of significant variation in the anisotropy profile between the trial points, the shape of the porosity profiles was fairly constant, see Figure 55. The profiles shown were measured with lumen open, the profiles with lumen filled were not available

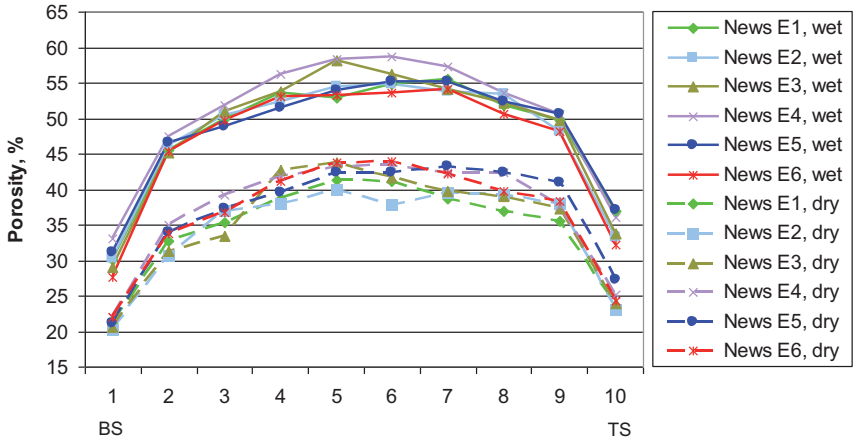

***Figure 55**. Porosity distributions for wet (DSC 56%) and dry papers. News E1–E6.*

Both visual examination and statistical methods were undertaken to determine whether the wet tensile and tensile stiffness indices (DSC 56% and 68%) correlate with total porosity, pore height, pore width, effective thickness and their standard deviations measured from wet samples. The same study was also undertaken for dry strength properties and porosity parameters measured from the dry papers. However, no correlation was found, not even an indication. The investigation of the papers divided into two groups according to the anisotropy profile, one maximum or seagull profile type, shows that Scott Bond (T 569 om-00) is better and Bendtsen porosity (Autoline 300) lower in the one maximum group, cf. Table 14. However, there are no differences in terms of total porosity, effective thickness and pore height or pore width determined by image analysis.

***Table 14**. Comparison of the papers with a one maximum anisotropy profile type (E1, E2, E4 and E5) with the papers with a seagull anisotropy profile type (E3 and E6). Total porosity, pore height and pore width are measured with lumen filled.*

	Property	One maximum	Seagull	Percentage difference
Dry papers	Porosity, ml/min	243	263	-7.6
	Scott Bond, J/m²	209	180	16.1
	Total porosity, %	30.4	30.2	0.8
	Effective thickness, µm	53.2	53.1	0.0
	Pore height, µm	2.74	2.77	-1.3
	Pore width, µm	4.39	4.37	0.4
Wet papers	Total porosity, %	41.1	40.5	1.6
	Effective thickness, µm	68.2	68.8	-0.9
	Pore height, µm	3.28	3.35	-2.1
	Pore width, µm	4.92	4.97	-1.1

All the z-direction ash profiles are fairly typical for gap formers (Odell 2000, Puurtinen 2003). Trial papers E2, E3 and E4, run with high vacuums, display a symmetrical and slightly U-shaped z-direction ash profile, cf. Appendix 6. In contrast, in the low vacuum papers E1, E5 and E6, the ash content tended to be two-sided regarding the outermost paper layers. However, neither of the profile types provided better wet or dry tensile index or tensile stiffness index values.

4.3 Effect of grammage variation and fibre orientation on the strength properties of LWC base papers

LWC base papers A1–A3, basis weight 40 g/m², were manufactured on a roll-blade gap former with A1 being run with standard blades and A2 and A3 with loadable blades. In addition, the jet-wire ratio was altered between the trial points. The furnish, consisting of TMP and bleached softwood kraft, was not possible to control due to the long delay between the runs. There was less kraft in furnish A1 than in furnishes A2 and A3, which were fairly equal. Consequently, there are differences in fibre length, bendability and fibre fines content between furnish A1 and furnishes A2–A3, see Appendix 2.

LWC base papers B1 and B2, basis weight 48 g/m², are from a roll-blade gap former. According to the measurements the furnish, consisting of PGW and bleached softwood kraft, was fairly similar for both papers, see Appendix 2. The aim was to select two different types of trial papers to test, one run on rush having a clear seagull-type layered orientation profile and the other run on drag having a one-maximum type profile. However, the target was not realised and both profiles were fairly similar, see Figure 56.

.

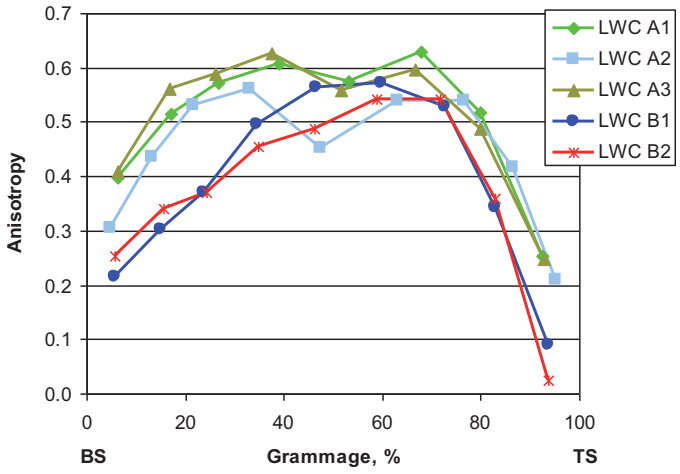

***Figure 56**. Anisotropy in different paper layers starting from bottom side. LWC base papers.*

The installation of loadable blades clearly improved the formation, see Table 15. The improvement was especially remarkable in the wavelength band of 2–8 mm, 1.5 times the max-min difference in News series E1–E6. The improvement was also significant in terms of total void area in the size range of 2–16 mm², see Figure 57. The results are analogous with floc size results, see Table 15. In addition, according to Tapio measurements, trial paper A3 shows improvement at all wavelengths starting from 2 mm with the strongest improvement being in the wavelength band of 16–32 mm, see Figure 58. Before the installation, the formation was comparable to that of LWC base paper B1, which in turn has slightly better formation than paper B2.

***Table 15**. Formation parameters (standard deviation, standard deviation in different wavelength bands (mm) and floc size) as well as tensile MD/CD ratio and averages of tensile indices measured at DSC 56% and 68%. LWC base papers A1–A3 and B1–B2. Formation results from β-radiography and Tapio Paper Machine Analyzer.*

Tp	β-radiography					Tapio	Tens. md/cd ratio	TSI MNm/kg	Tens. index Nm/g
	SD g/m²	$SD_{0.25-2}$ g/m²	SD_{2-8} g/m²	SD_{8-32} g/m²	Floc size mm	SD_{2-64} g/m²			
A1	4.95	3.34	3.29	1.59	2.77	3.21	3.75	1.36	9.61
A2	4.40	3.20	2.69	1.38	2.43	2.75	3.32	1.22	7.87
A3	4.20	3.07	2.55	1.31	2.38	2.59	3.74	1.29	8.51
B1	4.91	3.29	3.33	1.47	2.88	3.28	3.26	0.96	6.35
B2	5.12	3.41	3.48	1.59	2.92	3.41	2.99	1.00	6.00

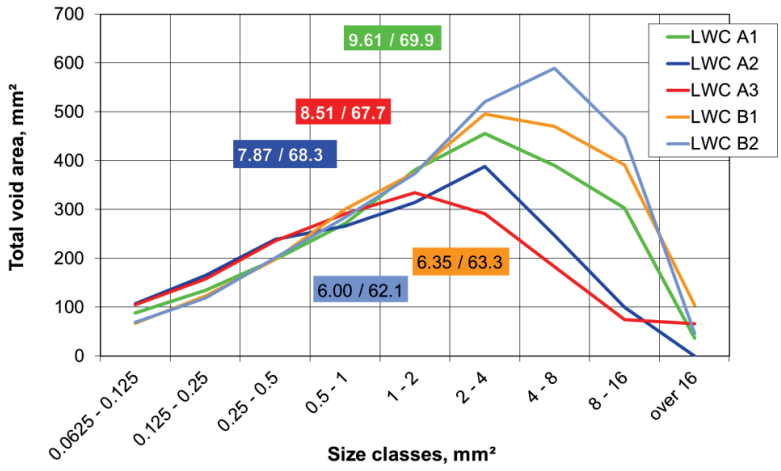

***Figure 57**. Total area of voids (median - 4 g/m²) belonging to different size classes. The averages of tensile indices at DSC 56% and 68% and tensile indices of dry papers are shown in colour-coed boxes. The distance between the boxes in the vertical direction denotes the relative difference in the average wet tensile indices of the trial papers. Specimen size was 12x12 cm².*

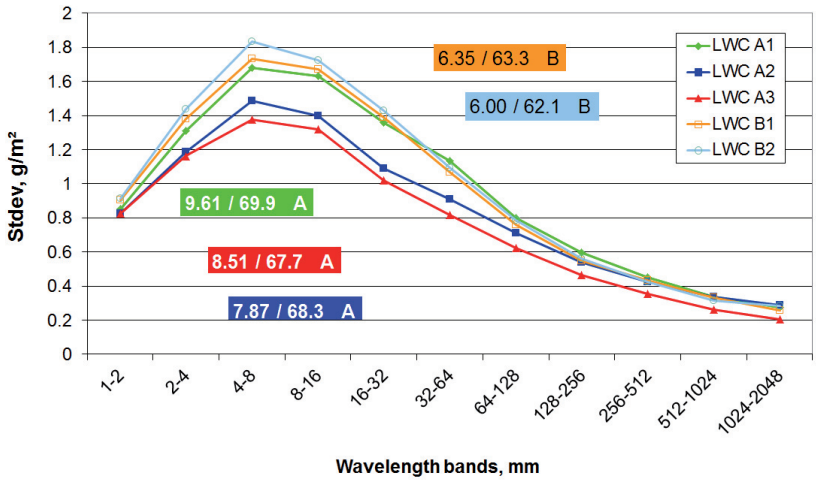

***Figure 58**. Standard deviation of basis weight in octave bands for LWC base papers A1–A3 and B1–B2. The averages of tensile indices at DSC 56% and 68% are shown in colour-coded boxes together with tensile indices of dry papers. The distance between the boxes in the vertical direction denotes the relative difference in the average wet tensile indices of the trial papers (Set 'A' papers (A) are compared with each other and set 'B' papers (B) with each other).*

In spite of a significant improvement in formation and mesoscale grammage variation, the wet tensile indices (DSC 56% and 68%) of papers A2 and A3 remained considerably lower than those of paper A1, Table 15. The same is valid for TSI. The higher fibre fines amount in paper A1, Appendix 2, is most likely a strong contributor to the good wet strength properties in that paper, cf. discussion in Chapter 2.3.1. In addition, the lower chemical pulp content may also have a minor positive effect.

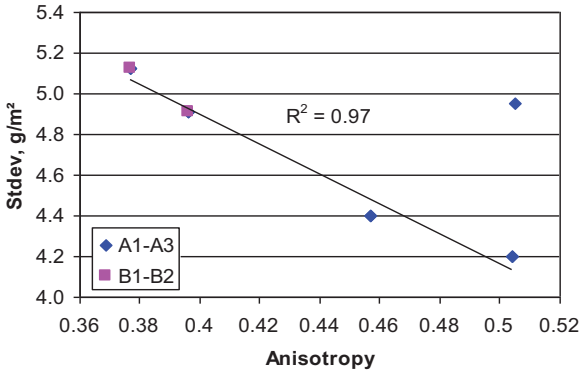

***Figure 59**. Correlation between layered anisotropy and formation measured by β-radiography with wavelength band being 0.25–32 mm. R^2 is computed for LWC base papers A2, A3, B1 and B2.*

When the comparison is made at equal furnish, A2 vs. A3 and B1 vs. B2, the effect of the fibre orientation and formation on strength properties is difficult to distinguish due to simultaneous changes. Interestingly, when these four papers are examined together, the correlation between the fibre orientation and formation is strong although papers A and B come from different paper machines, see Figure 59. The same is valid for the correlations of wet and dry tensile indices with formation and fibre orientation, cf. Figure 60. This interdependence and the deviation of paper A1 from the correlation line can be used to differentiate between the effect of formation and fibre orientation.

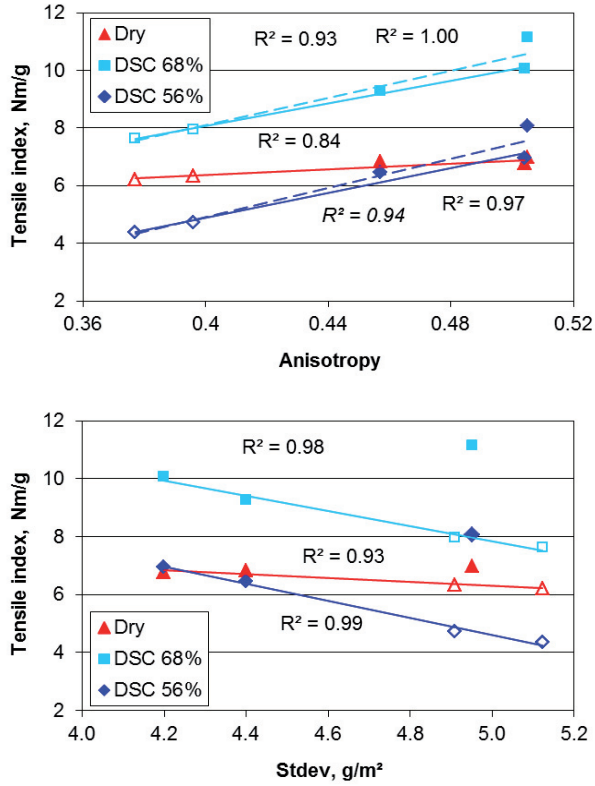

Figure 60. *Tensile index of LWC base papers A1–A3 and B1–B2 as a function of layered anisotropy and formation (β-radiography, wavelength band 0.25–32 mm). Solid symbols denote papers A1–A3 and open symbols papers B1–B2. A1 has the highest tensile index at all DSC levels. R^2 values in italics denote correlations computed for all the papers. All the other correlations are computed for papers A2, A3, B1 and B2 only. Tensile index values for dry papers are divided by 10 to accommodate the curves in the same figures.*

The examination of papers A1 and A3 at the same layered anisotropy level 0.505 shows that paper A1 has a 1.1 Nm/g higher wet tensile index than paper A3, both at DSC 56% and 68%, cf. Table 15. The difference is most likely caused by different

furnish as discussed above. Roughly speaking, all tensile index values at DSC 56% are on the same correlation line (also paper A1), as are the values at DSC 68% on their own line, cf. top Figure 60. R^2 values are high.

When the same examination is done between the wet tensile index and formation, there is a clear difference. The wet tensile indices of paper A1 need to be compared with the values taken from the correlation lines at the same formation value as paper A1. Tensile indices at DSC 56% and 68% taken from the respective correlation lines are on average 3.2 Nm/g smaller than the values of paper A1, see bottom Figure 60. Thus paper A1 strongly deviates from the correlation line. If the formation had an impact on the wet tensile index, this difference should be much smaller, as in the case of the fibre orientation. Thus the results suggest that the fibre orientation affects the wet tensile strength but that formation is not a major contributor. This is the case with dry papers as well. However, the effect of the fibre orientation on the tensile strength seems to mitigate when paper is dry.

Because the analysis is based on a limited number of data points and utilises the coincidence of strong correlations, no universal conclusions can be made. Thus the result should be considered as an indication only. However, although this is an indication, it supports the results from News series E1–E6.

TSI is not computed at DSC 56% for the same reason as papers E1–E6. Because TSI did not behave as unequivocally as tensile index (cf. Figure 61), the same kind of analysis referenced above cannot be performed to distinguish the effect of formation and fibre orientation.

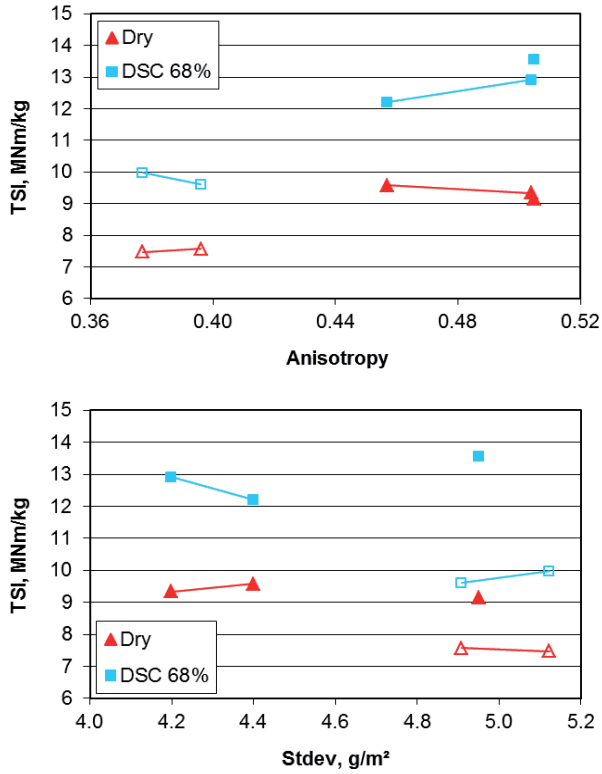

Figure 61. *Tensile stiffness index of LWC base papers A1–A3 and B1–B2 as a function of layered anisotropy and formation (β-radiography, wavelength band 0.25–32 mm). Solid symbols denote papers A1–A3 and open symbols papers B1–B2. Tensile stiffness index values for wet papers are multiplied by 10 to accommodate the curves in the same figures.*

4.4 Pilot papers

In order to have a larger formation range for analyses, four trial papers with poor formation were included in the study, trial series IV. The papers, basis weight 56.6–58.9 g/m², were manufactured on a pilot Fourdrinier from 100% TMP, see Appendix 8. The furnish was the same for all four trial papers. Formation was altered with headbox consistency and wire section vacuums. Breaking tension was measured in situ by the wet web winder installed right after the third press, see Figure 62, (Tanaka et al. 2009). Speed difference variation cycles between the 3rd press and the winder have been noticed to produce very similar stress-strain behaviour with the strong bending of the stress-strain curve near the break, see Figure 62. This enables fairly accurate breaking tension estimation with only one break per trial point. In the trial, the testing procedure included three speed difference cycles. The web was strained close to breaking point during the first two cycles and to breaking point during the third cycle. The dry solids content was 40%.

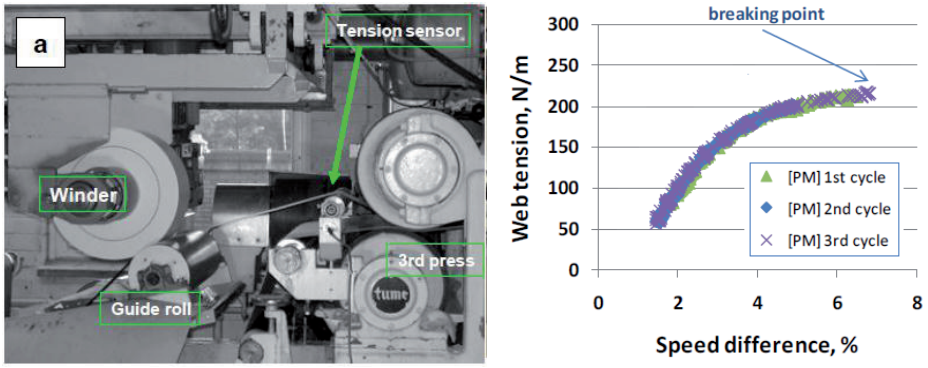

***Figure 62**. Left: The wet web winder located right after the third press on a pilot Fourdrinier. Right: An example of a stress-strain curve measured by the wet web winder. The curve consists of three cycles with the last one ending in a break. (Tanaka et al. 2009.)*

Local basis weight variation is much higher in the pilot papers compared with the mill papers, see Table 16. For example, Ambertec formation values are between 5.2 and 6.2, whereas for newsprint E1–E6 they are between 2.9 and 3.5. In addition, the widest max-min difference in the pilot papers appears to be in wavelength band 8–32 mm, whereas it is in wavelength band 2–8 mm for the other papers tested. The β-radiograph measurements were taken only for pilot papers 1, 2 and 3. It was not possible to carry out Tapio measurements. The investigation of Figure 63 confirms that the pilot papers are of a different nature to the mill papers. For the LWC base papers, the total area of large voids (>16 mm²) per 12x12 cm² was as an average 61 mm² and newsprint specimens E1–E6 typically had no large voids. Instead, for pilot papers 1, 2 and 3 the figure was 655 mm², 1256 mm² and 1409 mm² respectively. In addition, the maximum total area of voids in the mill papers occurred typically in size classes 1–2 mm² or 2–4 mm², but in the pilot papers the situation was quite different. This can be also observed from the floc size figures, see Table 16.

***Table 16**. Formation parameters (standard deviation, standard deviation in different wavelength bands and floc size) as well as tensile index (DSC 40%) for pilot papers. Formation measurements were taken with Ambertec Formation Tester and β-radiography.*

Tp	A-tec	β-radiography					Anisotropy	Tens. md/cd ratio	Tens. index Nm/g
	SD g/m²	SD g/m²	$SD_{0.25-2}$ g/m²	SD_{2-8} g/m²	SD_{8-32} g/m²	Floc size mm			
1	5.2	6.07	3.90	3.99	2.37	3.03	0.485	2.31	3.6
2	6.0	6.86	4.26	4.55	2.87	3.23	0.489	2.29	3.2
3	6.2	6.97	4.27	4.60	3.04	3.33	0.475	2.12	3.0
4	5.9	--	--	--	--	--	--	2.19	3.2

Because the furnish was constant and the fibre orientation was almost the same in all the trial papers, the differences in Figure 64 most probably originate from the differences in formation. Indeed, according to the R^2 values, the correlations are very good and the results suggest that, when the formation is at a very poor level, further deterioration has a negative effect on the wet tensile and tensile stiffness indices.

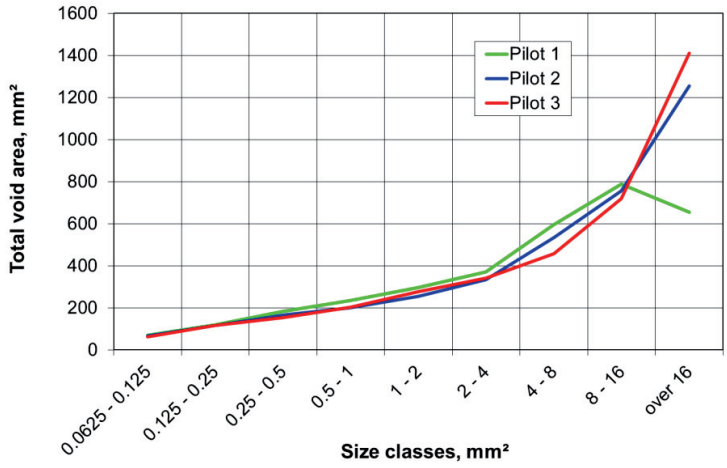

***Figure 63**. Total area of voids (median - 4 g/m²) belonging to different size classes. Pilot papers. Specimen size 12x12 cm².*

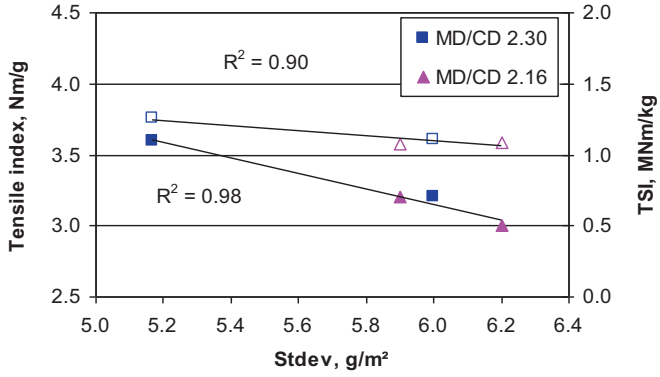

***Figure 64**. Tensile index (left axis and solid symbols) and tensile stiffness index (right axis and open symbols) as a function of formation (Ambertec). Tensile stiffness index values are multiplied by 10 to accommodate the curves in the same figure. Tensile MD/CD ratios 2.3 and 2.16. DSC 40%.*

4.5 The effect of MD effective shear on strength properties

The way in which each paper layer is formed during dewatering is governed by the conditions of the flow field that were prevailing as that layer was drained. As such, the effective shear map contains information of the shear field during dewatering and the paper structure. The evenness of the map may therefore correlate with strength properties. In the following, the effective shear maps are evaluated visually.

Pilot papers 1 and 2 have exactly the same fibre orientation, with paper 3 being only marginally lower, cf. Table 16. Tensile indices were 3.6, 3.2 and 3.0 respectively. When the papers are visually compared, it turns out that the strongest paper, paper no. 1, has the most even effective shear map in CD, see Figure 65. In addition, there is what appears to be a strong belt in the middle of the specimen. This originates from the anisotropy profile in the z-direction, see Figure 66. Papers 2 and 3 are much more fragmented.

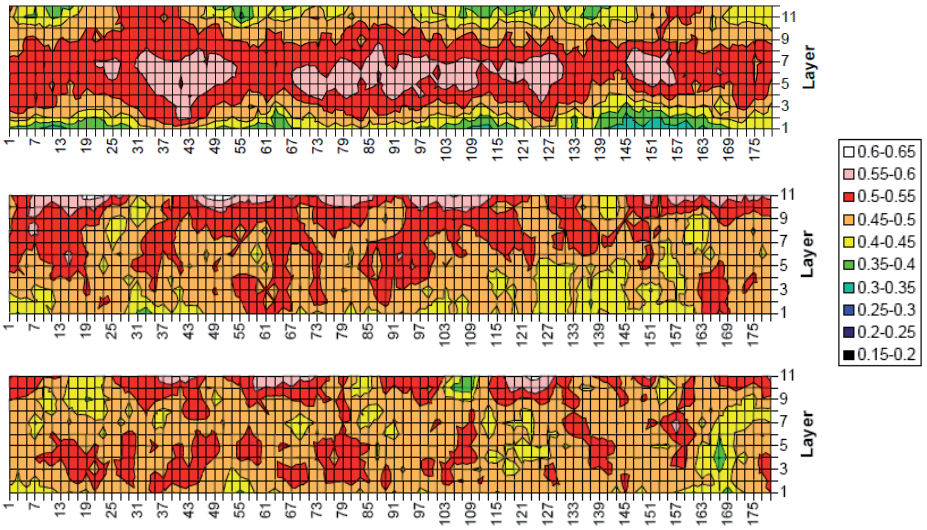

Figure 65. *Effective shear maps for pilot papers 1 (top), 2 (middle) and 3 (bottom). CD position in millimetre scale. Layer no. 1 is the bottom layer.*

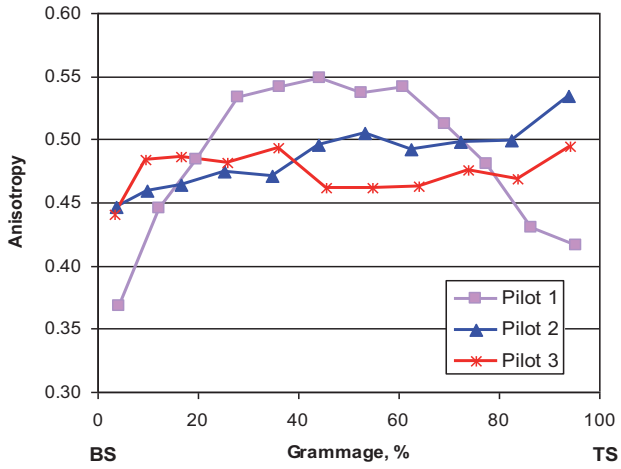

***Figure 66**. Layered anisotropy of the pilot papers in different paper layers, starting from bottom side.*

The influence of MD effective shear evenness gets support from the comparison of LWC base papers A1 and A3, see Figure 67. Both papers have very similar layered anisotropy profiles in the z-direction (Figure 56, Page 124), exactly the same mean fibre orientation according to layered anisotropy and tensile MD/CD ratio but paper A1 has much poorer formation, cf. Table 15 (Page 125). However, it seems to have a more even MD effective shear map in CD and 13% higher wet tensile strength and 5% higher wet TSI.

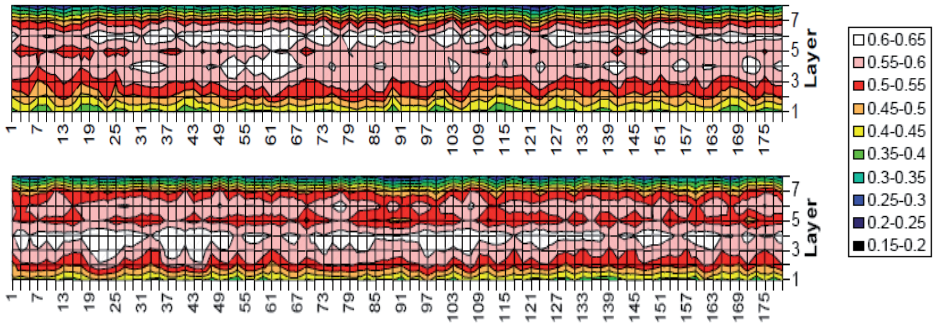

***Figure 67**. Effective shear maps for LWC base papers A1 (top) and A3 (bottom). CD position in millimetre scale. Layer no. 1 is the bottom layer.*

Figure 68 shows the comparison of papers News E2, E5 and E6. All three papers have fairly similar mean layered anisotropy values, cf. Figure 53 (Page 120), but the type of anisotropy profile varies. Papers E2 and E5 have a very similar one-maximum anisotropy profile type but paper E6 shows a clear seagull profile. It is difficult to rank the papers but the evenness of the MD effective shear map of paper E5 appears

to be slightly more uneven compared with the others. Paper E5 should therefore have the lowest wet strength values. Indeed, it has the lowest wet tensile index and wet TSI but the differences between the papers are minor.

On the whole, the results suggest that in addition to the mean fibre orientation the evenness of MD effective shear may have at least some effect on wet strength properties. However, a visual evaluation is not accurate enough and a better method should be developed.

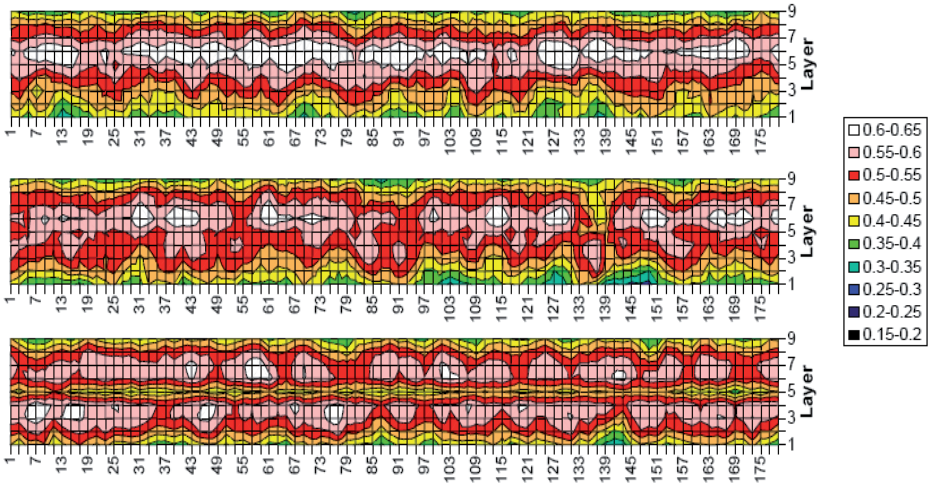

Figure 68. *Effective shear maps for News E2 (top), E5 (middle) and E6 (bottom). CD position in millimetre scale. Layer no. 1 is the bottom layer.*

5 STRENGTH DISTRIBUTIONS IN AHMA TRIALS

5.1 Is the tensile strength of wet paper normally distributed or does it follow an extreme value distribution?

Strength values of individual breaks were available only for newsprint trial points E1–E6 and LWC base paper trial points A1–A3 and B1–B2 for the purpose of investigating strength distributions. Unfortunately, the break signal data for the first two trials, News A, B, C and D, was corrupted due to a computer failure and was not available for distribution analysis.

Based on the references Gregersen (1998), Korteoja et al. (1998b), Uesaka et al. (2001), Hristopulos and Uesaka (2003) and Wathén and Niskanen (2006), the two-parameter Weibull and modified Gumbel distributions can be considered appropriate candidate models for the tensile strength of dry paper webs. However, because it is not known whether the strength distribution of a wet paper web can be described by any extreme value distribution at all, Gaussian distribution was included in the comparison. In addition, the modified Gumbel distribution was replaced with the Gumbel distribution for minimum, Equation (4), due to the reason explained below.

There are two very different analysis paradigms available to clarify the applicability of the model. They are the traditional statistical approach by testing the null hypothesis and Akaike's Information Criterion (AIC) (Akaike 1973). AIC is not a "test" in any sense, and there are no associated concepts such as test power, p values, subjective α levels or subjective partition of the measured data into bins as in a χ^2-test. It is good to bear in mind that there is a theoretical basis to information-theoretic approaches to model selection criteria, while the null hypothesis testing for model selection provides no general way to rank models, even if the models are nested (the model is nested if it is a special case of another model; for example, a second-degree polynomial is nested within a third-degree one). (Burnham and Anderson 2002.)

For these reasons, the model fit and selection of the best model from the set of candidate distribution models (two-parameter Weibull, Gumbel for minimum and Gaussian) were performed using Akaike's Information Criterion (AIC), cf. Chapter 3.6.4.

One additional reason for the decision to use AIC is that it allows a ranking of models and the identification of models that are nearly equally useful versus those that are clearly poor explanations for the data at hand (Burnham and Anderson 2002). For example, the shapes of the Weibull and Gumbel distributions may be very similar but with the selected procedure they can be ranked for estimating a probability distribution for a particular data set.

Maximum likelihood estimates and AIC values were computed with Matlab using the Wafo toolbox (2009). Because the toolbox does not provide the maximum likelihood estimates for the modified Gumbel distribution, the distribution was replaced with the Gumbel distribution for minimum. However, the toolbox provides maximum

likelihood estimates only for the Gumbel distribution for maximum, Equation (19) (Bury 1975, p. 371), and not for the Gumbel distribution for minimum, Equation (4). The computation was therefore performed using data multiplied by -1 and Equation (19). This made it possible to obtain the maximum likelihood estimates required.

$$G(\sigma) = \exp\left[-\exp\left(-\frac{\sigma - \mu}{\alpha} \right) \right] \tag{19}$$

where μ is the location parameter
α is the scale parameter, $\alpha > 0$.

There is a close relationship between the least square and maximum likelihood methods for linear and nonlinear models, where the error terms are normally distributed (Burnham and Anderson 2002). Thus the maximum likelihood estimates could have been computed using the least squares theory. However, when considering the candidate distribution models (modified) Gumbel and Weibull, the error terms cannot be expected to be normally distributed.

The Gumbel distribution is widely used to describe the strength of materials. However, in contrast to the Weibull and modified Gumbel distributions there is a finite probability of failure, even at zero stress, as discussed in Chapter 2.2.2. Due to this reason the Gumbel distribution overestimates the failure probability at low stress levels, which are a long way from the median stress level. However, the cumulative failure distribution usually approaches either the Weibull or Gumbel form near its median (Duxbury et al. 1994). Thus it is likely that if the weak tail of the distribution is slender, the Gumbel distribution is a reasonable candidate for modelling strength behaviour. This may especially be the case with wet paper webs, which may demonstrate only a very minor weak tail or no tail at all.

Due to the reasons discussed above, the replacement of the modified Gumbel distribution with the Gumbel distribution for minimum was considered reasonable.

Burnham and Anderson (2002) recommend the use of a second-order variant of AIC (AICc) instead of AIC when the ratio *n/K* (*n* is sample size and *K* the number of estimable parameters in an approximating model) is less than 40. In AICc, the bias correction term is multiplied by a constant, the size of which depends on *K* and *n*. In our trials, the average number of breaks per trial paper was 87. More accurately, for News E1–E6 there were an average of 83 breaks at DSC 56%, 96 at DSC 68% and 99 with dry papers. For LWC base papers A1–A3 and B1–B3, the respective figures were 61, 84 and 100. This suggests that AICc would be the recommended option. However, *K* is the same for all of the candidate models — in our case *K* is 2. This means that the difference between the models is the same, irrespective of whether AIC or AICc is used. AIC was therefore selected for reasons of simplicity.

The value of the maximised log-likelihood (i.e. $\log(L(\hat{\theta}))$ and the value of AIC varies substantially from sample to sample. For example, sample size and absolute values of data points have an influence here. However, all the comparisons of models are made

using the same data, making the sample-to-sample variation irrelevant. This all means that it is the relative values and particularly the AIC differences (Δ_i) that are important, not the absolute magnitudes. (Burnham and Anderson 2002.) AIC differences were computed according to formula (20).

$$\Delta_i = AIC_i - AIC_{min} \quad (20)$$

There are no strict rules to indicate how large an AIC difference must be to be of significance. However, Burnham and Anderson (2002) provide the following rough rules for nested models:

Δ_i	Level of empirical support on model
0–2	Substantial
4–7	Considerably less
> 10	Essentially none.

According to the rough rules above, models having Δ_i within 1–2 of the best model have substantial support and should receive consideration in making inferences. Models having Δ_i within about 4–7 of the best model have considerably less support, while models with $\Delta_i > 10$ have either essentially no support, and might be omitted from further consideration, or at least those models fail to explain some substantial explainable variation in the data. (Burnham and Anderson 2002.)

The guideline values may be somewhat larger for non-nested models, and more research is needed in this area (Burnham and Anderson 2002). Because the literature survey did not provide any better guidelines, the above values are employed.

Table 17 shows both computed AIC values and AIC differences. A colour code, based on the guidelines above, was established to visualise possible differences between the Gaussian and extreme value distributions. As the table shows, there is strong evidence that, at the lowest DSC of 56%, tensile strength is distributed normally and both the extreme value distributions, two-parameter Weibull and Gumbel to minimum, provide a poor fit to the actual strength distribution — see Figure 69, where the actual and modelled cumulative distributions are compared. The figure shows both the actual and modelled Gumbel distributions as a mirror image due to the computational method used for the computation of the Gumbel function.

Based on AIC differences, the Gaussian distribution also provides a better fit at the higher DSC of 68%. However, the performance of the Gaussian and extreme value distributions of newsprint series E start to resemble each other. According to visual evaluation, both the extreme value distributions perform well on the middle area of the distribution. However, they provide a poorer fit at the low end of the strength distribution, although the difference to the Gaussian distribution is much smaller than at DSC 56%. At DSC 68%, the LWC base papers show stronger Gaussian behaviour than newsprint series E based on AIC values and visual evaluation. However, Gaussian behaviour also weakened in their case according to AIC differences; only two papers out of five show strong Gaussian behaviour instead of four at DSC 56%.

The final piece of strong evidence in favour of the Gaussian distribution for wet papers is that it has the smallest AIC value 21 times out of 22.

***Table 17**. AIC differences and AIC values for News series E and LWC base paper series A and B. Colour code: Green = substantial evidence that both Gaussian and extreme value distributions can be used to describe the strength data. Yellow = considerably less support for that. Pink = it is very unlikely that both Gaussian and extreme value distributions are suitable choices.*

Dry Solids Content 56%						
	Δ_i			**AIC**		
Data Set	**Weibull**	**Gumbel**	**Gaussian**	**Weibull**	**Gumbel**	**Gaussian**
E1	8.8	10.3	**0**	552.5	554	**543.7**
E2	8.3	9.9	**0**	608.5	610.1	**600.2**
E3	16.1	18.5	**0**	585.8	588.2	**569.7**
E4	19.7	22.3	**0**	698	700.6	**678.3**
E5	1.6	2.5	**0**	550.1	551	**548.5**
E6	5.7	6.8	**0**	394.1	395.2	**388.4**
A1	0.6	1	**0**	361.1	361.5	**360.5**
A2	17.9	19.7	**0**	419.2	421	**401.3**
A3	21.3	23.3	**0**	424.4	426.4	**403.1**
B1	11.7	13.6	**0**	371	372.9	**359.3**
B2	8.3	10.2	**0**	524.7	526.6	**516.4**
Dry Solids Content 68%						
	Δ_i			**AIC**		
Data Set	**Weibull**	**Gumbel**	**Gaussian**	**Weibull**	**Gumbel**	**Gaussian**
E1	0.4	1.7	**0**	758.3	759.6	**757.9**
E2	2.8	4.3	**0**	736.8	738.3	**734**
E3	1.2	2.9	**0**	892.5	894.2	**891.3**
E4	0.9	3	**0**	752.2	754.3	**751.3**
E5	**0**	0.6	5.4	**714.9**	715.5	720.3
E6	16.4	19.1	**0**	807.2	809.9	**790.8**
A1	4.3	5.5	**0**	608.1	609.3	**603.8**
A2	19.1	22.1	**0**	656.8	659.8	**637.7**
A3	6.5	7.7	**0**	672	673.2	**665.5**
B1	7.2	9.2	**0**	586.7	588.7	**579.5**
B2	10.6	12.8	**0**	796.5	798.7	**785.9**
Dry						
	Δ_i			**AIC**		
Data Set	**Weibull**	**Gumbel**	**Gaussian**	**Weibull**	**Gumbel**	**Gaussian**
E1	1.6	**0**	40.4	1149	**1147.4**	1187.8
E2	7.6	**0**	71.4	1190.9	**1183.3**	1254.7
E3	5.8	**0**	65.9	1218.9	**1213.1**	1279
E4	**0**	**0**	13.5	**1118.8**	**1118.8**	1132.3
E5	2.8	**0**	52	1159.3	**1156.5**	1208.5
E6	**0**	0.5	8.3	**1136.5**	1137	1144.8
A1	0.2	**0**	17.4	1104.3	**1104.1**	1121.5
A2	4.5	6.4	**0**	1182.9	1184.8	**1178.4**
A3	**0**	0.1	11.1	**1125**	1125.1	1136.1
B1	**0**	0.7	4	**1273.5**	1274.2	1277.5
B2	**0**	2.1	0.7	**1238.5**	1240.6	1239.2

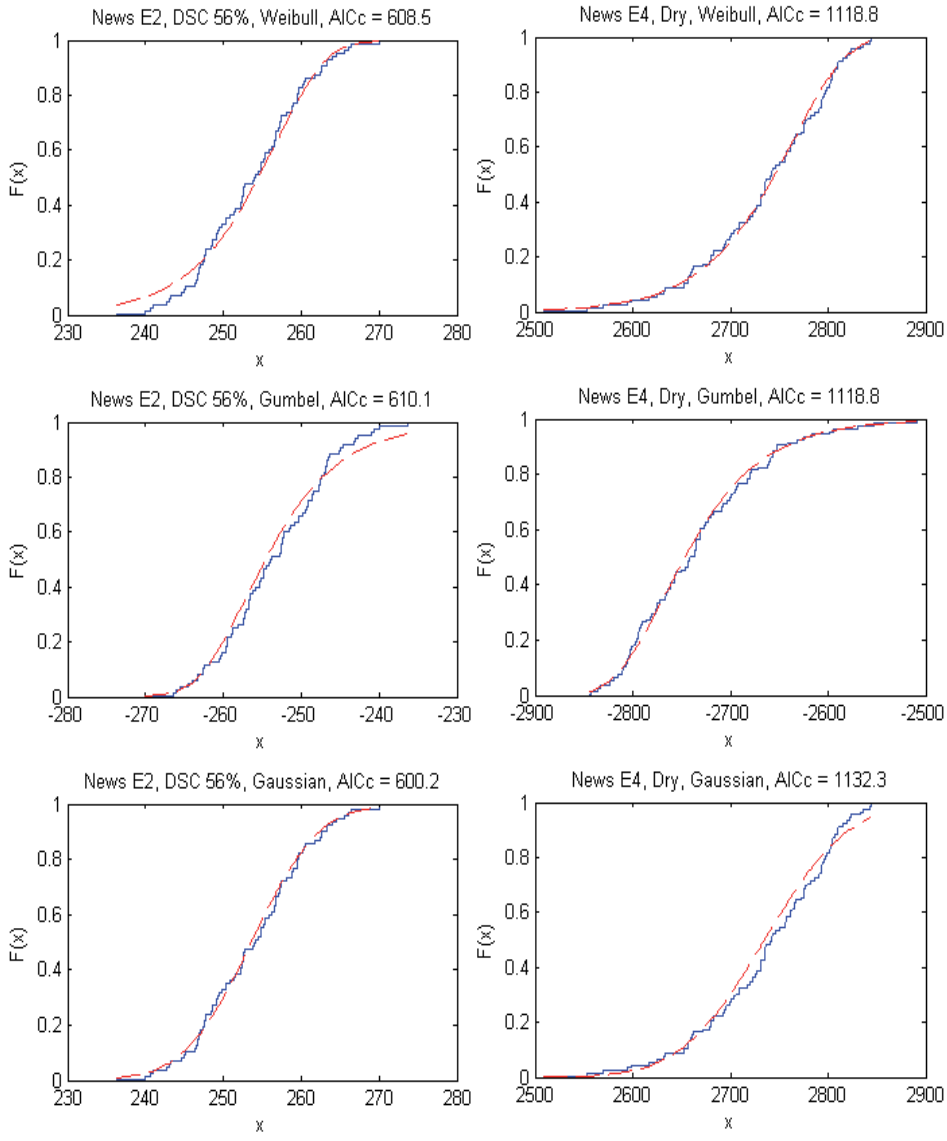

Figure 69. *An example of measured and modelled cumulative tensile strength distributions. The measured tensile strength values on x-axis as N/m. News E2 at DSC 56% on the left and News E4 dry on the right. Fitted models are two-parameter Weibull, Gumbel for minimum and Gaussian distributions. The measured data (blue solid line) and the modelled distribution (red dashed line) in the Gumbel distribution plots are shown as mirror images due to the computational method used.*

According to Table 17 and Figure 69, the tensile strength distribution of dry papers follows extreme value statistics. Based on AIC difference, the two distributions—two-parameter Weibull and Gumbel for minimum—seem to perform fairly equally

except in two cases: two newsprint trial points where the Gumbel distribution outperforms the Weibull distribution. Based on a visual evaluation of the distributions fitted to the data of all dry papers, it is impossible to give any priority to either of the extreme distributions when both the low tail and middle area of the distributions are considered.

To conclude, the results suggest that the tensile strength of wet paper—at least at dry solids contents typical to the press section and the first part of the drying section—is normally distributed instead of any extreme value distribution.

5.2 The effect of paper structure on the strength distribution of wet and dry paper webs

Focus has been so far on the interaction between a web structure and average strength properties. For example, the pilot results showed that when formation is poor, it reduces the average tensile strength and tensile stiffness of wet webs, see Figure 64 (Page 131). On the other hand, if formation is good or fairly good, no negative effect exists. Instead, another structural property—fibre orientation—has an influence on the average tensile strength and tensile stiffness in wet paper, cf. Figures 49 and 51 (Pages 116 and 118).

Hristopulos and Uesaka (2003) showed formation on the length scale smaller than a few mm to have an effect on the tensile strength distribution of dry paper. In this chapter, the aim is to investigate whether paper structure has some influence on the tensile strength distribution of wet paper. Any possible effects are measured for tensile indices as a change of Coefficient of Variation (subsequently referred to as COV) and Weibull modulus. However, the latter is computed for dry papers only. Paper structure is described by means of fibre orientation and local basis weight variation in different wavelength bands and void size classes.

Table 18. *COV (computed as an average of the papers) for the tensile index of News and LWC base papers, differences between the maximum and minimum COV in each paper group and the weighted averages (two last rows) for COV and skewness (weighting by the number of papers in each paper group).*

	DSC 56%		DSC 68%		Dry	
	COV	Max-Min	COV	Max-Min	COV	Max-Min
News E1–E6	2.70	0.25	3.31	1.11	4.05	3.97
LWC A1–A3	2.14	0.15	2.70	0.58	3.23	0.48
LWC B1–B2	3.39	0.09	3.56	0.55	3.43	0.36
COV, average	2.67		3.19		3.71	
Skewness, average	0.19		-0.15		-1.37	

According to Table 18, COV is smaller and varies considerably less at a DSC of 56% compared with those at DSC 68%. In addition, the skewness values suggest the

strength distribution to turn from Gaussian into a left tailed extreme value distribution as paper dries. This result is consistent with the results shown in Table 17 (Page 138).

Because COV varied only slightly at a DSC of 56%, it is understandable that no statistically significant correlation was found between COV and structural parameters, see Figures 70 and 71 as examples.

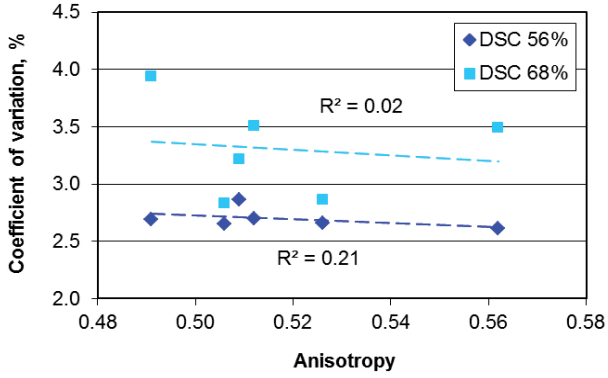

Figure 70. *COV of tensile index as a function of layered anisotropy. News E1–E6.*

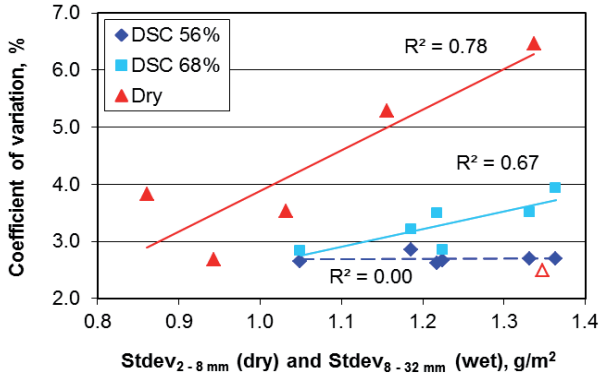

Figure 71. *COV of tensile index as a function of local basis weight variation in wavelength bands 8–32 mm (wet papers) and 2–8 mm (dry papers). Formation measurements by β-radiography. All the formation values of dry papers are deducted by 1.5 g/m² in order to accommodate both wavelength bands in the same figure. News E1–E6. The result of dry trial paper E4 (open symbol) is excluded from the correlation analysis due to an extraordinary high Weibull modulus.*

According to Table 19 and Figure 70, fibre orientation does not influence the strength distribution of wet or dry paper although it has an effect on average strength values as shown earlier. On the contrary, formation seems to have a significant effect on the width of the strength distribution at a DSC of 68% and in dry paper, cf. COV and

Weibull modulus values in Table 19 and in Figure 71. Interestingly, the results suggest that the intensity of the effect depends both on the scale of formation and on DSC (no effect at DSC 56% and the greatest effect in dry papers). At a DSC of 68%, correlation becomes stronger when the scale of formation increases. Finally, on the large scale—wavelength range 8–32 mm and total void area in size class 8–16 mm²—correlation is statistically significant at a 95% confidence level. Conversely, in dry papers correlation is strongest on the wavelength band 2–8 mm.

Table 19. *Correlation coefficients and respective p values for the correlations between structural parameters and COV and Weibull modulus β for the tensile index of News E1–E6. Highlighted correlations are statistically significant at a confidence level of 95%.*

	COV, DSC 68%		COV, dry *)		Weibull modulus, dry *)	
Measurement	p value	R	p value	R	p value	R
Layered anisotropy	0.791	-0.141	0.580	0.336	0.544	-0.369
Tensile MD/CD ratio	0.721	0.188	0.470	0.430	0.419	-0.475
β-radiography	0.064	0.786	0.048	0.881	0.027	-0.920
β-radiography $_{0.25–2\ mm}$	0.303	0.508	0.281	0.604	0.215	-0.671
β-radiography $_{2–8\ mm}$	0.063	0.787	0.045	0.886	0.028	-0.918
β-radiography $_{8–32\ mm}$	0.047	0.818	0.053	0.874	0.069	-0.849
Voids $_{1–8\ mm^2}$	0.232	0.575	0.084	0.828	0.059	-0.865
Voids $_{8–16\ mm^2}$	0.037	0.838	0.162	0.730	0.212	-0.675

*) Trial paper E4 is excluded due to an exceptionally high Weibull modulus, c.f. Chapter 7.

Although the results of newsprint series E1–E6 were consistent, those of LWC base papers A1–A3 and B1–B2 were not. In the first-mentioned LWC base paper series, COV had a tendency to increase at dry solids contents 56% and 68% when formation deteriorated, irrespective of a formation parameter, but papers B1–B2 behaved conversely, cf. Figure 72. Fibre orientation results were also inconsistent, see Figure 73. In addition, because fibre orientation and formation strongly correlated in LWC base papers, no conclusions can be drawn.

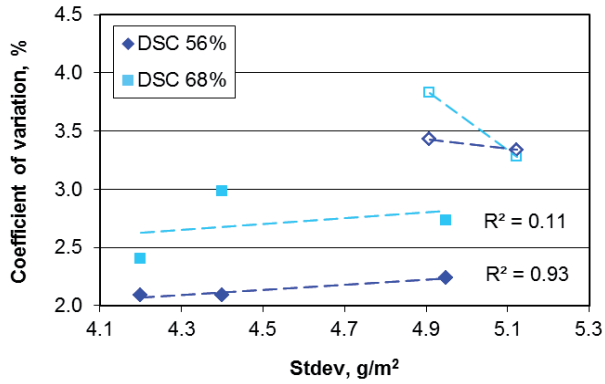

Figure 72. *COV of tensile index as a function of formation (β-radiography, wavelength band 0.25–32 mm). R² values are computed for papers A1–A3. Solid symbols denote papers A1–A3 and open symbols papers B1–B2.*

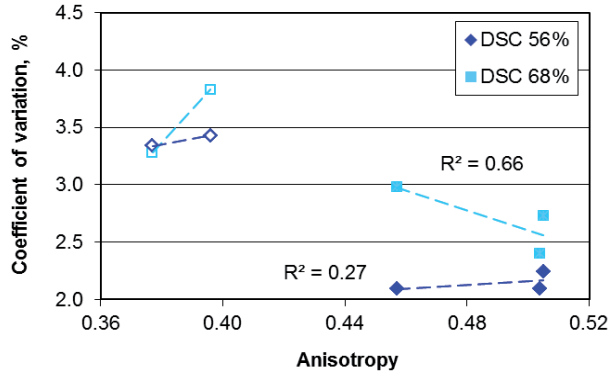

Figure 73. *COV of tensile index as a function of layered anisotropy. Solid symbols denote papers A1–A3 and open symbols papers B1–B2.*

6 EFFECT OF DEFECTS

The effect of defects was tested by making CD notches in the middle of the web. Instead, edge notches were not used because it was conceivable that the long web lead might cause the web to move sideways leading to variable notch length. The notch-making device was located in the AHMA runnability device between the spray unit and the lower nip moistening unit, item 6 in Figure 24. Table 20 shows the trial settings. In the first trial series, 94 breaks per trial point were measured on average with notches from wet papers and 177 from dry papers. The figures without notches were 258 and 237 respectively. In the third trial series, measurements comprised on average 44 breaks per trial point with notches and 87 breaks without notches.

Table 20. *Trial settings for notching runs.*

Trial series	I	III
Papers	News A and B	News E1-E6, LWC base papers A1–A3 and B1–B2
Web speed, m/s	2	1
Delay time, s	1.5–2.8 (DSC 80%) 3.6–4.9 (DSC 65%)	12.2 (DSC 68%) 8.5 / 12.2 (DSC 56%)
Moistening method	2 nips, DSC 80% Two-sided spray, DSC 65%	Spray, DSC 68% Spray + 1nip, DSC 56%

According to Figure 74, the effect of CD centre notches decreases rapidly as a function of lowering DSC. The results suggest that even 4 cm wide CD centre notches do not weaken the wet web at DSC typical for the first part of the drying section.

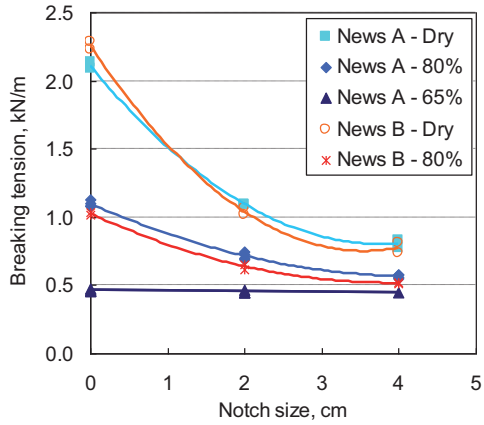

Figure 74. *Breaking tension as a function of the width of CD centre notches and dry solids content.*

Figure 75 shows that, irrespective of furnish, formation and orientation, the effect of 2 cm wide CD centre notches has already disappeared at DSC 68%. This result

confirms the insensitivity of the wet web to defects in the first open draw after the press section and in the first part of the drying section.

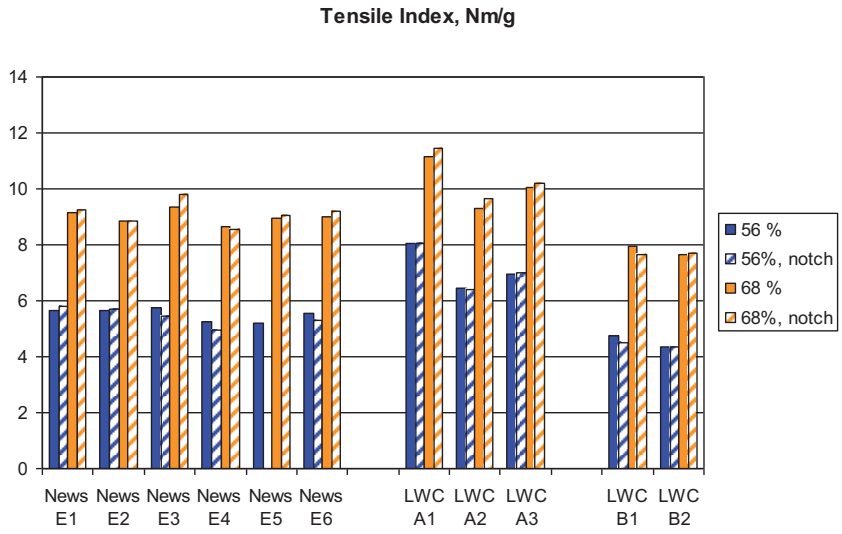

***Figure 75**. Breaking tension of webs affected by 2cm wide CD centre notches compared with intact webs. DSC 56% and 68%. Newsprint E and LWC base papers A and B.*

7 DISCUSSION

Tensile strength, elastic modulus (tensile stiffness) and residual tension were considered the important parameters describing wet web runnability, cf. Chapter 2.1. The first two can be measured using the AHMA runnability pilot. However, before proceeding to any pilot trials, a considerable amount of methodology development was needed because wet web properties were studied by running re-wetted paper webs on AHMA. Although the device has been used to apply water amounts typical to offset printing, the method enabling paper re-wetting down to DSC typical to the press section and the first part of drying section has been missing. A re-wetting system therefore needed to be developed. An inevitable question arose: "What is the congruence between the web taken from the press section and the re-wetted web?" The answer to this question was based on the following clarifications: firstly, it was studied how the hornification of fibres and fines induced by wet pressing and drying on a paper machine affects the congruence, and whether there is some structural hornification that affects the relative contact area (RCA) between fibres. Secondly, it was clarified whether AHMA provides similar wet strength results with in-situ measurements on a pilot paper machine.

The effect of hornification and the bonding mechanism in a wet web

The effect of hornification was thoroughly discussed in Chapters 3.1.2–3.1.4, and the bonding mechanism was covered in Chapter 2.3.2; therefore only a short summary is provided here. Fibres and fines experience hornification with the effect depending on morphology and chemical composition. Hornification makes chemical pulp fibres stiffer, improving the tensile stiffness of a wet web, but has no influence on wet web tensile strength (Miettinen et al. 2007b, Kulachenko 2008, Kulachenko et al. 2008, Tanaka et al. 2009).

Interestingly, based on recycling studies (without chemicals), Brancato and Banerjee (2010) noticed that hornification reduced nanoscale roughness of dry chemical pulp fibres measured at RH 50% but TMP fibres were relatively unaffected. If this effect stays when the fibres are re-wetted, the reduced roughness may or may not have an influence on wet tensile strength originating from the bonding mechanism in a wet web.

Although the bonding mechanism is not fully understood (cf. the discussion in Chapter 2.3.2), the entanglement friction (de Oliveira et al. 2008, van de Ven 2008, Tejado and van de Ven 2009a, 2009b, 2009c) plays an important role in wet strength. The entangled fibre network provides the normal force on fibre crossings. This force multiplied by the coefficient of friction constitutes a part of the friction force operating on the fibre contacts with the other part consisting of the initial tangent adhesive force (Andersson and Rasmuson 1997, Huang et al. 2009). The latter is independent of the normal force. Instead, its origin is in various attractive forces, such as capillary, electrostatic, van der Waals and chemical bonding under different circumstances (Maboudian and Howe 1997). In addition, provided that water menisci

exist on the fibre contact points, the shear resistance of those menisci between fibres affects the initial tangent adhesion force (Kulachenko 2008, Kulachenko et al. 2008).

Based on the work of Andersson et al. (2000) and Kulachenko (2008) and Huang et al. (2009), it is obvious that increasing the nanoscale surface roughness of fibre contact areas increases the coefficient of friction but simultaneously reduces the initial tangent adhesion at dry solids contents typical to a press section and initial part of the drying section. According to the results of Huang et al. (2009) the higher the DSC the higher the coefficient of friction. Instead, the results of Andersson et al. (2000) showed wet fibres to have both higher coefficient of friction and initial tangent adhesion compared with dry fibres. In addition, because both friction components may develop at different rates as a function of DSC, the general effect on wet strength properties cannot be unequivocally predicted.

Mechanical pulp fines have an important role in improving the wet strength properties of wood-containing papers. Depending on the morphology, they perform different kinds of structural functions in a fibre network. For example, they can act as the "filling" in a "sandwich" and forming bonds between two fibres, or they can fill interstices and bridge gaps in the fibre network, shortening the deflection distance required to constitute additional fibre contacts in wet pressing, or they can simply have a neutral filling role without having any effect on strength. (de Silveira et al. 1995, Görres et al. 1996.) Mechanical pulp fines are likely to coagulate irreversibly to some degree due to wet pressing and high web temperature in the final part of the drying section, causing reduced pore volume between the fines particles (Maloney et al. 1997, Weise 1997). This might reduce their capability to act as bridge makers in a re-wetted web, leading to slightly deteriorated wet strength properties compared with a never-dried web.

However, our clarifications related to possible structural hornification showed that wet pressing and drying followed by re-wetting of the specimen did not change the relative contact area in the fibre network. Neither the mean pore height nor the pore width changed (cf. Chapter 3.1.3). This result suggests that hornification does not cause structural alterations that could reduce wet strength properties. Certainly there remains a small uncertainty in the results because the wet pressing was done too gently compared with machine-made papers and drying was performed at room temperature rather than high temperature.

In any case, when considering the bonding mechanism in the wet web based on the current understanding, it is evident that the microstructure of the re-wetted web does not differ so much from that of a never-dried web that it would lead to faulty results or conclusions if the wet web strength properties were studied using re-wetted paper webs instead of never-dried webs. This is an important result.

Correspondence between wet strength properties measured by AHMA and in situ on the press section

The issue was studied by using the results of Barnet and Harvey (1980), Mäkinen (2003) and Tanaka et al. (2009), cf. Chapter 3.4. The results of Tanaka et al. (2009)

showed that the tensile strength of wet webs measured in situ on the press section were similar to the results of AHMA when the wet webs were wound by the wet web winder located right after the press section (cf. Figure 62, Page 130) and measured after that on AHMA. However, stretch at break on AHMA remained much smaller but tensile stiffness was larger. The reason for that lies in the different straining history. In the press section, paper was strained by the wet web winder until rupture. However, on AHMA, paper straining consisted of straining during winding on the wet web winder, straining on the path from the unwinder to the test draw and straining until rupture on the test draw, cf. Figure 24 (Page 71).

Based on the results of Barnet and Harvey (1980), Mäkinen (2003) and Tanaka et al. (2009), it was possible to show that the tensile strength and the total strain of a wet web is independent from the straining history if straining is not extensive. This means that the measured tensile strength does not change although the division of wet web straining between the test draw of AHMA (cf. Figure 24) and the path from re-wetting to the test draw would change. In addition, the total strain remains unchanged but the tensile stiffness naturally changes when the share of strain on the test draw changes.

If the speed differences from the unwinder to the draw nip were recorded in our trials, the total strain and the share of that performed on the test draw would be known. This would help when evaluating the tensile stiffness values measured in the different trial points. However, pre-tensions in our trials were at a very low level, for example in the trial series III, News E1–E6 and LWC base papers A1–A3 and B1–B2, they were 80 N/m in the first and second measurement points (items 5 and 8 in Figure 24) and 88 N/m in the last measurement point (item 11). This means that inside the run of each paper grade and at constant DSC, either 56% or 68%, any possible differences in the total pre-strain are most likely minimal, making the comparison of tensile stiffness values reliable.

To conclude, there is good correspondence between the wet tensile strength measured on AHMA and in situ on a paper machine. The stretch-at-break values are lower on AHMA due to all wet straining performed before the test draw on AHMA. However, if that straining is kept constant, the stretch-at-break and tensile stiffness values measured on AHMA accurately follow the in situ measured values, although on a different level. These are important conclusions.

Re-wetting system

An ideal re-wetting procedure would consist of re-wetting AHMA reels with a separate re-wetting device and sealing the re-wetted reels after this in plastic sacks for 1–2 hrs to even out the moisture. However, the test showed that the procedure generates wrinkles in the paper, leaving re-wetting on AHMA as the only option. Although water penetration into paper pores and diffusion into fibres are very quick phenomena as shown by the literature survey and laboratory tests (cf. Chapter 3.5), it is clear that diffusion cannot be fully completed in the time frame applicable on AHMA. This may lead to two conceivable effects at constant DSC: firstly, a slightly vaster amount of water between fibres somewhat reduces the tensile strength and

tensile stiffness of wet paper and secondly, chemical pulp fibres are a little stiffer, leading to slightly higher wet paper tensile stiffness but leaving the tensile strength intact. However, the theoretical examination and the tests carried out suggest that, for the type of papers tested (newsprint containing at least 50 RCF and LWC base paper), the delays varying from 4 s to 12 s—depending on the re-wetting arrangements and targeted DSC (below 70%)—were adequate (and at higher DSC levels even shorter delay times are adequate in a two-sided nip application). Strength values were also repeatable. This becomes evident when observing the results of individual trial points of papers News A and News B (trial series I). Two rolls were run at every trial point and the measured strength values were close to each other as Figure 26 shows.

When News E1–E6 and LWC base papers A1–A3 and B1–B2 were run, only one roll per trial point was measured. However, the repeatability can be evaluated by comparing the results measured at DSC 68% and 56%, see Figure 76. If the repeatability is good, the correlation should be 100%. Indeed, the correspondence between the measurements was extremely good with two exceptions. There were two deviations in the newsprint series, the reason for which could not be ascertained. Because of the deviations, analyses carried out in this thesis have been based not only on the results measured at DSC 56% and 68% but also on the averages of those measurements. This meant it was possible to reduce the effect of the deviations.

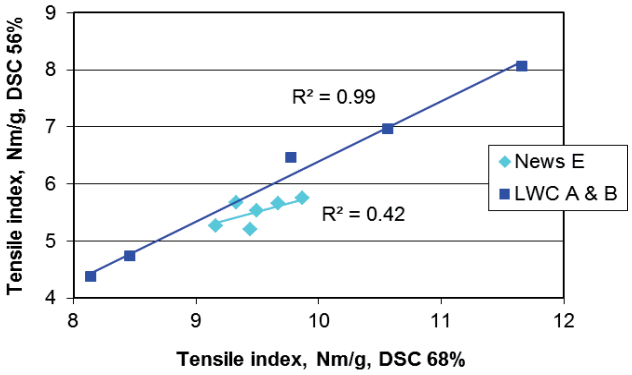

***Figure 76**. Correlation between the tensile indices measured at DSC 68% and 56%. Newsprints E1-E6 and LWC base papers A1-A2 and B1-B2.*

The evaluation of the re-wetting system has been based so far only on the average strength values. However, it can be speculated whether there existed any kind of moisture variation in a wet web in the z-direction and/or in the x-y plane that could have affected strength variation. Although it was shown that possible moisture variations did not affect the average strength values, this may not have been the case for strength variation.

The discussion is confined to News E1–E6 and LWC base papers, because the strength variation data was available only for those papers. Liquid flow through a porous medium is greatly complicated by the many time- and length-scales that are involved. For example, capillary flow can be a basic capillary rise (piston-type of

bulk flow), a flow along the channels formed by fibre overlaps and a film type of flow along the edges of the pores when the advancement is halted by discontinuities in the pore structure, c.f. the discussion in Chapter 3.5.1. A gradually thickening film collar in a pore may lead to a film collapse (i.e. snap-off type pore filling). The snap-off phenomenon is heavily weighted to the smaller pores but the larger pores remain partially wet along the pore edges (Roberts et al. 2003). Snap-off is relatively slow process since it requires the wetting phase to be transported by flow through wetting films. The rate at which the wetting phase can be transported depends on the area available for flow (film thickness and pressure) (Senden and Knackstedt 2000).

Based on the discussion above, it is conceivable that the moisture distribution may have had some influence. However, there is a strong probability that at DSC 56% water distribution throughout the entire sheet structure was very even. This is based the following reasoning. Firstly, as discussed in Chapters 3.5.1 and 3.5.4, fast capillary penetration is probably the most important water transport mechanism quantitatively when there is a surplus of water. The average interfibre porosity for News E1–E6 is 30.3%. This means that a theoretical "infinite" water amount to fill all the interfibre pores is 16.1 g/m². This is a considerably smaller amount compared with the applied water amount 28.9 g/m². Secondly, the big surplus of water enables a fast diffusion from the interfibre pores to the fibres. Thirdly, a long delay from the water application to the test draw (12.2 s from the spray application and 8.5 s from the nip application) is long enough to complete the equalization of water distribution in the sheet. In addition, the latter nip application provides an effective piston type of flow.

The situation is slightly more complicated at a DSC of 68%. The applied water amount 15.9 g/m² approximately equals the "infinite" water amount 16.1 g/m². It is therefore evident that the diffusion, the channel flow and the film type of flow have a more important role in moisture equalization in the z and x-y directions compared with the situation at DSC 56%. In addition, it is likely that the snap-off type of pore filling is also more important at DSC 68% leaving large pores partly unfilled. It is therefore conceivable that there would remain local moisture gradients in the z and x-y directions in the web going to the test draw in AHMA. However, the closed nip of the nip moistening device most likely effectively promotes moisture equalization in all the directions in the wet web. In addition, based on the discussion in Chapter 3.5, it is evident that the used re-wetting system with the delay of 12.2 s is adequate to provide fairly even water distribution into and between the fibres in the whole fibre network (important from wet strength properties point of view) leaving larger pores only partly filled.

As a summary, it is suggested that most of the water reaches "the final destination" in the time frame applicable in AHMA, meaning that the final equalization would not have any practical effect on the measured average wet strength properties or their distribution. It is therefore justified to conclude that any possible strength variation at DSC 56% or 68% is not caused by a water distribution in the sheet but by a variation in paper structure. As a comparison, there is most likely a formation originating small scale moisture variation also in the web coming from the press section on a paper machine.

Finally, because pressure in the nip moistening device was high, comparable with the average nip pressure on a paper machine, it can be speculated whether this somehow negatively affected the wet web structure and further strength distribution. In the first trial series, News A and News B, web speed 4 m/min indeed turned out to be too harsh causing reduction in breaking tension. It is assumed that forcing a large amount of water very quickly into a dry fibre network causes damage to it. It is plausible that the phenomenon resembles an oozing phenomenon on the press section where too much water is quickly transferred inside a wet network. Alternatively, in News series E1–E6 and LWC base paper series A1–A3 and B1–B2 web speed was only 1 m/min. Although the applied water amount was double to that applied in the first series, the wet web (already moistened by the spray) most likely tolerates fast piston type of capillary flows. As a comparison, water flows inside the wet web on the paper machine press section are very vigorous due to high water amounts removed during a short pressure pulse. To conclude, it is unlikely that the high nip pressure negatively affected the strength properties.

Based on the clarifications of hornification, bonding mechanism in a wet web, the re-wetting system, re-wetting trials and correspondence between wet strength measurements on AHMA and in situ on a pilot paper machine, it can be concluded that wet web strength properties at dry solids contents typical to the press section and the first part of drying section can be measured by running re-wetted paper webs on AHMA. This is a new result because, according to the writer's knowledge, there is no published data related to this issue. In addition, this is an important result because it provides an easy method for mills to study wet strength properties of their papers. The important wet strength properties related to wet web runnability were considered to be tensile strength, elastic modulus (tensile stiffness) and residual tension. The two first properties can be measured using AHMA.

Analysis procedure for the measured data

The AHMA runnability pilot can be run using two different methods, "rheology mode" and "web break mode" (Niskanen et al. 2003). The first is robust when it comes to signal noise because each tension value is an average of 300 readings of the tension signal recorded at 10 ms intervals. However, signal noise is not normally a problem for the latter option either because it can easily be filtered by a low-pass filter, cf. Figure 30. In addition, the "web break mode" allows a large number of breaks to be measured, which is needed for distribution studies. The "web break mode" was therefore employed in this thesis.

Unfortunately, a clear 0.61 s cyclic variation had appeared both in the tension and strain signals in News series E and LWC base paper series A and B. The noise component described above was also present. In addition, the initial tension needed to be kept at a high level, on average 185 N/m, for the reason explained in Chapter 3.6.1. This value is almost double in comparison with the situation involving News A, B, C and D without any cyclic variation. The breaking tension was low at DSC 56%, 250 N/m on average. The difference between the initial and breaking tension was only 65 N/m on average, which is a small number compared with the combined effect of the cycle variation and noise. This was roughly 100–150 N/m from peak to peak

(cf. Figures 31–33), making any curve fitting very challenging. The situation was better at DSC 68% due to the higher average breaking tension of 395 N/m. This increased the mean difference between the initial and break tension to 145 N/m, facilitating curve fitting. The same disturbances were also present in the dry paper measurements but due to high breaking tension values, 2800 N/m on average, they did not pose any difficulties for curve fitting.

One way of evaluating curve fitting at DSC 56% is to compare the coefficient of variation at DSC 56% and 68%. If the value is clearly larger at DSC 56%, that could be considered an indication of poor curve fitting, leading to increased tensile strength variation. However, this was not the case because the coefficient of variation was on average 2.67% at DSC 56% and 3.19% at DSC 68%. Thus it can be concluded that the developed curve fitting procedure worked well, irrespective of the disturbances in the tension and strain signals.

The vibration in the tension and strain signals originated from the vibrating top rolls in the brake and/or draw nip. However, the vibration occurred only in the measured signals but the paper web did not experience any cyclic straining as shown in Chapter 3.6.1.

Strength distributions, rupture and bonding mechanisms

The model fit and selection of the best model from the set of candidate distribution models (two-parameter Weibull, Gumbel and Gaussian) were performed using Akaike's Information Criterion (AIC) (Akaike 1973, Burnham and Anderson 2002), cf. Table 17 (Page 138). The fits were also evaluated visually.

The results at DSC 56% and 68% suggest that the strength of wet paper is normally distributed, although the difference between the Gaussian and extreme value distributions mitigates when DSC increases. According to the results, the tensile strength distribution of dry papers follows extreme value statistics and the results are thus congruent with the earlier published results of Gregersen (1998), Korteoja et al. (1998b), Uesaka et al. (2001), Hristopulos and Uesaka (2003) and Wathén and Niskanen (2006). It is evident that the strength distribution changes gradually from the Gaussian distribution to an extreme value distribution as a function of DSC, for example when the web runs from the press section to the reel. This suggestion is supported by the skewness values computed for the wet and dry papers. The values were on an average 0.19 and -0.15 for papers at DSC 56% and 68%, respectively, and -1.37 for dry papers. Qualitatively, a negative skew indicates that the tail on the left side of the strength distribution is longer than on the right side.

There was also another difference between the dry solids contents. COV for tensile index was on average 2.67% at DSC 56% and 3.18% at DSC 68%. As a comparison, it was 3.71% for dry papers. In addition, variation in COV between the wet trial papers was considerably smaller at the lower DSC, on average 22% of that at DSC 68%. It is likely that compared with the stronger structure at DSC 68%, the wetter and weaker structure at DSC 56% yields more evenly under external load leading to a lower variation in tensile strength.

The gradual change of the strength distribution can be understood on the grounds of the bonding mechanism. In wet paper, bonding between the fibres and fines is based on friction forces and shear resistance as discussed above. When DSC increases, hydrogen bonds start to emerge until, in the dry paper, fibre bonds are largely formed by hydrogen bonding accompanied by van der Waals' forces (Retulainen 1997). The rupture mechanism of paper naturally changes accordingly. The solids content at which actual interfibre bonds form is not exactly known. However, an estimate for the onset of bonding can be derived from the elastic modulus of paper during drying. The change in the modulus must be due to bond formation because wet fibres have a much higher rigidity than wet bonds — the fibres themselves would otherwise disintegrate in water solution. In the case of kraft pulp, the modulus starts to increase at approximately 50% solids content. (Retulainen et al. 1998.)

This means that, at least at the higher dry solids content of 68%, hydrogen bonds contribute to some degree to wet web strength properties. In order to form bonds, distances between particles, fibres and fines need to be short enough. It is natural to think that furnish and wet web microstructure have an influence on those distances and therefore determine the dry solids content for the onset of hydrogen bonding. This probably explains the difference between News E1–E6 and LWC base papers A1–A3 and B1–B2. In any case, the results strongly suggest that the tensile strength is normally distributed at dry solids content typical to the press section and the first part of drying section.

It is evident that the failure and bonding mechanisms and strength distributions are closely interrelated. The simulation work of Miettinen et al. (2007b) and Kulachenko et al. (2009) showed that the deformation of the wet sheet is driven by continuous stick-slip behaviour on the fibre level. This is understandable based on the bonding mechanism allowing individual fibres to slide in relation to each other, stick together, then continue the movement again etc. The works of Kulachenko et al. (2009) and Kulachenko and Uesaka (2012) suggested that at first, when wet paper is loaded, most of the fibre contacts are in the slipping state although the strain field shows a presence of a “criss-cross” type of shear band pattern, however, without any clear sign of strain localization. When external load is further increased, deformation concentrates more and more in the shear bands. Finally, the deformation reaches such a clear localization in some shear bands that a rupture path can develop; most of the slippage between fibres occurs in this region such that the wet specimen or the wet paper web breaks.

It has been an open question whether weak-link scaling occurs in wet paper. Weak-link scaling means that the mean strength of larger samples is lower than that of smaller ones. By means of a new network model, based on a non-linear finite element method, Kulachenko et al. (2009) tried to clarify the matter. However, due to computational restrictions the size of the modelled samples was small, i.e. the maximum length and width of the modelled specimens were 6.5 mm and 5 mm respectively. The results showed that the weak-link scaling does not apply on the scale studied but the writers admitted that it remained an open question whether weak-link scaling occurs at larger wet paper samples.

Based on the deformation model above, it can be concluded that the breaking mechanism in the wet web does not obey the weakest link model, i.e. the rupture does not initiate from a single weak spot, and the strength distribution cannot follow any extreme value distribution. This conclusion is supported by two new facts. Firstly, the tensile strength distribution was shown to be normally distributed at DSC 56% and 68%. Secondly, even a 4 cm wide cross cut in the wet web (DSC 65%) did not deteriorate the tensile strength. These are strong evidences against the weakest link model and these are important new findings.

As a comparison, according to Curtin (1988), Phoenix and Beyerlein (2000) and Sornette (2002), the rupture of heterogeneous brittle materials involves the creation, growth and multiplication of local microscopic cracks under increasing load. After the crack density reaches a critical threshold, a macroscopic crack develops that eventually leads to material failure. Uesaka et al. (2001) and Hristopulos and Uesaka (2003, 2004) provide the following rupture mechanism for dry paper. Due to increasing tensile load, some of the structural elements such as bonds and fibres start failing locally. Initially, the distribution of such failed areas in the entire system is almost random. The local failures cause stress redistribution among intact structural elements. As the stress further increases, the neighbouring failed areas interact and coalesce with each other, creating almost independently behaving critical clusters of damage areas. A group containing several critical clusters forms a mesoscopic "link", and the whole material can be viewed as a chain of such links. The final rupture is determined by the weakest of the links. According to experimental evidence, the length scale of the links is about 20 mm, and the dimensions of critical clusters are expected to be approximately on the millimetre scale (Hristopulos and Uesaka (2004).

The studies of Wong et al. (1996) and Korteoja et al. (1996, 1997, 1998c) support the dry paper fracture model above, cf. Chapter 2.3.3. Their results suggest that paper formation affects the way external elongation is distributed through paper into local strains. The low grammage points accumulate far more strain, and consequently more damage, than high grammage points. Thus the damage accumulates in low grammage points throughout the whole paper specimen or paper web but the final rupture process always starts from a single weak spot (i.e. a weak link) and paper breaks abruptly. This kind of rupture mechanism inevitably leads to an extreme value strength distribution. The simulations of Korteoja et al. (1996) suggest that plastic deformation in dry paper takes place in less than a quarter of the paper area when paper is loaded. Increased formation-type disorder reduces this fraction. It is evident that the breaking mechanism in dry and wet paper is not alike.

Interestingly, the performance of both extreme value models used in the current study was very similar, with the exception being papers E2 and E3 where the Gumbel distribution provided a better fit. However, on the whole it is difficult to give any preference to either of the two extreme value models. The reason is most likely the slender low strength tail in the measured strength distributions, which is seen as fairly high Weibull modulus values, on average 38.4. The narrow strength distribution also means that the overestimating problem related to the Gumbel distribution is avoided. Typically, the Gumbel distribution overestimates the failure probability at low stress levels, which are well away from the median stress level, cf. Chapter 2.2.2.

For comparison, based on AHMA trials Wathén and Niskanen (2006) reported that when the Weibull modulus of the two-parametric Weibull distribution was larger than 20, it was difficult to give statistical preference to any of the three models tested: two- and three-parameter Weibull and modified Gumbel distributions. In addition, based on model disordered microstructures, Duxbury et al. (1994) commented that even in simulations of model systems it is sometimes difficult to distinguish between the modified Gumbel and Weibull distributions.

For some reason, the AHMA runnability pilot seems to provide substantially higher Weibull modulus values compared with the laboratory measurements reported in the literature. The Weibull modulus measured by Korteoja et al. (1998b) was 13 for newsprint and 9 for copy paper. Deng et al. (2005) reported values from about 13 to 17.5 for newsprint. Wathén and Niskanen (2006) measured LWC base and wood-free papers made on a pilot paper machine. They used AHMA and the mean value for the LWC base papers was 17, with the maximum being roughly 37. The respective values for the wood-free papers were 25 and 35. Lehto et al. (2010) produced four different kinds of wood containing pilot papers and measured them on AHMA with the Weibull modulus varying from 12 to 46 and the average being 30.5. As a comparison, we measured in one project 13 different mill-made papers, both SC and newsprint, on AHMA. The average Weibull modulus was 34.0 with the range being from 26.5 to 41.7.

The average Weibull modulus values for the current News series E and LWC base paper series A and B were 40.2 and 36.2, respectively. The respective ranges were 28.1–50.8 and 32.9–43.2. The value 50.8 (News E4) is extraordinarily high and cannot be explained. Without that value the average for newsprint would have been 38.1 and the range 28.1–45.3. These figures together with those of LWC base paper series A and B, although being high, are not so far away from the earlier values measured on AHMA.

The effect of formation and defects

By altering the wire section and headbox settings, it was possible to manufacture trial papers, News E1–E6, with non-correlating formation and fibre orientation characteristics, irrespective of the orientation and formation measurement methods used, cf. Appendix 4. In addition, papers having practically the same fibre orientation but clearly different formation figures (cf. Table 16) were manufactured on a pilot Fourdrinier by altering the headbox consistency and wire section vacuums. Finally, LWC base papers A1–A3 and B1–B2 also provided the possibility of segregating the effects of formation and fibre orientation. All this provides an excellent opportunity to explore the effects of formation and fibre orientation separately.

In spite of a significant formation change in News series E1–E6, from 2.9 g/m² to 3.4 g/m², wet and dry tensile index and tensile stiffness index did not change, see Figure 49 and Appendix 5. None of the measured correlations between tensile index or TSI and total formation (Ambertec, β-radiography) or local basis weight variation in different wavelength bands and void size classes were statistically significant at a 95% confidence level, not even at 90%. However, although the results were otherwise

unequivocal, there existed, according to visual evaluation, an indication of a possible correlation at DSC 68% between tensile index and total void area in a size class 8–16 mm² (p value 0.11).

LWC base paper series A1–A3 showed that although the installation of the loadable blades changed formation at a wavelength band of 2–32 mm from 3.65 g/m² to 2.87 g/m² with the fibre orientation staying constant, the wet and dry tensile indices decreased by 11% and 2% respectively. The most probable reason is the furnish alteration. It is interesting that the effect of furnish was much smaller in dry than wet tensile strength.

It is suggested that when the formation is good or fairly good, it does not affect the average tensile strength or tensile stiffness of the wet and dry papers. With regard to wet papers, this is explained by the bonding mechanism. The formation did not have any influence on the dry tensile stiffness, which indeed it should not do because the elastic modulus (tensile stiffness) is insensitive to formation-like and other fluctuations in the paper structure (Alava and Niskanen 2008).

Instead, the results from the pilot paper machine suggest that when the formation is poor, i.e. the formation number has a high value and the web structure is (very) cloudy, further worsening lowers the wet tensile and tensile stiffness indices. As a comparison, formation at a wavelength band of 2–32 mm was 5.17 g/m² on average for pilot papers, 2.89 g/m² for News E1–E6 and 3.40 g/m² for LWC base papers A1–A3 and B1–B2.

Interestingly, in the pilot papers the total void area in the size class over 8 mm² and the basis weight variation measured at the wavelength band of 8–32 mm, which both describe a large-scale formation variation, provided the strongest correlations with the wet tensile index, cf. Figure 77. In addition, the correlation was almost statistically significant at a 95% confidence level for the wavelength band 8–32 mm (p value 0.057). These results are supported by the aforementioned indication of the interaction between tensile index and basis weight variation in the size class 8–16 mm² in News series E1–E6.

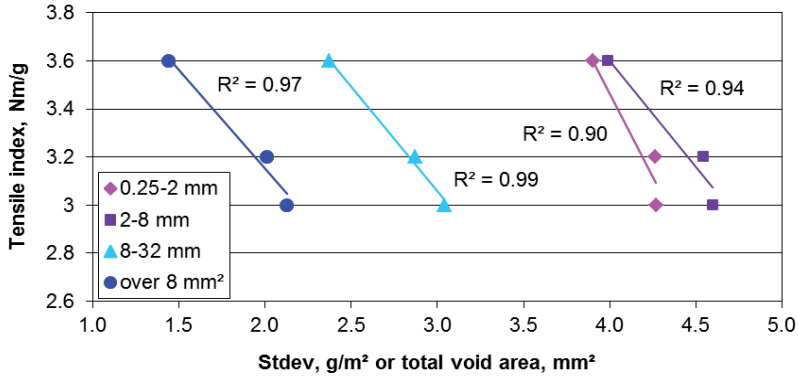

***Figure** 77. The effect of different formation parameters on the wet tensile index. Pilot papers at DSC 40%. The results at different wavelength bands are based on β-radiography as well as the total area of the voids belonging to the size class over 8 mm². The total void area numbers are divided by 1000 to accommodate the values in the same graph. The size of the measured area was 12x12 cm².*

As discussed above and in Chapter 2.3.3, external straining generates an uneven strain field in ductile materials (e.g. wet paper), in the form of shear bands. Structural properties, including formation and number of fibre contacts, have naturally an effect on the magnitude of individual shear bands. The more uniform the fibre network, the more uniform the magnitude of shear bands.

A wet fibre network is most likely capable to adapt fairly well to the strain field by sliding and averaging out or diffusing the external load. This could explain why the changes in formation in News E1–E6 and LWC base papers did not affect the average wet strength and tensile stiffness values. Instead, very poor formation in pilot papers presumably enhanced the damage localization in shear bands impairing any adaptation (c.f. formation Figures 40 and 41). This could explain why further deterioration in formation reduced the average strength and tensile stiffness values.

Although it was suggested that good or fairly good formation does not have an influence on the average tensile strength, it appeared to affect the tensile strength variation, both in wet and dry paper. The better the formation the smaller the variation (i.e. the smaller the COV and the bigger the Weibull modulus).

Interestingly, the results of the News series E1–E6 suggest that the effect depends both on the scale of formation and DSC (no effect at DSC 56% and the greatest effect in dry papers). In wet papers, large scale formation—basis weight variation at the wavelength band of 8–32 mm and total area of voids belonging to the size class of 8–16 mm²—turned out to have the greatest effect. As a reminder, a void in a paper sheet was determined to be an area where local basis weight is at least 4 g/m² lower than the median grammage. Although the total area of large voids was only a small fraction of the whole sheet area, it seemed effectively to bring forth differences in the evenness of paper structure between the trial papers.

Figures 78 and 79 demonstrate this as showing the COV of tensile index as a function of formation parameters for News E1–E6 at DSC 68%. The correlations for the large scale formation parameters are statistically significant at a 95% confidence level (p value for 8–32 mm 0.047 and for 8–16 mm² 0.037).

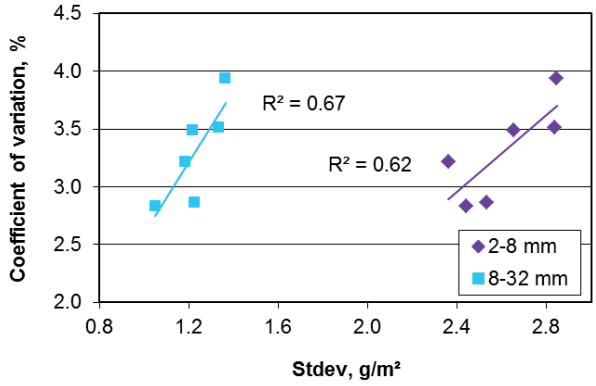

***Figure 78**. COV of tensile index as a function of basis weigh variation at wavelength bands 2–8 mm and 8–32 mm (β-radiography). News E1–E6 at DSC 68%.*

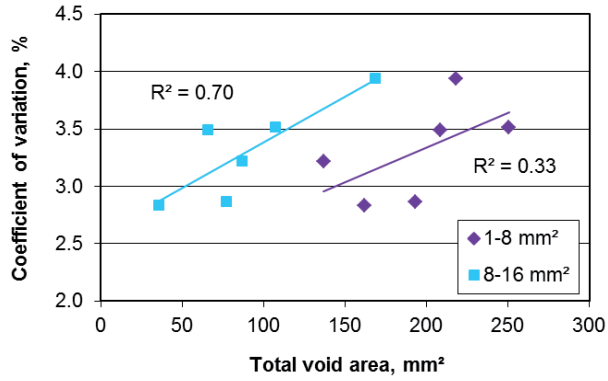

***Figure 79**. COV of tensile index as a function of total void area in size classes 1–8 mm² and 8–16 mm² (β-radiography). The area numbers for the class 1–8 mm² are divided by 5 to accommodate the graphs in the same figure. News E1–E6 at DSC 68%.*

In dry papers, the correlation was especially strong (0.92) and statistically significant at a 95% confidence level (p value 0.028) when the formation was measured at a wavelength band of 2–8 mm, cf. Figure 80. News E4, having an extraordinarily high Weibull modulus without good explanation, is not included in the correlation examination but is shown in the figure. The result supports the results of Hristopulos and Uesaka (2003, 2004), who showed that the reduction of local grammage variation

at the length scale less than a few millimetres, i.e. at the critical cluster size, has a clear effect on the Weibull modulus but the effect of the local grammage variation at large scales should have a minor effect. However, in our case the difference between the wavelength bands of 2–8 mm and 8–32 mm is small. It is possible that if the comparison was made, for example, between the bands 2–4 mm and 4–32 mm the difference might have been clearer.

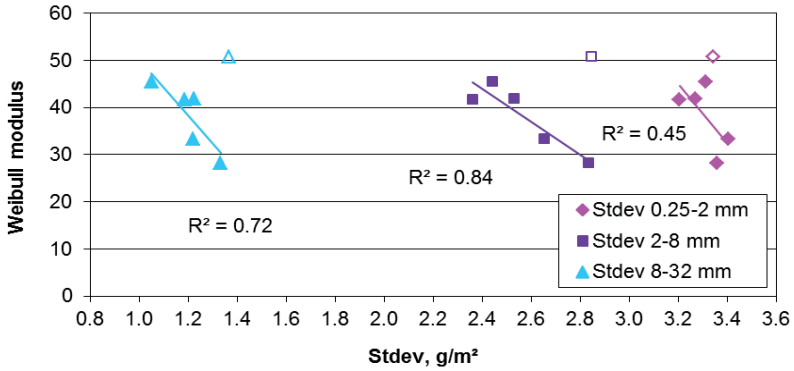

***Figure 80**. The Weibull modulus as a function of the formation measured at different wavelength bands (β-radiography). Trial paper E4 (Weibull modulus 50.8, open symbols) has been left out of the correlation calculations. News E1–E6.*

The importance of small scale formation variation is also evident from Figure 81 which shows the effect of formation variation in two different size classes. The correlation at the smaller class is almost statistically significant at a 95% confidence level with p value being 0.059.

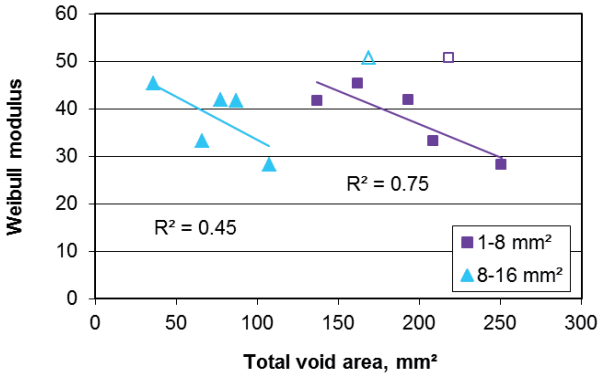

***Figure 81**. The Weibull modulus as a function of total void area in size classes 1–8 mm² and 8–16 mm² (β-radiography). The area numbers for the class 1–8 mm² are divided by 5 to accommodate the graphs in the same figure. Trial paper E4 (Weibull modulus 50.8, open symbols) has been left out of the correlation calculations. News E1–E6.*

The effect of formation and DSC on the strength variation can be explained by the breaking mechanism. At DSC 56%, fibres can easily slip in the wet network enabling effective averaging out or diffusing the external load. Alternatively, because bonding between the fibres is stronger at DSC 68%, it is plausible that the wet fibre network cannot adapt as easily to the strain field as at DSC 56%. The poorer the formation, the less uniform the magnitude of shear bands, the greater the damage localization, the more difficult the adaptation and the greater the strength variation in web breaks. This would explain the correlation between formation and COV at DSC 68%. In dry papers, bonding between fibres does not allow the slippage on bond sites preventing the adaptation mechanism proposed in wet fibre networks. Because plastic strain strongly concentrates in low grammage spots (c.f. Chapter 2.3.3), it is understandable that formation has greatest effect on COV in dry papers. The proposed mechanism would also explain the difference in the effect of the scale of formation on wet and dry papers.

It can be concluded that formation does not affect the average tensile strength or tensile stiffness of wet or dry papers, if formation is good or fairly good, but it does have an influence on the tensile strength variation of wet and dry papers. In addition, the effect depends both upon the scale of local basis weight variation and DSC. In wet papers, large scale formation has the greatest effect on the strength variation. In dry papers, the situation is opposite and the tensile strength variation is controlled by small scale formation.

These results mean that, on modern paper machines with good formation, further formation improvement does not lead to improved wet strength properties at the press section or in the first part of the drying section. Only if large scale formation can be improved, tensile strength variation is reduced. Instead, slow old Fourdrinier-type machines most probably benefit from the formation improvement. These are important new results.

Another interesting result is that the wet web is insensitive to even large defects. This is evident because even 4 cm CD notches in the middle of wet AHMA webs did not reduce the tensile strength. This is an important result because it shows that defects in the wet web cannot be a runnability-restricting or disturbing factor at the press section or in the first part of the drying section, at least if the defects are not located in the very edge of the web.

The effect of fibre orientation

It was not possible to distinguish the effect of local fibre orientation variation (i.e. local orientation evenness) from that of "bulk" fibre orientation, i.e. mean layered fibre orientation. Based on a visual evaluation, the effective shear maps, cf. Chapter 4.5, seem to provide an interesting means of studying the effect of fibre orientation. However, a quantitative method to evaluate the differences between the samples should be developed in order to utilize them fully.

The results from News series E1–E6 and LWC base paper series A1–A3 and B1–B2 suggest that the fibre orientation has a stronger effect on the tensile strength and

tensile stiffness of the wet paper webs than on those of dry webs. This provides some means of improving wet web runnability. However, its usage may be limited because the fibre orientation has an influence on the web behaviour in offset printing. Kouko et al. (2007) reported that fibre orientation had a positive effect on the tensile strength and residual tension of press dry fine paper. Their findings therefore support our results.

One maximum and seagull type orientation profiles in z-direction led to different Scott Bond and porosity values. However, there were no differences in tensile or tensile stiffness indices of wet papers between the two profile types, cf. Chapter 4.2.4. The porosity profile in the z-direction can be considered to reflect the relative contact area distribution in the z-direction, cf. Chapter 3.1.3. Because wet pressing controls the porosity profile distribution and because wet pressing was similar for all trial papers E1–E6, it is understandable that both orientation profiles, the one maximum type and the seagull type, provided similar wet strength properties.

Finally, the results suggest that the fibre orientation does not affect the tensile strength variation of wet or dry paper webs.

8 CONCLUSIONS

Good wet web runnability means that the web is strong enough to tolerate all the stresses imposed on it when running through the paper machine. This leads to a low number of breaks and defects in the ready-made paper. Based on the literature, it was concluded that MD tensile strength, MD tensile stiffness and MD residual tension are the important strength properties from the wet web runnability point of view. The first two properties can be measured with the AHMA pilot scale runnability device.

A research method was developed for re-wetting and running mill-made paper reels on AHMA at dry solids contents typical to the press section and the first part of the drying section. It was shown that the method is a relevant means of studying the wet web strength properties in dynamic conditions. These results are important because the method developed provides paper mills with a way to study and improve their wet web strength properties.

It was shown that, of the micro and mesoscale structural characteristics, only fibre orientation has a strong effect on the average wet tensile strength and wet tensile stiffness. The influence is lower in dry paper. Although it was not possible to distinguish the effect of variations in local fibre orientation (i.e. local orientation evenness) from that of "bulk" fibre orientation, it was possible to study the effect of the fibre orientation profile in the z-direction. It is suggested that the orientation profile does not affect the average wet tensile strength or wet tensile stiffness if the average fibre orientation remains unchanged. This means that, from a wet strength point of view, it should not matter whether the machine runs the jet-wire ratio in the rush or drag side; however, this may have influence on Scott Bond values.

When formation is good, as it typically is on modern paper machines, further formation improvement does not improve average wet strength properties. Only when formation is poor, i.e. the formation number has a high value and the web structure is cloudy, does this have an influence on average wet web tensile strength and tensile stiffness. Presumably this would be the situation on a Fourdrinier type machine.

Formation has an influence on the tensile strength variation of wet and dry papers. In addition, the effect depends on the scale of formation and dry solids content. In wet papers, large scale formation has the greatest effect on the strength variation. Conversely, in dry papers the strength variation is controlled by small scale variation. In addition to the scale of formation and DSC, it is suggested that the poorer the formation the lower the DSC at which the variability due to the effect of formation appears. Contrary to formation, fibre orientation does not affect the strength variation.

Another interesting result is that the wet web is insensitive to even large defects. This is evident because even 4 cm CD notches in the middle of 25 cm wide wet AHMA webs did not reduce the tensile strength. This is an important result because it shows that defects in the wet web cannot be a runnability-restricting or disturbing factor at the press section or in the first part of the drying section, at least if they are not located just at the edge of the web. However, CD defects are certainly detrimental in coating and in the latter part of the paper machine irrespective of the location of defects in the web.

The bonding mechanism, fracture mechanism and strength distribution are closely interrelated. The strength of wet paper is normally distributed. This means that wet paper does not show either weak-link behaviour or weak-link scaling. In wet paper, bonding between the fibres and fines is based on friction forces and shear resistance. The increase of DSC causes the emergence of hydrogen bonds, leading to a gradual change of the fracture mechanism and strength distribution. Finally, in dry paper, bonding is largely based on hydrogen bonds accompanied by van der Waals' forces and paper strength obeys an extreme value distribution

The conclusions above mean that the objectives:

- to clarify how web structure on the microscale and mesoscale (particularly formation and fibre orientation distribution) affects wet web strength properties
- to develop a relevant methodology to study re-wetted paper reels on a pilot scale
- to clarify whether the strength distribution of the wet web can be described by an extreme value strength distribution, does the wet web demonstrate a weak-link behaviour and does the wet web show any weak-link scaling,

were reached fairly well.

The hypothesis, that it is possible to affect the strength properties of the wet web by altering the wire section and headbox parameters, turned out to be partly valid. Because the tensile strength and tensile stiffness of wet paper develop faster as a function of fibre orientation compared with those of dry paper, it provides some means to affect wet web runnability without jeopardising the quality specifications of dry paper. If large scale formation can be improved, it provides a means to both reduce wet strength variation on gap formers and Fourdriniers and to improve average wet tensile strength and tensile stiffness on Fourdriniers. This should realize an improved wet web runnability.

REFERENCES

Adams, R. J. 1991. Controlling the web in the press section. In: Seminar notes of 1991 Sheet Flutter and Winder Problems Seminar. Nashville, TN, USA. 4-5.10.1991. Atlanta, GA, USA: Tappi Press. pp. 101-110.

Ahrens, F., Patterson, T. and Bloom, F. 2004. Mathematical modelling of web separation and dynamics on a web adhesion and drying simulator. Int. J. of Applied Mechanics and Engineering. Vol. 9:2. 227-271.

Akaike, H. 1973. Information theory and an extension of the maximum likelihood principle. In: Petrov, B. N. and Csaki, F. (eds.) Proceedings of the 2nd International Symposium on Information Theory. Budapest, Hungary: Akademia Kiado. pp. 267-281.

Alava, M. and Niskanen, K. 2008. In-plane tensile properties. In: Papermaking Science and Technology. Niskanen, K. (ed.) Book 16, Paper Physics. 2nd ed. Helsinki, Finland: Finnish Paper Engineers' Association/Paperi ja Puu Oy. pp. 181-228.

Alén, R. 2000. Structure and chemical composition of wood. In: Papermaking Science and Technology. Stenius, P. (ed.) Book 3, Forest Products Chemistry. Helsinki, Finland: Fapet Oy. pp. 11-57.

Alince, B., Vanerek, A., de Oliveira, M. H. and van de Ven, T. G. M. 2006. The effect of polyelectrolytes on the wet-web strength of paper. Nordic Pulp and Paper Research Journal. Vol. 21:5. 653-658.

Andersson, S. R. and Rasmuson, A. 1997. Dry and wet friction of single pulp and synthetic fibres. Journal of Pulp and Paper Science. Vol. 23:1. J5-J11.

Andersson, S. R., Nordstrand, T. and Rasmuson, A. 2000. The influence of some fibre and solution properties on pulp fibre friction. Journal of Pulp and Paper Science. Vol. 26:2. 67-71.

Asplund, G. and Norman, B. 2004. Fibre orientation anisotropy profile over the thickness of a headbox jet. Journal of Pulp and Paper Science. Vol. 30:8. 217-221.

Avikainen, M. and Erkkilä, A-L. 2003. Comparison of traditional β-radiography and storage phosphor screen formation measurement techniques. Paperi ja Puu. Vol. 85:5. 279-286.

Barnet, A. J. and Harvey, D. M. 1979. Stock properties required for high speed paper machines. Pulp and Paper Canada. Vol. 80:4. T132-T134.

Barnet, A. J. and Harvey, D. M. 1980. Wet web characteristics and relation to wet end draws. Part II – Wet behaviour in the press section of an experimental paper machine. Pulp and Paper Canada. Vol. 81:11. T306-T310.

Baum, G. A., Pers K., Shepard D. R. and Ave'Lallemant T.R. 1984. Wet straining of paper. Tappi Journal. Vol. 67:5. 100-104.

Bernard, P. and Charlebois, A. 1991. Comparison of basis weight, fiber orientation and alignment angle distributions for different spatial resolutions. In: 1991 International Paper Physics Conference. Kona, HI, USA. 22-26.9.1991. Atlanta, GA, USA: TAPPI Press. Book 1. pp. 71-79.

Berthold, J. and Salmén, L. 1997. Effects of mechanical and chemical treatments on the pore-size distribution in wood pulps examined by inverse size-exclusion chromatography. Journal of Pulp and Paper Science. Vol. 23:6. J245-J253.

Brancato, A. and Banerjee, S. 2010. Effect of recycling on the surface and pore structure of wood fibre. Appita Journal. Vol. 63:1. 42-44, 52.

Bristow, J. A. 1986. The pore structure and the sorption of liquids. In: Bristow, J. A. and Kolseth, P. (eds.) Paper structure and properties. New York, USA: Dekker. pp. 183-201.

Burnham, K. P. and Anderson D. R. 2002. Model selection and multimodel inference. A practical information-theoretic approach. 2nd ed. Springer. 488 p.

Bury, K. V. 1975. Statistical models in applied science. John Wiley and Sons, Inc. 625 p.

Campbell, W. B. 1933. The cellulose – water relationship in papermaking. Forest Service Bulletin 84. Ottawa, Canada: Department of the Interior.

Carlsson, A. 2007. Orientation of fibres in suspensions flowing over a solid surface. Licentiate Thesis. Royal Institute of Technology, Mechanics. Stockholm, Sweden. 80 p.

Carlsson, G. and Lindström, T. 1984. Hornification of cellulosic fibers during wet pressing. Svensk Papperstidning. Vol. 87:15. R119-R125.

Corso, F.D. 2009. Cracks, shear bands and lamellar inclusions in homogenously prestressed materials. Doctoral thesis. University of Trento, Department of Mechanical and Structural Engineering. Trento, Italy. 142 p.

Corson, S. R. and Lobben, T. H. 1980. Wet web properties are increased by fines fraction. Pulp and Paper Canada. Vol. 81:11. 90-95.

Curtin, W. A. 1998. Size scaling of strength in heterogeneous materials. Physical Review Letters. Vol. 80:7. 1445-1448.

Curtin, W. A. and Scher, H. 1992. Algebraic scaling of material strength. Physical Review B. Vol. 45:6. 2620-2627.

Deng, M. and Dodson, C. T. J. 1994. Paper: An engineered stochastic structure. Atlanta, GA, USA: TAPPI Press. 284 p.

Deng, N., Ferahi, M. and Uesaka, T. 2005. Pressroom runnability: A comprehensive analysis of pressroom and mill databases. In: Preprints of PAPTAC 91st Annual Meeting. Montreal, Canada. 8-10.2.2005. Montreal, Canada: Pulp and Paper Association of Canada. Book C. pp. C217-C228.

Dulemba, M., Qi, D. and Aravamuthan, R. 1999. The effect of repeated drying and wetting on single fiber flexibility. Progress in Paper Recycling. Vol. 9:1. 38-45.

Duxbury, P. M., Kim, S. G. and Leath, P. H. 1994. Size effect and statistics of fracture in random materials. Materials Science and Engineering. Vol. 176:1-2. 25-31.

Edvardsson, S. and Uesaka, T. 2009a. System stability of the open draw section and paper machine runnability. In: I'Anson, S. J. (ed.) Advances in Pulp and Paper Research, Transactions of 14th Fundamental Research Symposium. Oxford, UK. September 2009. Bury, UK: The Pulp and Paper Fundamental Research Society. Vol. 1. pp. 557-575

Edvardsson, S. and Uesaka, T. 2009b. Web tension variations and runnability of the open draw section. In: Madetoja, E., Niskanen, H. and Hämäläinen, J. (eds.) Proceedings of Papermaking Research Symposium. Kuopio, Finland, 1-4.6.2009. University of Kuopio. 11 p.

Edvardsson, S. and Uesaka, T. 2010. System dynamics of the open-draw with web adhesion: Particle approach. Journal of Applied Mechanics. Vol. 77. 021009-1-021009-11.

Eklund, D. and Salminen, P. 1987. Water sorption in paper during short times. Appita Journal. Vol. 40:5. 340-346.

Erkkilä A-L. 1995. Mechanisms and measurements of the layered orientation structure of paper sheets (in Finnish). Licentiate thesis. University of Jyväskylä, Department of Physics. Jyväskylä, Finland. 97 p.

Erkkilä, A-L, Pakarinen, P. and Odell, M. 1998. Sheet forming studies using layered orientation analysis. Pulp and Paper Canada. Vol. 99:1. 81-85.

Erkkilä, A-L, Pakarinen, P. and Odell, M. 1999. The effect of forming mechanisms on layered fiber structure in roll and blade gap forming. In: Proceedings of TAPPI 99 – Preparing for the Next Millennium. Atlanta, GA, USA. 1-4.3.1999. Atlanta, GA, USA: TAPPI Press. Vol. 2. pp. 389-400.

Fabritius, T. 2007. Optical method for liquid sorption measurements in paper. Doctoral thesis. University of Oulu, Faculty of Technology, Department of Electrical and Information Engineering. Oulu, Finland. Acta Universitas Ouluensis, C Technica 269. Oulu, Finland: Oulu University Press. 48 p.

Fahlén, J. and Salmén, L. 2003. Cross-sectional structure of the secondary wall of wood fibers as affected by processing. Journal of Materials Science. Vol 38. 119-126.

Forsström, J., Andreasson, B. and Wåberg, L. 2005. Influence of pore structure and water retaining ability of fibres on the strength of papers from unbleached kraft fibres. Nordic Pulp and Paper Research Journal. Vol. 20:2. 176-185.

Gregersen, O. W. 1998. On the assessment of effective paper web strength. Doctoral thesis. Norwegian University of Science and Technology, Department of Chemical Engineering. Trondheim, Norway. 76 p.

Görres, J., Amiri, R., Wood, J. R. and Karnis, A. 1996. Mechanical pulp fines and sheet structure. Journal of Pulp and Paper Science. Vol. 22:12. J491-J496.

Hakkila, P. and Verkasalo, E. 2009. Structure and properties of wood and woody biomass. In: Papermaking Science and Technology. Kellomäki, S. (ed.) Book 2, Forest Resources and Sustainable Management. 2nd ed. Helsinki, Finland: Paper Engineers' Association/Paperi ja Puu Oy. pp. 133-215.

Hasuike, M., Johansson P-Å., Fellers, C. Terland, O. 1987. Fiber orientation and its relation to paper formation studied by image analysis. In: Proceedings of 1987 International Paper Physics Conference. Mont Rolland, Canada. Montreal, Canada: Canadian Pulp and Paper Association. pp. 185-188.

Hauptmann, E. G. and Cutshall, K. A. 1977. Dynamic mechanical properties of wet paper webs. In: Proceedings of TAPPI Annual Meeting. Atlanta, Georgia, USA. 14-16.2.1977. Atlanta, GA, USA: Technical Association of the Pulp and Paper Industry. pp. 193-202.

Heikkilä, P., Timofeev, O. and Kiiskinen, H. 2000. Multicylinder dryer. In: Papermaking Science and Technology. Karlsson, M. (ed.) Book 9, Papermaking Part 2, Drying. Helsinki, Finland: Fapet Oy. pp. 84-125

Heikkinen, A. 1998. Controlling the moisture distribution of board in surface moistening. Master's thesis (in Finnish). Helsinki University of Technology, Department of Forest Products Technology. Espoo, Finland. 204 p.

Hilden, K. and Perento, J. 2000. Paper analysis - the key to optimizing and troubleshooting paper machines. In: Proceedings of 2000 Pulping/process and product quality conference. Boston, MA, USA. 5-8.11.2000. Atlanta, GA, USA: TAPPI Press. 8 p.

Hoyland, R. W. 1977a. A review of the transudation of water into paper – in five parts. Part 5: The mechanism of penetration, and conclusions. Paper Technology and Industry. Vol. 18:1. 7-9.

Hoyland, R. W. 1977b. Swelling during the penetration of aqueous liquids into paper. In: Fibre-Water Interactions in Paper-Making. Transactions of 6th Fundamental Research Symposium. Oxford, UK. September 1977. London, UK: The British Paper and Board Industry Federation. Vol. 2. pp. 557-579.

Hoyland , R. W., Howarth, P. and Field, R. 1973. Fundamental parameters relating to performance of paper as a base for aqueous coatings. In: Bolam, F. (ed.) The Fundamental Properties of Paper Related to its Uses, Transactions of the symposium. Cambridge, UK. September 1973. London, UK: The British Paper and Board Industry Federation. pp. 464-510.

Hristopulos, D. T. and Uesaka, T. 2003. Factors that control the tensile strength distribution in paper. In: Preprint of 2003 International Paper Physics Conference. Victoria, Canada. 7-11.2003. Montreal, Canada: Pulp and Paper Technical Association of Canada. pp. 5-17.

Hristopulos, D. T. and Uesaka, T. 2004. Structural disorder effects on the tensile strength distribution of heterogeneous brittle materials with emphasis on fiber networks. Physical Review B. Vol. 70:6. 064108-1-064108-18.

Htun, M. and de Ruvo, A. 1978. Correlation between the drying stress and the internal stress in paper. Tappi Journal. Vol. 61:6. 75-77.

Huang, F., Li, K. and Kulachenko, A. 2009. Measurement of interfiber friction force by atomic force microscopy. In: Proceedings of Annual Meeting 2009. Montreal, Canada. 3-4.2.2009. Montreal, Canada: PAPTAC. pp. 183-190.

Huang, T. and LePoutre, P. 1996. Effect of basestock absorbency on coating "hold-out" and coated paper properties. In: Proceedings of 1996 Tappi Coating Conference. Nashville, TN, USA. 19-22.5.1996. Atlanta, GA, USA: TAPPI Press. pp. 167-176.

Hämäläinen, T. and Hämäläinen, J. 2007. Modelling of fibre orientation in the headbox jet. Journal of Pulp and Paper Science. Vol. 33:1. 49-53.

Ionides, G. N., Jackson, M., Smith, M. K. and Forgacs, O. L. 1977. Factors influencing the strength properties of wet-webs. In: Fibre – Water Interactions in Paper-Making, Transactions of 6th Fundamental Research Symposium. Oxford, UK. September 1977. London, UK: The British Paper and Board Industry Federation. Vol. 1. pp. 357-374, 375-376.

Ilvespää, H. 1996. A new era in pressing. In: Valmet Paper Machine Days. Jyväskylä, Finland. 13-14.6.1996. Jyväskylä, Finland: Valmet Corporation. pp. 49-61.

Ilvespää, H. 1998. Challenging the speed potential. In: Valmet Paper Technology Days 1998. Jyväskylä, Finland. 11-12.6.1998. Jyväskylä, Finland: Valmet Corporation. pp. 63-71.

Ilvespää, H., Kokkonen, O., Haavisto, J., Kangas, J. and Haavanlammi, A. 2003. Rebuild opportunities in paper machine sections. In: Metso Paper Technology Days 2003, Shaping the World of Papermaking. Lahti, Finland. 10-12.6.2003. Metso Paper Inc. pp. 88-101.

Jantunen, J. 1985. Visco-elastic properties of wet webs under dynamic conditions. In: Punton, E.V. (ed.) Papermaking Raw Materials, Transactions of the 8th Fundamental Research Symposium. Oxford, UK. September 1985. London, UK: Mechanical Engineering Publications Limited. Vol. 1. pp. 133-162.

Juppi, K. 2006. Improved runnability and drying capacity through new technology. In: Metso Paper Technology Days 2006, Technology for Lifecycle Results. Jyväskylä, Finland. 15-16.6.2006. Metso Paper Inc. pp. 66-75.

Juppi, K. and Kaihovirta, J. 2002. The effect of the dryer section on paper quality. In: Preprints of 88th Annual Meeting. Montreal, Canada. 30.1.2002. Montreal, Canada: Pulp and paper Technical Association of Canada. Preprints 'B'. pp. B23-B26.

Kajanto, I., Laamanen, J. and Kainulainen, M. 1998. Paper bulk and surface. In: Papermaking Science and Technology. Niskanen, K. (ed.) Book 16, Paper Physics. Helsinki, Finland: Fapet Oy. pp. 88-115.

Kananen, J. 2003. Water transfer and dimensional changes of paper in a wet nip. Licentiate thesis. Helsinki University of Technology, Department of Forest Products Technology. Espoo, Finland. 177 p.

Kangas, H. 2007. Surface chemical and morphological properties of mechanical pulps, fibres and fines. Doctoral thesis. Helsinki University of Technology, Department of Forest Products Technology. Espoo, Finland. KCL Communications 13. Espoo, Finland: KCL. 141 p.

Karppinen, T. 2008. Characterizing physical properties of wetting paper by air coupled ultrasound and light. Doctoral thesis. University of Helsinki, Faculty of Science, Department of Physics. Helsinki, Finland. Report Series in Physics HU-P-D154. Helsinki, Finland: University of Helsinki. 58 p.

Kartovaara, I. 1989. Gradienttikalanterointi: gradienttien syntymisen ja kalanterointituloksen arvostelun perusteet (in Finnish). Licentiate thesis. Helsinki University of Technology, Department of Forest Products Technology. Espoo, Finland. 140 p.

Kekko P., Kouko, J., Retulainen, E. and Timonen, J. 2009. Effects of strain rate on the stress relaxation of wet paper. In: Proceedings of 6th International Symposium: Moisture and Creep Effects on Paper, Board and Containers. Madison, WI, USA. 14-15.7.2009. U.S. Department of Agriculture, Forest Service, Forest Products Laboratory. 10 p.

Kent, H. J. and Lyne, M. B. 1989. On the penetration of printing ink into paper. Nordic Pulp and Paper Research Journal. Vol. 4:2. 141-145.

Kerr, A. J. and Goring, D. A. I. 1975. The ultrastructural arrangement of the wood cell wall. Cellulose Chemistry and Technology. Vol. 9:6. 563-573.

Kimura, M. and Shimizu, H. 1985. Stress and strain behavior of low grammage spot in paper during elongation. 1985. Japan Tappi Journal. Vol. 39:8. 777-784.

Kitayama, T., Okayama, T. and Oye, R. 1983. Changes of chemical pulp fibres during recycling. In: 1983 International Symposium on Wood and Pulping Chemistry. Tsukuba Science City, Japan. 23-27.5.1983. Tokyo, Japan: Japanese Technical Association of the Pulp and Paper Industry. Vol. 3. pp. 118-123.

Ketoja, J. A., Kananen, J., Niskanen, K. J. and Tattari, H. 2001. Sorption and web expansion mechanisms. In: Baker, C. F. (ed.) The science of Papermaking, The 12th Fundamental Research Symposium. Oxford, UK. 17-21.9.2001. Bury, UK: The Pulp and Paper Fundamental Research Society. Vol. 2. pp. 1357-1370.

Ketoja, J. A., Tanaka, A., Asikainen, J. and Lehti, S. T. 2007. Creep of wet paper. In: Proceedings of 61st Appita Annual Conference and Exhibition/2007 International Paper Physics Conference. Gold Coast, Australia. 6-10.5.2007. Carlton Australia: Appita. Vol. 2. pp. 179-183.

Kiiskinen, H., Paltakari, J. and Pakarinen, P. 2000. Drying and paper quality. In: Papermaking Science and Technology. Karlsson, M. (ed.) Book 9, Papermaking Part 2, Drying. Helsinki, Finland: Fapet Oy. pp. 332-368.

Kortschot, M. T. 1997. The role of the fibre in the structural hierarchy of paper. In: Baker, C. F. (ed.) The Fundamentals of Papermaking Materials, Transactions of 11th Fundamental Research Symposium. Cambridge, UK. September 1997. Leatherhead, UK: Fundamental Research Committee and Pira International. Vol. 1. pp. 351-399.

Korteoja, M. J., Lukkarinen, A., Kaski, K., Gunderson, D. E., Dahlke, J. L. and Niskanen, K. J. 1996. Local strain fields in paper. Tappi Journal. Vol. 79:4. 217-223.

Korteoja, M. J. 1997. Damage and fracture in fibrous compounds: The effect of structural disorder. Doctoral thesis. Helsinki University of Technology, Laboratory of Computational Engineering. Espoo, Finland. 159 p.

Korteoja, M. J., Lukkarinen, A., Kaski, K. and Niskanen K. J. 1997. Computational study of formation effects on paper strength. Journal of Pulp and Paper Science. Vol. 23:1. J18-J22.

Korteoja, M., Salminen, L. I., Niskanen K. J. and Alava, M. 1998a. Statistical variation of paper strength. Journal of pulp and paper Science. Vol. 24:1. 1-7.

Korteoja, M., Salminen, L. I., Niskanen K. J. and Alava, M. 1998b. Strength distribution in paper. Materials Science and Engineering A248. pp. 173-180.

Korteoja, M. J., Niskanen, K. J., Kortschot, M. T. and Kaski, K. K. 1998c. Progressive damage in paper. Paperi ja Puu. Vol. 80:5. 364-372.

Kouko, J., Kekko, P. and Kurki, M. 2006a. Effect of strain rate on the strength properties of paper. In: Proceedings of the 2006 Progress in Paper Physics – A seminar. Oxford, OH, USA. pp. 90-94.

Kouko, J., Kekko, P., Liimatainen, H., Saari, T. and Kurki, M.2006b. Wet runnability of fibre furnish for magazine papers. Paperi ja Puu. Vol. 88:3. 169-174.

Kouko, J. Salminen, K. and Kurki, M. 2007. Laboratory scale measurement procedure for the runnability of a wet web on a paper machine, Part 2. Paperi ja Puu. Vol. 89:7-8. 424-430.

Kuhasalo, A., Niskanen, J., Paltakari, J. and Karlsson, M. 2000. Introduction to paper drying and principles and structure of a dryer section. In: Papermaking Science and Technology. Karlsson, M. (ed.) Book 9, Papermaking Part 2, Drying. Helsinki, Finland: Fapet Oy. pp. 14-53.

Kulachenko, A. 2008. New network model. In: Wet Web Runnability: Effect of Furnish Characteristics. Unpublished KCL report.

Kulachenko, A., Uesaka, T. and Lindstrom, S. 2008. Reinventing mechanics of fibre network. In: Kotomäki, K., Koivunen, K. and Paulapuro, H. (eds.) Proceedings of Progress in Paper Physics Seminar 2008. Espoo, Finland. 2-5.6.2008. Espoo, Finland: Helsinki University of Technology and TAPPI. pp. 185-187, 193.

Kulachenko, A., Lindström, S. and Uesaka, T. 2009, Strength of wet fiber networks – Strength scaling. In: Madetoja, E., Niskanen, H. and Hämäläinen, J. (eds.) Proceedings of Papermaking Research Symposium. Kuopio, Finland. 1-4.6.2009. Kuopio, Finland: University of Kuopio. 10 p.

Kulachenko, A. and Uesaka, T. 2012. Direct simulations of fiber network deformation and failure. To appear in Journal of Mechanics of Materials.

Kurki, M. 2001. New web handling techniques and paper property developments in single tier dryer section. In: Improving Paper Machine Runnability, Pira International conference proceedings. Gothenburg, Sweden. 22-23.1.2001. Leatherhead, UK: Pira International. Paper 16. 13 p.

Kurki, M. 2004. Efficiency improvements by runnability components in the press and drying section of the paper machine. In: Improving Paper Machine Runnability, Pira International conference proceedings. Brussels, Belgium. 9-10.6.2004. Leatherhead, UK: Pira International. Paper 16, 22 p.

Kurki, M. 2005. Modelling of kinematical and rheological web line behaviour in a papermaking environment. Licentiate thesis. Lappeenranta University of Technology, Mechanical Engineering Department. Lappeenranta, Finland. 142 p.

Kurki, M., Juppi, K., Ryymin, R. Taskinen, P. and Pakarinen, P. 1995. On the web tension dynamics in an open draw. In: Proceedings of the Third International Conference on Web Handling. Web Handling Research Center, Stillwater, OK, USA. 18-21.6.1995. pp. 230-246.

Kurki, M., Vestola, J., Martikainen, P. and Pakarinen, P. 1997. The effect of web rheology and peeling on web transfer in open draw. In: Proceedings of the Fourth International Conference on Web Handling. Web Handling Research Center, Stillwater, OK, USA. 1-4.6.1997. pp. 527-543.

Kurki, M. Kekko, P., Kouko, J. and Saari, T. 2004. Laboratory scale measurement procedure of paper machine wet web runnability. Part 1. Paperi ja Puu. Vol. 86:4. 256-258, 260-262.

Kurki, M. and Martikainen, P. 2005. Adaptive, self-underpressurizing suction roll for fast web handling concepts. In: Proceedings of the Eighth International Conference on Web Handling. Stillwater, Oklahoma, USA. 5-8.2005. Stillwater, OK, USA: Oklahoma State University. pp. 375-390.

Kurki, M., Martikainen, P., Pakarinen, P., Salminen, K. and Juppi, K. 2010. Web handling. In: Papermaking Science and Technology. Karlsson, M. (ed.) Book 9, Papermaking Part 2, Drying. 2nd ed. Helsinki, Finland: Paper Engineers' Association/Paperi ja Puu Oy. pp. 484-541.

Laine, J. and Stenius, P. 1997. Effect of charge on the fibre and paper properties of bleached industrial kraft pulps. Paperi ja Puu. Vol. 79:4. 257-266.

Laivins, G. V. and Scallan, A. M. 1993. The mechanism of hornification of wood pulps. In: Baker, C. F. (ed.) Products of Papermaking, Transactions of the 10th Fundamental Research Symposium. Oxford, UK. 1993. Leatherhead, UK: Pira International. Vol. 2. pp. 1235-1260.

Laivins, G. V. and Scallan, A. M. 1996. The influence of drying and beating on the swelling of fines. Journal of Pulp and Paper Science. Vol. 22:5. J178-J184.

Lamminmäki, T., Kettle, J., Puukko, P., Ketoja, J. and Gane, P. 2010. The role of binder type in determining inkjet print quality. Nordic Pulp and Paper Research Journal. Vol. 25:3. 380-390.

Lange, D. 1996. Extended nip pressing of paper grades. In: Preprints of 82nd Annual Meeting, Technical Section - Creating an Environment for the Future. Montreal, Canada. 30.1-2.2.1996. Montreal, Canada: Canadian Pulp and Paper Association. Preprints 'B'. pp. 97-100.

Lappalainen, T. and Kouko, J. 2011. Determination of local strains and breaking behaviour of wet paper using high-speed camera. Nordic Pulp and Paper Research Journal. Vol. 26:3. 288-296.

Lauterbach, T. J. 1990. Controlling the web in the press section. In: Seminar notes of 1990 Sheet Flutter and Windage Problems Seminar. Seattle, WA, USA. 28-29.9.1990. Atlanta, GA, USA: TAPPI Press. pp. 59-75.

Lehto, J. H. 2004. Characterization of mechanical and chemical pulp fibers. In: Proceedings of 58th Appita Annual Conference and Exhibition. Canberra, Australia. 19-21.4.2004. Carlton, Australia: Appita. Vol. 2. pp. 349-356.

Lehto, J., Hiltunen, E. and Paulapuro, H. 2010. TMP long fibres as reinforcement pulp. Part 2. Pilot tests. Accepted for publication in Nordic Pulp and Paper Research Journal. Vol. 25:3. 340-350.

Lehtonen, P. 2005. Paper moisture depth profiling by using near infrared spectroscopy and gloss measurement (in Finnish). Master's thesis. University of Oulu, The Department of Electrical and Information Engineering. Oulu, Finland. 79 p.

Li, T., Henrikssson, U., Klason, T. and Ödberg, L. 1992. Water diffusion in wood pulp cellulose fibres studied by means of the pulsed gradient spin-echo method. Journal of Colloid and Interface Science. Vol. 154:2. 305-315.

Lindström, S. B. and Uesaka, T. 2008. Particle-level simulation of forming of the fiber network in papermaking. International Journal of Engineering Science. Vol. 46:9. 858-876.

Lindström, S. B., Kulachenko, A. and Uesaka, T. 2009. New insights in paper forming from particle-level process simulations. In: Madetoja, E., Niskanen, H. and Hämäläinen, J. (eds.) Proceedings of Papermaking Research Symposium. Kuopio, Finland. 1-4.6.2009. Kuopio, Finland: University of Kuopio. 10 p.

Lindström, T. 1986. The porous lamellar structure of the cell wall. In: Bristow, J. A. and Kolseth, P. (eds.) Paper Structure and Properties. New York, NY, USA: Marcel Dekker Inc. pp. 99-119.

Lipponen, P., Erkkilä, A-L., Leppänen, T. and Hämäläinen, J. 2009. On the importance of in-plane shrinkage and through-thickness moisture gradient during drying on cockling and curling phenomena. In: I'Anson, S. J. (ed.) Advances in Pulp and Paper Research, Transactions of the 14th Fundamental Research Symposium. Oxford, UK. September 2009. Bury, UK: Pulp and Paper Fundamental Research Society. Vol. 1. pp. 389-436.

Lu, C., Danzer, R. and Fischer, F. D. 2002. Influence of threshold stress on the estimation of the Weibull statistics. Journal of the American Ceramic Society. Vol. 85:6. 1640-1642.

Lundberg, R. and de Ruvo, A. 1978. The influence of drying conditions on the recovery of swelling and strength of recycled fibres. Svensk Papperstidning. Vol. 81:11. 355-358.

Luukko, K. and Maloney, T. C. 1999. Swelling of mechanical pulp fines. Cellulose. Vol. 6:2. 123-135.

Lyne, M. B. 1993. On the interaction of liquids with paper under dynamic conditions. In: Baker, C. F. (ed.) Products of Papermaking, Transactions of the 10th Fundamental Research Symposium. Oxford, UK. September 1993. Leatherhead, UK: Pira International. Vol. 2. pp. 885-911, Vol. 3. pp. 1645-1651.

Lyne, M. B. 2002. Wetting and the penetration of liquids into paper. In: Borch, J., Lyne, M. B., Mark, R. E. and Habeger, C. C. Jr. (eds.) Handbook of Physical Testing of Paper. 2nd ed. New York, NY, USA: Marcel Dekker Inc. Vol. 2. pp. 303-332.

Maboudian, R. and Howe, R. T. 1997. Critical review: Adhesion in surface micromechanical structures. Journal of Vacuum Science and Technology B. Vol. 15:1. 1-20.

Maloney, T. C., Li, T-Q., Weise, U. and Paulapuro, H. 1997. Intra- and inter-fibre pore closure in wet pressing. Appita Journal. Vol. 50:4. 301-306.

Maloney, T. C. and Paulapuro, H. 1999. The formation of pores in the cell wall. Journal of Pulp and Paper Science. Vol. 25:12. 430-436.

Maloney, T. C., Laine, J. E. and Paulapuro, H. 1999. Comments on the measurement of cell water. Tappi Journal. Vol. 82:9. 125-127.

Maloney, T. C. 2000. On the pore structure and dewatering properties of the pulp fiber cell wall. Doctoral thesis. Helsinki University of Technology, Department of Forest Products Technology. Espoo, Finland. Acta Polytechnica Scandinavica Chemical Technology Series, No. 275. Espoo, Finland: The Finnish Academy of Technology. 106 p.

Maloney, T. C. and Paulapuro, H. 2000. The effect of drying conditions on the swelling and bonding properties of bleached kraft hardwood pulp. In: Proceedings of 54th Appita Annual Conference. Melbourne, Australia. 3-6.4.2000. Carlton, Australia: Appita. Vol. 1. pp. 41-45

Mardon, J., Cutshall, K., Smook, G., Branion, R. and Michie, I. 1975. Effects of wet-web furnish properties on newsprint runnability. Pulp and Paper Canada. Vol. 75:5. 92-100.

Mardon, J. 1976. Theoretical and experimental investigations into the peeling of paper from solid surfaces. Paperi ja Puu. Vol. 58:11. 797-802, 807-808, 810, 812, 814-815.

Mardon, J. 1979. A comparative study of the peeling of paper webs from common press roll cover materials. Paperi ja Puu. Vol. 61:5. 402-410.

Mayer, R. 2002. Web run from press to dryers. In: International Customer Conference, "Science Dialog". Salzburg, Austria. 4-6.9.2002. Voith. pp. 35-39.

McDonald, J. D., Pikulik, I. I. and Daunais, R. 1988. On-machine stress-strain behaviour of newsprint. Journal of Pulp and Paper Science. Vol. 14:3. J53-J58.

McDonald, J. D., Daunais, R., Pikulik, I. I. and Pye I. T. 1990. A new web transfer system for closing the draw between the last press and the dryer section. In: Preprints of 76th Annual Meeting, Technical Section. Montreal, Canada. 30.1.-2.2.1990. Montreal, Canada: Canadian Pulp and Paper Association. Preprints 'A'. pp. A19-A23.

Miettinen, P. P. J., Ketoja, J. A. and Hjelt, T. 2007a. Simulated structure of wet fiber networks. Nordic Pulp and Paper Research Journal. Vol. 22:4. 516-522.

Miettinen, P. P. J., Ketoja, J. A. and Klingenberg, D. J. 2007b. Simulated strength of wet fibre networks. Journal of Pulp and Paper Science. Vol. 33:4. 198-205.

Miettinen, P. P. J. and Ketoja, J. A. 2008. Simulation of triaxial deformation of wet fiber networks. Nordic Pulp and Paper Research Journal. Vol. 23:3. 264-271.

Miettinen, P. P. J., Kekko, P. and Kouko, J. 2009. Relaxation of wet paper by simulations and laboratory-scale experiments. Nordic Pulp and Paper Research Journal. Vol. 24:4. 381-387.

Moffat, J.M., Beath, L.R. and Mihelich, W.G. 1976. Major factors governing newsprint strength. In: Bolam, F. (ed.) The Fundamental Properties of Paper Related to its Uses. Transactions of the 5th Fundamental Research Symposium. Cambridge, UK. September 1973. London, UK: The British Paper and Board Industry Federation. Vol. 1. pp. 104-127.

Mäkinen, J. 2003. Testing of wet webs with KCL AHMA. Unpublished KCL report.

Nanko, H. and Ohsawa, J. 1989. Mechanisms of fibre bond formation. In: Baker, C. F. and Punton, V. W. (eds.) Fundamentals of Papermaking, Transactions of the 9th Fundamental Research Symposium. Cambridge, UK. 17-22.9.1989. London, UK: Mechanical Engineering Publications Ltd. Vol. 2. pp. 783-830.

Nanko, H., Asano, S. and Ohsawa, J. 1991. Shrinkage behaviour of pulp fibres during drying. In: Proceedings of 1991 International Paper Physics Conference. Kona, Hawaii. 22-26.9.1991. Atlanta, GA, USA: TAPPI Press. Book 2. pp. 365-373.

Neimo, L. 1999. Internal sizing of paper. In: Papermaking Science and Technology. Gullichsen, J., Paulapuro. H. and Neimo, L. (eds.) Book 4, Papermaking Chemistry. Helsinki, Finland: Fapet Oy. pp. 150-203.

Niskanen, K. J. 1989. Distribution of fibre orientations in paper. In: Baker, C. F. and Punton, V. W. (eds.) Fundamentals of Papermaking, Transactions of the 9th Fundamental Research Symposium. Cambridge, UK. 17-22.9.1989. London, UK: Mechanical Engineering Publications Ltd. Vol. 1. pp. 275-308.

Niskanen K. 1993. Strength and fracture of paper. In: Baker C. F. (ed.) Products of Papermaking, Transactions of the 10th Fundamental Research Symposium. Oxford, UK. September 1993. Leatherhead, UK: Pira International. Vol. 2. pp. 641-725.

Niskanen, K. and Rajatora, H. 2002. Statistical geometry of paper cross-sections. Journal of Pulp and Paper Science. Vol. 28:7. 228-233.

Niskanen, K., Mäkinen, J., Ketoja, J., Kananen, J. and Wathén, R. 2003. Paper industry invests in better web runnability. Paperi ja Puu. Vol. 85:5. 274-278.

Niskanen, K. and Pakarinen, P. 2008. Paper structure. In: Papermaking Science and Technology. Niskanen, K. (ed.) Book 16, Paper Physics. 2nd ed. Helsinki, Finland: Finnish Paper Engineers' Association/Paperi ja Puu Oy. pp. 11-58.

Nordström, B. 2003. Effects of pulp type and headbox design on anisotropy and other sheet properties in twin-wire roll forming. Nordic Pulp and Paper Research Journal. Vol. 18:3. 288-295.

Nordstrom, B. and Norman, B. 1994. Influence on sheet anisotropy, formation, Z-toughness and tensile stiffness of reduced feed area to a headbox nozzle. Nordic Pulp and Paper Research Journal. Vol. 9:1. 53-59.

Nordstrom, B. and Norman, B. 1995. Effects of headbox jet quality and blade pulse force on formation, retention and mechanical properties during roll-blade forming with curved blades. Nordic Pulp and Paper Research Journal. Vol. 10:1. 33-40, 45.

Norman B. 1989. Overview of the physics of forming. In: Baker C. F. (ed.) Fundamentals of Papermaking, Transactions of the 9th Fundamental Research symposium. Cambridge, UK. September 1989. London, UK: Mechanical Engineering Publications Limited. Vol. 3. pp. 73-149, 153-158.

Norman, B. 2008. Web forming. In: Papermaking Science and Technology. Paulapuro, H. (ed.) Book 8, Papermaking Part 1, Stock Preparation and Wet End. 2nd ed. Helsinki, Finland: Finnish Paper Engineers' Association/Paperi ja Puu Oy. pp. 216-288.

Norman, B. and Söderberg, D. 2001. Overview of forming literature, 1990-2000. In: The Science of Papermaking, Transactions of the 12th Fundamental Research Symposium. Oxford, UK. 17-21.9.2001. Bury, UK: The Pulp and Paper Fundamental Research Society. Vol. 1. pp. 431-558.

O'Connor, P. D. T. 1985. Practical reliability engineering. 2nd ed. John Wiley and Sons Ltd. 398 p.

de Oliveira, M. H., Maric, M. and van de Ven, T. G. M. 2008. The role of fiber entanglement in the strength of wet papers. Nordic Pulp and Paper Research Journal. Vol. 23:4. 426-431.

Odell, M. H. 2000. Paper structure engineering. Appita Journal. Vol. 53:5. 371-377.

Odell, M. H. and Pakarinen, P. 2001. The compleat fibre orientation control and effects on diverse paper properties. In: 2001 Papermakers Conference. Cincinnati, OH, USA. 11-14.3. 2001. Atlanta, GA, USA: TAPPI Press. Session 11. 27p.

Odell, M. H. and Pakarinen, P. 2003. Formation – influences and tuning. In: Proceedings of 28th EUCEPA Conference, Sustainable Development for the Pulp and Paper Industry. Lisbon, Portugal. 2-4.4.2003. Lisbon, Portugal: TECNICELPA. Session 3. pp. 152-168.

Oliver, J.F. 1982. Adhesive film properties affect web adhesion and release from press rolls. Tappi Journal. Vol. 65:3. 119-123.

Paaso, J. 2007. Moisture depth profiling in paper using near-infrared spectroscopy. Doctoral Thesis. University of Oulu, The Faculty of Technology. Oulu, Finland. VTT Publications 664. Espoo, Finland: VTT. 199 p.

Page, D. H. 1993. A quantitative theory of the strength of wet webs. Journal of Pulp and Paper Science. Vol. 19:4. J175-J176.

Pakarinen, P., Ryymin, R., Kurki, M. and Taskinen, P. 1993. On the dynamics of web transfer in an open draw. In: Proceedings of the Second International Conference on Web Handling. Web Handling Research Center, Stillwater, OK, USA. 6-9.6.1993. pp. 117-134.

Pakarinen, P., Juppi, K. and Karlsson M. 1995. A study of air flows in single-tier pockets at high machine speeds. Journal of Pulp and Paper Science. Vol. 21:2. J68-J73.

Park, S. Venditti, R. A., Jameel, H. and Pawlak J. J. 2006. A novel method to evaluate fibre hornification by high resolution thermogravimetric analysis. Appita Journal. Vol. 59:6. 481-485.

Parker, D. 1985. A study of wet sheet adhesion. In: Preprints of 71st Annual Meeting, Technical Section. Montreal, Canada. 29-30.1.1985. Montreal, Canada: Canadian Pulp and Paper Association. Preprints 'A'. pp. A117-A122.

Parker, J. D. 1972. The sheet-forming process. Atlanta, GA, USA: Technical Association of the Pulp and Paper Industry. 110 p. TAPPI STAP Series, no. 9.

Paulapuro, H. 2007. Wet pressing. In: Papermaking Science and Technology. Paulapuro, H. (ed.) Book 8, Papermaking Part 1, Stock Preparation and Wet End. 2nd ed. Helsinki, Finland: Finnish Paper Engineers' Association/Paperi ja Puu Oy. pp. 343-401.

Pikulik, I. I., McDonald, J. D. and Aitcin, P.-C. 1993. Pulp and Paper Canada. Vol. 94:4. 46-51.

Pikulik, I. I. 1997. Wet-web properties and their effect on picking and machine runnability. In: Preprints of 83rd Annual Meeting, Technical Section. Montreal, Canada. 30-31.1.1997. Montreal, Canada: Canadian Pulp and Paper Association. Preprints 'B'. pp. B23-B30.

Praast, H. and Göttsching, L. 1997. Local orientation of flocs in paper. In: Baker, C. F. (ed.) The Fundamentals of Paper Making Materials, Transactions of the 11th Fundamental Research Symposium. Cambridge, UK. September 1997. Leatherhead, UK: Pira International. Vol. 2. pp. 1293-1324, 1613-1615.

Puurtinen, A. 2003. Control of mobility and filler distribution in wet end layering. Nordic Pulp and Paper Research Journal. Vol. 18:2. 217-225.

Pye, I.T., Daunais, R. and Batty, R. C. 1985. Journal of Pulp and Paper Science. Vol. 11:5. J145-J149.

Ramarao, B. V., Massoquete, A., Lavrykov, S. and Ramaswamy, S. 2003. Moisture diffusion inside paper materials in the hygroscopic range and characteristics of diffusivity parameters. Drying Technology. Vol. 21:10. 2007-2056.

Ramaswamy, S., Ramarao, B. V., Goel, A. Lee, G., Choi, D. and Lavrykov, S. 2002. Theoretical and experimental investigation on liquid penetration in porous media. In: Keller, D. S. and Ramarao, B. V. (eds.) Proceedings of 2002 Progress in Paper Physics Seminar. Syracuse, NY, USA. 8-13.9.2002. Syracuse, NY, USA: State University of New York. pp. 136-140.

Ranger, A.E. and Hopkins, L.F. 1962. A new theory of the tensile behaviour of paper. In: Bolam, F. (ed.) The Formation and Sructure of Paper, Transactions of the Symposium. Oxford, UK. September 1961. London, UK: The British Paper and Board Makers' Association. pp. 277-318.

Retulainen, E. 1997. The role of fibre bonding in paper properties. Doctoral thesis. Helsinki University of Technology, Laboratory of Paper Technology. Reports series A 7. Espoo, Finland. 195 p.

Retulainen, E. and Salminen, K. 2009. Effects of furnish-related factors on tension and relaxation of wet webs. In: I'Anson, S. J. (ed.) Advances in Pulp and Paper Research, Transactions of 14th Fundamental Research Symposium. Oxford, UK. September 2009. Bury, UK: The Pulp and Paper Fundamental Research Society. Vol. 2. pp. 1019-1037, Vol. 3. pp. 1523-1527.

Rice, J.R. 1976. The localization of plastic deformation. In: Koiter, W.T. (ed.) Theoretical and Apllied Mechanics, Proceedings of the 14th International Congress on Theoretical and Applied Mechanics. Delft, Netherlands. 1976. North-Holland Publishing Co. pp. 207-220.

Roberts, R. J., Senden, T. J., Knackstedt, M. A. and Lyne M. B. 2003a. Spreading of aqueous liquids in unsized papers is by film flow. Journal of Pulp and Paper Science. Vol. 29:4. 123-131.

Roberts, R. J., Senden, T. J., Knackstedt, M. A., Lyne, M. B. and Schrof, W. 2003b. 3D imaging of the spreading and penetration of aqueous liquids into unsized and sized papers. In: Proceedings of 5th International Paper and Coating Chemistry Symposium. Montreal, Canada. 16-19.6.2003. Montreal, Canada: Pulp and Paper Technical Association of Canada. pp. 303-311.

de Ruvo, A. and Htun, M. 1981. Fundamental and practical aspects of paper making with recycled fibres. In: Brander, J. (ed.) The Role of Fundamental Research in Paper Making, Transactions of the Symposium. Cambridge, UK. September 1981. London, UK: Mechanical Engineering Publications LTD. Vol. 1. pp. 195-225.

Salminen, P. 1988. Studies of water transport in paper during short contact times. Doctoral thesis. Åbo Akademi, Department of Chemical Engineering, Laboratory of paper Chemistry. Åbo, Finland. 94 p.

Salminen, P. 2010. Oral communication 10.3.2010.

Scallan, A. M. 1974. The structure of the cell wall of wood - a consequence of anisotropic inter-microfibrillar bonding? Wood Science. Vol. 6:3. 266-271.

Scallan, A. M. 1977. The accommodation of water within pulp fibres. In: Fibre-Water Interactions in Paper-making, Transactions of the 6th Fundamental Research Symposium. Oxford, UK. September 1977. London, UK: The British Paper and Board Industry Federation. Vol. 1. pp. 9-29.

Scallan, A. M. and Tigerström, A. C. 1992. Swelling and elasticity of the cell walls of pulp fibres. Journal of Pulp and Paper Science. Vol. 18:5. J188-J193.

Senden, T. J. and Knackstedt, M. A. 2000. Droplet penetration into porous networks: Role of pore morphology. Nordic Pulp and Paper Research Journal. Vol. 15:5. 554-563.

Senden, T. J., Bauer, A., Roberts, R. J., Salminen, L., Ettl, R., Champ, S. and Knackstedt, M. 2007. Experimental imaging of fluid penetration into papers. In: Proceedings of 61st Appita Annual Conference and Exhibition/2007 International Paper Physics Conference. Gold Coast, Australia. 6-9.5.2007. Carlton, Australia: Appita. 5 p.

Seth, R. J. 1995. The effect of fibre length and coarseness on the tensile strength of wet webs: a statistical geometry explanation. Tappi Journal. Vol. 78:3. 99-102.

Seth, R. S., Page, D. H., Barbe, M., C. and Byron, D. J. 1984. The mechanism of the strength and extensibility of wet webs. Svensk Papperstidning. Vol. 87:6. R36-R43.

Shallhorn, P. M. 2002. Effect of moisture content on wet-web tensile properties. Journal of Pulp and Paper Science. Vol. 28:11. 384-387.

Shallhorn, P. M. and Karnis, A. 1975. The mechanism of picking at the presses of a papermachine. In: Preprints of 61st Annual Meeting, Technical Section. Montreal, Canada. Canadian Pulp and Paper Association. Preprints 'B'. pp. B127-B132.

Shmulski, R., Haygreen, J. G. and Bowyer, J. L. 2007. Forest products and wood science. An introduction. 5th revised edition. The Iowa State University Press, Ames. 576 p.

de Silveira, G., Zhang, X., Berry, R. and Wood J. R. 1995. Location of fines in mechanical pulp handsheets using scanning electron microscopy. In: 1995 International Mechanical Pulping Conference. Ottawa, Canada. 12-15.1995. Montreal, Canada: Canadian Pulp and Paper Association. pp. 85-92.

Skowronski, J., Lépoutre, P. and Bichard, W. 1988. Measuring the swelling pressure of paper. In: Proceedings of Tappi Coating Conference. New Orleans, USA. 8-12.5. 1988. Atlanta, USA: TAPPI. pp. 97-101.

Sonka, M., Hlavac, V. and Boyle, R. 1998. Image processing, analysis, and machine vision. 2nd ed. Pacific Grove, CA, USA: Brooks/Cole Publishing Company. 800 p.

Stone, J. E. and Scallan, A. M. 1965. Influence of drying on the pore structures of the cell wall. In: Bolam, F. (ed.) Consolidation of the Paper Web, Transactions of the Symposium. Cambridge, UK. September 1965. London, UK: The British Paper and Board Makers Association. Vol. 1. pp. 145-173.

Stone, J. E. and Scallan, A. M. 1967. The effect of component removal upon the porous structure of the cell wall of wood. II. Swelling in water and the fibre saturation point. Tappi Journal. Vol. 50:10. 496-501.

Stone, J. E. and Scallan, A. M. 1968a. A structural model for the cell wall of water swollen wood pulp fibres based on their accessibility to macromolecules. Cellulose Chemistry and Technology. Vol. 2:3. 343-358.

Stone, J. E. and Scallan, A. M. 1968b. The effect of component removal upon the porous structure of the cell wall of wood. Pulp and Paper Canada. Vol. 69:6. T288-T293.

Stone, J. E. and Scallan, A. M. 1968c. Influence of beating on cell wall swelling and internal fibrillation. Svensk Papperstidning. Vol. 71:19. 687-694.

Söderberg, L. D. and Alfredsson, P. H. 1998. Experimental and theoretical stability investigations of plane liquid jets. European Journal of Mechanics – B/Fluids. Vol. 17:5. 689-737

Szikla, Z. and Paulapuro, H. 1989. Changes in Z-direction density distribution of paper in wet pressing. Journal of Pulp and Paper Science. Vol. 15:1. J11-J17.

Takahashi, A., Häggkvist, M. and Li, T-Q. 1997. Capillary penetration in fibrous matrices by dynamic spiral magnetic resonance imaging. Physical Review E. Vol. 56:2. 2035-2042.

Tanaka, A., Asikainen, J. and Ketoja, A. 2009. Wet web rheology on a paper machine. In: I'Anson, S. J. (ed.) Advances in pulp and paper research, 14th Fundamental Research Symposium. Oxford, UK. September 2009. Bury, UK: Pulp and Paper Fundamental Research Society. Vol. 1. pp. 577-595.

Tejado, A. and van de Ven, T. G. M. 2009a. The strength of wet paper: Beyond capillary forces. In: Madetoja, E., Niskanen, H. and Hämäläinen, J. (eds.) Proceedings of Papermaking Research Symposium. Kuopio, Finland. 1-4.6.2009. Kuopio, Finland: University of Kuopio. 9 p.

Tejado, A. and van de Ven, T. G. M. 2009b. The strength of wet paper: Capillary forces or entanglement friction? In: Proceedings of 7th International Paper and Coating Chemistry Symposium. Hamilton, Canada. 10-12.6.2009. Montreal, Canada: PAPTAC. pp. 51-56.

Tejado, A. and van de Ven, T. G. M. 2009c. Effect of fiber hydrophobicity on the wet web strength of paper. In: Proceedings of 7th International Paper and Coating Chemistry Symposium. Hamilton, Canada. 10-12.6.2009. Montreal, Canada: PAPTAC. pp. 83-90.

Thorpe, J. 1981. Paper as an orthotropic thin plate. Tappi Journal. Vol. 64:3. 119-121.

Thorpe, J. and Yang, C. 1979. The influence of local variation in grammage on wet web straining of newsprint. Svensk Papperstidning. Vol. 82:7. 207-211.

Uesaka, T., Ferahi, M., Hristopulos, D., Deng, N. and Moss, C. 2001. Factors controlling pressroom runnability of paper. In: Baker, C. F. (ed.) The Science of Papermaking, Transactions of the 12th Fundamental Research Symposium. Oxford, UK. September 2001. Bury, UK: The Pulp and Paper Fundamental Research Society. Vol. 2. pp. 1423-1440.

Uesaka, T. and Ferahi, M. 1999. Principal factors controlling press room breaks. In: Proceedings of 1999 TAPPI International Paper Physics Conference. San Diego, California, USA. 26-30.9.1999. Atlanta, GA, USA: TAPPI Press. pp. 229-245.

Ullmar, M. 1998. On fiber alignment mechanisms in a headbox nozzle. Licentiate thesis. Royal Institute of Technology, Department of Pulp and Paper Chemistry and Technology. Stockholm, Sweden. 73 p. TRITA – PMT Report 1998:8.

van de Ven, T. G. M. 2008. Capillary forces in wet paper. Industrial and Engineering Chemistry Research. Vol. 47:19. pp. 7250-7256.

Vuorinen, T. and Alén, R. 1998. Carbohydrates. In: Sjöström, E. and Alén, R. (eds.) Analytical Methods in Wood Chemistry, Pulping and Papermaking. Heidelberg, Germany: Springer Verlag. pp. 37-75.

Wafo toolbox 2009. A Matlab toolbox for analysis of random waves and loads. Lund University, Lund Institute of Technology, Centre for Mathematical Sciences, Mathematical statistics. Version 2.5.

Wahren, D. 1981. Wet webs in open draws. An engineering analysis. Tappi Journal. Vol. 64:3. 89-93.

Wahren, D. 1989. Stability of webs in open draws. In: Preprints of 75th Annual Meeting, Technical Section. Montreal, Canada. 31.1-3.2.1989. Montreal, Canada: Canadian Pulp and Paper Association. Preprints 'B'. pp. B19-B33.

Wang, X., Maloney, T. C. and Paulapuro, H. 2003. Internal fibrillation in never-dried and once-dried chemical pulps. Appita Journal.Vol. 56:6. 455-459.

Wathén, R. 2003. Characterizing the influence of paper structure on web breaks. Licentiate thesis. Helsinki University of Technology, Department of Forest Products Technology. Espoo, Finland. KCL Communications 5, Espoo, Finland: KCL. 104 p.

Wathén, R. and Niskanen, K. 2006. Strength distributions of running paper webs. Journal of Pulp and Paper Science. Vol. 32:3. 137-144.

Weise, U. 1997. Characterization and mechanisms of changes in wood pulp fibres caused by water removal. Doctoral thesis. Helsinki University of Technology, Department of Forest Products Technology. Espoo, Finland. Acta Polytechnica Scandinavica Chemical Technology Series No. 249. Espoo, Finland: The Finnish Academy of Technology. 141 p.

Weise, U. 1998. Hornification – mechanisms and terminology. Paperi ja Puu. Vol. 80:2. 110-115.

Weise, U. and Paulapuro, H. 1995. Changes of fibre dimensions during drying. In: 1995 International Paper Physics Conference. Niagara-on-the-Lake, Canada. 11-14.9.1995. Montreal, Canada: Canadian Pulp and Paper Association. pp. 121-124.

Weise, U., Maloney, T and Paulapuro, H. 1996. Quantification of water in different states of interaction with wood pulp fibres. Cellulose. Vol. 3:4. 189-202.

Weise, U. and Paulapuro, H. 1998. Relation between fiber shrinkage and hornification. Progress in Paper Recycling. Vol. 7:3. 14-21.

Weise, U. and Paulapuro, H. 1999. Effect of drying and rewetting cycles on fibre swelling. Journal of Pulp and Paper Science. Vol. 25:5. 163-166.

Wong, L., Kortschot, M. T. and Dodson, C. T. J. 1996. Effect of formation on local strain fields and fracture of paper. Journal of Pulp and Paper Science. Vol. 22:6. J213-J219.

Yamazaki, H. 1995. Mathematical modelling of absorption process of aqueous liquid into paper. In: 1995 International Paper Physics Conference. Niagara-on-the-Lake, Canada. 11-14.9.1995. Montreal, Canada: Canadian Pulp and Paper Association. pp. 95-98.

Yang, C. and Thorpe, J. 1977. Density distribution vs. wet strain in paper sheets. Tappi Journal. Vol. 60:12. 141-145.

Zapperi, S. and Nukala, P. M. V. V. 2006. Fracture statistics in three-dimensional random fuse model. International Journal of Fracture. Vol. 140:1-4. 99-111.

Österberg, A. V. 1962. Pappersbanors avtagning från pressvalsar. Svensk Papperstidning. Vol. 65:6. 222 – 233.

Hornification data collected from literature

Hornification was measured either as a water retention value (WRV) using the centrifugation technique or as a fibre saturation point (FSP) using the solute exclusion method.

When looking at the tables, it needs to be remembered that WRV is affected not only by fibre swelling, but also by the surface properties of fibres, fines and fines quantity. For example, mechanical pulps retain a significant amount of water in the fine-scale interfibre pores or spaces due to high fines content. In addition, WRV results depend on the g-forces used. In contrast, FSP is very good at estimating the amount of water inside the fibre wall. (Weise et al. 1996, Laine and Stenius 1997, Maloney and Paulapuro 1999, Maloney et al. 1999, Maloney 2000, Forsström et al. 2005.)

BK = bleached softwood kraft, BK-HW = bleached hardwood kraft, UBK = unbleached softwood kraft and DIP = deinked pulp.

Table 1.

Weise 1997		WRV 3000g, g water / g solids		
		WRV 1 *)	WRV 3 **)	Dried 105°C
• All pulps never dried except DIP_{Finn}. • Difference to other refs: Intact sheet centrifuged instead of a pad formed from dispersed fibres. • Lab-recycled (LRC) pulps recycled four times to simulate deinking.	BK, no fines	1.65	1.19	0.97
	BK, SR° 47, no fines	1.88	0.95	0.86
	DIP_{Finn}	1.38	1.22	1.04
	DIP_{German}	1.50	1.27	1.04
	BK beaten, 4x LRC	1.47	1.07	1.03
		WRV 900g, g water / g solids		
		WRV 1 *)	WRV 3 **)	Dried 105°C
			DSC 60-75%	
	BK beaten, 4x LRC	1.78	1.45	1.21
	DIP_{German}	2.45	2.09	1.81
	$DIP_{German,}$ no fines	1.45	1.32	1.11
	TMP, 4x LRC	2.33	2.08	1.66
	TMP, no fines, 4x LRC	1.51	1.37	-
	UBK,PFI-5000, no fines	2.04	1.55	1.34
	BK-HW, PFI-4000 rev.	2.74	1.75	1.57

*) All free water should have been removed from interfibre voids or from larger pores that refill reversibly when re-wetted.
**) Virtually all free water should have disappeared from macropores between lamellae in the cell wall, causing them to laminate irreversibly (wet hornification)

Table 2.

Park et al. 1331	Pulp	WRV, g water / g solids	
		Never dried	Dried 105°C
Dried values were measured from defibrated handsheets.	BK, PFI 6000 rev.	3.05	2.27
	BK unbeaten	2.51	1.92
	UBK unbeaten	2.46	2.00
	BK-HW, PFI 4000 rev.	2.92	2.18
	BK-HW unbeaten	2.40	1.89
	TMP	2.20	2.01

Table 3.

Laivins & Scallan 1996	Pulp	FSP, g water / g solids		Fines content, % *)
		Never dried	Air dried	
• Kraft pulps unbeaten. • Results of BK and UBK, an average of two pulps. • Fines < 200 mesh. • *) in never dried pulp / in dried pulp • **) Calculated based on results of whole pulp and fibres.	UBK whole pulp	1.47	1.20	4.9 / 4.3
	UBK fibres	1.40	1.16	
	UBK < 200 mesh **)	2.9	2.2	
	BK whole pulp	1.28	1.03	4.6 / 4.4
	BK fibres	1.21	0.96	
	BK < 200 mesh **)	2.6	2.3	
	BK-HW whole pulp	1.36	0.99	18.3 / 18.4
	BK-HW fibres	1.1	0.89	
	BK-HW < 200 mesh **)	2.5	1.4	
	Refiner whole pulp	0.81	0.77	27.7 / -
	Refiner fibres	0.67	0.62	
	Refiner < 200 mesh **)	1.2	1.2	
	TMP whole pulp	0.99	0.91	29.2 / 28.6
	TMP fibres	0.73	0.72	
	TMP < 200 mesh **)	1.6	1.4	

Table 4.

Scallan & Tigerström 1992	Pulp	FSP, g water / g solids	
		Never dried	Air dried
• Kraft pulps unbeaten.	UBK >200 mesh	1.44	1.14
	BK >200 mesh	1.37	0.97
	GW >200 mesh	0.71	0.67
	Refiner >200 mesh	0.72	0.69

Table 5.

Lundberg & de Ruvo 1978	Pulp	WRV, g water / g solids			
• Measurements from restrained dried and disintegrated handsheets.		Never dried	Air dried	Dried 120°C	Bone dry 120°C
	BK beaten	1.90	1.47	1.38	1.31
	BK beaten > 150 mesh	1.73	1.30	1.22	1.15

Furnish properties for papers News E1–E6 from disintegrated paper samples

News	E1	E2	E3	E4	E5	E6
L&W Fiber Master results						
Fibre length, mm	1.375	1.370	1.384	1.389	1.390	1.373
Fibre width, µm	29.0	29.0	28.9	28.9	28.9	28.7
Fibre shape factor	88.1	88.1	88.2	88.0	88.1	88.0
Bendability, %	4.6	4.6	4.8	4.8	4.8	4.6
Coarseness, µg/m	111.7	114.4	113.9	108.7	110.3	110.0
Fiber Master fines, %	28.05	27.30	27.75	27.05	27.20	27.80
Length weighted proportion %						
0.2–0.5 mm	0.23	0.23	0.23	0.22	0.23	0.23
0.5–1.5 mm	0.43	0.43	0.43	0.44	0.43	0.43
1.5–3.0 mm	0.24	0.24	0.24	0.24	0.23	0.24
3.0–4.5 mm	0.09	0.08	0.09	0.09	0.09	0.09
4.5–> mm	0.01	0.02	0.02	0.02	0.02	0.02
Width 0.2–0.5 mm, µm	20.7	20.7	20.7	20.7	20.7	20.9
Width 0.5–1.5 mm, µm	27.6	27.3	27.4	27.2	27.4	27.2
Width 1.5–3 mm, µm	36.1	36.6	36.0	36.2	36.1	35.9
Width 3–4.5 mm, µm	36.5	37.0	36.3	36.3	36.7	36.0
Width 4.5–> mm, µm	36.4	37.0	36.2	37.9	37.6	36.6
Shape factor 0.2–0.5 mm	87.4	87.5	87.4	87.5	87.3	87.5
Shape factor 0.5–1.5 mm	89.7	89.7	89.9	89.6	89.9	89.7
Shape factor 1.5–3.0 mm	88.8	88.6	89.0	88.6	88.7	88.5
Shape factor 3.0–4.5 mm	83.2	83.5	84.0	83.9	83.6	83.2
Shape factor 4.5–> mm	68.8	70.8	69.1	68.7	71.0	69.3
Bendability 0.2–0.5 mm, %	1.3	1.8	1.4	1.6	1.3	1.5
Bendability 0.5–1.5 mm, %	3.7	3.7	3.7	3.8	4.0	3.9
Bendability 1.5–3.0 mm, %	8.7	8.3	8.9	8.6	8.8	8.6
Bendability 3.0–4.5 mm, %	9.6	10.5	11.0	10.6	10.5	9.7
Bendability 4.5–> mm, %	4.9	7.1	6.0	5.0	7.3	5.2
BMcN 28, %	30.1	30.3	30.3	30.2	30.2	29.6
BMcN 48, %	24.7	24.6	24.4	25.3	25.1	24.6
BMcN 100, %	14.2	14.1	13.9	14.8	14.5	14.2
BMcN 200, %	8.8	8.3	8.5	9.3	8.4	8.9
BMcN <200, %	22.1	22.7	22.9	20.3	21.8	22.7
Ash 525°C, %	9.4	9.0	9.3	9.1	9.0	9.1
Softwood mechanical pulp, %	69	NA	58	61	NA	61
Hardwood mechanical pulp, %	1	NA	2	2	NA	1
Softwood chemical pulp, %	18	NA	25	23	NA	22
Hardwood chemical pulp, %	12	NA	15	14	NA	16

Because ash was assumed to be located as a whole in BMcN fraction < 200 mesh, the amount of fibre fines was calculated by subtracting ash content from BMcN fraction < 200 mesh. After this, fines and fibre fractions were scaled so that the sum of the fractions equalled 100%.
Disintegration ISO 5263:1995, BauerMcNett classification SCAN-CM 6:05, Fiber Master furnish analyses ISO 16065-2:2007, ash 525°C ISO 1762:2001 and fibre furnish analysis ISO 9184-1:1990 and ISO 9184-4:1990.

Furnish properties for LWC base papers A1– A3 and B1–B2 from disintegrated paper samples.

LWC base papers	A1	A2	A3	B1	B2
L&W Fiber Master results					
Average fibre length, mm	1.951	2.102	2.077	1.478	1.470
Average fibre width, µm	33.1	33.3	33.2	28.9	29.2
Average fibre shape factor	86.4	85.6	85.8	85.8	85.8
Coarseness, µg/m	147.1	136.1	132.5	NA	NA
Average bendability, %	5.7	6.2	6.3	5.1	5.2
Fiber master fines, %	23.8	22.40	23.30	37.20	36.15
Length weighted proportion 0.2–0.5 mm, %	0.17	0.16	0.16	0.32	0.31
Length weighted proportion 0.5–1.5 mm, %	0.25	0.23	0.23	0.30	0.31
Length weighted proportion 1.5–3.0 mm, %	0.35	0.35	0.35	0.22	0.23
Length weighted proportion 3.0–4.5 mm, %	0.18	0.21	0.21	0.14	0.13
Length weighted proportion 4.5–> mm, %	0.04	0.05	0.05	0.02	0.02
Width 0.2–0.5 mm, µm	23.6	24.3	24.4	21.2	21.6
Width 0.5–1.5 mm, µm	33.9	33.6	33.7	30.8	30.9
Width 1.5–3 mm, µm	35.7	35.7	35.4	34.1	34.2
Width 3–4.5 mm, µm	35.0	35.1	34.9	33.7	33.8
Width 4.5–> mm, µm	36.8	36.5	37.0	34.2	34.7
Shape factor 0.2–0.5 mm	84.6	84.3	84.2	86.9	86.6
Shape factor 0.5–1.5 mm	88.4	87.2	88.1	86.9	86.7
Shape factor 1.5–3.0 mm	89.1	88.3	88.4	86.0	86.4
Shape factor 3.0–4.5 mm	83.7	84.0	83.8	83.0	82.8
Shape factor 4.5–> mm	69.4	70.0	69.1	72.2	72.0
Bendability 0.2–0.5 mm, %	1.5	1.9	1.7	1.5	1.7
Bendability 0.5–1.5 mm, %	3.0	3.2	3.8	3.9	3.6
Bendability 1.5–3.0 mm, %	9.4	9.6	9.6	10.0	10.4
Bendability 3.0–4.5 mm, %	11.3	11.2	11.5	11.3	11.3
Bendability 4.5–> mm, %	6.6	7.8	6.4	8.6	8.1
BMcN 28, %	55.3	61.5	61.3	39.7	40.2
BMcN 48, %	9.8	7.4	8.7	12.2	13.6
BMcN 100, %	8.1	7.0	7.3	12.5	11.4
BMcN 200, %	8.5	8.3	8.7	12.8	12.1
BMcN <200, %	18.3	15.9	14.0	22.8	22.9
Ash 525°C, %	7.2	8.0	7.7	13.6	14.6
Softwood mechanical pulp, %	60	55	54	54	55
Hardwood mechanical pulp, %	0	0	0	0	0
Softwood chemical pulp, %	40	45	46	46	45
Hardwood chemical pulp, %	0	0	0	0	0

Because ash was assumed to be located as a whole in BMcN fraction < 200 mesh, the amount of fibre fines was calculated by subtracting ash content from BMcN fraction < 200 mesh. After this, fines and fibre fractions were scaled so that the sum of the fractions equalled 100%.
Disintegration ISO 5263:1995, BauerMcNett classification SCAN-CM 6:05, Fiber Master furnish analyses ISO 16065-2:2007, ash 525°C ISO 1762:2001 and fibre furnish analysis ISO 9184-1:1990 and ISO 9184-4:1990.

Porosity results based on ESEM measurements

- News E1–E6, wet samples (DSC 56%) in the top table and dry samples in the bottom table
- Instead of the settings used in Chapter 3.1.3., the magnification was 600x and resolution 0.29 µm/pixel.
- The measurements were executed both with the lumen open and filled.

	E1	E2	E3	E4	E5	E6
Total porosity without lumen, %	40.5	40.6	41.5	42.9	40.5	39.5
Standard deviation, %	3.65	4.65	4.26	3.34	4.36	4.52
Total porosity with lumen, %	47.3	46.9	47.6	49.6	47.5	45.9
Standard deviation, %	3.86	3.99	3.46	3.33	3.94	4.00
Effective thickness of sheet, µm	67.2	68.3	69.8	68.6	68.6	67.8
Standard deviation, µm	10.29	9.60	9.31	9.11	8.69	8.89
Pore height without lumen, µm	3.34	3.25	3.33	3.31	3.20	3.36
Standard deviation, µm	3.44	3.34	3.50	3.46	3.33	3.48
Pore height with lumen, µm	3.35	3.26	3.33	3.32	3.27	3.38
Standard deviation, µm	3.35	3.28	3.41	3.38	3.29	3.39
Pore width without lumen, µm	5.02	4.85	4.93	4.92	4.89	5.02
Standard deviation, µm	6.34	6.10	6.16	6.08	6.12	6.44
Pore width with lumen, µm	5.24	5.02	5.07	5.15	5.15	5.22
Standard deviation, µm	6.54	6.26	6.25	6.26	6.35	6.57

	E1	E2	E3	E4	E5	E6
Total porosity without lumen, %	29.2	29.0	29.1	31.7	31.7	31.3
Standard deviation, %	5.19	5.42	4.64	4.69	5.33	3.83
Total porosity with lumen, %	33.6	33.3	34.4	36.2	36.1	35.8
Standard deviation, %	5.18	5.48	5.01	4.70	4.97	4.00
Effective thickness of sheet, µm	53.4	53.6	53.7	53.1	52.5	52.6
Standard deviation, µm	5.97	6.39	6.13	5.47	5.58	5.77
Pore height without lumen, µm	2.71	2.67	2.75	2.74	2.83	2.80
Standard deviation, µm	2.41	2.36	2.51	2.58	2.57	2.62
Pore height with lumen, µm	2.69	2.63	2.71	2.71	2.79	2.78
Standard deviation, µm	2.35	2.29	2.42	2.49	2.48	2.54
Pore width without lumen, µm	4.25	4.34	4.30	4.39	4.56	4.43
Standard deviation, µm	5.03	5.04	5.04	5.21	5.48	5.35
Pore width with lumen, µm	4.42	4.47	4.47	4.52	4.69	4.59
Standard deviation, µm	5.19	5.14	5.19	5.35	5.59	5.50

Examples of the ESEM images obtained from wet samples, DSC 56%. The images are taken in the cross machine direction.

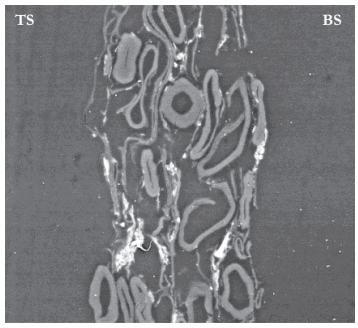

News E1

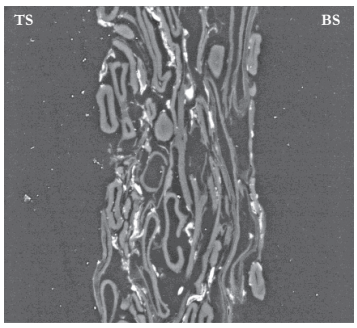

News E4

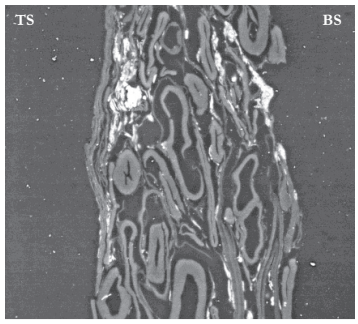

News E2

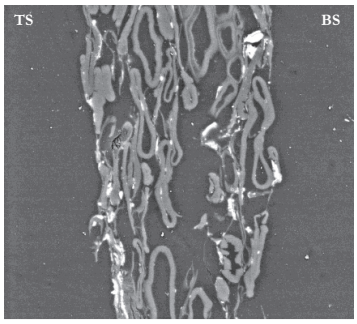

News E5

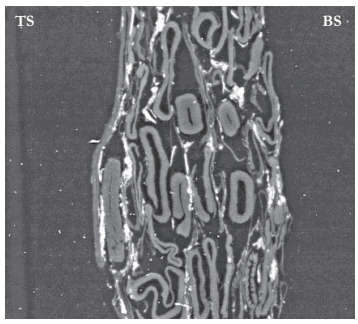

News E3

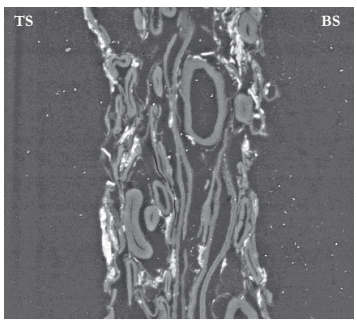

News E6

Examples of the ESEM images obtained from dry samples, DSC 92%. The images are taken in the cross machine direction.

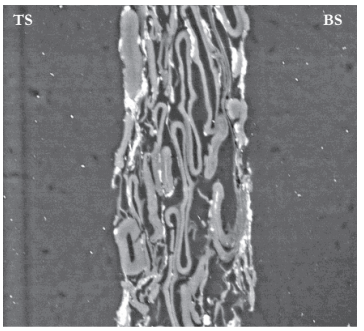

News E1

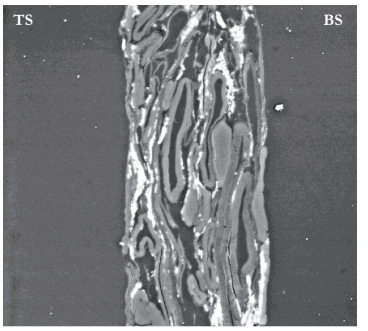

News E4

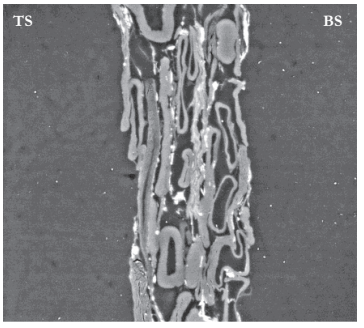

News E2

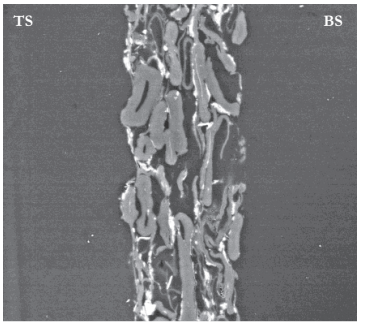

News E5

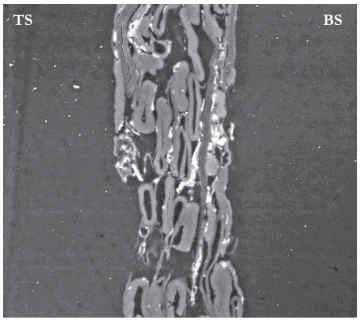

News E3

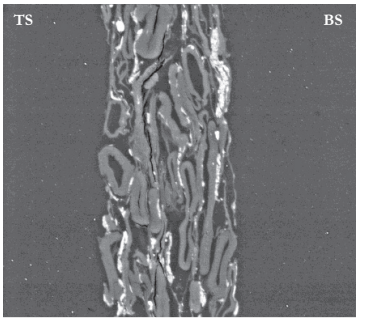

News E6

Correlation between fibre orientation and grammage variation measured in formation and mesoscale. News E1–E6.

The intensity of the correlation is indicated by p value, t value and coefficient of determination. None of the correlations is statistically significant.

	Layered anisotropy			Tensile MD/CD ratio		
Measurement	p value	t value	R^2	p value	t value	R^2
Ambertec	0.908	-0.123	0.004	0.744	0.351	0.030
β-radiography	0.964	0.049	0.001	0.500	0.741	0.121
β-radiography $_{2–8\ mm}$	0.871	-0.173	0.007	0.667	0.464	0.051
β-radiography $_{8–32\ mm}$	0.757	-0.332	0.027	0.956	-0.059	0.001
Tapio $_{2–8\ mm}$	0.624	-0.530	0.066	0.773	0.308	0.023
Tapio $_{8–16\ mm}$	0.564	-0.629	0.090	0.982	-0.024	0.000
Tapio $_{16–32\ mm}$	0.557	-0.641	0.093	0.852	-0.199	0.010
Tapio $_{32–64\ mm}$	0.677	-0.449	0.048	0.939	0.082	0.002
Tapio $_{2–128\ mm}$	0.598	-0.572	0.075	0.958	0.056	0.001
Voids $_{1–4\ mm^2}$	0.547	0.657	0.097	0.220	1.453	0.346
Voids $_{4–8\ mm^2}$	0.807	-0.261	0.017	0.979	-0.027	0.000
Voids $_{1–8\ mm^2}$	0.832	0.226	0.013	0.526	0.694	0.108
Voids $_{8–16\ mm^2}$	0.322	-1.128	0.241	0.571	-0.616	0.087

The lower index in the left column refers either to a wavelength band as mm or void size class as mm^2.

Correlation between tensile strength and grammage variation measured in formation and mesoscale. News E1–E6.

The intensity of the correlation is indicated by p value, t value and coefficient of determination. None of the correlations is statistically significant.

	DSC 56%			DSC 68%		
Measurement	p value	t value	R2	p value	t value	R2
Ambertec	0.546	0.659	0.098	0.533	-0.682	0.104
β-radiography	0.573	0.613	0.086	0.578	-0.604	0.084
β-radiography $_{2–8\ mm}$	0.670	0.458	0.050	0.445	-0.846	0.152
β-radiography $_{8–32\ mm}$	0.876	-0.167	0.007	0.363	-1.027	0.209
Tapio $_{2–8\ mm}$	0.911	0.119	0.004	0.321	-1.131	0.243
Tapio $_{8–16\ mm}$	0.907	0.125	0.004	0.264	-1.298	0.296
Tapio $_{16–32\ mm}$	0.904	0.128	0.004	0.263	-1.302	0.298
Tapio $_{32–64\ mm}$	0.760	0.326	0.026	0.348	-1.062	0.220
Tapio $_{2–128\ mm}$	0.876	0.166	0.007	0.285	-1.232	0.275
Voids $_{1–4\ mm^2}$	0.186	1.595	0.389	0.938	0.083	0.002
Voids $_{4\ 8\ mm^2}$	0.554	0.645	0.094	0.455	-0.827	0.146
Voids $_{1–8\ mm^2}$	0.301	1.186	0.260	0.749	-0.343	0.029
Voids $_{8–16\ mm^2}$	0.344	-1.073	0.223	0.115	-2.012	0.503
	Mean of tensile strength at DSC 56% and 68%			Dry		
Measurement	p value	t value	R2	p value	t value	R2
Ambertec	0.967	-0.044	0.000	0.844	-0.210	0.011
β-radiography	0.981	-0.028	0.000	0.820	0.243	0.015
β-radiography $_{2–8\ mm}$	0.840	-0.215	0.011	0.972	0.037	0.000
β-radiography $_{8–32\ mm}$	0.554	-0.644	0.094	0.945	0.073	0.001
Tapio $_{2–8\ mm}$	0.630	-0.521	0.064	0.965	-0.047	0.001
Tapio $_{8–16\ mm}$	0.590	-0.585	0.079	0.738	-0.359	0.031
Tapio $_{16–32\ mm}$	0.590	-0.585	0.079	0.635	-0.513	0.062
Tapio $_{32–64\ mm}$	0.725	-0.378	0.034	0.744	-0.350	0.030
Tapio $_{2–128\ mm}$	0.621	-0.535	0.067	0.781	-0.298	0.022
Voids $_{1–4\ mm^2}$	0.495	0.750	0.123	0.738	0.358	0.031
Voids $_{4–8\ mm^2}$	0.912	-0.118	0.003	0.597	-0.573	0.076
Voids $_{1–8\ mm^2}$	0.747	0.345	0.029	0.942	-0.077	0.001
Voids $_{8–16\ mm^2}$	0.157	-1.741	0.431	0.923	-0.103	0.003

The lower index in the left column refers either to a wavelength band as mm or void size class as mm².

Correlation between TSI and grammage variation measured in formation and mesoscale. News E1–E6.

The intensity of the correlation is indicated by p value, t value and coefficient of determination. None of the correlations is statistically significant.

	DSC 68%			Dry		
Measurement	p value	t value	R^2	p value	t value	R^2
Ambertec	0.963	0.050	0.001	0.822	0.240	0.014
β-radiography	0.866	0.180	0.008	0.504	0.733	0.118
β-radiography $_{2\ 8\ mm}$	0.977	-0.031	0.000	0.654	0.483	0.055
β-radiography $_{8–32\ mm}$	0.805	-0.264	0.017	0.838	0.219	0.012
Tapio $_{2–8\ mm}$	0.692	-0.426	0.043	0.853	0.197	0.010
Tapio $_{8–16\ mm}$	0.659	-0.476	0.054	0.955	-0.060	0.001
Tapio $_{16\ 32\ mm}$	0.664	-0.468	0.052	0.869	-0.175	0.008
Tapio $_{32–64\ mm}$	0.790	-0.284	0.020	0.986	0.018	0.000
Tapio $_{2\ 128\ mm}$	0.694	-0.424	0.043	0.993	0.009	0.000
Voids $_{1–4\ mm^2}$	0.437	0.862	0.157	0.335	1.096	0.231
Voids $_{4\ 8\ mm^2}$	0.971	-0.038	0.000	0.960	0.054	0.001
Voids $_{1–8\ mm^2}$	0.681	0.442	0.047	0.581	0.600	0.083
Voids $_{8–16\ mm^2}$	0.314	-1.151	0.249	0.784	-0.293	0.021

The lower index in the left column refers either to a wavelength band as mm or void size class as mm^2.

Ash distribution in z-direction

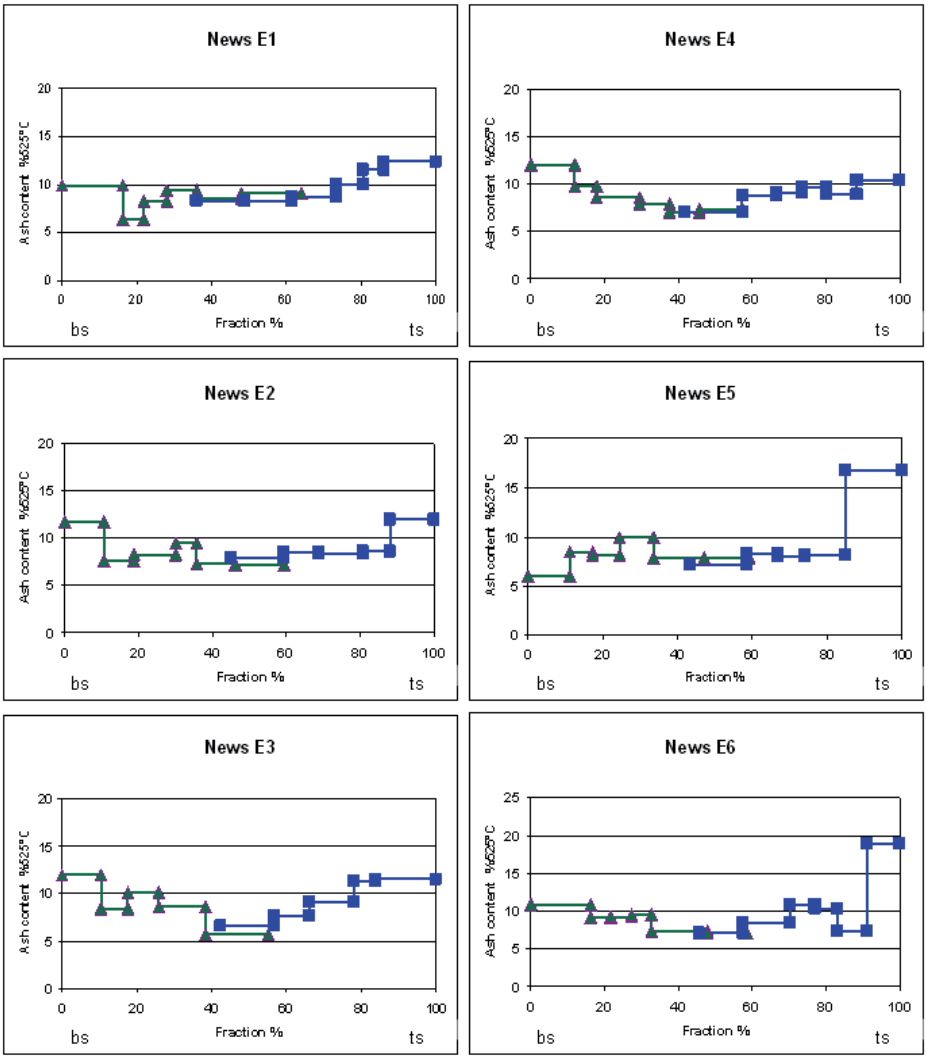

The samples of 50 mm x 180 mm were split by a tape method. The basis weight and ash content (525°C) of each layer were measured according to standard methods ISO 536:1995 and ISO 1762:2001 respectively.

The layout of the wire section of the gap former used for News series E1–E6

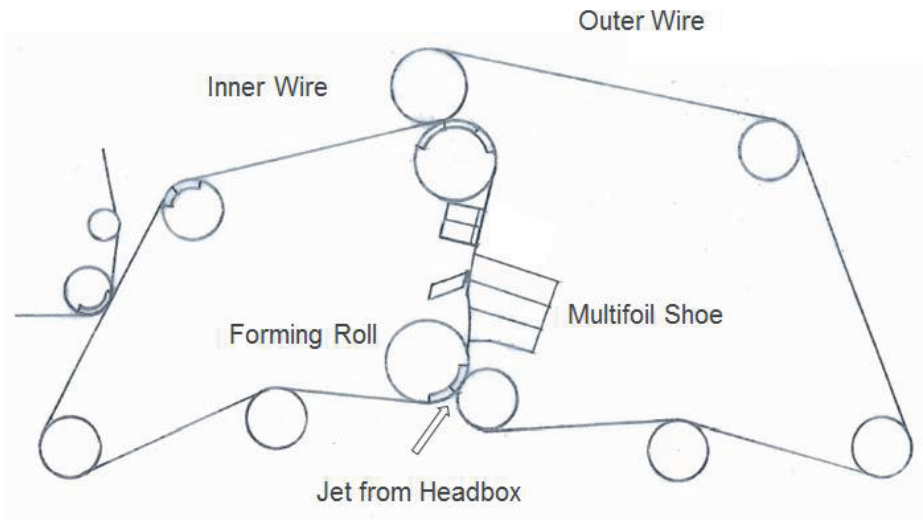

The layout of the pilot paper machine

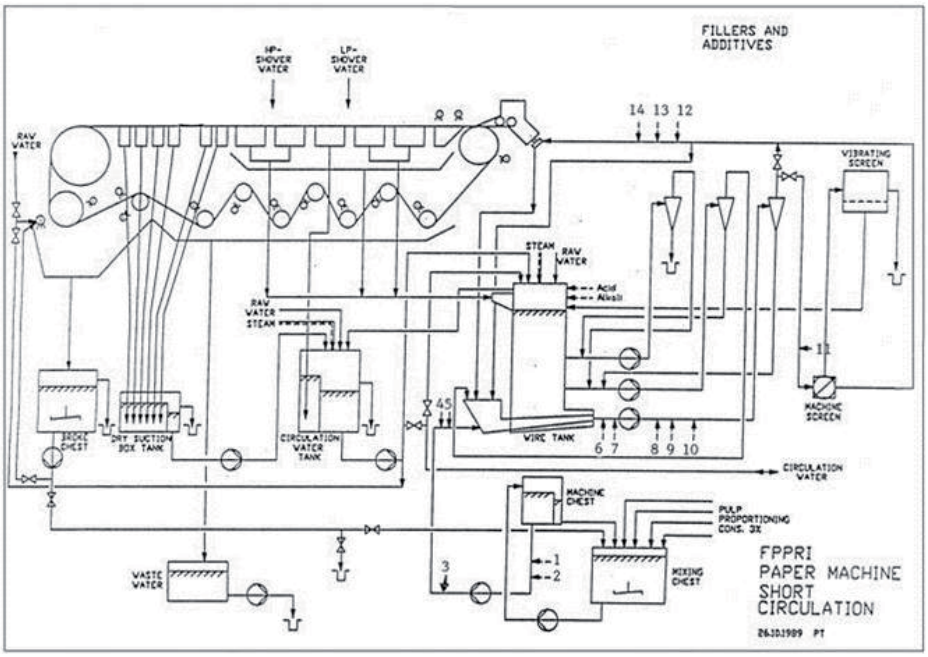

Aalto-DD 38/2012

ISBN 978-952-60-4568-9
ISBN 978-952-60-4569-6 (pdf)
ISSN-L 1799-4934
ISSN 1799-4934
ISSN 1799-4942 (pdf)

Aalto University
School of Chemical Technology
Department of Forest Products Technology
www.aalto.fi

BUSINESS +
ECONOMY

ART +
DESIGN +
ARCHITECTURE

SCIENCE +
TECHNOLOGY

CROSSOVER

DOCTORAL
DISSERTATIONS